01 May 1990

Design of automotive structural components using high strength sheet steels structural strengths of cold-formed steel members under dynamic loads

Maher Kassar

Wei-Wen Yu
Missouri University of Science and Technology, wwy4@mst.edu

Civil Engineering Study 90-1
Structural Series

Thirteenth Progress Report

DESIGN OF AUTOMOTIVE STRUCTURAL COMPONENTS USING HIGH STRENGTH SHEET STEELS

STRUCTURAL STRENGTHS OF COLD-FORMED STEEL MEMBERS UNDER DYNAMIC LOADS

by

Maher Kassar
Research Assistant

Wei-Wen Yu
Project Director

A Research Project Sponsored by the American Iron and Steel Institute

May 1990

Department of Civil Engineering
University of Missouri-Rolla
Rolla, Missouri

TABLE OF CONTENTS

TABLE OF CONTENTS (Cont.)

TABLE OF CONTENTS (Cont.)

LIST OF TABLES

LIST OF TABLES (cont.)

LIST OF TABLES (cont.)

LIST OF TABLES (cont.)

LIST OF Figures

LIST OF FIGURES (Cont.)

LIST OF FIGURES (Cont.)

LIST OF FIGURES (Cont.)

LIST OF FIGURES (Cont.)

LIST OF FIGURES (Cont.)

LIST OF FIGURES (Cont.)

LIST OF FIGURES (Cont.)

I. INTRODUCTION

Since May 1988, the research project on automotive components sponsored by American Iron and Steel Institute (AISI) at University of Missouri-Rolla (UMR) has been concentrated on a study of the effect of strain rate on mechanical properties of sheet steels and the structural behavior and strength of cold-formed steel members subjected to impact loads.

The results of the static and dynamic tensile mechanical properties of three selected sheet steels in the virgin condition as well as for the steels subjected to different amount of cold stretchings, were established in 1988 and early 1989. Details of the tension coupon tests were presented in the Eleventh Progress Report.[1]

During the period from January through August 1989, the UMR study primarily involved the experimental determination of the static and dynamic mechanical properties in compression for the same sheet steels used in the Eleventh Progress Report. The strain rates used for these compression coupon tests were similar to those used for the tension tests. They ranged from 10^{-4} to 1.0 in./in./sec. Details of the compression coupon tests are discussed in the Twelfth Progress Report.[2]

The study of the structural behavior and strength of cold-formed steel members subjected to impact loads (phase II of the project) was initiated in August 1989. Two materials (35XF and 50XF) were used in this phase of study.

Up to January 1990, thirty-seven (37) stub-columns and thirty (30) beam specimens fabricated from 35XF sheet steel have been tested under different strain rates. Specimens using channel and I-shaped sections were tested to study the strength of structural members having unstiffened compression elements. Specimens using hat and box sections were tested to study the strength of structural members having stiffened compression elements.

The ranges of w/t ratios varied from 8.93 to 20.87 for unstiffened compression elements and from 26.92 to 76.64 for stiffened compression elements. The strain rate ranged from 10^{-5} to 0.1 in./in./sec.

Chapter II includes review of the literature related to local buckling and post-buckling behavior of stiffened and unstiffened compression elements. Also discussed in chapter II is the available literature on the effect of the impact loads and strain rates on the structural strength of beams and columns. Details of test specimens, test procedures, and test results are presented in Chapter III. The test results are evaluated in Chapter IV. Finally, the research findings are summarized in Chapter V.

II. REVIEW OF LITERATURE

A. GENERAL

This literature review covers both theoretical and experimental work for the following two major subjects:

1. The structural behavior of stiffened and unstiffened compression elements under static loads presented in Section B.

2. The response of structural members to dynamic loads discussed in Section C.

The literature survey on the effect of strain rate on mechanical behavior of materials in tension and compression was presented early in the Eleventh and Twelfth Progress Reports.[1,2] This survey focuses on those cases related to flexural and axially loaded members for the purpose of studying the effect of strain rate due to the dynamic loads on the structural strengths of these members.

B. STRUCTURAL BEHAVIOR OF COMPRESSION ELEMENT UNDER STATIC LOADS

The analytical solutions of the elastic local buckling strengths of both stiffened and unstiffened compression elements are presented in Section II.B.1. The buckling stress in the inelastic range is discussed in Section II.B.2. In Section II.B.3, the theoretical background of the postbuckling behavior of rectangular stiffened and unstiffened compression elements is briefly reviewed. The development of effective width formulas for the prediction of the maximum strength

of stiffened and unstiffened compression elements is presented in Section II.B.4. Also presented in this section are the effective width formulas used in the current AISI Cold Formed Steel Design Manual[3] and AISI Automotive Design Manual[4].

1. Elastic Local Buckling of Flat Compression Elements. The elastic local buckling behavior of thin elements is governed by a differential equation based on the small deflection theory of plates. The analytical solution for the critical buckling stress of plates is available from solving the differential equation by using the energy method.[5,6] Timoshenko[5] has presented a series of solutions of plate buckling for several different types of compression elements, considering various boundary conditions. Figure 2.1 shows different sructural members with stiffened and unstiffened compression elements.

The methods of determining the critical buckling stresses of compression elements are summarized in Sections II.B.1.a and II.B.1.b for stiffened and unstiffened elements, respectively.

a. Stiffened Elements. The critical buckling stress of compression elements can be determined by solving the following differential equation. This equation was originally derived by Saint Venant in 1883.[7]

$$\frac{\partial^4\omega}{\partial x^4} + 2\frac{\partial^4\omega}{\partial x^2\partial y^2} + \frac{\partial^4\omega}{\partial y^4} = \frac{1}{D}\left[q + f_x t\frac{\partial^2\omega}{\partial x^2} + f_y t\frac{\partial^2\omega}{\partial y^2} + 2\tau_{xy}t\frac{\partial^2\omega}{\partial x\partial y}\right] \qquad (2.1)$$

where ω = lateral deflection of the plate

q = lateral uniform load applied to the plate

t = thickness of the plate

$D = Et^3/(12(1-\mu^2))$

E = modulus of elasticity

μ = Poisson's ratio = 0.3 for steel

f_x, f_y = stress components normal to the edges of the plate and lying in the x-y plane

τ_{xy} = shear stress component on the edges of the plate in the x-z and y-z plane

As shown in Fig. 2.2, a rectangular plate simply supported on four edges is compressed in its middle plane by stresses uniformly distributed along the sides x=0 and x=a. According to the loading conditions of the compressed plate, the nonexistent stress terms were eliminated in Equation (2.1) and the governing differential equation is as follows:

$$\frac{\partial^4\omega}{\partial x^4} + 2\frac{\partial^4\omega}{\partial x^2\partial y^2} + \frac{\partial^4\omega}{\partial y^4} = -\frac{f_x t}{D}\frac{\partial^2\omega}{\partial x^2} \qquad (2.2)$$

The change of the sign in front of the f_x term indicates that the stress is considered to be positive for compression. Timoshenko[3] assumed that a double Fourier series can be used to represent the deflected surface of the buckled plates as follows:

$$\omega = \sum_{m=1}^{\infty} \sum_{n=1}^{\infty} A_{mn} \sin\left(\frac{m\pi x}{a}\right) \sin\left(\frac{n\pi y}{w}\right) \qquad (2.3)$$

where A_{mn} = coefficient

m = number of half sine waves in x-direction

n = number of half sine waves in y-direction

a = length of plate

w = width of plate

Equation (2.3) satisfies the boundary conditions along the four simply supported edges. The boundary conditions at the unloaded edges are

$$[\omega = 0]_{y=0,\, w}, \quad \left[\frac{\partial^2 \omega}{\partial x^2} + \mu \frac{\partial^2 \omega}{\partial y^2} = 0 \right]_{y=0,\, w} \qquad (2.4)$$

Solving Equation (2.2) by using Equations (2.3) and (2.4), the expression for the critical buckling stress of stiffened compression elements is

$$f_{cr} = f_x = \frac{k\pi D}{tw^2} \qquad (2.5)$$

where $$k = \left[m\left(\frac{w}{a}\right) + \left(\frac{1}{m}\right)\left(\frac{a}{w}\right) \right]^2 \qquad (2.6)$$

In Equation (2.5), only one half sine wave in the y direction was assumed. Substituting the equation for D into Equation (2.5), one can obtain the following expression for the critical buckling stress.

$$f_{cr} = \frac{k\pi^2 E}{12(1-\mu^2)(w/t)^2} . \qquad (2.7)$$

The value of k, as shown in Fig. 2.3, depends on the magnitude of the aspect ratio (a/w) of the plate and the number of half sine waves in the direction of compression. In Fig. 2.3, it is noted that the value of k is equal to four for a square plate and for any plate with an aspect ratio equal to an integer. In addition, for a long plate with an aspect ratio larger than four, the value of k approaches to four. Therefore, a minimum value of k equal to four is conservatively used in practical design without considering the rotational restraint along the unloaded edges.

b. Unstiffened Elements. The same governing Equation (2.2) can also be used for unstiffened plates, as shown in Fig. 2.4, which are simply supported on three edges and the other edge free. Timoshenko[5] assumed that a plate under the action of compressive forces will buckle in m sinusoidal half-waves. The expression of the deflected surface of the plate is

$$\omega = f(y) \sin\left(\frac{m\pi x}{a}\right) \tag{2.8}$$

where a = length of plate

$f(y)$ = function of y alone.

Equation (2.8) satisfies the boundary conditions along the simply supported edges x=0 and x=a. The boundary conditions along the supported edge, y=0, and the free edge, y=w, are as follows:

$$\left[\omega = 0\right]_{y=0}, \quad \left[\frac{\partial^2\omega}{\partial y^2} + \mu \frac{\partial^2\omega}{\partial x^2} = 0\right]_{y=0}$$

$$\left[\frac{\partial^2\omega}{\partial y^2} + \mu \frac{\partial^2\omega}{\partial x^2} = 0\right]_{y=w}, \quad \left[\frac{\partial^3\omega}{\partial y^3} + (2-\mu) \frac{\partial^3\omega}{\partial x^2 \partial y} = 0\right]_{y=w} \tag{2.9}$$

Solving Equation (2.2) by using Equations (2.8) and (2.9), one can obtain the following expression for the critical buckling stress of unstiffened compression elements in which the buckled plate has only one half sine wave in the direction of compression regardless of the length of plate.

$$f_{cr} = \frac{k\pi^2 D}{tw^2} \tag{2.10}$$

in which k is a numerical factor depending on the magnitude of the ratio of a/w. An approximate solution based on an energy method has been

presented by both Timoshenko[5] and Bulson[6]. The buckling coefficient was found to be

$$k = \left(\frac{w}{a}\right)^2 + 6\frac{1-\mu}{\pi^2} . \qquad (2.11)$$

Figure 2.5 shows the relationship between buckling coefficient and aspect ratio of the rectangular unstiffened plate. Reference 6 indicates that the approximate solution is close to the exact solution. Figure 2.5 also shows that the value of k approaches to a constant of 0.425 as the aspect ratio of the plate approaches infinity. Poisson's ratio μ is equal to 0.3.

2. Inelastic Buckling of Flat Compression Elements. A plate may buckle at a stress level beyond the proportional limit of the steel when the flat width-to-thickness (w/t) ratio is small. The plate becomes an anisotropic plate when it buckles in the inelastic range. The analytical study of local buckling in the inelastic range is complicated because of the anisotropic nature of the material. However, analytical investigations of plates that buckled in the inelastic range have been considered by numerous researchers.[8-12] A brief discussion of plate buckling in the inelastic range is presented in this section.

In 1924, Bleich[8] extended the theory of flat plate stability into the inelastic range by considering the plate as an anisotropic type and by introducing a reduced modulus into Eq. (2.2). He assumed that the

reduced modulus is effective only for strips of a plate in the direction of the compressive stress, whereas the elastic modulus remains valid for strips in the perpendicular direction of compression stress. The differential equation proposed by Bleich for inelastic buckling is

$$\tau \frac{\partial^4 \omega}{\partial x^4} + 2\sqrt{\tau} \frac{\partial^4 \omega}{\partial x^2 \partial y^2} + \frac{\partial^4 \omega}{\partial y^4} + \frac{f_x t}{D} \frac{\partial^2 \omega}{\partial x^2} = 0 \qquad (2.12)$$

where $\tau = E_t/E$, and E_t = tangent modulus of steel.

The following equation for the buckling stress in the inelastic range, given by the solution of Eq. (2.12), is in terms of the elastic buckling stress $(f_{cr})_e$ and the plasticity reduction factor, η.

$$(f_{cr})_{in} = \eta (f_{cr})_e = \frac{\eta k \pi^2 E}{12(1 - \mu^2)(w/t)^2} \qquad (2.13)$$

In Eq. (2.13), $\eta = \sqrt{\tau} = \sqrt{E_t/E}$, which is the plasticity reduction factor for a simply supported plate subjected to uniform compressive stresses in one direction.

3. Post-Buckling Behavior of Flat Compression Elements. Some one-dimensional structural members, such as columns, normally fail at or slightly below the theoretical critical buckling load. However, compression flanges of thin-walled structural members, with relatively

large w/t ratios as shown in Fig. 2.1, can continue to carry increasing loads after the onset of local buckling of the compression elements. This phenomenon is well-known as the post-buckling strength of a plate.

The deflected shape of a stiffened compression element in the post-buckling range can be visualized from a grid model as shown in Fig. 2.6. The transverse bars, which are anchored at the sides of the grid, act as tie rods to support the deflection of the longitudinal struts. This means that the membrane stresses developed in the transverse direction in the real stiffened plate act as hoop stresses, which restrain the lateral displacements caused by the longitudinal load.

Because of the transverse membrane stresses and the resulting redistribution of stress occurring in the plate, additional load may be carried by the plate after the critical buckling load is reached. In a stiffened plate, the stress distribution is uniform prior to its buckling as shown in Fig. 2.7(a). After buckling, the stress distribution is nonuniform while the load continues to increase as shown in Fig. 2.7(b). The redistribution of stress will continue until the stress at the supported edges reaches the yield stress of the steel. Failure normally occurs when the edge stress reaches the yield point of the material as shown in Fig. 2.7(c).

Because the membrane stresses are developed in the transverse direction and because the deflection of the plate is usually much larger than its thickness after buckling, small deflection theory of plate bending, which was used to derive the critical local buckling stress of plates, can not be applied for the post-buckling range. For these

reasons, the large deflection theory of plates is used for the analysis of plates in the post-buckling range.

In 1910,[13] von Karman developed large deflection equations for plates in the post-buckling range by taking the membrane stresses into account. The differential equation is given by Timoshenko in the following form:[5]

$$\frac{\partial^4\omega}{\partial x^4}+2\frac{\partial^4\omega}{\partial x^2\partial y^2}+\frac{\partial^4\omega}{\partial y^4}=\frac{t}{D}\left[\frac{\partial^2 F}{\partial y^2}\frac{\partial^2\omega}{\partial x^2}-2\frac{\partial^2 F}{\partial x\partial y}\frac{\partial^2\omega}{\partial x\partial y}+\frac{\partial^2 F}{\partial x^2}\frac{\partial^2\omega}{\partial y^2}\right] \quad (2.14)$$

where F is a stress function. The median fiber stresses are defined as follows:

$$f_x=\frac{\partial^2 F}{\partial y^2}, \qquad f_y=\frac{\partial^2 F}{\partial x^2}, \qquad \tau_{xy}=-\frac{\partial^2 F}{\partial x\partial y} \quad (2.15)$$

This equation has been used by many researchers to study the post-buckling behavior of square plates. The exact solution for Eq. (2.14) is very difficult because this equation is a fourth order, nonlinear differential equation. Approximate solutions for the differential equation have been proposed by Schnadel,[14] Timoshenko,[5] Cox,[15] Marguerre,[16] and Levy.[17] They used the energy method and assumed a wave form of the deflected plate to study the post-buckling behavior of the plate.

An approximate solution of the differential equation based on the large deflection theory was found to be too difficult for use in practical design because of its complexity. Therefore, the effective width design formulas are currently empirical in nature. In the past, the effective width concept has been successfully used for the prediction of post-buckling strengths of stiffened and unstiffened compression elements. The development of Winter's formulas is reviewed in the following section.

4. Development of Effective Width Formulas. In 1932,[18] von Karman introduced a concept of "Effective Width" to determine the ultimate strength of thin metal sheets in aeronautical structures. In his approach, it was assumed that the entire load is carried by two effective strips with a uniformly distributed stress equal to the edge stress, f_{max}, as shown in Fig. 2.8, instead of using the full width of the compression element with actual, nonuniform stress distribution.

To extend the use of the effective width formula for practical design of plates with small w/t ratios and for stress levels lower than the yield point, in the 1940s Winter[19-21] performed extensive tests for the compression flanges of cold-formed steel sections at Cornell University. Based on his test results, Winter derived effective width formulas for the design of both stiffened and unstiffened compression elements under uniform compression as follows:

(1) Stiffened Elements:

$$b = 1.9t\sqrt{\frac{E}{f_{max}}}\left[1 - 0.475\left(\frac{t}{w}\right)\sqrt{\frac{E}{f_{max}}}\right] \qquad (2.16)$$

or

$$b = \left[\sqrt{\frac{f_{cr}}{f_{max}}}\left(1 - 0.25\sqrt{\frac{f_{cr}}{f_{max}}}\right)\right]w \qquad (2.17)$$

This equation is similar to von Karmam's equation given in Reference 16 with the addition of an empirical correction factor which accounts for the effect of initial imperfections of compression elements. The correction factor is

$$1 - 0.475\left(\frac{t}{w}\right)\sqrt{\frac{E}{f_{max}}} \qquad (2.18)$$

(2) Unstiffened Elements:

$$b = 0.8t\sqrt{\frac{E}{f_{max}}}\left[1 - 0.202\left(\frac{t}{w}\right)\sqrt{\frac{E}{f_{max}}}\right] \qquad (2.19)$$

The effective width of unstiffened compression elements can be calculated from Eq. (2.19), in which the post-buckling strength of unstiffened elements is considered. In this approach, the entire load is assumed to be carried by an effective strip with a uniformly distributed stress equal to the edge stress, f_{max}, as shown in Fig. 2.9, instead of using the full width of the compression element with a varying stress distribution. Additional research conducted by Kalyanaraman[22-24] at Cornell University has shown good agreement with Eq. (2.19).

It is noted that Eqs. (2.16) and (2.19) depend not only on the edge stresses but also on the w/t ratio. Because the maximum edge stress, f_{max}, was introduced for F_y, these two equations can be applied to any range of stress levels.

The effective width approach has been used for the design of stiffened compression elements since 1946, whereas the reduced allowable stress method was used for the design of unstiffened compression elements until the AISI Specification was revised in 1986.

Equation (2.16) had been used for the design of cold-formed steel structural members until 1968. Based on the accumulated design experience with a restudy of original and additional test results, the following less conservative and more accurate equation was recommended for determination of the effective width, b, of stiffened compression elements

$$b = 1.9t\sqrt{\frac{E}{f_{max}}}\left[1 - 0.415\left(\frac{t}{w}\right)\sqrt{\frac{E}{f_{max}}}\right] \qquad (2.20)$$

or

$$b = \left[\sqrt{\frac{f_{cr}}{f_{max}}} \left(1 - 0.22 \sqrt{\frac{f_{cr}}{f_{max}}} \right) \right] w \qquad (2.21)$$

Equation (2.20) was used in the AISI Specification[25] since 1968 and maintained in the 1980 AISI Specification[26]. Based on the research conducted by Pekoz[27], a different format of effective width formula, which is based on Eq. (2.21), is used in the 1986 AISI Design Manual[3]. The same effective width formula is also used in the current AISI Specification for unstiffened compression elements by specifying a different buckling coefficient.

In Sections B2.1 and B3.1 of the 1986 AISI Specification, the effective widths of stiffened and unstiffened compression elements can be determined by using the following equations:

(1) For Load Capacity Determination: The effective width b for computing the load-carrying capacity of uniformly compressed elements can be determined from the following formulas:

$$b = w \qquad \text{when} \quad \lambda \leq 0.673, \qquad (2.22)$$

$$b = \rho w \qquad \text{when} \quad \lambda > 0.673, \qquad (2.23)$$

where b = effective width of a compression element

w = flat width of a compression element

$$\rho = (1 - 0.22/\lambda)/\lambda \qquad (2.24)$$

λ is a slenderness factor determined as follows:

$$\lambda = \frac{1.052}{\sqrt{k}}\left(\frac{w}{t}\right)\left(\sqrt{\frac{f}{E}}\right) \qquad (2.25)$$

where f = the edge stress

E = modulus of elasticity, 29500 ksi

k = plate buckling coefficient

= 4 for stiffened elements supported by a web on each longitudinal edge

= 0.43 for unstiffened elements supported by a web on a longitudinal edge and free on the other.

(2) For Deflection Determination: The effective widths b_d in computing deflections shall be determined from the following formulas:

$$b_d = w \qquad \text{when} \qquad \lambda \leq 0.673, \qquad (2.26)$$

$$b_d = \rho w \qquad \text{when} \qquad \lambda > 0.673, \qquad (2.27)$$

where w = flat width of a compression element

ρ = reduction factor determined by either of the following two procedures:

(1) Procedure I.

A low estimate of the effective width may be obtained from Eqs. (2.24) and (2.25) where f_d is substituted for f. f_d is defined as the computed compressive stress in the element being considered (calculations are based on the effective section at the load for which deflections are determined).

(2) Procedure II.

For stiffened elements supported by a web on each longitudinal edge an improved estimate of the effective width can be obtained by calculating ρ as follows:

$$\rho = 1 \qquad \text{when} \quad \lambda \leq 0.673 \qquad (2.28)$$

$$\rho = (1.358 - 0.461/\lambda)/\lambda \qquad \text{when} \quad 0.673 < \lambda < \lambda_c \qquad (2.29)$$

$$\rho = (0.41 + 0.59\sqrt{F_y/f} - 0.22/\lambda)/\lambda \qquad \text{when} \quad \lambda \geq \lambda_c \qquad (2.30)$$

where $$\lambda_c = 0.256 + 0.328(w/t)(\sqrt{F_y/E}). \qquad (2.31)$$

and λ is as defined by Eq. (2.25) except that f_d is substituted for f.

For the uniformly compressed unstiffened elements, the effective widths used in computing deflections shall be determined in accordance with Procedure I except that f_d is substituted for f.

Based on the extensive research work sponsored by the American Iron and Steel Institute, the effective width approach has been extended in the 1986 AISI Specification for the design of beem webs and stiffened elements with stress gradient, perforated elements, and elements with edge stiffeners or intermediate stiffeners. Detailed information on the effective width formulas used for these types of elements can be found in Ref. 3.

The effective width formulas (Eq. 2.22 through 2.25) are also presented in Sections 3.1.2.1(a) and (b) of the AISI Automotive Steel Design Manual[4] for steels with yield strengths up to 80 ksi. These equations calculate the effective widths of fully stiffened and unstiffened compression elements based on the effective width formulas used in the 1986 AISI Specification. Also included in these sections are the effective width formulas for steels with yield strengths higher than 80 ksi (84 to 153 ksi) based on the recent research conducted by Pan at University of Missouri-Rolla in 1988.[28] In addition, Sections 3.1.2.3 and 3.1.2.4 of the Automotive Design Manual discuss the effective width formulas for sections having 1) curve plate elements, and 2) curve and straight plate elements, respectively. The latter formulas were based on Parks' research findings.[29]

C. RESPONSE OF STRUCTURAL MEMBERS TO DYNAMIC LOADS

It has been a general practice for the structural designer to increase the live load for the effect of dynamic loading and to assume

that the properties of the material he employs are unaffected by the nature of the loading.

Developments in several separate fields has reached a point where proper analysis of structural behavior under impact overload conditions could take place. The understanding of material properties under static and dynamic loading has been developed to the stage where dynamic stress-strain curves could be produced for common engineering materials. The instrumentation used in the dynamic tests has been developed to a degree that accurate studies could be made of high speed effects without the introduction of significant errors from the instrumentation itself. The digital computers provide a facility for studying systems too tedious or intractable to attempt by manual means.[30]

In this section, some of the developments used in the past research for the response of structures to dynamic overloads are reviewed. Particular attention has been directed to those items related to beams, and columns.

1. Flexural Members. Impacts on flexural members have been the subject of investigation, especially during the last three decades. In this section, some of these investigations will be summarized in chronological order.

In 1958, Parkes[31] studied encastre beams with impact loading applied transversely at any point on their span. One of the main objectives of his work was to evaluate the effect of material strain-rate sensitivity on the accuracy of the analysis. Test specimens were

fabricated from mild steel, brass and duralumin. It was found that mild steel is the most sensitive to strain-rate as compared with other two materials. The correlation between theoretical and experimental results can be improved with taking the strain-rate sensitivity into account.

A developement of an analysis to determine the response of a simply-supported beam subject to a concentrated impact load at midspan was presented by Ezra[30] in 1958. He was actually attempting to develop a theory for comparison with the test results of Duwez and Clark.[33] His mathematical model allows the use of full-plastic moment, taking account of yield stress as affected by the strain-rate. The theoretical values show increasingly better agreements with the test results as the impact speed of the test increases. This indicates that the strain-rate sensitivity is a significant factor for the tests.

For small-scale cantilever beams with tip mass, two series of tests were performed by Bodner and Symonds[34] in 1962. In the first series, the base of the cantilever was impacted against a solid support, and in the second the tip mass was loaded either by an explosive charge, or being hit by a rifle bullet. Two materials were used for the specimens. They were mild steel and a less strain-rate sensitive aluminum alloy. Theoretical results were initially obtained from the use of a simple "rigid-plastic" theory. Comparisons between these results and the test results showed that any discrepancies between the two results were sensibly independent of the angle of rotation of the hinge at fixed support. It was concluded that strain-rate sensitivity was the only significant factor causing error, as all other factors would

be dependent on the rotation angle at fixed support. To check this conclusion, an analysis including strain-rate effects gave good agreements with the test results. An important point, that the authors made, is that the use of an overall percentage increase of yield atress may lead to errors in some situations.

In 1963, Rawlings[35] reported on an experimental investigation of strain-rate effects on yield loads for beam tests. He tested a series of simply supported mild-steel beams using tow-point loading system so that a plastic hinge could be formed in the central portion of the beam. All loads were applied by large falling masses. The force pulse applied to the beam was measured at the lever by electric-resistance atrain-gages. Repeated tests were performed on beam specimens to investigate the behavior under different cycles of stress. Original specimens showed a marked upper yield peak for short duration, and a major amount of lower yield bending for long duration as shown in Fig. 2.10. The results for the relationship between lower yield value and the time taken to yield obtained from beam tests (Fig. 2.11) showed good agreements with the relationship obtained from material tests. The author concluded that the full plastic moment is independent of the method of loading.

Using the experimental results of Parkes, Ting[36] developed in 1965 a formula for cantilever beams loaded dynamically on the basis of rigid-plastic theory, which took into account large geometric changes. His results compare very favorably with Parkes' experimental results. He concluded that not all of the errors between the theory and

experimental results can be attributed to strain-rate effects, as had been previously assumed. Ting was concerned primarily with the high-speed, low-mass loading causing travelling hinges. For high-mass, low-speed loading, that characteristically causes root hinges only, then strain-rate effects probably do cause almost all the errors in a simple rigid-plastic theory. A verification of Ting 's research finding was given by Bodner[37] ,who tested cantilever specimens by detonating explosive charges which were attached to tip masses. Both cantilevers were attached to a pendulum to enable the impulse to be measured. Observation of final deformed shapes showed large root rotations, with little evidence of travelling hinges. On this basis, and using time-to-yield records from strain gages attached to the cantilever, a simple theory with an overall correction for strain-rate effects gave reasonable correlation with the test results.

Cowper and Symonds found that the following simple empirical expression with D = 40.4 in./in./sec., and p = 5, provides a reasonable estimate of dynamic yield stress recorded during many dynamic uniaxial tensile and compressive tests under constant strain rate for mild steel:[39]

$$\frac{\sigma}{\sigma_0} = 1 + \left(\frac{\dot{\varepsilon}}{D}\right)^{1/p} \qquad (2.32)$$

where σ = dynamic yield stress

σ_0 = static yield stress

$\dot{\varepsilon}$ = strain rate

D and p = material constants

The above Cowper-Symonds constitutive relation and its derivative forms are used almost exclusively in theoretical and numerical studies on the dynamic plastic behavior of structures made from strain-rate sensitive materials. The universal acceptance of this equation stems from the observation that analytical and numerical predictions agree remarkably well with experimental tests on beams.[39]

In 1966, Aspden and Campbell[40] were the first to conduct dynamic flexural tests in which transient records were taken of moment-rotation characteristics. They used small specimens 0.75 inches long by 0.375 inches wide by 0.125 inches thick, supported at their ends by beams, and loaded as a four point loading system by a falling weight. The bending moment transmitted to each specimen was measured by electric resistance strain gages mounted on the support beam and the strain-rate at surface of the specimen was determined by recording the velocity of the load frame using an inductive transducer. They compared their high speed flexural test results with those obtained under dynamic compression using a hydraulically operated machine, and with slow speed tests in an Instron machine. Moment-rotation curves obtained from double-beam oscilloscope traces of velocity and moment were corrected to take account of 1) the bending of the support beams, 2) zero errors, and 3) inertia effects caused by acceleration of the loading mechanism. Like Rawlings, Aspden and Campbell observed evidence of high initial peak moments of resistance. For the highest rate of strain in their beams, the dynamic 'upper yield moment' was about 80% higher than the corresponding moment in a low speed test. See Fig. 2.12 for the variation of upper and lower yield moments with strain-rate at surface

of specimen. Aspden and Campbell noticed that after attaining the maximum peak moment of resistance, the value decreased below that would be predicted by integration of dynamic axial stresses across the section as derived from test results by assuming plane sections remain plane. They attributed the difference of about 10% to non-uniform strain distribution throughout the experiment during the loading process. In their work, they integrated Eq. 2.32 through the thickness of a beam and found that the dynamic bending moment is related to the associated beam curvature rate according to the expression given in Eq. 2.33.

$$\frac{M}{M_0} = 1 + \frac{2p}{2p+1}\left(\frac{\dot{\kappa}H}{2D}\right)^{1/p} \qquad (2.33)$$

where M = dynamic bending moment

$M_0 = \sigma_y H^2/4$ static collapse moment

$\dot{\kappa}$ = curvature rate

H = thichness of the beam

D and p = material constants obtained from Eq. 2.32

Recent research has been directed to analytical procedures which take into account more precise constitutive relationships including strain rate sensitivity, strain hardening, and geometric changes arising from overloads. In some of these studies, relatively sophisticated algebraic solutions have been developed, while in others, numerical procedures have been derived.

In order to develop the methods applicable for analysis of the response of beams supported at the ends by immovable frictionless pins and loaded with a uniform impulse, Jones[41] in 1967 used the rigid-plastic theory taking into account strain hardening and strain rate sensitivity. Equation 2.32 was used to acount for the material strain rate sensitivity. Strain hardening was assumed to follow a linear relationship of the following form:

$$\frac{\sigma}{\sigma_0} = 1 + \frac{E\ \varepsilon}{r\ \sigma_0} \qquad (2.34)$$

where E/r is the equivalent modulus in the plastic range and r is the ratio of the slopes of the elastic and plastic portions of the stress-strain curve. Equations 2.32 and 2.34 were combined into the form as shown in Eq. 2.35.

$$\frac{\sigma}{\sigma_0} = \left[1 + \left(\frac{\dot{\varepsilon}}{D}\right)^{1/p}\right] (1 + \nu\varepsilon) \qquad (2.35)$$

where $\nu = E / (r\ \sigma_0)$

In his treatment of the problem, Jones allowed for membrane effects by adopting interaction curves for the yield condition of a beam element subjected to axial tension and bending. Jones acknowledged the difficulty of assessing the accuracy of his theory, because of the absence of experimental results.

In 1971, Culver, Zanoni and Osgood[42] of Carnegie-Mellon University reported on thin-walled beam sections subjected to dynamic loading, as part of a large program of dynamic loading on cold-formed steel structural sections. Two methods of analysis were used in this study. One is the linear elastic and the other is the non-linear method including local buckling effects. A comparison of results showed that it was sufficient to predict bending moments from normal linear elastic analysis considering local buckling effects.

In a paper published in 1972,[43] Symonds and Jones reviewed the earlier work on plastic response to impulsive loading of beams clamped against end rotations and axial displacements, taking account of small finite transverse displacements and of strain-rate dependence of the yield stress. New solutions were derived from rigid-plastic analysis which included both effects and were compared with the experimental results. They concluded that the strain-rate dependence of the yield stress can be used in the analysis because the dynamic yield stress varies slowly with strain rate. Therefore, an estimate of dynamic yield stress at one strain rate may serve as a good approximation over several decades of strain rate. It is then assumed that the static plastic moment and axial force can be replaced by dynamic values obtained by multiplying the static magnitudes by a factor calculated from the strain rate at time t^*, after which the plastification of the cross section occurs. The strain rates at t^* are taken as representative of the initial part of the motion. If the pattern of deformation of the structure with strain-rate sensitive material is the same as that for non-rate sensitive behavior, then this substitution of new dynamic constants can

give excellent results compared to those obtained by numerical integration. However, if the patterns differ considerably, then the use of dynamic correction factors may be entirely inappropriate, and can lead to large errors.

More recently, Forrestal, Wesenberg, and Sagartz[44,45] have developed a simple method for incorporating the approximate influence of material elasticity on the dynamic plastic response of beams. An exact elastic analysis is first undertaken for a dynamic beam problem which remains valid until the maximum stress reaches yield. If the beam material is strain-rate sensitive, then this yield stress is calculated from the Cowper-Symonds constitutive law, Eq. 2.32, using the corresponding strain-rate predicted by the elastic analysis. The subsequent plastic behavior is controlled by a constant yield stress. There was an excellent agreement with the peak displacements recorded during experiments on simply supported beams using 1018 steel, type 304 stainless steel, and aluminium 6061 T6 as shown in Fig. 2.13.

2. Columns. In view of the fact that a compression member is one of the common structural components, its behavior under impact loading conditions has attracted interest for a considerable period of time.[30]

The analysis of column behavior under impact loading conditions went back to 1933, when Koning and Taub[30] derived equations describing the axial and transverse oscillation of pin-ended columns subjected to dynamic axial load. They considered loads having a rectangular pulse form, of magnitude less than, equal to, or greater than the static Euler

load. However, they did not recognize the possibility of dynamic overloads.

In the 1940s, Meier, Pian and Siddal,[30] studied the response of pin-ended struts subjected to impact loads. They showed that struts could withstand loads well above Euler load without sustaining permanent damage. Pian and Siddal also conducted experiments on eccentrically loaded struts of very high slenderness ratios and demonstrated that they could withstand overloads of up to seven times the Euler value.

Some of the most significant work on the analysis of strut behavior under dynamic loading is due to Hoff.[47] His analysis was directed to study the dynamics of the buckling of elastic columns in a rapid compression test. Figure 2.14 is adopted from his study which shows that under rapid loading the lateral displacements of the column are less than those calculated from static considerations. As a consequence the load supported by the column can exceed the Euler load considerably.

In 1972, Roberts[48] made an extensive theoretical and experimental investigation of pin-ended columns subjected to axial impact conditions. The experimental study involved the testing of mild steel columns of rectangular box sections. The cross sectional dimensions and the length of columns were selected to provide a range of slenderness ratios from 100 to 400. For the high speed tests, in which the impact velocity was of the order 1 to 3 m/s, the columns developed peak loads many times the Euler load, particularly for the case of columns with high slenderness ratios, for which the sustained compressive loads may be 20 or more times the Euler value.

Axial impact on thin-walled columns was examined theoretically by Culver and Vaidya[49] and experimentally by Logue[50] , both published in 1971. The theoretical work was applied to short duration impact loading which was defined by prescribing the time variations of the load at the end of the columns. Nonlinearity due to local buckling was accounted for by using nonlinear axial load-curvature relations derived with the aid of the effective width concept. The results of the analytical study were shown as response spectra curves which described the effect of initial deflection, pulse duration, maximum dynamic load, and the static preload on the dynamic response. It was concluded from the experimental study that maximum loads in excess of the static failure loads may be carried dynamically. However, the failure modes for thin-walled columns subjected to shock loading were not established in this study. Further study was suggested by the author to determine the maximum dynamic carrying capacity of these members.

In 1974, Soden, Al-Hassani and Johnson[51] studied the crushing behavior of circular tubes under static and dynamic axial loads. The loads and deformations of tubes with various thicknesses were recorded and three failure modes were observed and studied. The majority of tubes tested collapsed by progressive folding into diamond shaped lobes, while thick tubes failed by collapsing into circumferential rings. The initial failure loads and post-buckling loads for various modes of deformation were predicted theoretically. All stresses increased with increasing strain rate. Figure 2.15 shows the variation of first maximum stress and mean post-buckling stress for tubes with thickness to diameter ratio equal to 0.067.

Wierzbicki[52] has studied the dynamic crushing strength of strain-rate sensitive box columns. The main purpose of his study was to identify material and geometrical parameters in the problem of impact loading for sheet metal and to derive an expression for the strain rate correction factor. As a particular structural component, a straight rectangular box column was considered to be representive of front or rear longitudinal members of an automobile body. He stated that during a vehicle collision the strain rates in the zones of localized deformation can be of the order of 10 to 100 in/in/sec. Consequently, dynamic forces in compressed mild steel members are much greater than static ones. An approximate analysis was presented to determine dynamic strength and energy absorption of axially loaded thin-walled box columns. In this analysis, the dynamic compressive force is a product of a static crushing strength of the column and a strain-rate correction factor. The strain-rate correction factor was found to be dependent on the initial impact velocity and parameters describing the sensitivity of the material to strain rate. He compared his analytical solution with the results of experimental work conducted by Ohkubo, Akamatsu, and Shirasawa[53] on closed-hat section members and the experimental work of Wimmer[54] on box sections. Wierzbicki concluded that in order to validate his theory, a much wider range of sectional dimensions and impact velocities is needed.

Wierzbicki and Abramowicz[55] used a simple method to calculate the dynamic correction factor for thin-walled strain-rate sensitive structures. For the experiments run at two crushing speeds v_1 and v_2 with associated strain rates $\dot{\varepsilon}_1$ and $\dot{\varepsilon}_2$, the correponding ratio of mean

crushing forces P_m^1 and P_m^2 is equal to the dynamic correction factor given as follows:

$$R = \frac{P_m^1}{P_m^2} = \left(\frac{\dot{\varepsilon}_1}{\dot{\varepsilon}_2}\right)^{\frac{1}{\bar{n}}} = \left(\frac{v_1}{v_2}\right)^{\frac{1}{\bar{n}}} \qquad (2.36)$$

where $\bar{n}$ is the material strain-rate sensitivity calculated from the following equation:

$$\frac{\sigma}{\sigma_0} = \left(\frac{\dot{\varepsilon}}{\dot{\varepsilon}_0}\right)^{\frac{1}{\bar{n}}} \qquad (2.37)$$

It is observed from Eq. 2.36 that the dynamic correction factor does not involve any geometrical and material parameters except the constant $\bar{n}$.

In another work published in 1984, Abramowicz and Jones[56] conducted 84 dynamic crushing tests on thin-walled square steel tubes with various lengths and two different cross sections. The columns were crushed axially on a drop hammer rig. Approximate theoretical predictions were developed for the axial progressive crushing of square box columns using a kinematic method of analysis. The effective crushing distance is considered in the analysis along with the influence of material strain-rate sensitivity. The theoretical study predicts four deformation modes which govern the behavior for different ranges of the parameter c/h (c being the width of a square box-section and h being the wall thickness). New asymmetric deformation modes were predicted

theoretically and confirmed by the experimental tests. These asymmetric modes cause an inclination of a column which could lead to collapse in the sense of overall buckling even for relatively short columns. The following equation was presented for the ratio of dynamic to static mean crush force:

$$\bar{P}_m^d / \bar{P}_m = 1 + \alpha v^{\beta} \qquad (2.38)$$

where α and β = constants given in Table 2.1 for different modes

v = impact velocity (m/sec)

Equation 2.38 gave reasonable agreement with the corresponding experimental results of Abamowicz and Jones.[56]

Also listed in Table 2.1 are the values of constants α and β used in Eq. 2.38 obtained from various references for calculation of the dynamic correction factor for thin-walled steel columns having different cross sections and different lengths.

III. EXPERIMENTAL INVESTIGATION

A. GENERAL

In cold-formed steel design, the effective width approach has been adopted in several specifications to predict the load-carrying capacities of structural members in building and other cold-formed steel structures. Because the effective width formulas included in the current AISI Specification and the Automotive Steel Design Manual [4] are primarily based on the results of static tests of cold-formed steel members corresponding to a strain rate of approximately 1.7×10^{-6} in./in./sec. [3], the objective of this experimental investigation was to study whether the available effective design formulas using dynamic material properties can be adequately used for the design of structural members subjected to dynamic loads. It should be noted that according to ASTM Specification E8, the stress rate should be 100 ksi/min. for obtaining the material static stress-strain curve. This stress rate could be converted to strain rate of $5.65\ 10^{-5}$ in./in./sec. by using Hooke's Law and modulus of elasticity of 29,500 ksi.

During the period from August 1989 through January 1990, 15 hat-section beams and 18 box-shaped stub columns were tested for the study of stiffened elements, while 15 channel-beams and 19 I-shaped stub columns were tested for unstiffened elements. The configurations of test specimens are shown in Figs. 3.1 and 3.2. All specimens used for this phase of study were fabricated from 35XF sheet steels. The stub column specimens were cold-formed by Butler Manufacturing Company in Grandview,

Missouri, while the beam specimens were cold-formed by Holloway Machine Company in Springfield, Missouri.

The strain rates used in the tests varied from 10^{-5} to 0.1 in./in./sec. In addition, the ranges of w/t ratios used in this study were from 26.67 to 76.08 for stiffened elements, and from 8.93 to 20.69 for unstiffened elements. The designation of test spcimens used in Chapter 3 and Chapter 4 of this study is presented in Table 3.1. The number of tests are given in Tables 3.2 to 3.5. As shown in these tables, a total of 67 specimens have been tested under different strain rates.

B. MATERIAL PROPERTIES

The 35XF sheet steel used in the present study is the same as that used in the Eleventh and Twelfth Progress Reports. The mechanical properties of this sheet steel in tension and compression have been established under different strain rates and documented in the aforementioned reports. Table 3.6 gives the average values of mechanical properties including yield stress (F_y), proportional limit (F_{pr}), tensile strength (F_u), and elongation in 2-in. gage length tested under different strain rates. The thickness of this sheet steel is 0.085 in. Typical stress-strain curves for longitudinal tension and longitudinal compression of this material under different strain rates are shown in Figs. 3.3 and 3.4, respectively. Figures 3.5 through 3.7 show comparisons of typical stress-strain curves for longitudinal tension and longitudinal compression under the strain rates of 0.0001, 0.01, and 1.0 in./in./sec. respectively. Other mechanical properties (transverse tension and transverse compression) and the corresponding stress-strain relationships

can be found in Refs. 1 and 2. Reference 1 also includes the mechanical properties of the 35XF steel for aged and non-aged materials tested under different amounts of cold-stretching and/or different strain rates.

C. BEAM TESTS FOR STIFFENED ELEMENTS

1. Specimens. Fifteen (15) beam specimens were tested to study the local buckling and post-buckling strengths of stiffened elements of the 35XF steel material using different strain rates. The strain rates used for the tests ranged from 10^{-5} to 0.01 in./in./sec. Three different beam sections were used. Figure 3.8 shows the hat sections designed for the study of post-buckling strength of stiffened elements. Table 3.7 gives the average cross-sectional dimensions of hat sections, thicknesses of sheet steels, w/t ratios, span lengths of specimens, and failure loads. The width-to-thickness ratios, w/t, ranged from 29.62 to 76.08.

All steel sheets were sheared to the designed sizes before the specimens were formed. All specimens were formed with an inside bend radius of 5/32 in.

2. Strain Measurements. Twelve foil strain gages were placed on the compression flange, tension flanges, and webs of each beam specimen for measuring compressive and tensile strains. Figure 3.9 shows the locations of strain gages, numbered from 1 to 12, placed on beam specimens. Eight strain gages (No. 3 through 8, 11, and 12) were placed at the midspan of beam specimens. In addition, two paired strain gages ((1,2) and (9,10)) were placed along the longitudinal centerline of the compression flange at a distance equal to the overall width of the

compression flange on each side of the midspan of specimens. All three paired strain gages along the centerline of the compression flange were used to detect local buckling of the compression flange. As shown in Fig. 3.10, the critical buckling load is determined from the load-versus-strain diagram by using the modified strain reversal method, which is discussed in Ref. 62. Strain gages (No. 5 and 6) placed along both edges of the compression flange were used to measure edge strains. The edge stress of stiffened elements can be determined from these strain readings using the stress-strain curve. On each side of the tension flanges, a strain gage (No. 11 or 12) was placed along the edge of each tension flange as shown in Fig. 3.9 to study the shift of the neutral axis during the test. Strain gages (No. 7 and 8) placed on the top of the webs were used to study the distribution of compressive stress in the web.

3. Instrumentation and Test Procedure. All beam specimens were tested in a 110 kips capacity 880 Material Test System (Figure 3.11) located in the Engineering Research Laboratory at the University of Missouri-Rolla. The data acquisition system used in this study conforms to the CAMAC standards. The main data acquisition module used in this system is a Kinetic Systems Model 4022 Transient Recorder. The unit has 64 simultaneously sampling input channels. The unit is capable of acquiring test data at the maximum rate of 25,000 sets of reading per second. The recorder has a storage capacity of 1,000,000 samples. Two channels were connected to the MTS machine to record loads and actuater displacements as the test runs. Thirty channels were connected to 2120 Measurements Group Strain Gage Conditioner and Amplifier System to measure the strain gage outputs. Four channels were connected to

Daytronic Linear Variable Differential Transformer (LVDT) Conditioners to measure the LVDT outputs. After the data have been acquired, it was downloaded into computer for analysis. A Data General mini computer was used to coordinate the electronic equipment and to store and analyze the test data.

Following fabrication of the test specimen and placement of strain gages, the beam specimen was placed in the 880 MTS test system. The test setup for beam specimens is shown in Figs. 3.12 through 3.14. One 8-feet long W-Shape steel beam was placed on the top of the lower compression platen of the MTS machine for the beam tests . As shown in Fig. 3.12, the beam was simply supported and the load was applied from the lower compression platen to the specimen. T-sections were used at L/8 points to support the beam for preventing web crippling failure. Six 1/4-in. dia., high strength bolts were used to connect each T-section to the web of the specimen. To prevent premature web crippling failure, one 4-in. wide bearing plate and a wooden block placed between specimen webs were used at each end of the specimen. The tension flanges at both ends of the beam specimens are clamped to bearing plates. During the fabrication of specimens, three aluminum bars were connected to the tension flanges at midspan and at quarter points to prevent hat section from opening. Beam deflections were measured with two LVDT which contacted the midspan aluminum bar at both sides of specimen.

The function generator was then programmed to produce the desired ramp. For all the tests, the range 2 of the stroke mode (maximum stroke = 2.5 in.) was selected as the control mode to maintain a constant actuator speed. The strain rates used in the tests ranged from 10^{-5} to

0.01 in./in./sec. and the corresponding test times ranged from 3000 to 3 sec.

During the tests, the applied load, actuator displacemnt, strains from twelve strain gage outputs, and deflections from two LVDT outputs were recorded and stored in the CAMAC memory. The CAMAC sampling rate depends on the test time and varied from 5 to 25000 readings per second. This rate depends on the test time and was set before the test started. Table 3.8 gives the frequency number and the corresponding readings per second. Following the completion of the test, the data were downloaded and stored into Data General Computer for later analysis. Each of the 64 CAMAC channels takes 16384 data points during the test (regardless of the test time). The test data file occupied 2 megabytes of the DG memory. All specimens were loaded to failure.

4. Test Results. For the study of post-buckling strengths of stiffened elements, beam specimens were designed to have various w/t ratios for the compression flange. Local buckling of the compression flange can be detected from the readings of the paired strain gages located on the centerline of the flange. Waving of the compression flange was observed as the load continued to increase beyond the buckling load. Because of the redistribution of compressive stress across the compression flange, the specimen failed when the maximum strength of the compression flange was reached. A typical development of the stiffened flange buckling waves during a slow hat-beam test is shown in Fig. 3.15. Typical failure of the beam specimen is shown in Fig. 3.16. Figure 3.17 shows the final deflected shape of the beam after the test. Failure of

test specimens always occurred in the middle portion of the beam close to the L/8 points.

The location of the neutral axis was determined from strain gage readings. Figure 3.18 shows the positions of the neutral axis. The neutral axis shifted away from the top flange as the load increased. As mentioned above, beam deflection was carefully measured at both sides of midspan of the specimen. In the early stage of the slow test, beam deflection increased linearly corresponding to the applied load. The nonlinear load-deflection relationship was noted when local buckling occurred in the compression flange of the specimen. A typical strain-time curve for the slow strain-rate test is presented in Fig. 3.19. Typical load-strain curves for the paired strain gages at the middle of the stiffened flange are shown in Fig. 3.20. This plot is used for determination of critical buckling load.

D. STUB COLUMN TESTS FOR STIFFENED ELEMENTS

1. Specimens. In this phase of experimental investigation, eighteen (18) stub column specimens were tested to study the effect of strain rate on the local and post-buckling strengths of stiffened elements for 35XF steel material.

As shown in Fig. 3.21, box-shaped stub columns were used for this phase of study. All stub columns were fabricated by connecting two identical hat sections through the unstiffened flanges. 1/4-in. dia. high strength bolts with washers were used for the fabrication of stub columns. The spacing of bolts was determined on the basis of the requirements of the AISI Specification. The steel sheets were sheared to the designed sizes of each hat section. Great care was taken when the

stub-column specimens were fabricated. Both ends of the stub-column specimens were milled to ensure that they were flat and parallel.

Table 3.9 gives the average cross sectional dimensions of stub-column specimens, the measured thicknesses of sheet steels, and the failure loads. In this phase of experimental study, the w/t ratios of stiffened elements ranged from 26.67 to 53.15. The strain rates ranged from 0.0001 to 0.1 in./in./sec. The webs of all hat sections were designed to be fully effective. The unstiffened flanges were connected to satisfy the requirements of the AISI Specification.

The lengths of stub-column specimens are also given in Table 3.9. In order to avoid overall column buckling, the length of each stub-column specimen is longer than three times the largest dimension of the cross section of the specimen and less than 20 times the least radius of gyration as recommended in Ref. 57. This criterion was also adopted in Part VII (Test Procedure) of the 1986 AISI Cold Formed Steel Design Manual.

2. Strain Measurements. Eight foil strain gages were used to measure strains at midheight of the stub column specimen. The location of strain gages, numbered from 1 to 8, is shown in Fig. 3.22. Additional eights strain gages were added only to the hat sections with large w/t ratio (w/t= 53.15). They were placed at a distance equal to half of the overall width of the compression flange as shown in Fig. 3.23. The critical buckling load of the specimen was determined from the load-versus-strain diagram using the modified strain reversal method as discussed in Ref. 62. The strains used in the load-versus-strain diagrams were obtained from the output of paired gages (No. 1,2,5,6 and 9 through

16) located at the centerline of each flange. Additional strain gages attached to the edges of compression flanges were used to measure the maximum edge strains for stiffened element. Prior to testing, all strain gages were used to align the stub-column specimen.

3. Instrumentation and Test Procedure. The 880 MTS material test system and the CAMAC data acquisition system used for the beam tests were also used for stub column tests.

Following fabrication of the specimen and placement of strain gages, the stub column was placed in the MTS testing machine. At the beginning of the test, a small preload was applied to the specimen and the resulting strains were recorded for all strain gages to see whether the strain distribution was uniform over the cross section of the specimen. If necessary, thin layers of aluminum foil were added to the ends of stub columns in the regions of low strain. This procedure was repeated until the strain distribution was essentially uniform over the cross section. Figure 3.24 shows the box-shaped stub column test setup.

The function generator was then programmed to produce the desired ramp. For all tests, the stroke mode was selected as the control mode to maintain a constant actuator speed which was obtained from multiplying the selected strain rate by the overall length of the specimen. For all tests, load range 1 (maximum load of 100 kips) and stroke range 4 (maximum displacement of 0.5 inch) were selected. Because the maximum actuator speed is 2.5 in./sec., a strain rate higher than 0.1 in./in./sec could not be obtained. The strain rates used in the tests ranged from 10^{-4} to 0.1 in./in./sec. and the corresponding test times ranged from 416 to 0.2 sec.

4. Test Results. The failure mode of the specimens varied with the width-to-thickness ratio of the compression flange. For stiffened elements with large w/t ratios, local buckling always occurred in the elastic range. Due to the stress redistribution across the cross section of the compression flange, the edge stress of the stiffened element continued to increase until the maximum edge stress was reached and the specimen failed. For stiffened elements with moderate w/t ratios, the compression flange normally buckled in or near the inelastic range. Yield failure occurred in stiffened elements with small w/t ratios, so that very little, if any, waving of the stiffened compression element occurred before failure. It was noted that the specimens with small w/t ratio failed always at either top or bottom ends. The specimen with moderate w/t ratio failed either at the end or at the middle or both, while the specimen with large w/t ratio failed most of the time at or near the middle height of the specimen regardless of the strain rate used in the test. Figures 3.25 and 3.26 show typical failure mode of box-shaped stub column specimens with moderate w/t ratios.

A typical strain-time curve for high strain-rate test is presented in Fig. 3.27. Typical load-strain curves for the paired strain gages at the middle of the stiffened flange are shown in Fig. 3.28. For the purpose of comparison, Figures 3.29 through 3.31 present three typical load-displacement curves for the specimens having the same w/t ratio but tested under different strain rates.

E. BEAM TESTS FOR UNSTIFFENED ELEMENTS

1. Specimens. Fifteen (15) channel-beam specimens were tested to study the effect of strain rate on local and post-buckling strengths of

unstiffened elements using 35XF steel material. Three different beam sections were studied. Aluminum bars were used to connect two channel specimens together to fabricate the beam specimen as demonstrated in Figure 3.32. The purpose of using the aluminum bars was to prevent the specimen from lateral buckling during the test. High strength, 1/4 in. dia. bolts were used in the fabrication of the test specimens. The cross section of the channel-beam specimens is shown in Fig. 3.33. Table 3.10 gives the average cross-sectional dimensions of channel-beam specimens and the failure loads. The span lengths of beam specimens are also given in Table 3.10. The w/t ratios of unstiffened elements ranged from 8.93 to 20.69.

All steel sheets were sheared to the designed sizes before the channel sections were formed. All specimens were formed with an inside bend radius of 5/32 in.

2. Strain Measurements. Eight foil strain gages were placed at midspan of the test specimen on the compression and tension flanges for measuring compressive and tensile strains. The locations of strain gages (numbered from 1 to 8) placed on beam specimens are shown in Fig. 3.34. These paired strain gages ((1,2) and (5,6)) were used to detect local buckling of the compression flanges. The modified strain reversal method was used to determine the critical buckling load from the load-versus-strain diagram, as recommended in Ref. 62.

Strain gages placed along the unsupported edges of the unstiffened compression flanges were used to measure edge strains. The edge stress of unstiffened elements can be determined from these strain readings using

the stress-strain curve. Strain gages on the tension flange were used to study the shift of the neutral axis.

3. Instrumentation and Test Procedure. The equipment and testing procedure were identical to those used in the beam tests for the study of stiffened elements as discussed in Section III.C.3. The test setup for channel-beams is shown in Figs. 3.35 and 3.36.

The load was applied to the beam specimen by the 880 MTS machine. Four-inch wide bearing plates were used under the loading points and at the ends of specimens. The stroke range 3 with maximum displacement equal to 1 in. was selected to be the control mode. The strain rates used in the tests ranged from 10^{-5} to 0.01 in./in./sec. and the corresponding test times ranged from 1400 to 1.4 sec.

During the tests, the applied load, actuator displacement, strains from eight strain gage outputs, and midspan deflections from two LVDT outputs were recorded at a preset frequency rate. As mentioned previously, the frequency rate depends on the test time.

4. Test Results. During the testing, waving of the compression flange was observed as the load continued to increase beyond the buckling load. Curling of the compression flanges near loading plates was observed in most specimens with small or moderate w/t ratios. For the specimens with large w/t ratio the curling occured always in the middle portion of the beam. As expected, the specimen failed between the loading points. The beam specimen failed when the maximum strength of the compression flange was reached. Possible failure by lateral buckling was prevented by providing lateral supports. Figure 3.37 shows typical flexural failure

of channel-beams with unstiffened elements having large w/t ratios. The deflected shape, after the test, is shown in Fig. 3.38.

A typical strain-time curve for medium strain-rate test is presented in Fig. 3.39. Typical load-strain curves for the paired strain gages at the middle of the stiffened flange are shown in Fig. 3.40. For the purpose of comparison, Figures 3.41 through 3.43 present three typical load-displacement curves for the specimens having the same w/t ratio but tested under different strain rates.

F. STUB COLUMN TESTS FOR I-SHAPED SECTIONS HAVING UNSTIFFENED FLANGES

1. Specimens. In this study, eighteen (18) I-shaped stub-column specimens have been tested for the study of local buckling and post-buckling strength of unstiffened elements of the 35XF steel material using different strain rates. The strain rates used for the tests ranged from 10^{-5} to 0.1 in./in./sec. Figure 3.44 shows the cross section of an I-shaped stub column. Table 3.11 gives the average cross-sectional dimensions of stub-column specimens and the failure loads. For the unstiffened flanges studied in this program, the ranges of w/t ratios were from 8.9 to 20.7.

The stub-column specimens were fabricated by bonding two identical channels back to back. Surfaces to be joined were paper sanded and cleaned with methyl alcohol and bonded by a thin layer of PC-7 epoxy. The webs of channels were held together by C-clamps after glue was placed on the web. Thin wires with 0.002 in. dia. were placed between the specimen webs to maintain uniform epoxy thickness. C-clamps were released after 24 hours. Great care was taken when the stub-columns were fabricated. Prior

to testing, the ends of stub-column specimens were milled flat and parallel.

The lengths of stub-column specimens are also given in Table 3.11. In order to prevent overall column buckling, the length of stub column is longer than three times the largest dimension of the cross section of the specimen and less than 20 times the least radius of gyration as recommended in Ref. 57. This criterion was also adopted in Part VII (Test Procedure) of the 1986 AISI Design Manual. The dimensions of webs of all stub column specimens were chosen to be fully effective.

2. Strain Measurements. Fourteen foil strain gages were used to measure strains at the midheight of the stub-column specimens. The locations of strain gages are shown in Fig. 3.45. The paired strain gages placed along the tips of compression flanges were used to determine the critical buckling load of stub columns. The buckling load of the specimen was determined from the modified strain reversal method. Strain gages (No. 3, 4, 9, and 10) were placed at the supported edges of the compression flanges to measure maximum edge strains at each load level for calculating the maximum edge stress in the unstiffened flanges. Paired strain gages (No. 13 and 14) were placed along the centerline of the web to monitor any premature failure of the web. All strain gages were used to align the stub-column specimen.

3. Instrumentation and Test Procedure. Equipment and test procedures used in this phase were the same as those used in the stub column tests for stiffened elements described in Section III.D.3. The test setup for stub stub-column specimens with unstiffened elements is shown

in Fig. 3.46. The strain rates used in the tests ranged from 10^{-5} to 0.1 in./in./sec. and the corresponding test times ranged from 3600 to 0.2 sec.

4. Test Results.

During the test, no bonding failure was observed prior to the attainment of the maximum load. The failure mode of stub-column specimens with unstiffened elements varied with the width-to-thickness ratio of the unstiffened compression flanges. The unstiffened flanges with large w/t ratios showed large waving deformations, whereas the unstiffened compression flanges with small w/t ratios showed no noticeable waving until failure. A typical development of unstiffened flanges buckling waves during a slow I-shaped stub column test is shown in Fig. 3.47. Typical failure mode of stub-column specimens with unstiffened compression flanges is shown in Fig. 3.48. A typical strain-time curve for high strain-rate test is presented in Fig. 3.49. It was observed during the I-shaped stub column tests that the webs of the test specimens showed no sign of buckling before the load reached the ultimate value. Typical stress-strain curves for the paired strain gages at the tip of the unstiffened flange are shown in Fig. 3.49. For the purpose of comparison, Figures 3.51 through 3.53 present three typical load-displacement curves for the specimens having the same w/t ratio but tested under different strain rates.

IV. EVALUATION OF EXPERIMENTAL DATA

A. GENERAL

Sections IV.B through IV.E of this chapter evaluate the experimental results of beams and stub columns fabricated from 35XF sheet steels and tested under different strain rates. The strain rates varied from 0.00001 to 0.1 in./in./sec. These sections compare the test results and the failure loads predicted by the current AISI Automotive Steel Design Manual[4] for structural members tested in this study. Also discussed in these sections is the effect of strain rate on the structural strengths of test specimens.

B. BEAM TESTS FOR THE STUDY OF STIFFENED ELEMENTS

Hat sections have been designed and fabricated for beam tests to study the post-buckling strengths of stiffened compression elements using 35XF sheet steels. All beam specimens were subjected to two point loads located at L/8 from end supports as shown in Figs. 3.12 and 3.13. Lateral torsional buckling of beam specimens was not critical according to the design of specimens. The webs of hat-section beams were designed to be fully effective. The weight of the test specimen and the weight of the cross beam placed on the top of the specimen (approx. 70 lbs.) are small as compared to the ultimate loads and were neglected in the evaluation of test results. The tested tensile yield stress was used for computing yield moment (M_y) and ultimate moment (M_u) for all beam specimens studied in this investigation.

1. Critical Local Buckling Strength. The compression flange of beam specimens may buckle locally in either the elastic or the inelastic range, depending on the w/t ratio of the flange. The elastic critical buckling stress of the stiffened flange subjected to a uniform compression can be computed by using Eq. (2.7).

$$(f_{cr})_E = \frac{k\pi^2 E}{12(1-\mu^2)(w/t)^2} \qquad (2.7)$$

where k = buckling coefficient

E = modulus of elasticity

w = width of plate

t = thickness of plate

μ = Poisson's ratio

If the critical buckling stress exceeds the proportional limit, the stiffened flange buckles in the inelastic range. The inelastic buckling stress, $(f_{cr})_I$, can be computed by using the following equation, which is based on the tangent modulus concept[63].

$$(f_{cr})_I = F_y - \frac{F_{pr}(F_y - F_{pr})}{(f_{cr})_E} \qquad (4.1)$$

where F_y = yield stress of steel

F_{pr} = proportional limit of steel

$(f_{cr})_E$ = elastic critical buckling stress defined in Eq. (2.7)

Therefore, the computed critical buckling moment, $(M_{cr})_{comp}$, of a beam corresponding to the initiation of local buckling of its compression flange can be calculated as follows:

$$(M_{cr})_{comp} = S_{xc} f_{cr} \quad (4.2)$$

where f_{cr} = critical buckling stress of the compression flange

S_{xc} = elastic section modulus of the full cross section relative to the compression flange.

The predicted and tested critical buckling moments of beam specimens are listed in columns (5) and (6) of Table 4.1, respectively. The predicted critical buckling moments were computed by using Eq. (4.2). The tested critical buckling moments were determined from the product of bending arm (L/8) and one half of the tested critical buckling load ($P_{cr}/2$) as follows:

$$(M_{cr})_{test} = \frac{P_{cr} L}{16} \quad (4.3)$$

In the above equation, the tested critical buckling loads (P_{cr}) were determined from load-strain diagrams by using a modified strain reversal method as discussed in Ref. 62. L is the span length of beam specimen. The values of S_{xc}, $f_{cr,}$, P_{cr}, and L are also given in Table 4.1.

The load versus strain diagrams of the hat sections with small w/t ratios (3A Sections) showed no sign of critical buckling. As presented in Table 4.1, most of the tested critical buckling moments were greater than the predicted values. This is because a minimum value of 4.0 was used as the buckling coefficient for stiffened compression flanges ignoring any effect of rotational edge restraint provided by the adjoining webs. The mean value of nine $(M_{cr})_{test}/(M_{cr})_{comp}$ ratios is equal to 1.076 with a standard deviation of 0.066. The tested critical loads of the hat sections with relatively large w/t ratios (3C Sections) increased with increasing strain rate.

\It was observed from 3C beam specimens that the number of half sine waves in the stiffened compression flange is the same for all tests regardless of the strain rate used for the test.

2. Ultimate Flexural Strength. The ultimate section strength can be calculated either on the basis of initiation of yielding in the effective section or on the basis of the inelastic reserve capacity.

a. Yield Flexural Strength. Based on the initiation of yielding in the effective section, the computed yield moment, $(M_y)_{comp}$, of a beam can be calculated by using the following equation:

$$(M_y)_{comp} = F_y S_e \qquad (4.4)$$

where F_y = static or dynamic yield stress of steel

S_e = elastic section modulus of the effective section calculated with the extreme compression or tension stress at F_y.

Tables 4.2(a) and 4.2(b) compare the computed and tested yield moments. Table 4.2(a) uses static yield stress for all tests, while Table 4.2(b) uses static or dynamic yield stress taking into account the effect of strain rate on yield stress value as discussed in Ref. 1. In these tables, the computed yield moment $(M_{y)comp}$ is listed in column (5) for each specimen. These yield moments were calculated by using Eq. (4.4) with effective section moduli (S_e) computed from the AISI effective width formula. The yield stress value is listed in column (2). Note that this value is a constant in Table 4.2(a), but it increases with strain rate in Table 4.2(b). The tested yield moments listed in column (6) were determined from the product of bending arm (L/8) and one half of the yield loads (P_y) determined from load-strain diagrams as follows:

$$(M_y)_{test} = \frac{P_y L}{16} \qquad (4.5)$$

The tested yield load and the effective section modulus computed for the extreme compression or tension stress at F_y are also given in Tables 4.2(a) and 4.2(b). As presented in these tables, all tested yield moments were greater than the predicted values. As expected, the ratios of tested to computed yield moments listed in Table 4.2(a) are larger than those listed in Table 4.2(b), because the latter table takes into

account the effect of strain rate on yield stress. In both tables the ratio of tested to computed yield moments increases with strain rate most of the time. As shown in Table 4.2(a), the average value of $(M_y)_{test}/(M_y)_{comp}$ ratios is equal to 1.321 with a standard deviation of 0.148, while in Table 4.2(b) the mean value of $(M_y)_{test}/(M_y)_{comp}$ ratios is equal to 1.237 with a standard deviation of 0.102.

b. Inelastic Reserve Capacity. The inelastic reserve capacity of flexural members, which allows partial yielding of a cross section, is recognized in the 1986 AISI Automotive Design Manual. It can be used to predict the ultimate load capacities of flexural members provided that such members satisfy the specific requirements.

The ultimate strengths of hat sections or track sections with yielded tension flanges may be calculated on the basis of inelastic reserve capacity. Figure 4.1 shows the stress distribution in sections with yielded tension flanges at ultimate moment. The following equations can be used to compute the values of y_c, y_t, y_p, and y_{tp} shown in Fig. 4.1 and the ultimate moment, M_u. For the purpose of simplicity, midline dimensions were used in the calculations.[58]

$$y_c = \frac{b_t - b_c + 2d}{4} \tag{4.6}$$

$$y_t = d - y_c \tag{4.7}$$

$$y_p = \frac{y_c}{C_y} \tag{4.8}$$

$$y_{cp} = y_c - y_p \tag{4.9}$$

$$y_{tp} = y_t - y_p \tag{4.10}$$

$$M_u = F_y t\left[b_c y_c + 2y_{cp}(y_p + \frac{y_{cp}}{2}) + \frac{4}{3}(y_p)^2 + 2y_{tp}(y_p + \frac{y_{tp}}{2}) + b_t y_t \right] \tag{4.11}$$

where b_c = effective width of the compression flange

b_t = total width of the tension flange

d = depth of the section

t = thickness of the section

C_y = compression strain factor for stiffened compression elements without intermediate stiffeners, which can be determined as follows:

$$C_y = 3 \qquad \text{for} \quad w/t \le \lambda_1 \tag{4.12(a)}$$

$$C_y = 3 - 2(\frac{w/t - \lambda_1}{\lambda_2 - \lambda_1}) \qquad \text{for} \quad \lambda_1 < w/t < \lambda_2 \tag{4.12(b)}$$

$$C_y = 1 \qquad \text{for} \quad w/t \ge \lambda_2 \tag{4.12(c)}$$

where $\lambda_1 = \frac{1.11}{\sqrt{F_y/E}}$ (4.13)

$$\lambda_2 = \frac{1.28}{\sqrt{F_y/E}} \qquad (4.14)$$

According to the AISI Automotive Design Manual, the ultimate moments computed by using the inelastic reserve capacity procedure should not exceed the limit of $(1.25\ S_e F_y)$

Tables 4.3(a) and 4.3(b) present the predicted and tested ultimate moments. Similar to Tables 4.2(a) and 4.2(b), Table 4.3(a) uses static yield stress while Table 4.3(b) uses static or dynamic yield stress corresponding to the strain-rate value used in the test. The tested ultimate moments were determined by the product of bending arm (L/8) and one half of the ultimate load $(P_u)/2$ as follows:

$$(M_u)_{test} = \frac{P_u\ L}{16} \qquad (4.15)$$

Ultimate loads were determined from the maximum loads reached during the tests and are listed in column (3). In both Tables 4.3(a) and 4.3(b), the tested ultimate moments of specimens were compared with the calculated ultimate moments. It is noted from column (7) of these tables that the ratio of the tested ultimate moment to the computed value decreases with increasing w/t ratio. For specimens having the same w/t ratios, the tested ultimate moment inceased with increasing strain rate. As shown in Table 4.3(a), the average value of $(M_u)_{test}/(M_u)_{comp}$ ratios is equal to 1.254 with a standard deviation of 0.200, while in Table

4.3(b) the mean value of $(M_u)_{test}/(M_u)_{comp}$ ratios is equal to 1.191 with a standard deviation of 0.169. Figures 4.2 through 4.4 show graphically typical moment-displacement curves for 3B sections under different strain rates. The computed critical, yield, and ultimate moments (based on inelastic reserve capacity) are marked in these figures for the comparison with the tested values. It is observed from these figures that the critical buckling moments are greater than the yield moments because the stress in the compression flange at the initiation of yielding (Fig. 4.5(b)) is less than the critical local buckling stress. The critical local buckling moments in these figures were calculated according to the stress distribution shown in Fig. 4.5(c) and assuming that the strain diagram is linear.

Tables 4.4 and 4.5 were prepared to study the effect of strain rate on ultimate momemts of hat-beam specimens. Table 4.4 lists average ultimate moments. Each ultimate moment value listed in this table is the average of two similar tests except that for the test conducted at the strain rate of 0.00001 in./in./sec., only one test was performed for each w/t ratio. For the purpose of comparison, Table 4.5 lists the ratios of average ultimate moments obtained from Table 4.4. Each value listed in this table represents the ratio of two ultimate moments for tests having the same w/t ratio but conducted at two different strain rates. It is noted from Tables 4.4 and 4.5 that the ultimate moment increases with strain rate for all w/t ratios. The percentage increase of the ultimate moments for specimens having the same w/t ratio is larger at higher strain rate as compared to this increase at lower strain rate for most of the cases.

Figure 4.6 shows graphically the effect of strain rate on the ultimate moments of the hat-beam specimens. The horizontal axis represents logarithmic strain rate while the vertical axis represents the ratio of dynamic to static ultimate moments. The tests performed at strain rate of 0.0001 in./in./sec. are considered to be the static loading condition.

C. STUB COLUMN TESTS FOR THE STUDY OF STIFFENED ELEMENTS

Box-shaped sections (Fig. 3.21) were designed and fabricated for stub column tests to study the post-buckling strengths of stiffened elements by using 35XF sheet steels. All stub columns were subjected to uniform compression. The overall column buckling is prevented by the design of stub columns. All webs of the stub columns were designed to be fully effective based on the 1986 AISI Automotive Design Manual. According to the same manual, all unstiffened elements are fully effective. The tested compressive yield stress was used for the evaluation of all stub column specimens studied in this investigation.

1. Critical Local Buckling Load. As discussed in Section IV.B.1, the critical local buckling stress, f_{cr}, of a stiffened element can be computed by using Eq. (2.7) or Eq. (4.1), depending on the w/t ratio of the stiffened element. Therefore, the critical buckling loads of stub columns can be computed by using the following equation:

$$P_{cr} = A_t f_{cr} \qquad (4.16)$$

where f_{cr} = critical local buckling stress of stiffened element

A_t = total cross-sectional area of stub column

The total cross-sectional areas of stub columns with stiffened elements are given in Table 3.9. The critical local buckling stress for each specimen, listed in column (1) of Table 4.6, is the average value of two critical local buckling stresses of stiffened compression flanges of stub columns. No signs of critical local buckling were observed from the load-strain diagrams of box-shaped stub columns with small and medium w/t ratios (1A and 1B sections).

Table 4.6 compares the computed and tested critical local buckling loads for stub column specimens fabricated from 35XF sheet steels. The tested critical local buckling loads listed in column (3) of Table 4.6 were determined from load-strain diagrams by using a modified strain reversal method. The buckling coefficient used to calculate the buckling stress of stiffened elements in Eq. (4.1) was equal to 4.0. The mean value of $(P_{cr})_{test}/(P_{cr})_{comp}$ ratios is equal to 1.168 with a standard deviation of 0.076. It is noted from column (4) of Table 4.6 that the ratio of tested to computed critical local buckling load $(P_{cr})_{test}/(P_{cr})_{comp}$ increases with increasing strain rate for stub columns with relatively large w/t ratios.

2. Ultimate Axial Load. By using the effective width concept discussed in Section II.D, a stub column specimen fails when the maximum edge stresses in the stiffened element reaches the yield stress of steel.

The ultimate load carrying capacities of stub columns can be calculated by using Eq. (4.17).

$$P_u = A_e F_y \tag{4.17}$$

where F_y = static or dynamic yield stress of steel

A_e = effective cross-sectional area of stub column for the maximum edge stress at F_y

Equation (4.17) was used to calculate the failure loads of the specimens. In using Eq. (4.17), F_y values are listed in column (3) of Tables 4.7(a) and 4.7(b). For the calculation of computed ultimate loads, Table 4.7(a) uses static yield stress, while Table 4.7(b) uses static or dynamic yield stress, corresponding to the strain rate used in the test. The effective cross-sectional area of each stub column is listed in column (4) of Tables 4.7(a) and 4.7(b) by using the current AISI Automotive Design Manual and the appropriate yield stress. The computed failure loads of stub columns, $(P_u)_{comp}$, are listed in column (5) of Tables 4.7(a) and 4.7(b). The tested failure loads of stub-column specimens are listed in column (6) of Tables 4.7(a) and 4.7(b). Comparisons of the computed and tested failure loads of stub columns are shown in column (7) of both tables. The mean values of $(P_u)_{test}/(P_u)_{comp}$ ratios and standard deviations are (1.265, 0.139) and (1.184, 0.093) for Tables 4.7(a) and 4.7(b), respectively. As expected, for specimens having the same w/t ratio, the tested ultimate load increases with strain rate. The tested to computed ultimate load ratios

in Table 4.7(a) are higher than the corresponding values in Table 4.7(b). Figures 4.7 through 4.9 show graphically typical load-displacement curves for 1B sections under different strain rates. The computed critical and ultimate loads are marked in these figures for the comparison with the tested ones.

Tables 4.8 and 4.9 were prepared to study the effect of strain rate on failure loads of box-shaped stub column specimens. Table 4.8 lists average failure loads obtained from Table 3.9. Each failure load value listed in this table is the average of two values obtained from similar tests. For the purpose of comparison, Table 4.9 shows the ratios of average failure loads obtained from the tests conducted at different strain rates. It is noted from Tables 4.8 and 4.9 that 1) the failure load increases with strain rate and 2) the ratio of dynamic to static failure loads increases with increasing w/t ratio. The percentage increase in failure loads is larger at higher strain rate as compared to the increase at lower strain rates.

Figure 4.10 shows graphically the effect of strain rate on the failure loads of stub column spcimens. The horizontal axis represents logarithmic strain rate, while the vertical axis represents the ratio of dynamic to static failure loads. The static failure loads are corresponding to the tests performed at strain rate of 0.0001 in./in./sec.

D. BEAM TESTS FOR THE STUDY OF UNSTIFFENED ELEMENTS

As mentioned in Chapter III, channel beams having small w/t ratios have been designed and fabricated to study the post-buckling strengths of unstiffened elements by using 35XF sheet steels. All the channel beams were subjected to two point loads at a distance of L/8 from end support as shown in Figs. 3.35 and 3.36. Lateral torsional buckling of channel beams was prevented by using lateral supports provided by aluminum angles connected to the compression flanges, as discussed in Chapter III. The webs of channel beam specimens were designed to be fully effective. The weight of the test specimen and the weight of the cross beam placed on the top of the specimen (approx. 70 lbs.) are small as compared to the ultimate loads and were neglected in the evaluation of test results. The tested tensile yield stress was used for computing yield moment (M_y) for all beam specimens studied in this investigation.

1. Critical Local Buckling Strength. The critical local buckling moments (M_{cr}) of channel beams can be computed by using Eq. (4.2). As discussed in Section IV.B.1, the critical local buckling stress (f_{cr}) can be computed by using Eq. (2.7) or Eq. (4.1), depending on the w/t ratio of the compression flange. In this phase of study, a value of 0.43 was used as the buckling coefficient for unstiffened flanges to calculate the critical local buckling stresses of compression flanges.

The computed critical buckling moments of channel beams, listed in column (5) of Table 4.10, were calculated by using Eq. (4.2). The critical local buckling stresses were computed by using Eq. (4.1) for all channel beam tests. The tested critical buckling moments listed in column (6) of the same table were determined from the product of

bending arm (L/8) and one half of the critical local buckling loads $(P_{cr})/2$ as given in Eq. (4.3). The critical local buckling loads were determined from load-strain diagrams by using the modified strain reversal method. The span length of channel beams and other parameters (S_x, f_{cr}, P_{cr}) for each channel beam are given in Table 4.10. No local buckling was observed from load-strain diagrams for channel beams with small and medium w/t ratios. As shown in column (3) of Table 4.10, the tested critical load increases with strain rate.

A comparison of the tested and predicted critical local buckling moments is given in Table 4.10. Note that all tested critical buckling moments are greater than the computed critical local buckling moments. This is because a value of 0.43 was used as the buckling coefficient for unstiffened compression flanges ignoring any effect of rotational edge restraint provided by the adjoining webs. The mean value of $(M_{cr})_{test}/(M_{cr})_{comp}$ ratios is equal to 1.405 with a standard deviation of 0.060.

2. Ultimate Flexural Strength. For channel beams having equal flanges, the ultimate section strengths of such flexural members can be calculated on the basis of initiation of yielding of the compression flanges in the effective section. The ultimate section strengths of all channel beams can be calculated by using Eq. (4.4).

As discussed earlier, the buckling coefficients of 0.43 was used in the 1986 AISI Automotive Design Manual to calculate the effective width of an unstiffened element. The computed ultimate moments of

channel beams fabricated from 35XF sheet steels are given in Tables 4.11(a) and 4.11(b). The latter table uses static or dynamic yield stress depending on strain rate used in the test while, the previous one uses static yield stress for all tests. The ultimate moments $(M_u)_{comp}$ listed in column (5) of both tables were calculated by using Eq. (4.4). Effective section modulus (S_e) was computed using the effective width formula for unstiffened element adopted in the current AISI Automotive Design Manual along with the appropriate yield stress value. The computed values of effective section modulus for all channel beam tests are listed in column (1) of both tables (4.11(a) and 4.11(b)). The span lengths of channel beams are given in column (4) of these tables. The tested ultimate moments listed in column (6) of Tables 4.11(a) and 4.11(b) were determined from the product of the bending arms (L/8) and one half of the tested failure loads as given in Eq. (4.5). The tested failure load for each channel beam test was considered to be the maximum load the member can sustain during the test. The tested ultimate moments are compared with the computed ultimate moments in Tables 4.11(a) and 4.11(b).

The mean value of $(M_u)_{test}/(M_u)_{comp}$ ratios and standard deviations are (1.299, 0.096) and (1.228, 0.052) for Tables 4.11(a) and 4.11(b), respectively.

As observed previously, the ratios of tested ultimate moments to the computed ones are greater in Table 4.11(a) as compared to those ratios in Table 4.11(b), because the latter table took into account the effect of strain rate on yield stress. For specimens having the same

dimensions, the tested ultimate load increases with the strain rate. Figures 4.11 through 4.13 show graphically typical moment-displacement curves for 4B sections under different strain rates. The computed critical and yield moments are marked in these figures for the comparison with the tested ones.

Tables 4.12 and 4.13 were prepared to study the effect of strain rate on ultimate moments of channel beam specimens. Table 4.12 lists the average ultimate moments. Each ultimate load value listed in this table is the average of two values obtained from similar tests except that for the tests conducted at strain rate of 0.00001 in./in./sec., only one test was performed. For the purpose of comparison, Table 4.13 shows the ratios of ultimate moments. Each value listed in this table is the ratio of two ultimate moments for the specimens with same dimensions but tested under different strain rates. It is observed from Tables 4.8 and 4.9 that 1) the failure load increases with strain rate and 2) the percentage increase of ultimate moments is larger at higher strain rate in most cases.

Figure 4.14 shows graphically the effect of strain rate on the ultimate moments of the channel beam specimens. The horizontal axis represents logarithmic strain rate while the vertical axis represents the ratio of dynamic to static ultimate moments. The tests performed at strain rate of 0.0001 in./in./sec. are considered to be the static loading conditions.

E. STUB COLUMN TESTS FOR THE STUDY OF UNSTIFFENED ELEMENTS

I-shaped stub columns were designed and fabricated to study the post-buckling strengths of unstiffened elements under different strain rates by using 35XF steel. All the stub columns were subjected to uniform compression. Overall column buckling was prevented by the design of stub columns. The thickness of the web in a stub column was twice the thickness of the unstiffened compression flange because the webs of stub columns were glued together. The tested compressive yield stress was used for the evaluation of all stub column specimens studied in this investigation.

1. Critical Local Buckling Load. The critical local buckling load of a stub-column specimen with unstiffened compression elements can be calculated using Eq. (4.16).

In Eq. (4.16), the critical local buckling stress of an unstiffened element can be calculated by using Eq. (2.7) or (4.1), depending on the w/t ratio of the unstiffened flange. A value of 0.43 was used as the buckling coefficient to calculate the critical local buckling stresses of unstiffened elements in this phase of study for using Eq. (4.1). The total cross-sectional areas of stub columns are given in Table 3.11. The critical local buckling stress listed in column (1) of Table 4.14 for each stub column is the average value of four critical local buckling stresses of unstiffened flanges.

The computed and tested critical local buckling loads of specimens fabricated from 35XF steel are given in columns (2) and (3) of Tables 4.14, respectively. The tested critical local buckling loads were determined from load-strain diagrams by using a modified strain reversal method. In Table 4.14, the tested critical local buckling load for each specimen is the average value of four tested critical local buckling loads determined from unstiffened flanges. The computed critical local buckling loads were determined from the product of the average critical local buckling stresses and the total cross-sectional areas. No critical local buckling was observed from the load-strain diagrams of I-shaped stub columns with small and medium w/t ratios. Note that the critical local buckling loads for stub columns with large w/t ratios tested in the present investigation were underestimated by using Eq (4.16). The mean values of $(P_{cr})_{test}/(P_{cr})_{comp}$ ratios and standard deviations are equal to 1.556 and 0.102, respectively. As shown in column (3) of Table 4.14, the tested critical buckling load increases with the strain rate.

2. Ultimate Axial Load. From the concept of the effective width approach, stub-column specimens reach the ultimate axial load when the maximum edge stresses of the unstiffened elements reach yield stresses of the steels. The ultimate load carrying capacities (P_u) of the stub-column specimens can be calculated from Eq. (4.17).

The computed and tested failure loads of stub columns were compared in Tables 4.15(a) and 4.15(b). Table 4.15(a) uses static yield stress, while Table 4.15(b) uses static or dynamic yield stress according to

the strain rate used in the test. Equation (4.17) was used to compute the failure loads listed in column (5) of both tables using appropriate yield stresses. The yield stress values are listed in column (3) of the same tables. The effective cross-sectional areas computed by using the current AISI Automotive Design Manual are also given in Tables 4.15(a) and 4.15(b).

The tested ultimate loads of stub columns are listed in column (6) of Tables 4.15(a) and 4.15(b). Comparisons of the computed and tested failure loads are listed in column (7) of these tables. The mean values of $(P_u)_{test}/(P_u)_{comp}$ ratios are 1.417 and 1.334 with standard deviations of 0.136 and 0.070 for Tables 4.15(a) and 4.15(b) , respectively.

As shown in these tables, the ultimate load increases with strain rate. Because the latter table takes into account the effect of strain rate on yield stress, the ratios of tested to computed failure loads listed in Table 4.15(a) are greater than that given in Table 4.15(b). Figures 4.15 through 4.17 show graphically typical load-displacement curves for 2B sections under different strain rates. The computed critical and ultimate loads are marked in these figures for comparison with the tested ones.

Tables 4.16 and 4.17 were prepared to study the effect of strain rate on failure loads for I-shaped stub column specimens. Table 4.16 lists the average failure loads obtained from Table 3.11. Each failure load value listed in this table is the average of two values obtained from similar tests. For the purpose of comparison, Table 4.17 shows the ratios of dynamic failure loads. Each value listed in this table

is the ratio of two average failure loads for specimens having the same dimensions but tested under different strain rates. It is observed from Tables 4.16 and 4.17 that 1) the failure load increases with strain rate and 2) the ratio of dynamic to static failure loads increases with increasing w/t ratio. As observed previously, the percentage increase of failure load is larger at higher strain rates.

Similar to the previous figures, Fig. 4.18 shows the effect of strain rate on the failure loads of the I-shaped stub column specimens graphically. The tests performed at strain rate of 0.0001 in./in./sec. are considered to be the static loading conditions.

F. DEFLECTION OF BEAM SPECIMENS

As mentioned in Chapter III, the deflections at midspan of beam specimens (d in Fig. 4.19) were measured by two LVDTs located on both sides of hat and channel beam specimens as shown in Figs. 3.17 and 3.37. Tables 4.18 and 4.19 compare the computed and measured deflections under service moments for hat and channel beam specimens, respectively. The service moments were considered to be 60% of the computed yield moments and are listed in Table 4.2(b) for hat-beam specimens and in Table 4.11(b) for channel beam specimens. The measured deflection under service moment was obtained from the moment-deflection curve, while the computed value was calculated by using the following theoretical deflection equation with effective moment of inertia:

$$\delta = \frac{9 M_s L^2}{128 E I_e} \qquad (4.18)$$

where M_s = moment under service load

$= 0.6\ (M_y)_{comp}$

L = span length of beam

E = modulus of elasticity

I_e = effective moment of inertia under service moment

In the above expression, Equations 2.28 through 2.31 (procedure II) were used to calculate the effective moment of inertia for hat beam specimens, while Procedure I was used to calculate the effective moment of inertia for channel beam specimens under service moments.

The computed and measured deflections under service moments are given in Tables 4.18 and 4.19 for hat and channel beam specimens, respectively. It is noted from these tables that most of the measured deflections were less than the computed values. It has been noted that the ratios of measured to computed deflections decrease with increasing strain rate for most of the cases which means that the deflections from the fast tests lag behind those from the slow tests at the same load level. The mean values of $(d)_{test}/(d)_{comp}$ ratios and standard deviations under service moments are equal to (0.808, 0.093) and (0.833, 0.121) for hat and channel beam specimens , respectively. Figure 4.20 shows graphically a typical moment-deflection curve for hat-beam specimens, while Fig. 4.21 shows a typical moment-deflection curve for channel beam specimens.

V. CONCLUSIONS

This study dealt with the effect of strain rate on mechanical properties of sheet steels and the structural strengths of cold-formed steel members subjected to dynamic loads.

During the period from May 1988 through July 1989, progress was made on a study of the effect of strain rate on tensile and compressive mechanical properties of sheet steels. The results of this investigation were presented in the Eleventh and Twelfth Progress Reports.

During the period from August 1989 through February 1990, the work continued to include the study of structural strengths of cold-formed steel members subjected to dynamic loads. This work included a review of literature and testing of 67 structural members, of which 30 specimens were tested as beams and 37 specimens were tested as stub columns. The literature survey is presented in Chapter II. Chapter III contains the detailed information on the experimental investigation, which includes materials, test specimens, equipment, test procedure, and test results. Evaluation of the test data is presented in Chapter IV.

Based on the available test data, the following conclusions may be drawn from the study of the effect of dynamic loads on the structural strengths of cold-formed steel beams and stub columns fabricated from 35XF sheet steel:

1. The critical local buckling strength, yield strength, and ultimate strength for most of the tests increased with increasing strain rates. The ultimate strengths showed larger increases at higher strain rates than at lower strain rates.

2. The effect of strain rate on member strength was found to be similar to those observed from the previous study of material properties as affected by different strain rates. However, ratios of dynamic to static ultimate strengths for beams and stub columns conducted in this study were found to be slightly higher than those for tensile or compressive material yield stresses reported in Ref. 1 and 2.

3. The computed ultimate strength based on the AISI Automotive Design Manual was found to be conservative for all beam and stub column tests. The mean and standard deviation values for the ratios of tested to computed ultimate strengths were improved by using the dynamic yield stresses rather than the static value for all cases studied in this investigation.

4. The computed midspan deflection under service moments are slightly larger than those measured from tests, except for two channel beams.

5. Future tests are planned for a study of the effect of strain rate on structural strengths of cold-formed steel members fabricated from 35XF sheet steel using larger w/t ratios than those used in previous tests.

6. Future tests are also planned to investigate the effect of strain rate on member strengths using 50XF and other high strength sheet steels as recommended by the AISI Task Force on Automotive Structural Design.

ACKNOWLEDGMENTS

The research work reported herein was conducted in the Department of Civil Engineering at the University of Missouri-Rolla under the sponsorship of the American Iron and Steel Institute.

The financial assistance granted by the Institute and the technical guidance provided by members of the Task Force on Automotive Structural Design, the AISI Automotive Applications Committee Design Panel, and the AISI staff are gratefully acknowledged. These members are: Messrs. S. J. Errera (Chairman), J. Borchelt, R. Cary, F. L. Cheng, A. M. Davies, J. D. Grozier, C. Haddad, J. D. Harrington, A. L. Johnson, C. M. Kim, K. H. Lin, J. N. Macadam, H. Mahmood, D. Malen, J. G. Schroth, P. G. Schurter, T. N. Seel, and M. T. Vecchio. An expression of thanks is also due to Mr. D. L. Douty for his help.

All materials used in the experimental study were donated by Inland Steel Company and LTV Steel Company.

Appreciation is expressed to Messrs. K. Haas, J. Bradshaw, F. Senter, and J. Tucker, staff of the Department of Civil Engineering, for their technical support and to Mr. C. L. Pan for his valuable assistance in the preparation and performance of the tests. The advice provided by Dr. J. E. Minor, Chairman of the UMR Department of Civil Engineering, is greatly appreciated.

REFERENCES

1. Kassar, M. and Yu, W.W., "Design of Automotive Structural Components Using High Strength Sheet Steels: The Effect of Strain Rate on Mechanical Properties of Sheet Steels", Eleventh Progress Report, Civil Engineering Study 89-2, University of Missouri- Rolla, January 1989.

2. Kassar, M. and Yu, W.W., "Design of Automotive Structural Components Using High Strength Sheet Steels: The Effect of Strain Rate on Compressive Mechanical Properties of Sheet Steels", Twelfth Progress Report, Civil Engineering Study 89-2, University of Missouri- Rolla, August 1989.

3. American Iron and Steel Institute, "Cold-Formed Steel Design Manual ," 1986 Edition.

4. American Iron and Steel Institute, "Automotive Steel Design Manual," 1986 Edition.

5. Timoshenko, S. P. and Gere, J. M., Theory of Elastic Stability, 2nd Edition, New York: McGraw-Hill Book Company, Inc., 1961.

6. Bulson, P. S., The Stability of Flat Plates, New York: American Elsevier Publishing Company, Inc., 1969.

7. Saint Venant, "Discussion in Theorre de l'elasticte' des Corps Solides," by Clebsch, P.704, 1883.

8. Bleich, F. "Theorie .und Berechnung der eisernen Brcicken," Julius Springer, Berlin, 1924.

9. Bijlaard, P. P., "Theory of Plastic Stability of Thin Plates," Pubs. International Association for Bridge and Structural Engineering, Vol. VI, 1940-41.

10. Bijlaard, P. P., "Theory and Tests on the Plastic Stability of Plates and Shells," Journal of the Aeronautical Sciences, V. 16, PP529-541, 1949.

11. Ilyushin, A. A., "The Elastic-Plastic Stability of Plates," Translation in NACA Technical Memorandum 1188.

12. Stowell, E. Z., "A Unified Theory of Plastic Buckling of Columns and Plates," NACA Technical Note No. 1556, April 1948.

13. Von Karman, T., "Festigkeitsprobleme in Meschinenbau," Encyklpadie der Mathematischen, Vol. 4, 1910, P. 349.

14. Schnadel, G., "Die Uberschreitung der Knickgrenze bei dunnen Platlen," Proceedings of Third International Congress for Applied Mechanics, Stockholm, Vol. 3, 1930.

15. Cox, H. L., "The Buckling of Thin Plates in Compression," Technical Report of the Aeronautical Committee, 1933-34.

16. Marguerre, K., "Die Mittrangende Breite der Gedrukten Platte," Luftfahrtforschung, Vol. 14, 1937.

17. Levy, S., "Bending of Rectangular Plates with Large Deflections," NACA Technical Report 737, 1942, P.139.

18. Von Karman, T., Sechler, E. E., and Donnell, L. H., "The Strength of Thin Plates in Compression," Transactions, ASME, Vol. 54, APM54-5, 1932.

19. Winter, G., "Strength of Thin Steel Compression Flanges," Bulletin No. 35, Part 3, Cornell University, Engineering Experiment Station, Ithaca, N.Y., 1947.

20. Winter, G., "Performance of Thin Steel Compression Flanges," Preliminary Publication, 3rd Congress of the International Association for Bridge and Structural Engineering, 1948, P.137.

21. Winter, G., "Performance of Compression Plates as Parts of Structural Mambers," Bulletin No. 35, Cornell University, Engineering Experiment Station, Ithaca, N.Y., 1947.

22. Kalyanaraman, V., Pekoz, T., and Winter, G., "Analytical Study of Unstiffened Elements," Journal of Structural Division, ASCE, Vol. 104, No. ST9, September, 1978.

23. Kalyanaraman, V., Pekoz, T., and Winter, G., "Unstiffened Compression Elements," Journal of Structural Division, ASCE, Vol. 103, No. ST9, September 1977.

24. Kalyanaraman, V., "Local Buckling of Cold-Formed Steel Members," Journal of Structural Division, ASCE, Vol. 105, No. ST5, May 1979.

25. American Iron and Steel Institute, "Specification for the Design of Cold-Formed Steel Structural Members," 1968 Edition.

26. American Iron and Steel Institute, "Specification for the Design of Cold-Formed Steel Structural Members," 1980 Edition.

27. Pekoz, T., "Development of a Unified Approach to the Design of Cold-Formed Steel Members," Report SG86-4, AISI, Washington , D. C., May 1986.

28. Pan, L. C., "Effective Design Width of High Strength Cold-Formed Steel Members," PhD Dissertation, University of Missouri-Rolla, 1987.

29. Parks, M. B., "Structural Behavior of Members Consisting of Flat and Curved Elements," PhD Dissertation, University of Missouri-Rolla, 1987.

30. Rawlings, B., "Response of Structures to Dynamic Loads," Mechanical Properties at High Rates of Strain, Institute of Physics, London, No.21, 1974.

31. Parkes, E. W.,"The Permanenet Deformation of an Encastre Beam Struck Transversely at any Point in its Span," Proc. Inst. Civil Eng., July, 1958.

32. Ezra, A. A., "The Plastic Response of a Simply Supported Beam to an Impact Load at the Center," Proc. III U. S. Nat. Cong. Appl. Mech., 1958.

33. Duwez, P. E., Clark, D. S., and Bohnenblust, H. F., "The Behavior of Long Beams Under Impact Loading," J. Appl. Mech., Vol. 117, No. 1, March, 1950.

34. Bodner, S. R. and Symonds, P. S., "Experimental and Theoretical Investication of the Plastic Deformation of Cantilever Beams Subjected to Impulsive Loading," Journal of Applied Mechanics, Vol. 29, Dec.1962.

35. Rawlings, B., "The Dynamic Behavior of Steel in Pure Flexure," Proc. Royal Soc. Series A, Vol. 275, 1963.

36. Ting, T. C. T., "Large Deformation of a Rigid-Ideally-Plastic Cantilever Beam," J. Appl. Mech., June, 1965.

37. Bodner, S. R., "Deformation of Rate-Sensitive Structures under Impulsive Loading," Engineering Plasticity, Heyman and Leckie, Ed., Cambridge Univ. Press, 1968.

38. Symonds, P. S., Behavior of Materials Under Dynamic Loading, ASME, Huffington, N. J., Ed., 1965.

39. Jones, N., "Response of Structures to Dynamic Loading," Mechanical Properties at High Rates of Strain, Institute of Physics, London, No.47, 1979.

40. Aspden, R. J., and Campbell, J. D., "The Effect of Loading Rate on the Elasto-Plastic Flexure of Steel Beams," Proceedings of Royal Society of London, Vol. A290, 1966.

41. Jones, N., "Influence of Strain-Hardening and Strain-Rate Sensitivity on the Permanent Deformation of Impulsively Loaded Rigid-Plastic Beams," International Journal of Mechanical Sciences, Vol.9, 1967.

42. Culver, C. G., Zanoni, E. A., and Osgood, A. H., "Response of Thin-Walled Beams to Impact Loading," Proceedings of the First Specialty Conference on Cold-Formed Steel Structures, University of Missouri-Rolla, Aug. 1971.

43. Symonds, P. S. and Jones, N., "Impulsive Loading of Fully Clamped Beams with Finite Plastic Deflections and Strain-Rate Sensitivity," Int. J. Mech. Sci., Vol. 14, 1972.

44. Forrestal, M. J. and Sagartz, M. J., "Elastic-Plastic Response of 304 Stainless Steel Beams to Impulse Loads," Journal of Applied Mechanics, Vol. 45, September 1978.

45. Forrestal, M. J. and Wesenberg, D. L., "Elastic Plastic Response of Simply Supported 1018 Steel Beams to Impulse Loads," Journal of Applied Mechanics, Dec. 1977.

46. Meier, J. H., "On the Dynamic of Elastic Buckling," Journal of the Aeronautical Sciences, Vol. 12, 1945.

47. Hoff, N., "Dynamic Stability of Structures," Proceedings of an International Conference on Dynamic Stability of Structures, Northwestern University, Evanston, Illinois, October 1965.

48. Roberts, T. M., "The Response of Steel Struts to Impact Overload," PhD Thesis, University of Sheffield, 1972.

49. Culver, C. G. and Vaidya, N. R., "Impact Loading of Thin-Walled Columns," Proceedings of the First Specialty Conference on Cold-Formed Steel Structures, University of Missouri-Rolla, Aug. 1971.

50. Logue, J. M., "Experimental Study of Thin-Walled Columns Subjected to Impact Loading," Master Thesis, Carnegie-Mellon University, April, 1971.

51. Soden, P. D., Al-Hassani, S. T. S., and Johnson, W., "The Crumpling of Polyvinylchloride Tubes Under Static and Dynamic Axial Loads," Mechanical Properties at High Rates of Strain, Institute of Physics, London, No.21, 1974.

52. Wierzbicki, T., "Dynamic Crushing of Strain Rate Sensitive Box Columns," SAE Second International Conference on Vehicle Structural Mechanics, April 1977.

53. Ohkubo, Y., Akamatsu, T., and Shirasawa, K., "Mean Crushing Strength of Closed-Hat Section Members," SAE Paper No. 740040, 1974.

54. Wimmer, A., "Einfluss der Belastungsgeschwindigheit auf das Festigkeitsund Verformungsverhaten von Blechkonstruktionen am Beispiel von Kraftfahrzengen," ATZ 77, 1975.

55. Wierzbicki, T. and Abramowicz, W., "Crushing of Thin-Walled Strain-Rate Sensitive Structures," Dynamic and Crushing Analysis of Plastic Structures, Euromech Colloquium No. 121, August, 1979.

56. Abramowicz, W. and Jones, N., "Dynamic Axial Crushing of Square Tubes," Int. J. Impact Engng., Vol. 2, No. 2, 1984.

57. Galambos, T. V. (ed.), Guide to Stability Design Criteria for Metal structures, 4th Edition, New York: John Wiley & Sons, Inc.,1988.

58. Yu, W. W., Cold-Formed Steel Design, New York: John Wiley & Sons Inc., 1985.

59. Gerard, G., and H. Becker, Handbook of Structural Stability, Part I-Buckling of Flat Plates, NACA Technical Note 3781, July, 1957.

60. Bulson, P. S., The Stability of Flat Plates, American Elsevier Publishing Company, New York, 1969.

61. Winter, G., "Commentary on the 1968 Edition of the Specification for the Design of Cold-Formed Steel Structural Members," American Iron and Steel Institute, 1970 Ed.

62. Johnson, A. L. and Winter, G., "The Structural Performance of Austenitic Stainless Steel Members," Report No. 327, Cornell University, Nov., 1966.

63. Bleich, F., Buckling Strength of Metal Structures, New York: McGraw-Hill Book Company, 1952.

64. Reck, H. P., Pekoz, T., and Winter, G., "Inelastic Strength of Cold-Formed Steel Beams," Journal of Structural Division, ASCE Proceedings, vol. 101, Nov. 1975.

Table 2.1

α and β Values of Equation 2.36 for the Calculation of Dynamic Correction Factor for Thin-Walled Steel Columns with Various Cross-Sections

Author and Reference Number	Cross Section	α	β
Wierzbicki (Ref. 52)	Box Sections	0.1000	0.714
Ohkubo, Akamatsu, and Shirasawa (Ref. 53)	Closed Hat Sections (70x60x1.2 mm)	0.0668	1.000
Wimmer (Ref. 54)	Box Sections (50x50x1.2 mm)	0.0700	0.820
Abramowicz and Jones (Ref. 56)	Box, Symmetric Mode (37x37x1.152 mm)	0.183	0.256
Abramowicz and Jones (Ref. 56)	Box, Symmetric Mode (49x49x1.63 mm)	0.170	0.256
Abramowicz and Jones (Ref. 56)	Box, Asymmetric Mode (37x37x1.152 mm)	0.193	0.256
Abramowicz and Jones (Ref. 56)	Box, Asymmetric Mode (49x49x1.63 mm)	0.180	0.256

Table 3.1

Designation of Test Specimens Used in This Study

1st Digit - Section Type	1st Letter - w/t Ratio	2nd Digit - Strain-Rate (in./in./sec.)	2nd Letter - Test No.
1- Box-Shaped Section Stub-Column Test (Fig. 3.1b)	A- Small Ratio	0- 0.00001	A- 1st Test
	B- Medium Ratio	1- 0.0001	B- 2nd Test
	C- Large Ratio	2- 0.01	
2- I-Shaped Section Stub-Column Test (Fig. 3.2b)		3- 0.1	
3- Hat Section for Beam Test (Fig. 3.1a)			
4- Channel Section for Beam Test (Fig. 3.2a)			

Table 3.2

Number of Performed Stub Column Tests

Box Sections Having Stiffened Compression Elements

Spec. No.	Test Speed in./min.	Strain Rate (in./in./sec.)	w/t	L/r	No. of Tests Performed
1A1A	0.072	0.0001	27.15	12.26	1
1A1B	0.072	0.0001	27.39	12.26	1
1A2A	7.2	0.01	26.92	12.26	1
1A2B	7.2	0.01	27.06	12.26	1
1A3A	72.0	0.1	27.31	12.26	1
1A3B	72.0	0.1	27.40	12.26	1
1B1A	0.084	0.0001	38.93	10.98	1
1B1B	0.084	0.0001	38.17	10.98	1
1B2A	8.4	0.01	38.86	10.98	1
1B2B	8.4	0.01	39.10	10.98	1
1B3A	84.0	0.1	38.86	10.98	1
1B3B	84.0	0.1	38.96	10.98	1
1C1A	0.09	0.0001	52.69	11.27	1
1C1B	0.09	0.0001	52.96	11.27	1
1C2A	9.0	0.01	52.20	11.27	1
1C2B	9.0	0.01	53.06	11.27	1
1C3A	90.0	0.1	53.15	11.27	1
1C3B	90.0	0.1	53.39	11.27	1
Total					18

Table 3.3

Number of Performed Stub Column Tests

I-Sections Having Unstiffened Compression Elements

Spec. No.	Test Speed in./min.	Strain Rate (in./in./sec.)	w/t	L/r	No. of Tests Performed
2A1A	0.054	0.0001	8.93	18.73	1
2A1B	0.054	0.0001	9.04	18.73	1
2A2A	5.4	0.01	8.93	18.73	1
2A2B	5.4	0.01	9.10	18.73	1
2A3A	54.0	0.1	8.93	18.73	1
2A3B	54.0	0.1	8.96	18.73	1
2B1A	0.06	0.0001	13.34	17.65	1
2B1B	0.06	0.0001	13.41	17.65	1
2B2A	6.0	0.01	13.40	17.65	1
2B2B	6.0	0.01	13.37	17.65	1
2B3A	60.0	0.1	13.34	17.65	1
2B3B	60.0	0.1	13.42	17.65	1
2C0A	0.0084	0.00001	20.69	15.64	1
2C1A	0.084	0.0001	20.85	15.64	1
2C1B	0.084	0.0001	20.76	15.64	1
2C2A	8.4	0.01	20.97	15.64	1
2C2B	8.4	0.01	20.81	15.64	1
2C3A	84.0	0.1	20.93	15.64	1
2C3B	84.0	0.1	20.87	15.64	1
Total					19

Table 3.4

Number of Performed Beam Tests

Hat Sections Having Stiffened Compression Flanges

Spec. No.	Test Speed in./min.	Strain Rate (in./in./sec.)	w/t	L (in.)	No. of Tests Performed
3A0A	0.023	0.00001	29.15	47	1
3A1A	0.23	0.0001	30.00	47	1
3A1B	0.23	0.0001	29.85	47	1
3A2A	23.0	0.01	29.05	47	1
3A2B	23.0	0.01	30.17	47	1
3B0A	0.038	0.00001	55.91	77	1
3B1A	0.38	0.0001	55.11	77	1
3B1B	0.38	0.0001	55.91	77	1
3B2A	38.0	0.01	55.82	77	1
3B2B	38.0	0.01	55.97	77	1
3C0A	0.15	0.00001	76.17	95	1
3C1A	1.50	0.0001	76.64	95	1
3C1B	1.50	0.0001	76.57	95	1
3C2A	150.0	0.01	76.62	95	1
3C2B	150.0	0.01	76.03	95	1
Total					15

Table 3.5

Number of Performed Beam Tests

Channel Sections Having Unstiffened Compression Flanges

Spec. No.	Test Speed in./min.	Strain Rate (in./in./sec.)	w/t	L (in.)	No. of Tests Performed
4A0A	0.043	0.00001	9.28	41	1
4A1A	0.43	0.0001	9.16	41	1
4A1B	0.43	0.0001	9.16	41	1
4A2A	43.0	0.01	9.22	41	1
4A2B	43.0	0.01	9.03	41	1
4B0A	0.045	0.00001	15.13	47	1
4B1A	0.45	0.0001	15.16	47	1
4B1B	0.45	0.0001	14.93	47	1
4B2A	45.0	0.01	15.04	47	1
4B2B	45.0	0.01	15.16	47	1
4C0A	0.082	0.00001	20.93	69	1
4C1A	0.82	0.0001	20.99	69	1
4C1B	0.82	0.0001	20.93	69	1
4C2A	82.0	0.01	20.99	69	1
4C2B	82.0	0.01	20.93	69	1
Total					15

Table 3.6

Average Mechanical Properties of 35XF Sheet Steel used in the Experimental Study Under Different Strain Rates[1-2]

Strain Rate in./in./sec.	$(F_y)_c$ (ksi)	$(F_{pr})_c$ (ksi)	$(F_y)_t$ (ksi)	$(F_u)_t$ (ksi)	Elongation (%)
0.0001	29.83	17.79	32.87	49.35	38.90
0.01	31.92	20.03	36.40	51.76	36.80
1.0	36.91	*****	42.37	56.63	40.90

Notes:

1) For other material properties, see Refs. 1 and 2

2) $(F_y)_c$ and $(F_{pr})_c$ are based on longitudinal compression coupon tests.

3) $(F_y)_t$ and $(F_u)_t$ and Elongation are determined from longitudinal tension coupon tests.

4) Elongation was measured by using a 2-in. gage length.

Table 3.7

Dimensions of Beam Specimens with Stiffened Flanges

Fabricated from 35XF Sheet Steel

Specimen	BC (in.)	D (in.)	BT (in.)	t	w/t (in.)	L (in.)	P_u (kips)
3A0A	2.960	1.510	1.010	0.085	29.15	43.00	5.69
3A1A	3.033	1.462	1.012	0.085	30.00	43.00	5.43
3A1B	3.020	1.477	1.017	0.085	29.85	43.00	5.72
3A2A	2.952	1.515	1.020	0.085	29.05	43.00	6.31
3A2B	3.047	1.470	1.012	0.085	30.17	43.00	6.39
3B0A	5.235	2.445	1.235	0.085	55.91	73.00	6.38
3B1A	5.167	2.460	1.255	0.085	55.11	73.00	6.54
3B1B	5.235	2.435	1.230	0.085	55.91	73.00	6.49
3B2A	5.227	2.435	1.220	0.085	55.82	73.00	6.97
3B2B	5.240	2.440	1.232	0.085	55.97	73.00	7.63
3C0A	6.957	2.926	1.490	0.085	76.17	91.00	6.53
3C1A	6.997	2.947	1.483	0.085	76.64	91.00	6.99
3C1B	6.991	2.954	1.481	0.085	76.57	91.00	6.96
3C2A	6.995	2.934	1.483	0.085	76.62	91.00	7.45
3C2B	6.945	2.945	1.485	0.085	76.03	91.00	7.42

Table 3.8

The CAMAC Frequencies and the

Corresponding Sampling Rates

Frequency Number	Reading Per Seconds
0	5
1	10
2	25
3	50
4	100
5	250
6	500
7	1000
8	2500
9	5000
10	10000
11	25000

Table 3.9

Dimensions of Stub Columns with Stiffened Flanges

Fabricated from 35XF Sheet Steel

Specimen	BF (in.)	BW (in.)	BL (in.)	w/t	Gross Area ($in.^2$)	L (in.)	P_u (kips)
1A1A	2.790	1.492	0.916	27.15	1.2060	12.03	46.12
1A1B	2.811	1.482	0.915	27.39	1.2060	12.02	44.89
1A2A	2.771	1.484	0.918	26.92	1.2010	12.03	50.02
1A2B	2.783	1.482	0.916	27.06	1.2060	12.03	49.29
1A3A	2.804	1.470	0.916	27.31	1.2009	12.03	53.54
1A3B	2.812	1.467	0.915	27.40	1.2009	12.03	54.37
1B1A	3.792	1.990	0.922	38.93	1.5477	14.99	49.19
1B1B	3.812	1.985	0.918	39.17	1.5480	13.97	53.54
1B2A	3.786	1.978	0.918	38.86	1.5412	13.84	56.28
1B2B	3.806	1.982	0.919	39.10	1.5463	13.94	57.01
1B3A	3.786	1.992	0.919	38.86	1.5463	13.84	64.78
1B3B	3.794	1.982	0.918	38.96	1.5440	13.94	60.87
1C1A	4.961	2.523	0.919	52.69	1.9266	15.06	56.76
1C1B	4.984	2.513	0.922	52.96	1.9282	15.06	56.52
1C2A	4.920	2.524	0.920	52.20	1.9203	14.81	61.02
1C2B	4.993	2.519	0.922	53.06	1.9317	15.12	64.58
1C3A	5.000	2.526	0.919	53.15	1.9343	15.09	73.96
1C3B	5.021	2.510	0.922	53.39	1.9334	15.00	69.27

Table 3.10

Dimensions of Beam Specimens with Unstiffened Flanges

Fabricated from 35XF Sheet Steel

Specimen	BC (in.)	D (in.)	t (in.)	w/t	L (in.)	P_u (kips)
4A0A	1.030	2.020	0.085	9.28	37.00	6.41
4A1A	1.020	2.007	0.085	9.16	37.00	7.15
4A1B	1.020	2.025	0.085	9.16	37.00	7.18
4A2A	1.025	2.012	0.085	9.22	37.00	7.53
4A2B	1.009	2.020	0.085	9.03	37.00	7.63
4B0A	1.527	2.517	0.085	15.13	43.00	9.77
4B1A	1.530	2.510	0.085	15.16	43.00	10.12
4B1B	1.510	2.530	0.085	14.93	43.00	9.87
4B2A	1.520	2.520	0.085	15.04	43.00	10.97
4B2B	1.530	2.510	0.085	15.16	43.00	10.98
4C0A	2.020	3.020	0.085	20.93	65.00	8.49
4C1B	2.025	3.010	0.085	20.99	65.00	8.83
4C1C	2.020	3.010	0.085	20.93	65.00	9.15
4C2A	2.025	3.030	0.085	20.99	65.00	10.23
4C2B	2.020	3.020	0.085	20.93	65.00	10.22

Table 3.11

Dimensions of Stub Columns with Unstiffened Flanges

Fabricated from 35XF Sheet Steel

Specimen	BC (in.)	D (in.)	w/t	Gross Area ($in.^2$)	L (in.)	P_u (kips)
2A1A	1.000	2.000	8.93	0.6220	7.90	25.26
2A1B	1.010	2.018	9.04	0.6285	7.97	25.35
2A2A	1.000	2.040	8.93	0.6288	7.95	26.04
2A2B	1.015	2.002	9.10	0.6275	7.94	27.70
2A3A	1.000	2.040	8.93	0.6288	7.98	31.41
2A3B	1.003	2.014	8.96	0.6254	7.94	29.41
2B1A	1.375	3.025	13.34	0.9238	9.95	34.20
2B1B	1.381	2.981	13.41	0.9184	9.97	34.20
2B2A	1.380	2.987	13.40	0.9190	9.96	36.30
2B2B	1.378	3.007	13.37	0.9217	9.94	37.52
2B3A	1.375	3.020	13.34	0.9229	10.01	41.67
2B3B	1.382	3.006	13.42	0.9229	9.99	42.70
2C0A	2.000	3.000	20.69	1.1320	14.00	36.30
2C1A	2.014	2.976	20.85	1.1327	14.00	37.23
2C1B	2.006	3.018	20.76	1.1371	13.94	37.66
2C2A	2.024	2.967	20.97	1.1346	14.09	41.28
2C2B	2.010	3.015	20.81	1.1380	13.95	41.52
2C3A	2.020	2.970	20.93	1.1337	14.06	47.92
2C3B	2.015	2.977	20.87	1.1332	13.91	46.16

Table 4.1

Comparison of Computed and Tested Critical Buckling Moments
Beam Specimens with a Stiffened Flange (Based on k=4.0)
35XF Sheet Steel

Specimen	S_{xc}	f_{cr}	$(P_{cr})_{test}$	L	$(M_{cr})_{comp}$	$(M_{cr})_{test}$	(6)/(5)
	($in.^3$)	(ksi)	(kips)	(in.)	(in.-kips)	(in.-kips)	
	(1)	(2)	(3)	(4)	(5)	(6)	(7)
3A0A	0.342	28.12	N/A	43.00	9.62	N/A	N/A
3A1A	0.335	28.02	N/A	43.00	9.39	N/A	N/A
3A1B	0.338	28.04	N/A	43.00	9.48	N/A	N/A
3A2A	0.343	30.22	N/A	43.00	10.36	N/A	N/A
3A2B	0.338	30.09	N/A	43.00	10.17	N/A	N/A
3B0A	1.011	23.55	5.833	73.00	23.81	26.61	1.117
3B1A	1.010	23.73	6.214	73.00	23.97	28.35	1.183
3B1B	1.005	23.55	5.774	73.00	23.67	26.34	1.113
3B2A	1.003	25.66	6.106	73.00	25.74	27.86	1.082
3B2B	1.009	25.63	N/A	73.00	25.86	N/A	N/A
3C0A	1.615	18.38	5.042	91.00	29.68	28.68	0.966
3C1A	1.635	18.16	5.291	91.00	29.69	30.10	1.014
3C1B	1.638	18.19	5.217	91.00	29.79	29.67	0.996
3C2A	1.626	18.17	5.823	91.00	29.54	33.12	1.121
3C2B	1.624	18.45	5.760	91.00	29.96	32.76	1.093
Mean							1.076
Standard Deviation							0.066

Table 4.2(a)

Comparison of Computed and Tested Yield Moments
Beam Specimens with a Stiffened Flange
35XF Sheet Steel
(Based on Static Yield Stress)

Specimen	S_e	F_y	$(P_y)_{test}$	L	$(M_y)_{comp}$	$(M_y)_{test}$	(6)/(5)
	($in.^3$)	(ksi)	(kips)	(in.)	(in.-kips)	(in.-kips)	
	(1)	(2)	(3)	(4)	(5)	(6)	(7)
3A0A	.268	32.02	3.773	43.00	8.58	10.14	1.182
3A1A	.258	32.02	3.936	43.00	8.25	10.58	1.282
3A1B	.262	32.02	4.137	43.00	8.39	11.12	1.325
3A2A	.271	32.02	4.799	43.00	8.68	12.90	1.486
3A2B	.260	32.02	4.844	43.00	8.32	13.02	1.565
3B0A	.635	32.02	5.824	73.00	20.32	26.57	1.307
3B1A	.646	32.02	4.894	73.00	20.69	22.33	1.079
3B1B	.629	32.02	5.668	73.00	20.15	25.86	1.283
3B2A	.626	32.02	6.511	73.00	20.04	29.71	1.482
3B2B	.632	32.02	7.130	73.00	20.23	32.53	1.608
3C0A	.924	32.02	6.038	91.00	29.58	34.34	1.161
3C1A	.930	32.02	6.825	91.00	29.79	38.82	1.303
3C1B	.932	32.02	6.112	91.00	29.86	34.76	1.164
3C2A	.925	32.02	6.873	91.00	29.61	39.09	1.320
3C2B	.930	32.02	6.684	91.00	29.78	38.01	1.276
Mean							1.321
Standard Deviation							0.148

Note :

S_e is the effective section modulus relative to tension flange

Table 4.2(b)

Comparison of Computed and Tested Yield Moments
Beam Specimens with a Stiffened Flange
35XF Sheet Steel
(Based on Dynamic Yield Stress)

Specimen	S_e	F_y	$(P_y)_{test}$	L	$(M_y)_{comp}$	$(M_y)_{test}$	(6)/(5)
	($in.^3$)	(ksi)	(kips)	(in.)	(in.-kips)	(in.-kips)	
	(1)	(2)	(3)	(4)	(5)	(6)	(7)
3A0A	.268	32.02	3.773	43.00	8.58	10.14	1.182
3A1A	.258	32.87	3.936	43.00	8.46	10.58	1.251
3A1B	.262	32.87	4.137	43.00	8.62	11.12	1.290
3A2A	.271	36.40	4.799	43.00	9.87	12.90	1.307
3A2B	.260	36.40	4.844	43.00	9.45	13.02	1.378
3B0A	.635	32.02	5.824	73.00	20.32	26.57	1.307
3B1A	.645	32.87	4.894	73.00	21.21	22.33	1.053
3B1B	.629	32.87	5.668	73.00	20.66	25.86	1.252
3B2A	.623	36.40	6.511	73.00	22.66	29.71	1.311
3B2B	.628	36.40	7.130	73.00	22.87	32.53	1.422
3C0A	.924	32.02	6.038	91.00	29.58	34.34	1.161
3C1A	.929	32.87	6.825	91.00	30.53	38.82	1.271
3C1B	.931	32.87	6.112	91.00	30.61	34.76	1.135
3C2A	.917	36.40	6.873	91.00	34.33	39.09	1.139
3C2B	.922	36.40	6.684	91.00	34.52	38.01	1.101
Mean							1.237
Standard Deviation							0.102

Note :

S_e is the effective section modulus relative to tension flange

Table 4.3(a)

Comparison of Computed and Tested Failure Moments Based on the Effective Width Formulas in the 1986 AISI Automotive Steel Design Manual for Beam Specimens with a Stiffened Flange
(35XF Sheet Steel)
(Based on Static Yield Stress)

Specimen	Strain Rate	F_y	$(P_u)_{test}$	L	$(M_u)_{comp}$	$(M_u)_{test}$	(6)/(5)
	(in./in./sec.)	(ksi)	(kips)	(in.)	(in.-kips)	(in.-kips)	
	(1)	(2)	(3)	(4)	(5)	(6)	(7)
3A0A	0.00001	32.02	5.69	43.00	10.73	15.29	1.425
3A1A	0.0001	32.02	5.43	43.00	10.33	14.59	1.412
3A1B	0.0001	32.02	5.72	43.00	10.49	15.37	1.465
3A2A	0.01	32.02	6.31	43.00	10.85	16.96	1.563
3A2B	0.01	32.02	6.39	43.00	10.41	17.17	1.649
3B0A	0.00001	32.02	6.38	73.00	25.41	29.11	1.146
3B1A	0.0001	32.02	6.54	73.00	25.86	29.84	1.154
3B1B	0.0001	32.02	6.49	73.00	25.17	29.61	1.037
3B2A	0.01	32.02	6.97	73.00	25.05	31.80	1.176
3B2B	0.01	32.02	7.63	73.00	25.29	34.81	1.376
3C0A	0.00001	32.02	6.53	91.00	36.98	37.14	1.004
3C1A	0.0001	32.02	6.99	91.00	37.22	39.75	1.068
3C1B	0.0001	32.02	6.96	91.00	37.30	39.58	1.061
3C2A	0.01	32.02	7.45	91.00	37.02	42.37	1.144
3C2B	0.01	32.02	7.42	91.00	37.22	42.20	1.134
Mean							1.254
Standard Deviation							0.200

Table 4.3(b)

Comparison of Computed and Tested Failure Moments Based on the Effective Width Formulas in the 1986 AISI Automotive Steel Design Manual for Beam Specimens with a Stiffened Flange (35XF Sheet Steel) (Based on Dynamic Yield Stress)

Specimen	Strain Rate (in./in./sec.) (1)	F_y (ksi) (2)	$(P_u)_{test}$ (kips) (3)	L (in.) (4)	$(M_u)_{comp}$ (in.-kips) (5)	$(M_u)_{test}$ (in.-kips) (6)	(6)/(5) (7)
3A0A	0.00001	32.02	5.69	43.00	10.73	15.29	1.425
3A1A	0.0001	32.87	5.43	43.00	10.57	14.59	1.380
3A1B	0.0001	32.87	5.72	43.00	10.77	15.37	1.427
3A2A	0.01	36.40	6.31	43.00	12.34	16.96	1.374
3A2B	0.01	36.40	6.39	43.00	11.81	17.17	1.454
3B0A	0.00001	32.02	6.38	73.00	25.40	29.11	1.146
3B1A	0.0001	32.87	6.54	73.00	26.51	29.84	1.126
3B1B	0.0001	32.87	6.49	73.00	25.82	29.61	1.147
3B2A	0.01	36.40	6.97	73.00	28.32	31.80	1.123
3B2B	0.01	36.40	7.63	73.00	28.59	34.81	1.217
3C0A	0.00001	32.02	6.53	91.00	36.97	37.14	1.004
3C1A	0.0001	32.87	6.99	91.00	38.16	39.75	1.042
3C1B	0.0001	32.87	6.96	91.00	38.26	39.58	1.034
3C2A	0.01	36.40	7.45	91.00	42.91	42.37	0.987
3C2B	0.01	36.40	7.42	91.00	43.15	42.20	0.978
Mean							1.191
Standard Deviation							0.169

Table 4.4

Average Tested Ultimate Moments for Hat-Beam Specimens with a Stiffened Flange (35XF Sheet Steel)

Strain Rate	Ultimate Moment, $(M_u)_{test}$, in.-kips		
in./in./sec.	w/t		
	29.62	56.09	76.08
0.00001	15.29	29.11	37.14
0.0001	14.98	29.72	39.66
0.01	17.06	33.30	42.28

Table 4.5

Average Ultimate Moment Ratios for Hat-Beam Specimens Having Stiffened Flanges (35XF Sheet Steel)

w/t	$(M_u)_0/(M_u)_1$	$(M_u)_2/(M_u)_1$
29.69	1.02	1.14
56.09	0.98	1.12
76.08	0.94	1.07

Notes :

$(M_u)_0$= Average ultimate moment for the hat-beam specimens tested at the strain rate of 0.00001 in./in./sec.

$(M_u)_1$= Average ultimate moment for the hat-beam specimens tested at the strain rate of 0.0001 in./in./sec.

$(M_u)_2$= Average ultimate moment for the hat-beam specimens tested at the strain rate of 0.01 in./in./sec.

Table 4.6

Comparison of Computed and Tested Critical Buckling Loads
Stub Columns with Stiffened Flanges (Based on k=4.0)
35XF Sheet Steel

Specimen	f_{cr} (ksi) (1)	$(P_{cr})_{comp}$ (kips) (2)	$(P_{cr})_{test}$ (kips) (3)	(3)/(2) (4)
1A1A	28.35	34.19	N/A	N/A
1A1B	28.32	34.15	N/A	N/A
1A2A	30.30	36.39	N/A	N/A
1A2B	30.28	36.52	N/A	N/A
1A3A	32.16	38.62	N/A	N/A
1A3B	32.15	38.61	N/A	N/A
1B1A	26.79	41.46	N/A	N/A
1B1B	26.75	41.41	N/A	N/A
1B2A	28.55	44.00	N/A	N/A
1B2B	28.51	44.08	N/A	N/A
1B3A	30.22	46.73	N/A	N/A
1B3B	30.20	46.63	N/A	N/A
1C1A	24.25	46.72	50.56	1.082
1C1B	24.20	46.66	50.90	1.091
1C2A	25.83	49.60	58.09	1.171
1C2B	25.63	49.51	55.94	1.130
1C3A	26.88	51.99	66.15	1.272
1C3B	26.81	51.83	65.51	1.264
Mean				1.168
Standard Deviation				0.076

Table 4.7(a)

Comparison of Computed and Tested Failure Loads Based on the Effective Width Formulas in the 1986 AISI Automotive Steel Design Manual for Stub Columns with Stiffened Flanges
(35XF Sheet Steel)
(Based on Static Yield Stress)

Spec.	Strain Rate (in./in./sec.)	w/t	F_y (ksi)	A_e (in.^{2})	$(P_u)_{comp}$ (kips)	$(P_u)_{test}$ (kips)	(6)/(5)
	(1)	(2)	(3)	(4)	(5)	(6)	(7)
1A1A	0.0001	27.15	29.83	1.2060	35.97	46.12	1.28
1A1B	0.0001	27.39	29.83	1.2060	35.97	44.89	1.25
1A2A	0.01	26.92	29.83	1.2010	35.82	50.02	1.40
1A2B	0.01	27.06	29.83	1.2010	35.82	49.29	1.38
1A3A	0.10	27.31	29.83	1.2009	35.82	53.54	1.49
1A3B	0.10	27.40	29.83	1.2009	35.82	54.37	1.52
1B1A	0.0001	38.93	29.83	1.5477	46.17	49.19	1.06
1B1B	0.0001	39.17	29.83	1.5480	46.18	53.54	1.16
1B2A	0.01	38.86	29.83	1.5412	45.97	56.28	1.22
1B2B	0.01	39.10	29.83	1.5463	46.13	57.01	1.23
1B3A	0.10	38.86	29.83	1.5463	46.13	64.78	1.40
1B3B	0.10	38.96	29.83	1.5440	46.06	60.87	1.32
1C1A	0.0001	52.69	29.83	1.8135	54.10	56.76	1.05
1C1B	0.0001	52.96	29.83	1.8122	54.06	56.52	1.05
1C2A	0.01	52.20	29.83	1.8122	54.06	61.02	1.13
1C2B	0.01	53.06	29.83	1.8147	54.13	64.58	1.19
1C3A	0.10	53.15	29.83	1.8164	54.18	73.96	1.36
1C3B	0.10	53.39	29.83	1.8130	54.08	69.27	1.28
Mean							1.265
Standard Deviation							0.139

Table 4.7(b)

Comparison of Computed and Tested Failure Loads Based on the Effective Width Formulas in the 1986 AISI Automotive Steel Design Manual for Stub Columns with Stiffened Flanges (35XF Sheet Steel) (Based on Dynamic Yield Stress)

Spec.	Strain Rate (in./in./sec.) (1)	w/t (2)	F_y (ksi) (3)	A_e ($in.^2$) (4)	$(P_u)_{comp}$ (kips) (5)	$(P_u)_{test}$ (kips) (6)	(6)/(5) (7)
1A1A	0.0001	27.15	29.83	1.2060	35.97	46.12	1.28
1A1B	0.0001	27.39	29.83	1.2060	35.97	44.89	1.25
1A2A	0.01	26.92	31.92	1.2010	38.33	50.02	1.30
1A2B	0.01	27.06	31.92	1.2010	38.35	49.29	1.29
1A3A	0.10	27.31	34.06	1.2009	40.90	53.54	1.31
1A3B	0.10	27.40	34.06	1.2009	40.90	54.37	1.33
1B1A	0.0001	38.93	29.83	1.5477	46.17	49.19	1.06
1B1B	0.0001	39.17	29.83	1.5480	46.18	53.54	1.16
1B2A	0.01	38.86	31.92	1.5412	49.20	56.28	1.14
1B2B	0.01	39.10	31.92	1.5449	49.31	57.01	1.16
1B3A	0.10	38.86	34.06	1.5372	52.36	64.78	1.24
1B3B	0.10	38.96	34.06	1.5340	52.25	60.87	1.16
1C1A	0.0001	52.69	29.83	1.8135	54.10	56.76	1.05
1C1B	0.0001	52.96	29.83	1.8122	54.06	56.52	1.05
1C2A	0.01	52.20	31.92	1.7977	57.38	61.02	1.06
1C2B	0.01	53.06	31.92	1.8000	57.46	64.58	1.12
1C3A	0.10	53.15	34.06	1.7875	60.88	73.96	1.21
1C3B	0.10	53.39	34.06	1.7840	60.76	69.27	1.14
Mean							1.184
Standard Deviation							0.093

Table 4.8

Average Tested Failure Loads for Stub Column Specimens with Stiffened Flanges (35XF Sheet Steel)

Strain Rate	Failure Load, $(P_u)_{test}$, kips		
in./in./sec.	w/t		
	26.67	38.44	53.15
0.0001	45.50	51.36	56.64
0.01	49.65	56.64	62.80
0.1	53.95	62.82	71.48

Table 4.9

Ratios of Average Ultimate Loads for Stub Column Specimens Having Stiffened Flanges (35XF Sheet Steel)

w/t	$(P_u)_2/(P_u)_1$	$(P_u)_3/(P_u)_1$
29.67	1.09	1.18
38.44	1.10	1.22
53.15	1.11	1.26

Notes :

$(P_u)_1$= Average ultimate load for stub column specimens tested at strain rate of 0.0001 in./in./sec.

$(P_u)_2$= Average ultimate load for stub column specimens tested at strain rate of 0.01 in./in./sec.

$(P_u)_3$= Average ultimate load for stub column specimens tested at strain rate of 0.1 in./in./sec.

Table 4.10

Comparison of Computed and Tested Critical Buckling Moments
Beam Specimens with Unstiffened Flanges (Based on k=0.43)
35XF Sheet Steel

Specimen	S_{xc} ($in.^3$) (1)	f_{cr} (ksi) (2)	$(P_{cr})_{test}$ (kips) (3)	L (in.) (4)	$(M_{cr})_{comp}$ (in.-kips) (5)	$(M_{cr})_{test}$ (in.-kips) (6)	(6)/(5) (7)
4A0A	0.384	28.22	N/A	37.00	10.84	N/A	N/A
4A1A	0.377	28.26	N/A	37.00	10.65	N/A	N/A
4A1B	0.382	28.26	N/A	37.00	10.79	N/A	N/A
4A2A	0.380	30.15	N/A	37.00	11.46	N/A	N/A
4A2B	0.377	30.23	N/A	37.00	11.40	N/A	N/A
4B0A	0.719	25.55	N/A	43.00	18.37	N/A	N/A
4B1A	0.717	25.53	N/A	43.00	18.30	N/A	N/A
4B1B	0.717	25.66	N/A	43.00	18.40	N/A	N/A
4B2A	0.717	27.22	N/A	43.00	19.52	N/A	N/A
4B2B	0.717	27.14	N/A	43.00	19.46	N/A	N/A
4C0A	1.153	21.64	8.22	65.00	24.95	33.39	1.338
4C1A	1.150	21.60	8.15	65.00	24.84	33.11	1.333
4C1B	1.148	21.64	8.63	65.00	24.84	35.06	1.411
4C2A	1.160	22.77	9.56	65.00	26.41	38.84	1.471
4C2B	1.153	22.82	9.52	65.00	26.31	38.67	1.470
Mean							1.405
Standard Deviation							0.060

Table 4.11(a)

Comparison of Computed and Tested Ultimate Moments
Beam Specimens with Unstiffened Flanges
35XF Sheet Steels
(Based on Static Yield Stress)

Specimen	S_e	F_y	$(P_u)_{test}$	L	$(M_y)_{comp}$	$(M_u)_{test}$	(6)/(5)
	($in.^3$)	(ksi)	(kips)	(in.)	(in.-kips)	(in.-kips)	
	(1)	(2)	(3)	(4)	(5)	(6)	(7)
4A0A	.3837	32.02	6.41	37.00	12.29	14.82	1.206
4A1A	.3772	32.02	7.15	37.00	12.08	16.53	1.369
4A1B	.3819	32.02	7.18	37.00	12.23	16.60	1.357
4A2A	.3801	32.02	7.53	37.00	12.17	17.41	1.430
4A2B	.3771	32.02	7.63	37.00	12.07	17.64	1.461
4B0A	.6788	32.02	9.77	43.00	21.73	26.26	1.208
4B1A	.6736	32.02	10.12	43.00	21.67	27.20	1.255
4B1B	.6772	32.02	9.87	43.00	21.78	26.52	1.218
4B2A	.6631	32.02	10.97	43.00	21.73	29.48	1.357
4B2B	.6613	32.02	10.98	43.00	21.67	29.51	1.361
4C0A	.9515	32.02	8.49	65.00	30.47	34.49	1.132
4C1A	.9428	32.02	8.83	65.00	30.35	35.87	1.182
4C1B	.9421	32.02	9.15	65.00	30.33	37.17	1.225
4C2A	.9311	32.02	10.23	65.00	30.62	41.56	1.357
4C2B	.9263	32.02	10.22	65.00	30.47	41.52	1.363
Mean							1.299
Standard Deviation							0.096

Table 4.11(b)

Comparison of Computed and Tested Ultimate Moments
Beam Specimens with Unstiffened Flanges
35XF Sheet Steels
(Based on Dynamic Yield Stress)

Specimen	S_e	F_y	$(P_u)_{test}$	L	$(M_y)_{comp}$	$(M_u)_{test}$	(6)/(5)
	($in.^3$)	(ksi)	(kips)	(in.)	(in.-kips)	(in.-kips)	
	(1)	(2)	(3)	(4)	(5)	(6)	(7)
4A0A	.3837	32.02	6.41	37.00	12.29	14.82	1.206
4A1A	.3772	32.87	7.15	37.00	12.40	16.53	1.333
4A1B	.3819	32.87	7.18	37.00	12.55	16.60	1.322
4A2A	.3801	36.40	7.53	37.00	13.83	17.41	1.259
4A2B	.3771	36.40	7.63	37.00	13.73	17.64	1.285
4B0A	.6788	32.02	9.77	43.00	21.73	26.26	1.208
4B1A	.6736	32.87	10.12	43.00	22.14	27.20	1.228
4B1B	.6772	32.87	9.87	43.00	22.26	26.52	1.191
4B2A	.6631	36.40	10.97	43.00	24.14	29.48	1.221
4B2B	.6613	36.40	10.98	43.00	24.07	29.51	1.226
4C0A	.9515	32.02	8.49	65.00	30.47	34.49	1.132
4C1A	.9428	32.87	8.83	65.00	30.99	35.87	1.157
4C1B	.9421	32.87	9.15	65.00	30.97	37.17	1.200
4C2A	.9311	36.40	10.23	65.00	33.89	41.56	1.226
4C2B	.9263	36.40	10.22	65.00	33.72	41.52	1.231
Mean							1.228
Standard Deviation							0.052

Table 4.12

Average Tested Failure Moments for Channel Beam Specimens with Unstiffened Flanges (35XF Sheet Steel)

Strain Rate	Failure Moment, $(M_u)_{test}$, in.-kips		
in./in./sec.	w/t		
	8.93	14.81	20.69
0.00001	14.82	26.26	34.49
0.0001	16.56	26.85	36.52
0.01	17.53	29.48	41.54

Table 4.13

Ratios of Average Ultimate Moments for Channel Beam Specimens Having Unstiffened Flanges (35XF Sheet Steel)

w/t	$(M_u)_0/(M_u)_1$	$(M_u)_2/(M_u)_1$
8.93	0.89	1.06
14.81	0.98	1.10
20.69	0.94	1.14

Notes :

$(M_u)_0$= Average ultimate moment for channel beam specimens tested at strain rate of 0.00001 in./in./sec.

$(M_u)_1$= Average ultimate moment for channel beam specimens tested at strain rate of 0.0001 in./in./sec.

$(M_u)_2$= Average ultimate moment for channel beam specimens tested at strain rate of 0.01 in./in./sec.

Table 4.14

Comparison of Computed and Tested Critical Buckling Loads
Stub Columns with Unstiffened Flanges (Based on k=0.43)
(35XF Sheet Steel)

Specimen	$(f_{cr})_{comp}$ (ksi) (1)	$(P_{cr})_{comp}$ (kips) (2)	$(P_{cr})_{test}$ (kips) (3)	(3)/(2) (4)
2A1A	28.34	17.63	N/A	N/A
2A1B	28.30	17.79	N/A	N/A
2A2A	30.26	19.03	N/A	N/A
2A2B	30.20	18.95	N/A	N/A
2A3A	32.17	20.23	N/A	N/A
2A3B	32.16	20.11	N/A	N/A
2B1A	26.50	24.48	N/A	N/A
2B1B	26.47	24.31	N/A	N/A
2B2A	28.19	25.91	N/A	N/A
2B2B	28.21	26.00	N/A	N/A
2B3A	29.85	27.55	N/A	N/A
2B3B	29.80	27.50	N/A	N/A
2C0A	21.81	24.69	35.42	1.434
2C1A	21.71	24.59	36.44	1.482
2C1B	21.78	24.77	36.44	1.471
2C2A	22.78	25.85	40.40	1.563
2C2B	22.92	26.08	40.35	1.547
2C3A	23.70	26.87	46.95	1.747
2C3B	23.76	26.92	44.38	1.648
Mean				1.556
Standard Deviation				0.102

Table 4.15(a)

Comparison of Computed and Tested Failure Loads Based on the Effective Width Formulas in the 1986 AISI Automotive Steel Design Manual for Stub Columns with Unstiffened Flanges (35XF Sheet Steels) (Based on Static Yield Stress)

Spec.	Strain Rate (in./in./sec.) (1)	w/t (2)	F_y (ksi) (3)	A_e ($in.^2$) (4)	$(P_u)_{comp}$ (kips) (5)	$(P_u)_{test}$ (kips) (6)	(6)/(5) (7)
2A1A	0.0001	8.93	29.83	.6220	18.55	25.26	1.36
2A1B	0.0001	9.04	29.83	.6285	18.75	25.35	1.35
2A2A	0.01	8.93	29.83	.6288	18.76	26.04	1.39
2A2B	0.01	9.10	29.83	.6275	18.72	27.70	1.48
2A3A	0.10	8.93	29.83	.6288	18.76	31.41	1.67
2A3B	0.10	8.96	29.83	.6254	18.65	29.41	1.58
2B1A	0.0001	13.34	29.83	.9216	27.49	34.20	1.24
2B1B	0.0001	13.41	29.83	.9151	27.30	34.20	1.25
2B2A	0.01	13.40	29.83	.9160	27.32	36.30	1.33
2B2B	0.01	13.37	29.83	.9191	27.42	37.52	1.37
2B3A	0.10	13.34	29.83	.9208	27.47	41.67	1.52
2B3B	0.10	13.42	29.83	.9195	27.43	42.70	1.56
2C0A	0.00001	20.69	29.83	.9825	29.31	36.30	1.24
2C1A	0.0001	20.85	29.83	.9793	29.21	37.23	1.27
2C1B	0.0001	20.76	29.83	.9860	29.41	37.66	1.28
2C2A	0.01	20.97	29.83	.9785	29.19	41.28	1.41
2C2B	0.01	20.81	29.83	.9857	29.40	41.52	1.41
2C3A	0.10	20.93	29.83	.9787	29.19	47.92	1.64
2C3B	0.10	20.87	29.83	.9796	29.22	46.16	1.58
Mean							1.417
Standard Deviation							0.136

Table 4.15(b)

Comparison of Computed and Tested Failure Loads Based on the Effective Width Formulas in the 1986 AISI Automotive Steel Design Manual for Stub Columns with Unstiffened Flanges (35XF Sheet Steels) (Based on Dynamic Yield Stress)

Spec.	Strain Rate (in./in./sec.)	w/t	F_y (ksi)	A_e ($in.^2$)	$(P_u)_{comp}$ (kips)	$(P_u)_{test}$ (kips)	(6)/(5)
	(1)	(2)	(3)	(4)	(5)	(6)	(7)
2A1A	0.0001	8.93	29.83	.6220	18.55	25.26	1.36
2A1B	0.0001	9.04	29.83	.6285	18.75	25.35	1.35
2A2A	0.01	8.93	31.92	.6288	20.07	26.04	1.30
2A2B	0.01	9.10	31.92	.6275	20.03	27.70	1.38
2A3A	0.10	8.93	34.06	.6288	21.42	31.41	1.47
2A3B	0.10	8.96	34.06	.6254	21.30	29.41	1.38
2B1A	0.0001	13.34	29.83	.9216	27.49	34.20	1.24
2B1B	0.0001	13.41	29.83	.9151	27.30	34.20	1.25
2B2A	0.01	13.40	31.92	.9091	29.02	36.30	1.25
2B2B	0.01	13.37	31.92	.9122	29.12	37.52	1.29
2B3A	0.10	13.34	34.06	.9069	30.89	41.67	1.35
2B3B	0.10	13.42	34.06	.9049	30.82	42.70	1.38
2C0A	0.00001	20.69	29.77	.9828	29.26	36.30	1.24
2C1A	0.0001	20.85	29.83	.9793	29.21	37.23	1.27
2C1B	0.0001	20.76	29.83	.9859	29.41	37.66	1.28
2C2A	0.01	20.97	31.92	.9672	30.87	41.28	1.34
2C2B	0.01	20.81	31.92	.9745	31.11	41.52	1.33
2C3A	0.10	20.93	34.06	.9587	32.65	47.92	1.47
2C3B	0.10	20.87	34.06	.9637	32.82	46.16	1.41
Mean							1.334
Standard Deviation							0.070

Table 4.16

Average Tested Failure Loads for I-Shaped Stub Column Specimens with Unstiffened Flanges (35XF Sheet Steels)

Strain Rate	Failure Load, $(P_u)_{test}$, kips		
in./in./sec.	w/t		
	8.93	13.34	20.69
0.0001	25.30	34.20	37.44
0.01	26.87	36.91	41.40
0.1	30.41	42.18	47.04

Table 4.17

Ratios of Ultimate Loads for I-Shaped Stub Column Specimens Having Unstiffened Flanges (35XF Sheet Steels)

w/t	$(P_u)_2/(P_u)_1$	$(P_u)_3/(P_u)_1$
8.93	1.06	1.20
13.34	1.08	1.23
20.69	1.11	1.26

Note :

$(P_u)_1$= Average ultimate load for I-shaped stub column specimens tested at strain rate of 0.0001 in./in./sec.

$(P_u)_2$= Average ultimate load for I-shaped stub column specimens tested at strain rate of 0.01 in./in./sec.

$(P_u)_3$= Average ultimate load for I-shaped stub column specimens tested at strain rate of 0.1 in./in./sec.

Table 4.18

Deflections under Service Moments Based on Effective Sections for Hat-Beam Specimens with Stiffened Flanges (35XF Sheet Steel)

Specimen	$(M_s)_{test}$ (kips-in.) (1)	$(d)_{test}$ (in.) (2)	$(d)_{comp}$ (in.) (3)	(2)/(3) (4)
3B1A	12.73	0.1213	0.1658	0.732
3B1B	12.40	0.1319	0.1661	0.794
3B2A	13.60	0.1350	0.1830	0.738
3B2B	13.72	0.1396	0.1827	0.764
3C0A	17.75	0.1518	0.2003	0.758
3C1A	18.32	0.1974	0.2037	0.969
3C1B	18.37	0.2002	0.2033	0.985
3C2A	20.60	0.1835	0.2329	0.788
3C2B	20.71	0.1727	0.2325	0.743
Mean				0.808
Standard Deviation				0.093

Table 4.19

Deflections under Service Moments Based on Effective Sections for Channel Beam Specimens with Unstiffened Flanges (35XF Sheet Steel)

Specimen	$(M_s)_{test}$ (kips-in.) (1)	$(d)_{test}$ (in.) (2)	$(d)_{comp}$ (in.) (3)	(2)/(3) (4)
4A0A	7.37	0.0639	0.0620	1.031
4A1A	7.44	0.0609	0.0641	0.950
4A1B	7.53	0.0715	0.0649	1.102
4A2A	8.30	0.0542	0.0708	0.765
4A2B	8.24	0.0471	0.0706	0.667
4B0A	13.04	0.0511	0.0635	0.805
4B1A	13.28	0.0491	0.0650	0.755
4B1B	13.36	0.0445	0.0649	0.701
4B2A	14.48	0.0588	0.0706	0.833
4B2B	14.44	0.0527	0.0707	0.745
4C0A	18.28	0.0929	0.1097	0.847
4C1A	18.59	0.0924	0.1126	0.821*
4C1B	18.58	0.0630	0.1127	0.559*
4C2A	20.33	0.0992	0.1227	0.808*
3C2B	20.23	0.0639	0.1232	0.519*
Mean				0.833
Standard Deviation				0.121

(*) This value was not considered in the calculation of mean and standard deviation because the LVDT which measured the midspan deflection was not functioning properly during the test.

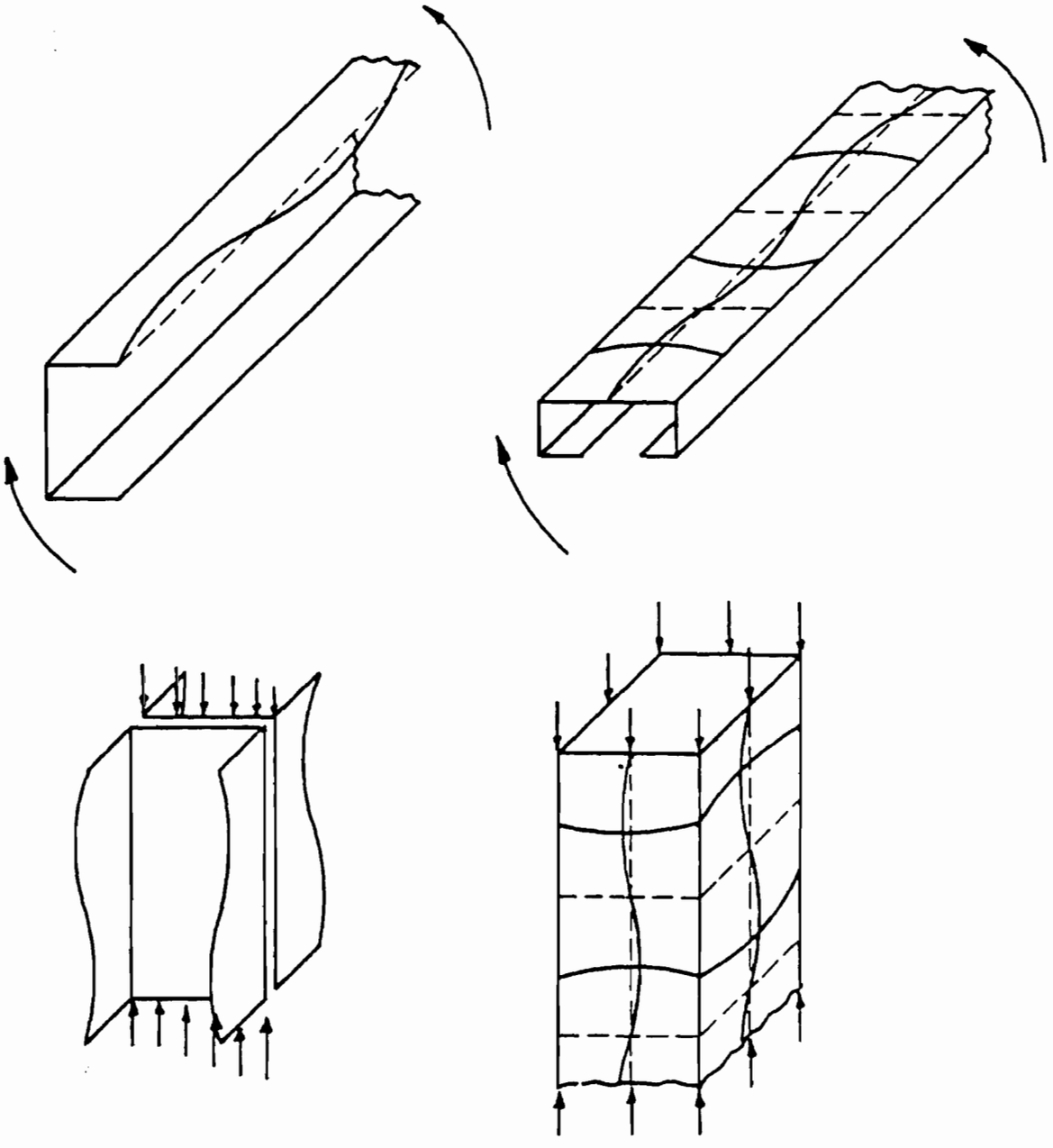

(a) Members with Unstiffened Compression Elements

(b) Members with Stiffened Compression Elements

Fig. 2.1 Structural Members with Stiffened and Unstiffened Elements [58]

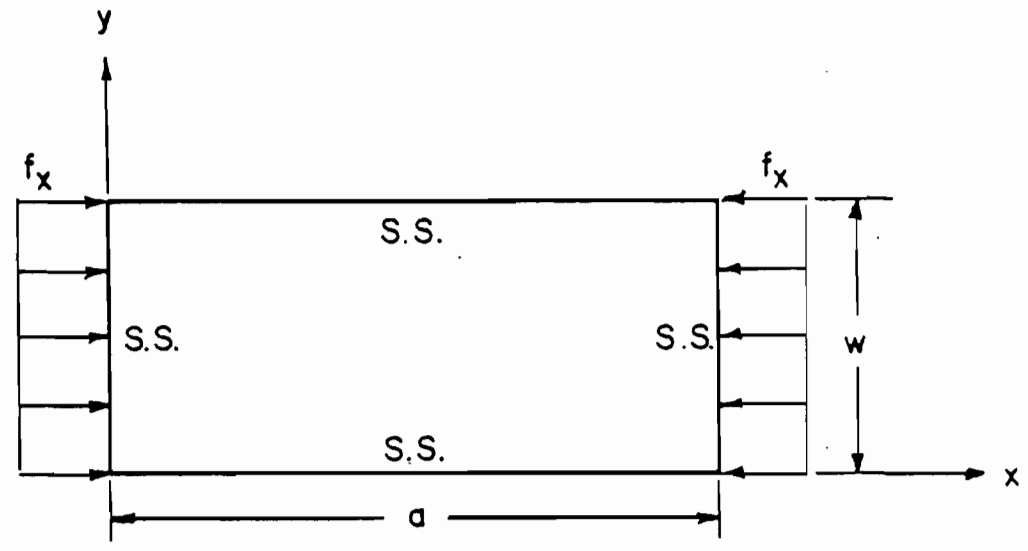

Figure 2.2 Rectangular Plate Simply Supported on Four Edges and Under Uniform Compression Stress [59]

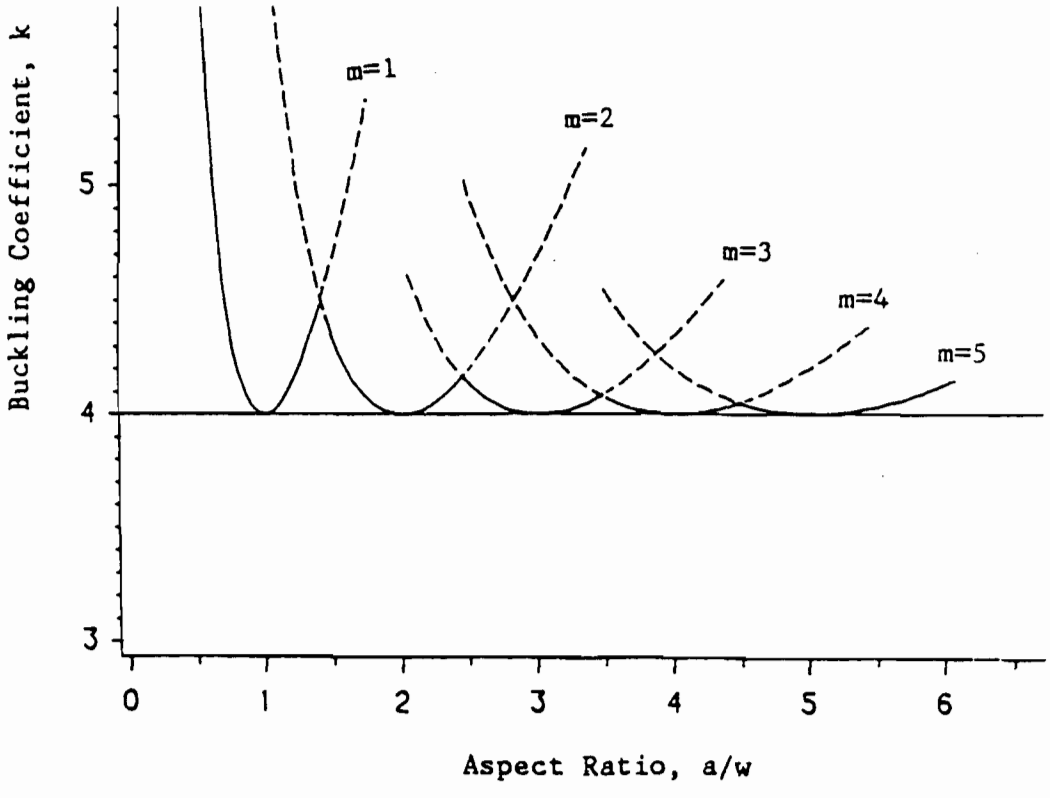

Figure 2.3 Buckling Coefficients for Flat Rectangular Stiffened Plates [59]

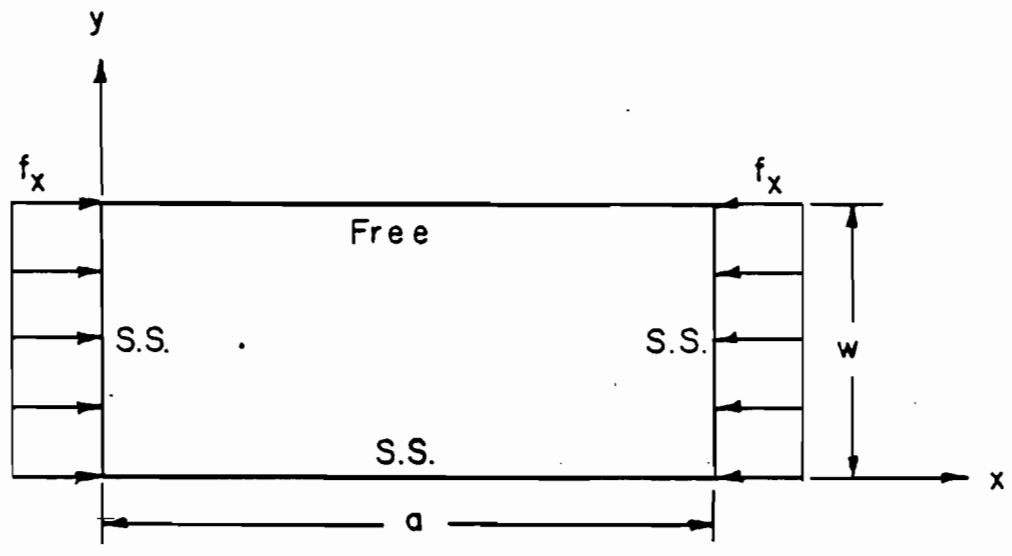

Figure 2.4 Rectangular Plate Simply Supported on Three Edges and Under Uniform Compression Stress [60]

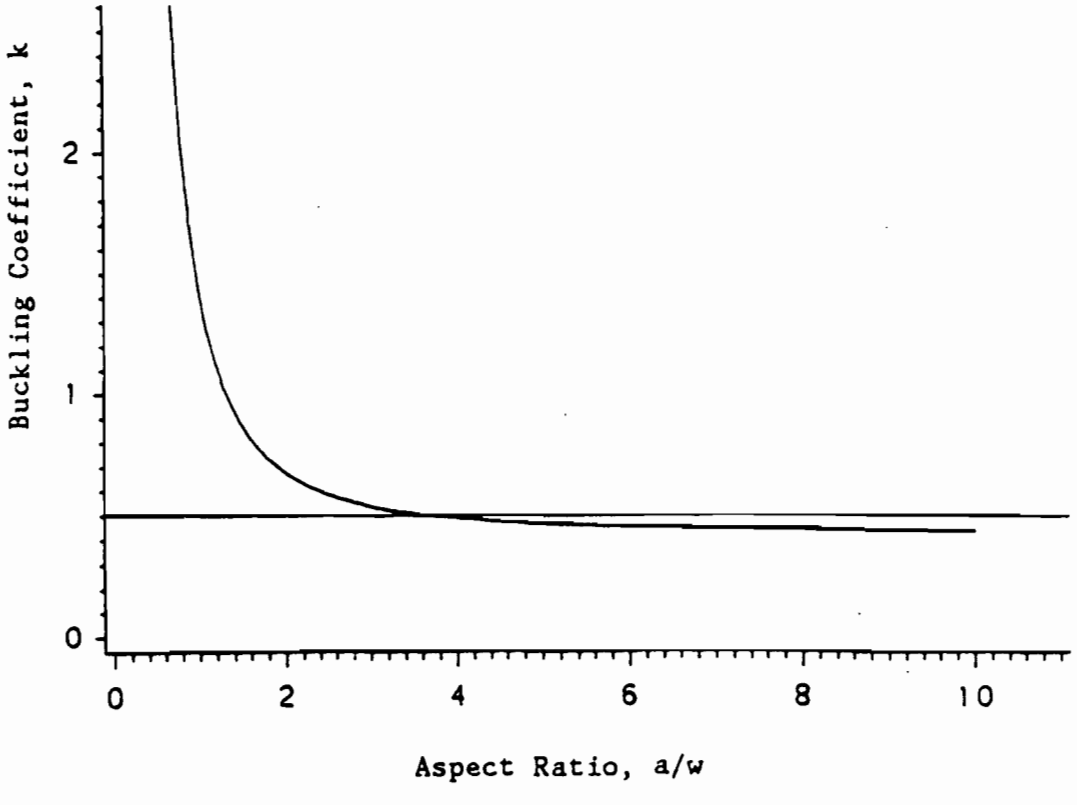

Figure 2.5 Buckling Coefficients for Flat Rectangular Unstiffened Plates [60]

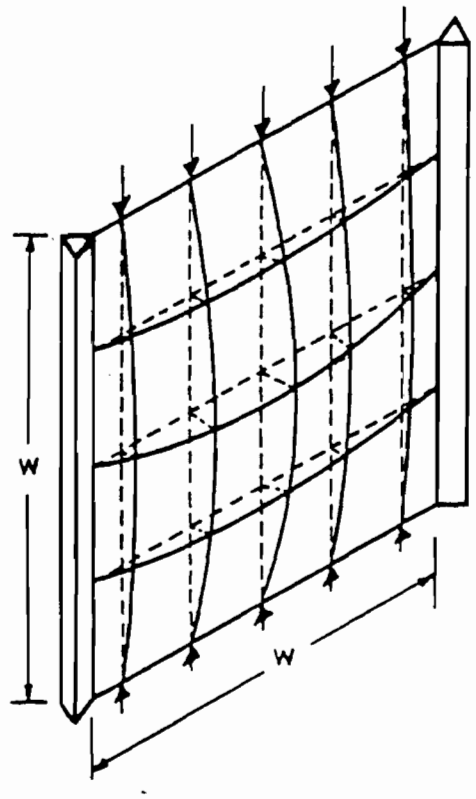

Fig. 2.6 Strut and Bar Grid Model Simply Supported Along Its Edges and Subjected to End Loading[58]

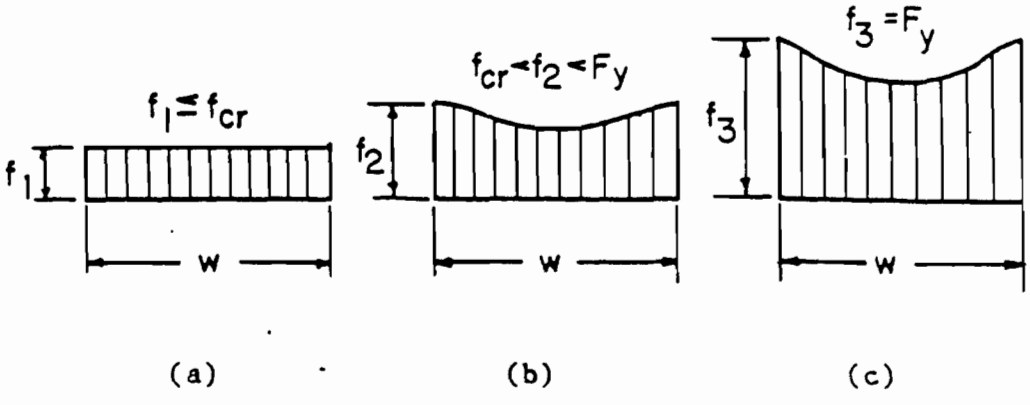

Fig. 2.7 Consecutive Stages of Stress Distribution in Stiffened Compression Elements[58]

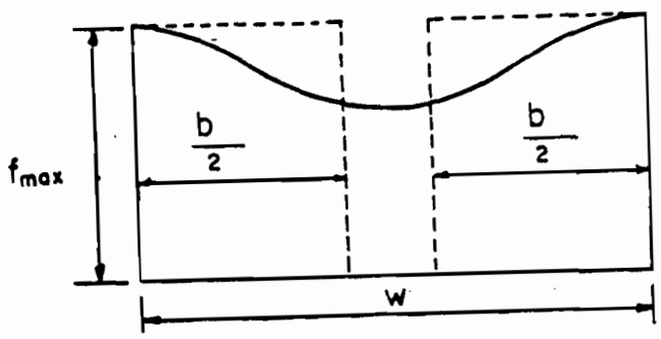

Fig. 2.8 Effective Design Width of a Stiffened Compression Element [58]

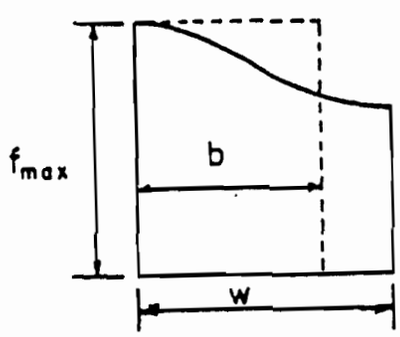

Fig. 2.9 Effective Design Width of an Unstiffened Compression Element [58]

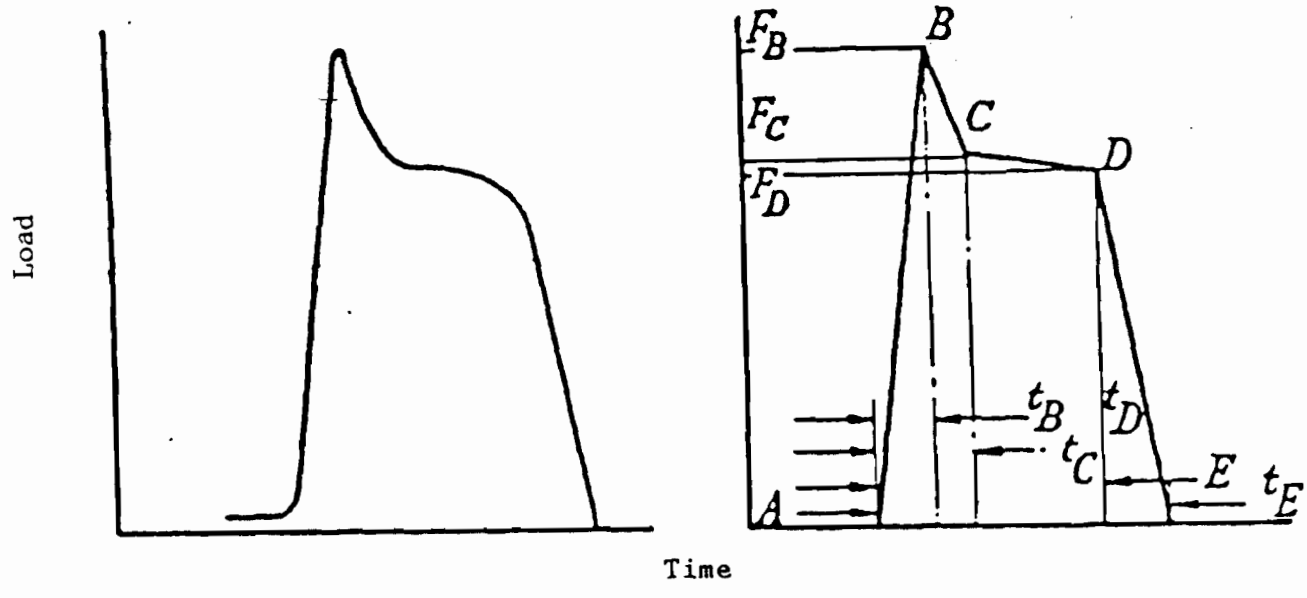

a) Typical Pulse

b) Assumed Shape

Fig. 2.10 Recorded Load Time Pulse [35]

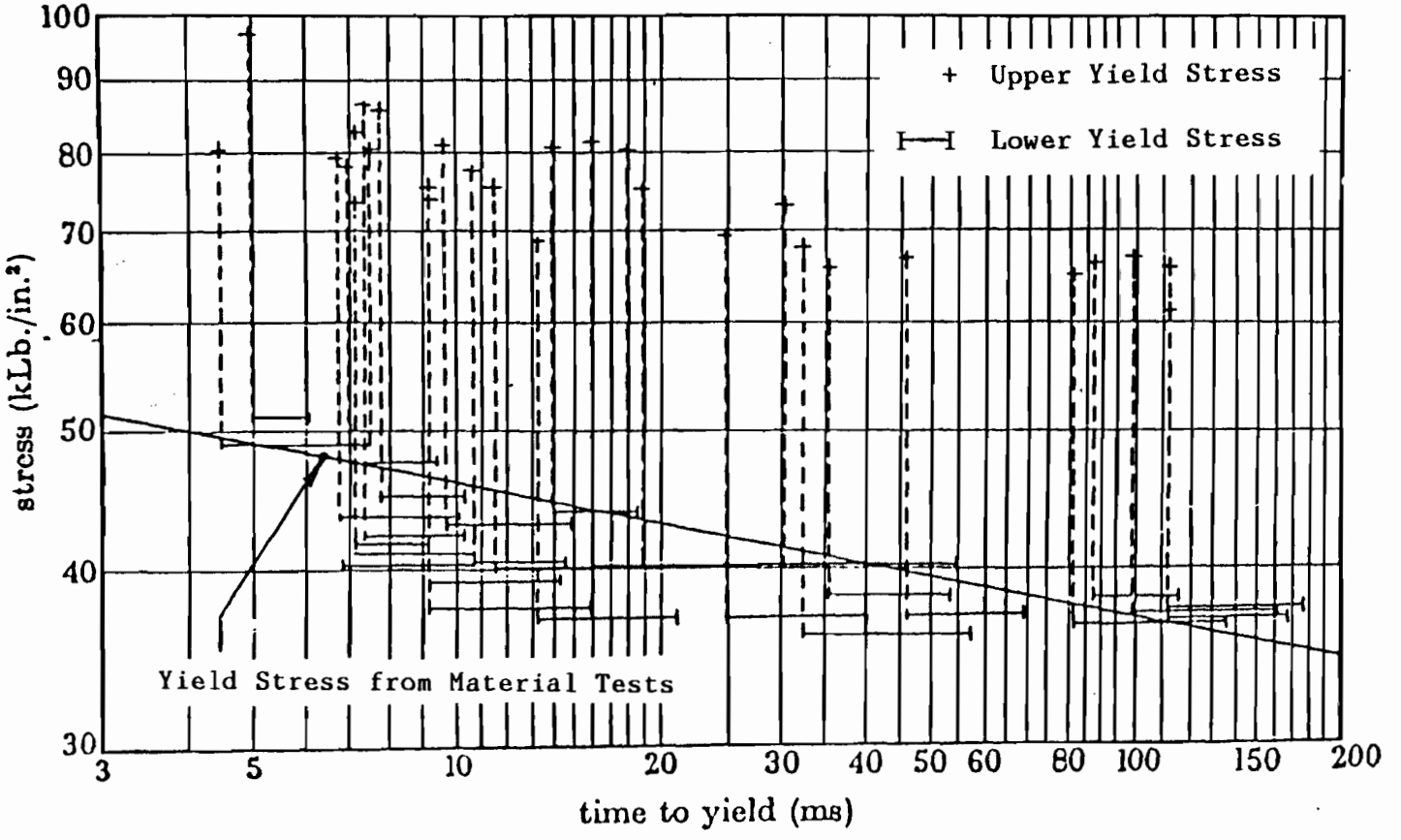

Fig. 2.11 Yield Stresses vs. Time to Yield [35]

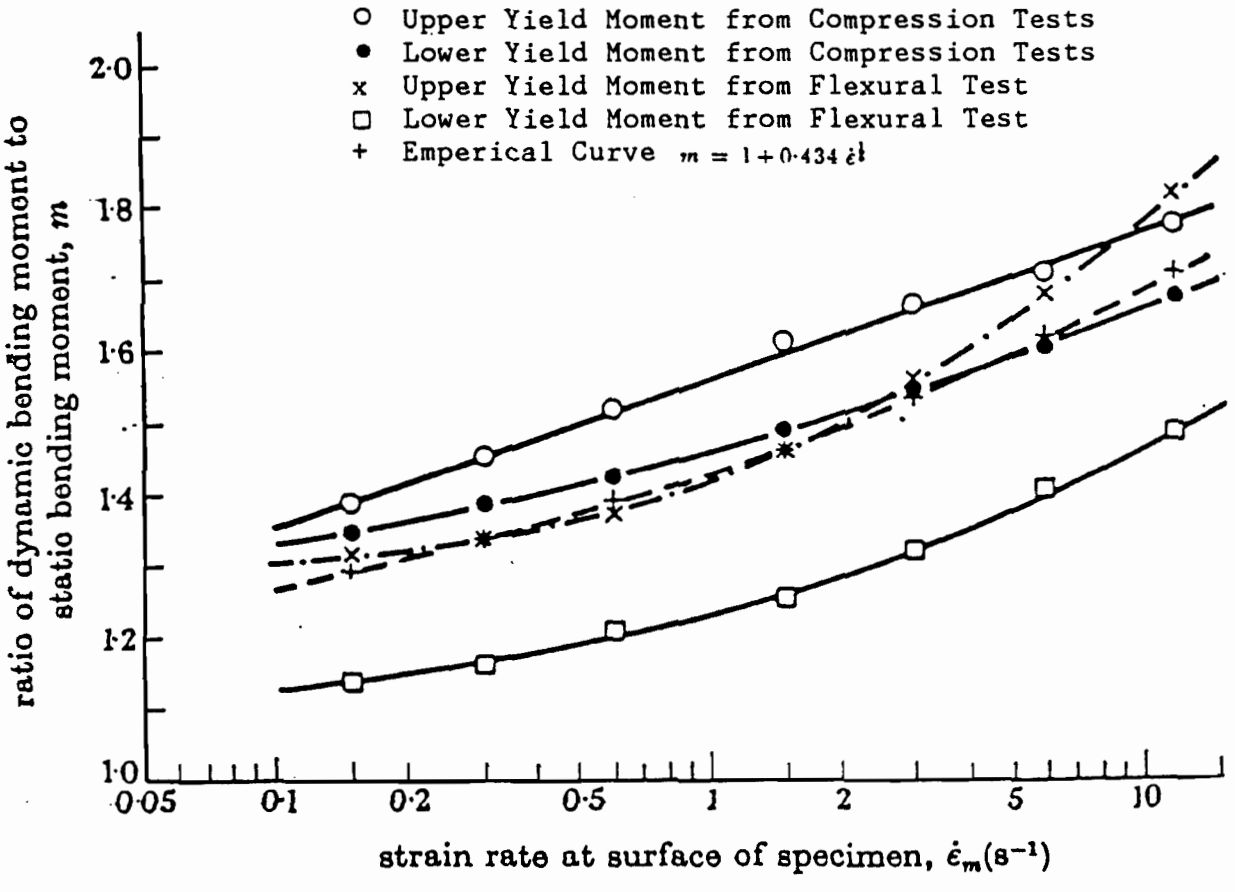

Fig. 2.12 Variation of Upper and Lower Yield Moments with Strain Rate at Surface of Specimen [40]

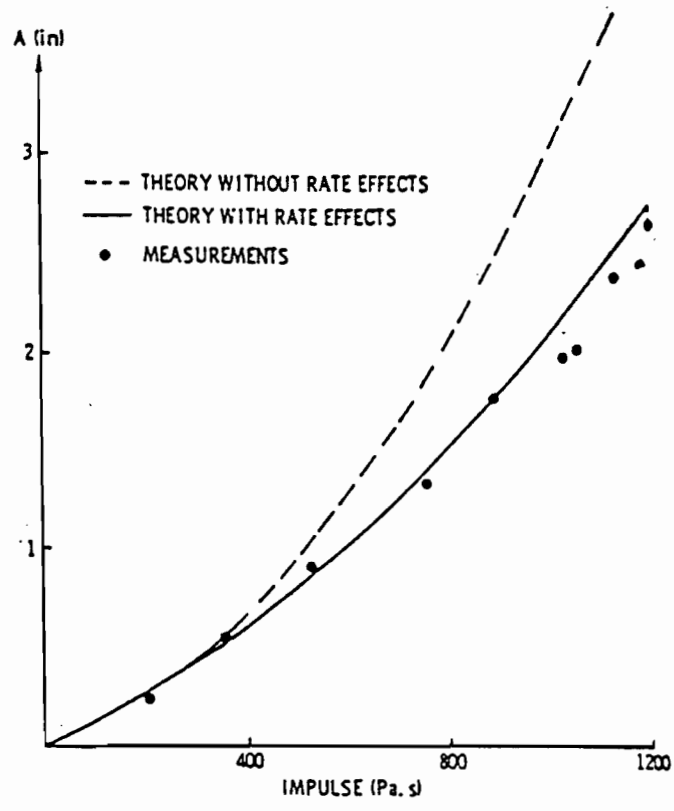

a) AISI 1018 Steel Beams [45]

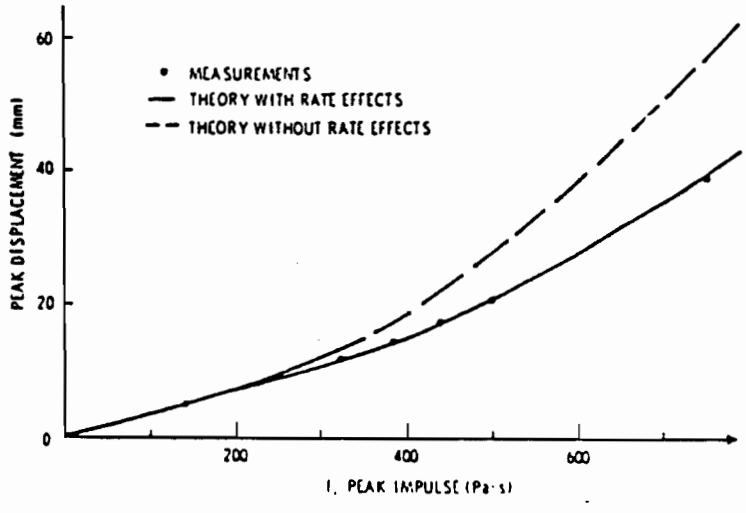

b) Type 304 Stainless Steel Beams [44]

Fig. 2.13 Peak Displacement Versus Impulse

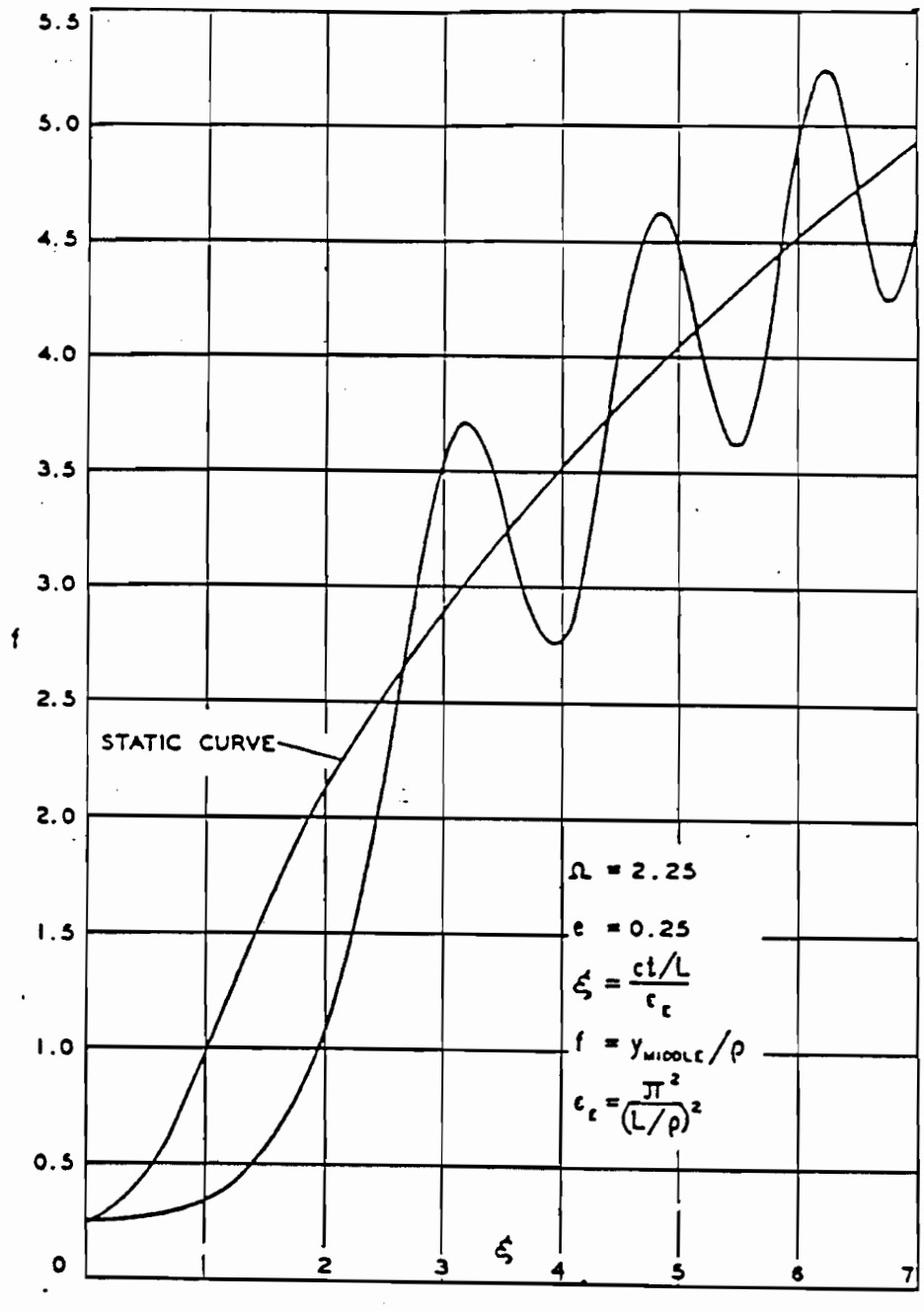

Fig. 2.14 Deflection of Mid-Point of Column [47]

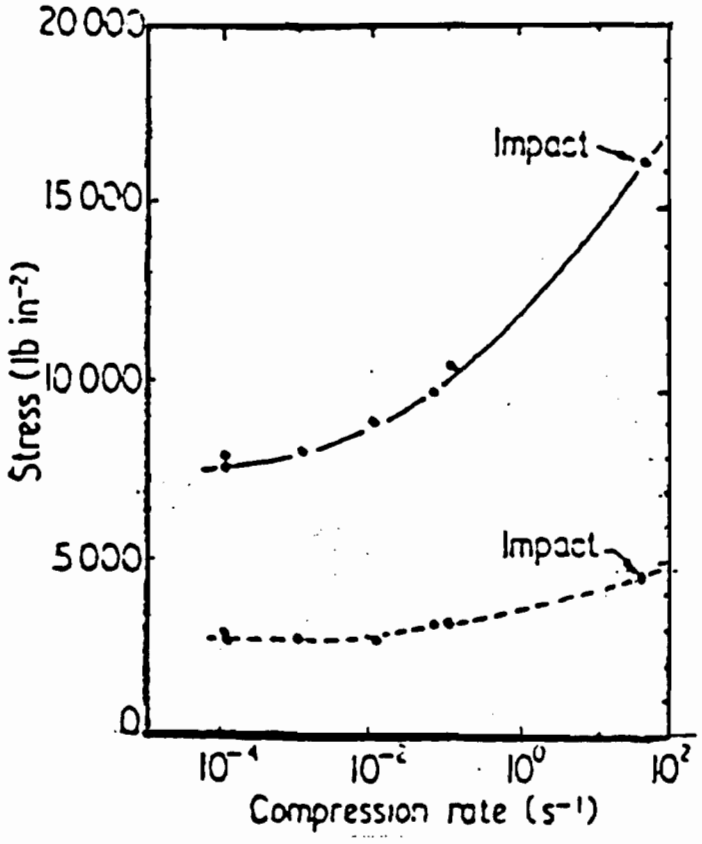

Fig. 2.15 Variation of First Maximum Stress (Solid Curve) and Mean Post-Buckling Stress (Broken Curve) with Compression Rate, for Column with t/D= 0.067 [51]

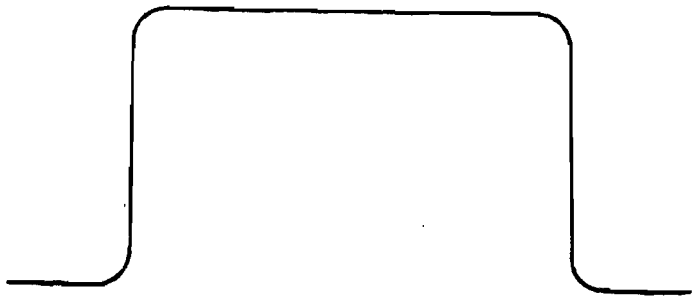

a. Beams

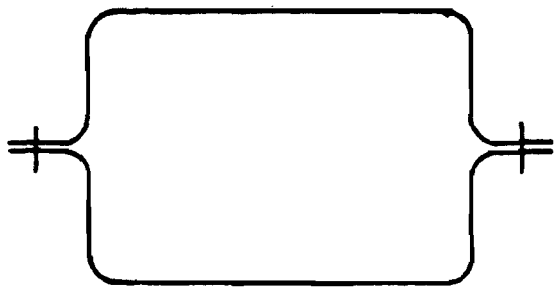

b. Stub Columns

Figure 3.1 Configurations of Test Specimens for Members Having Stiffened Compression Flanges

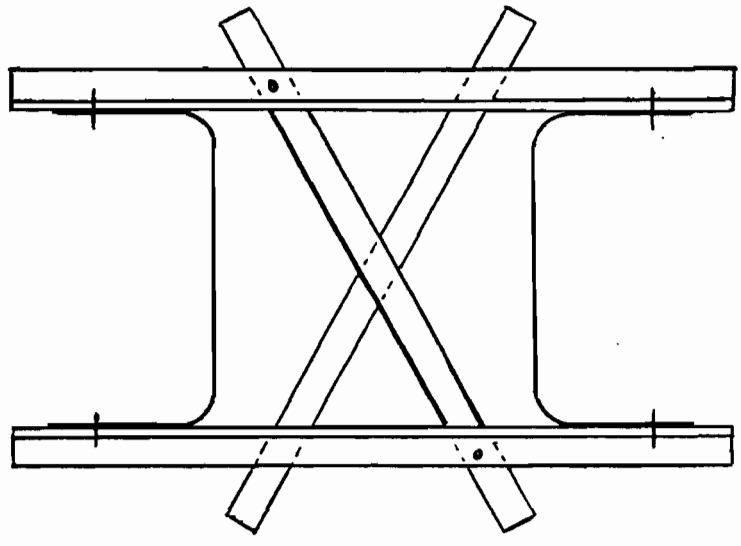

a. Beams

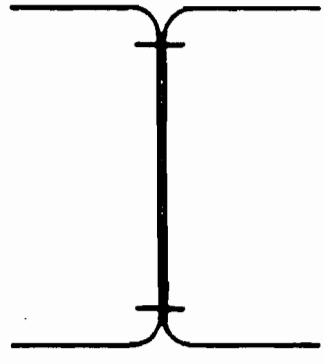

b. Stub Columns

Figure 3.2 Configurations of Test Specimens for Members Having Unstiffened Compression Flanges

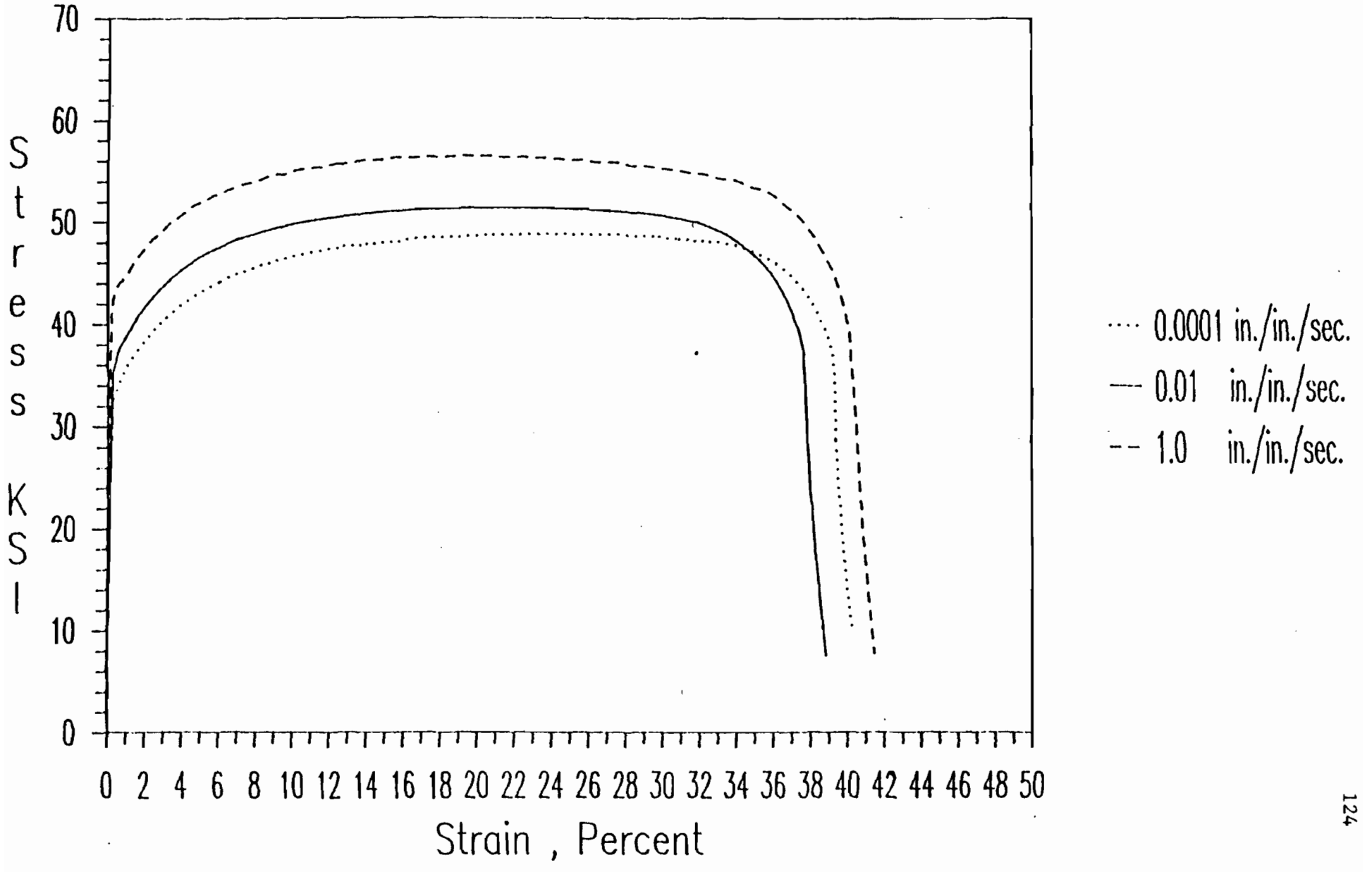

Figure 3.3 Stress-Strain Curves for 35XF Steel Tested Under Different Strain Rates, Longitudinal Tension[1]

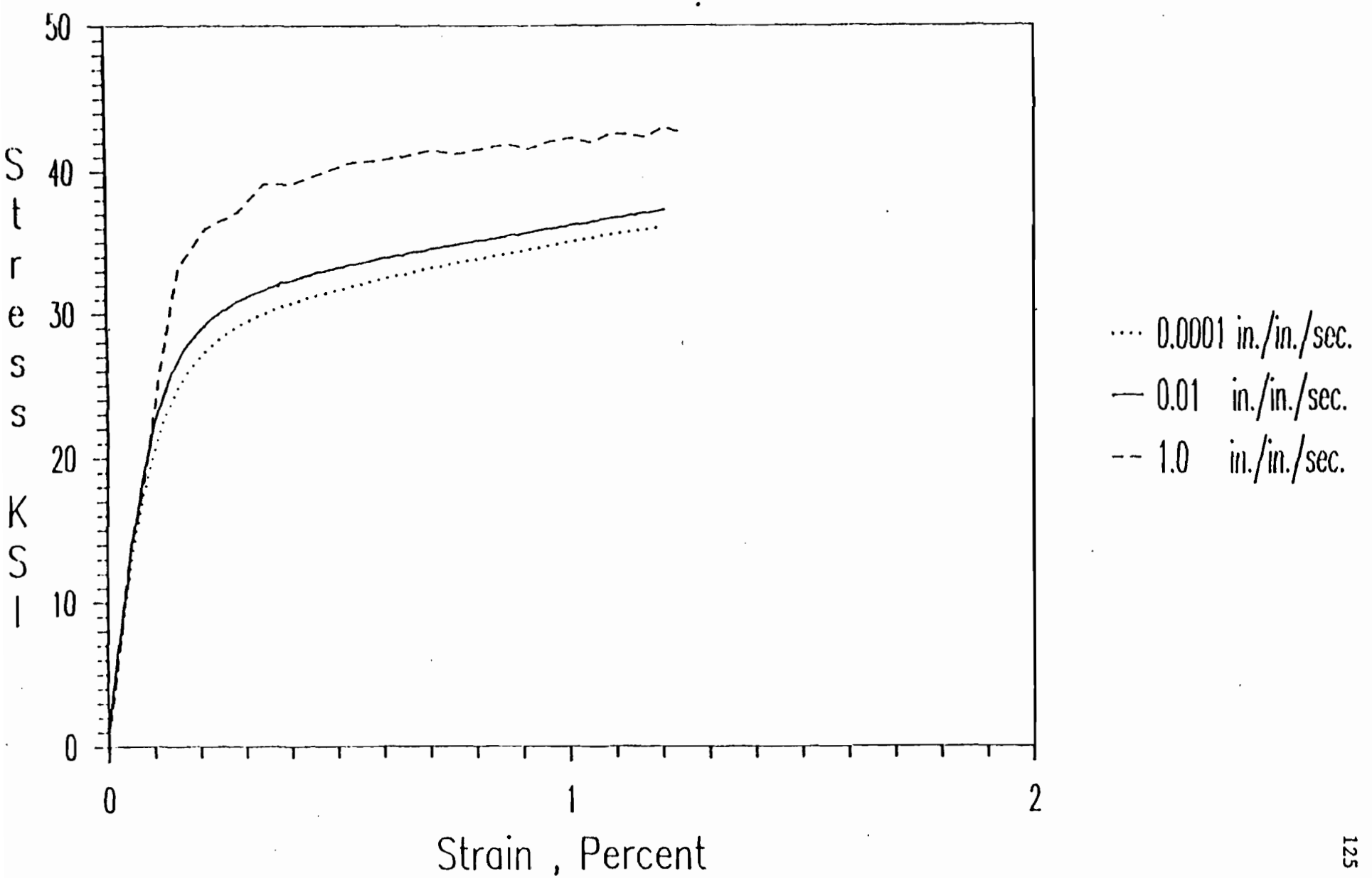

Figure 3.4 Stress-Strain Curves for 35XF Steel Tested Under Different Strain Rates, Longitudinal Compression[2]

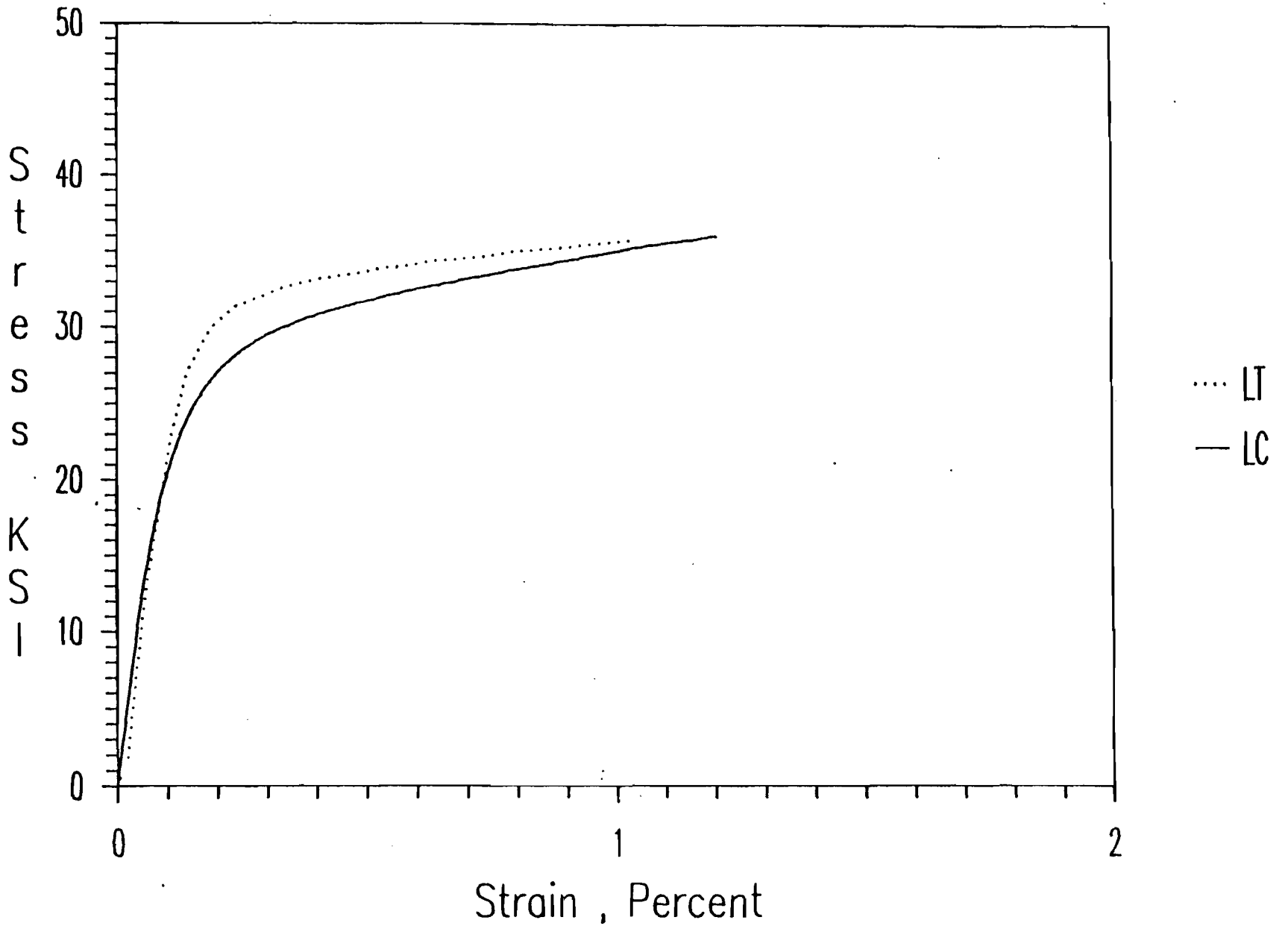

Figure 3.5 Comparison of Stress-Strain Curves of Longitudinal Tension and Compression for 35XF Steel Under Strain Rate of 0.0001 in./in./sec.

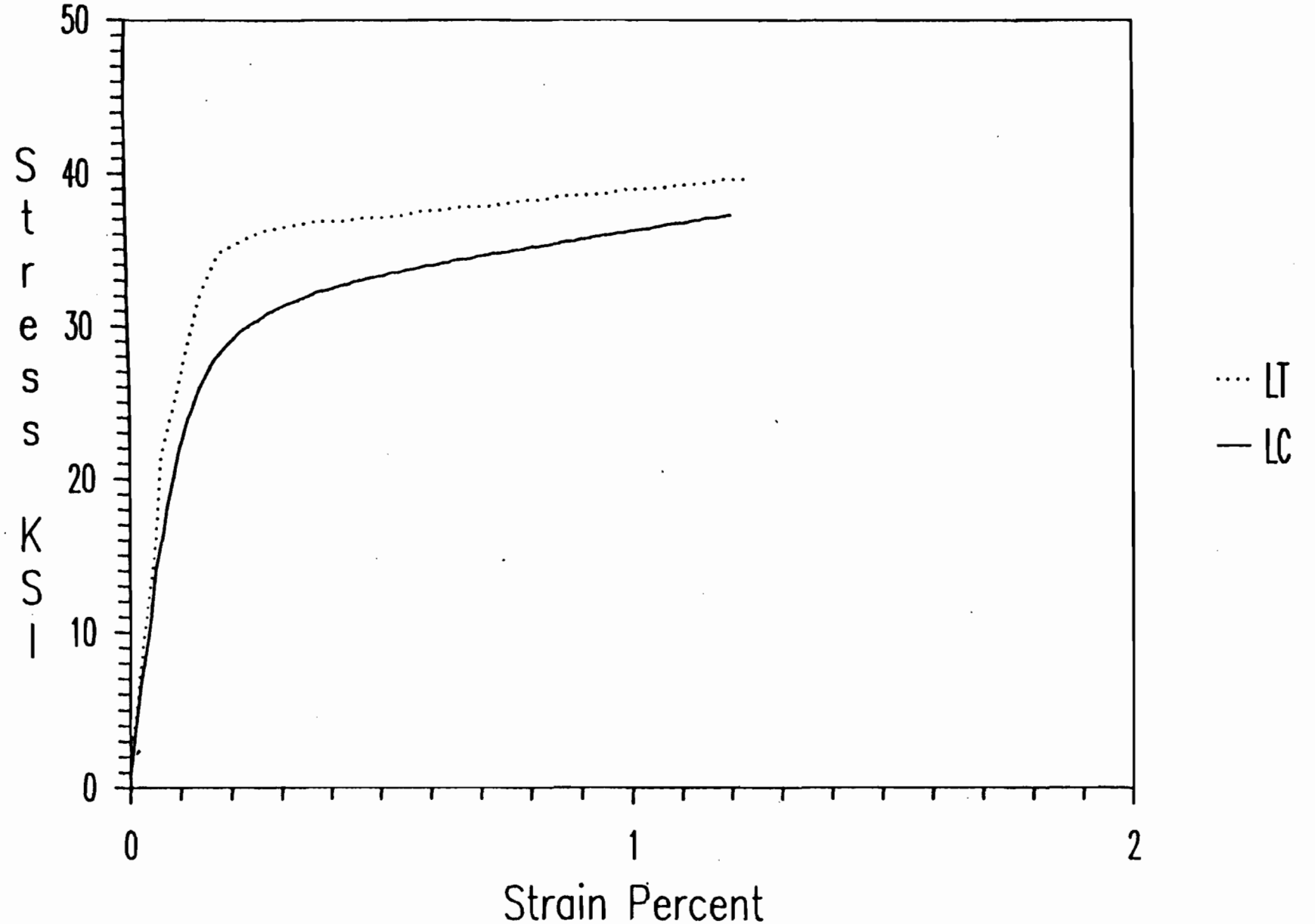

Figure 3.6 Comparison of Stress-Strain Curves of Longitudinal Tension and Compression for 35XF Steel Under Strain Rate of 0.01 in./in./sec.

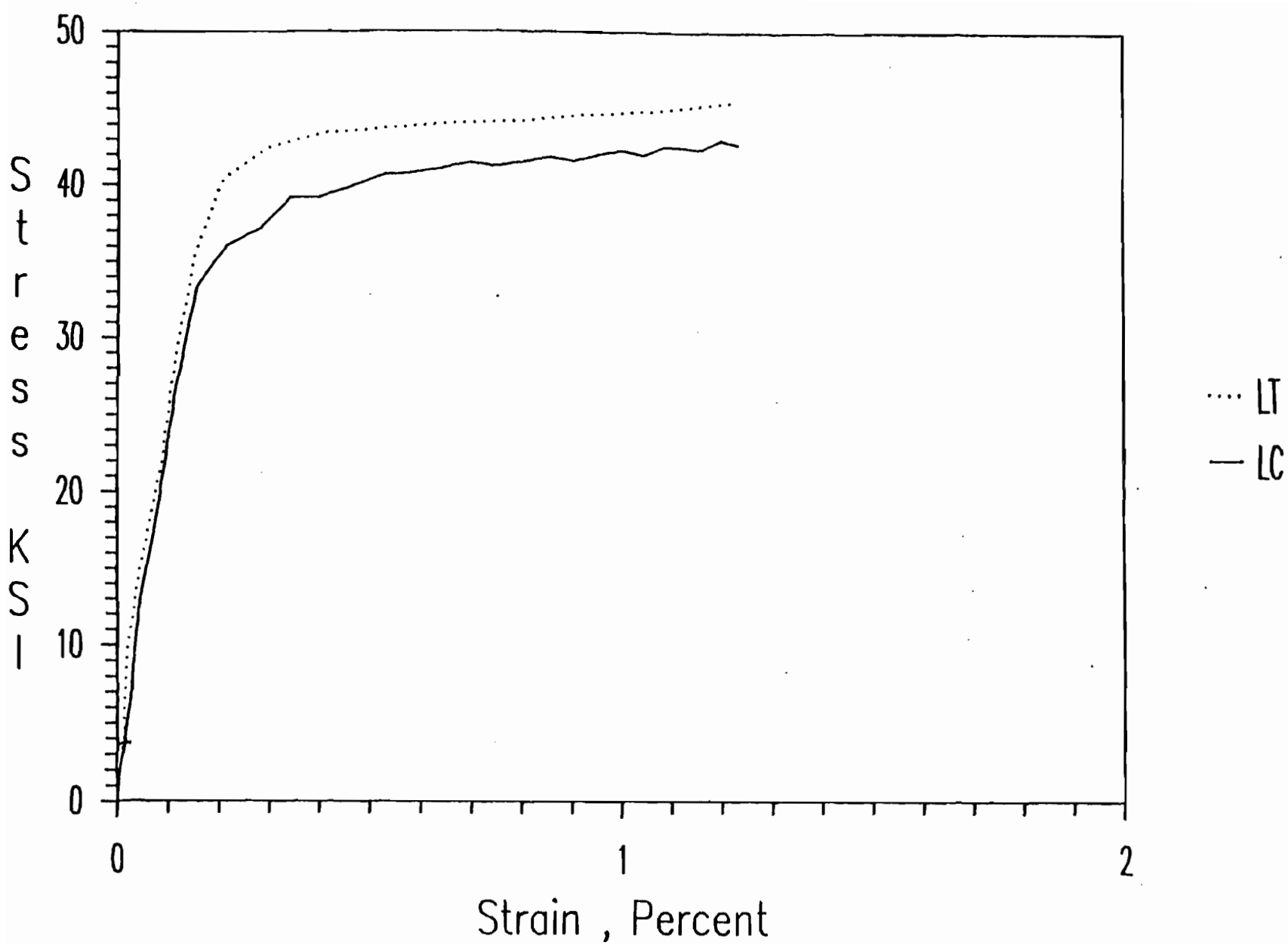

Figure 3.7 Comparison of Stress-Strain Curves of Longitudinal Tension and Compression for 35XF Steel Under Strain Rate of 1.0 in./in./sec.

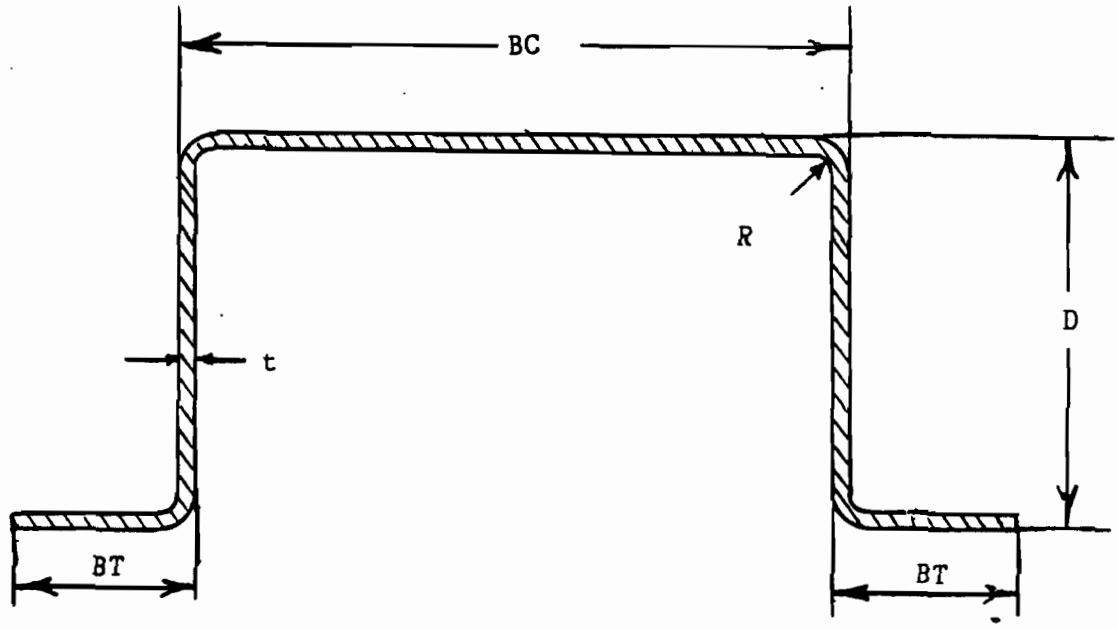

Figure 3.8 Hat Sections Used for Beam Tests

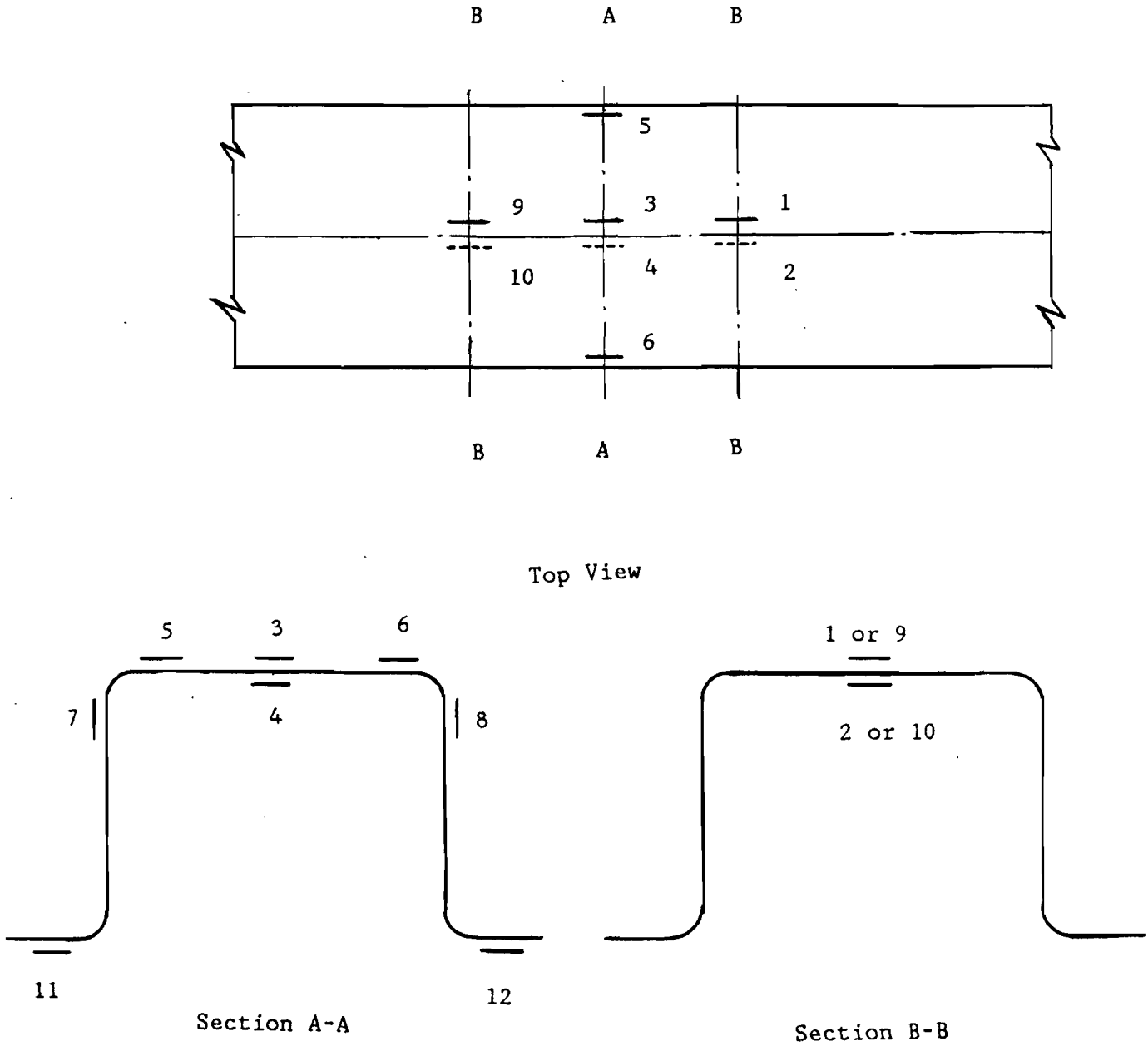

Figure 3.9 Locations of Strain Gages on Hat Sections

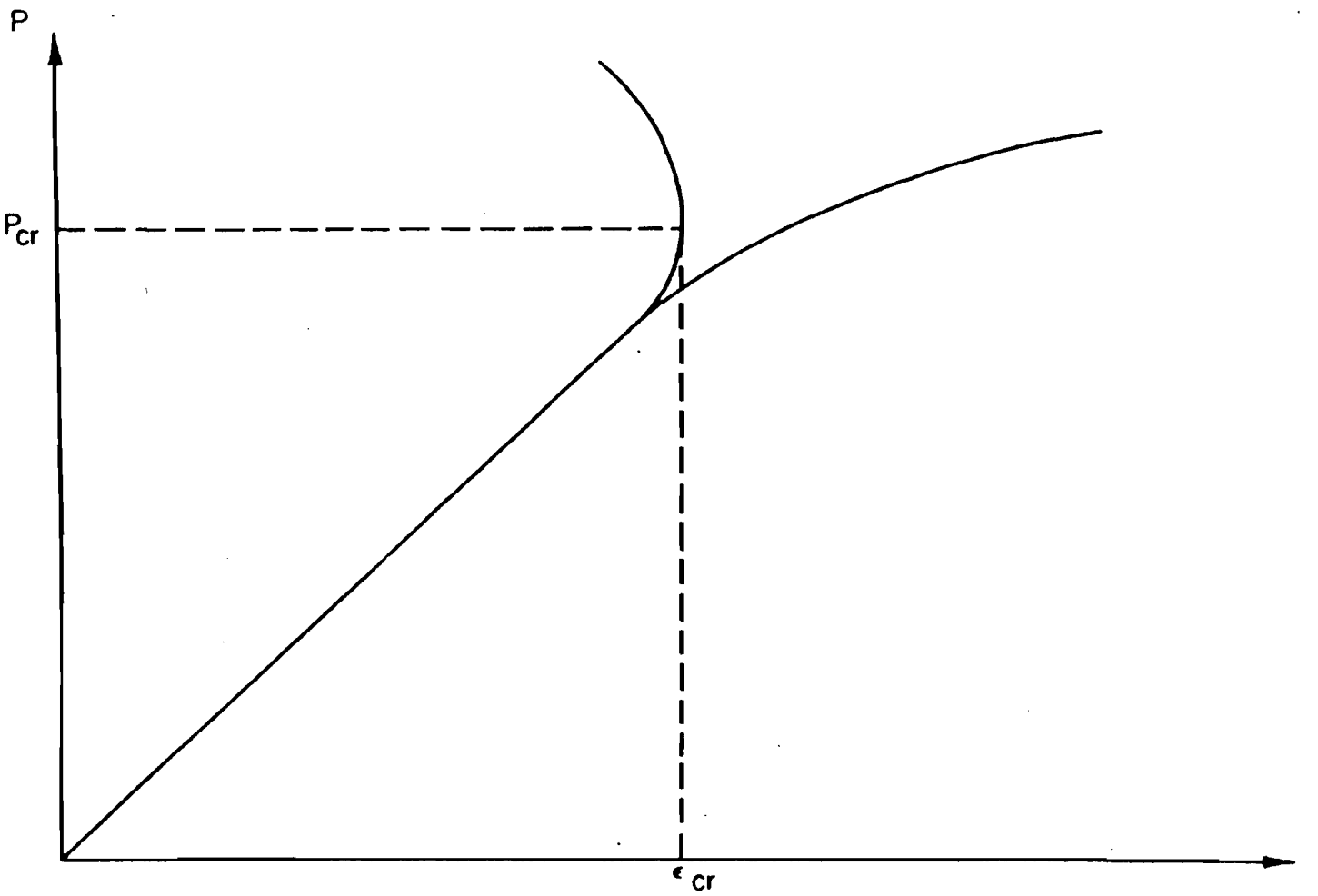

Figure 3.10 Modified Strain Reversal Method Used to Determine the Critical Buckling Load

Figure 3.11 MTS 880 Material Test System and CAMAC Data Acquisition System Used for Beam and Stub Column Tests

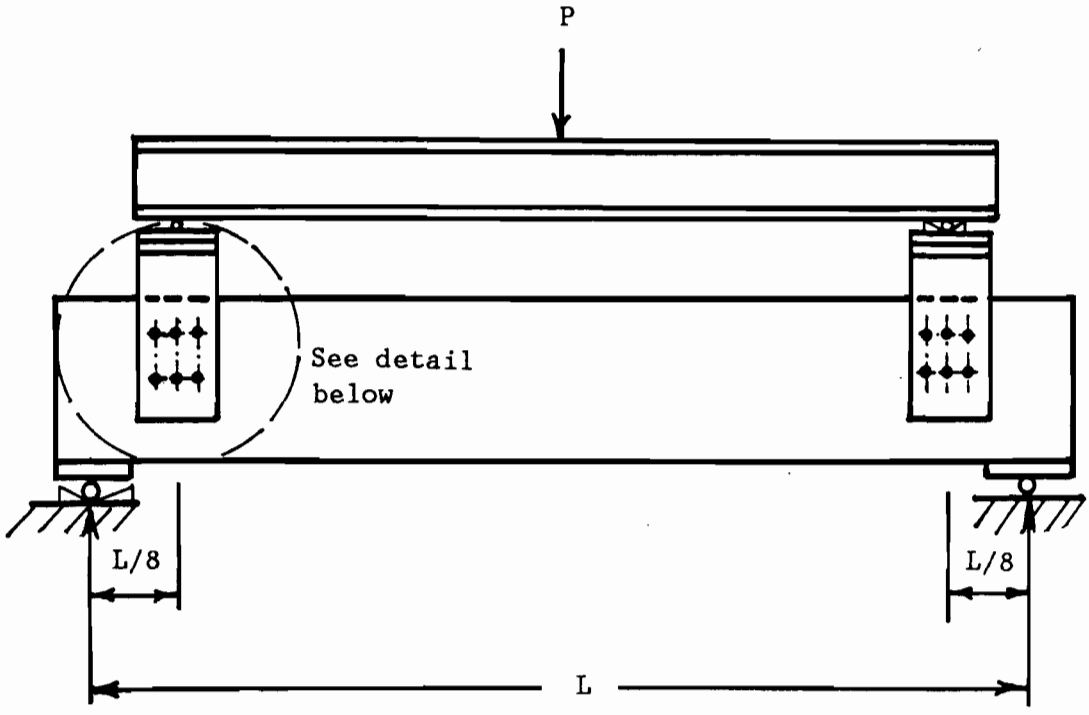

(a) Test Setup

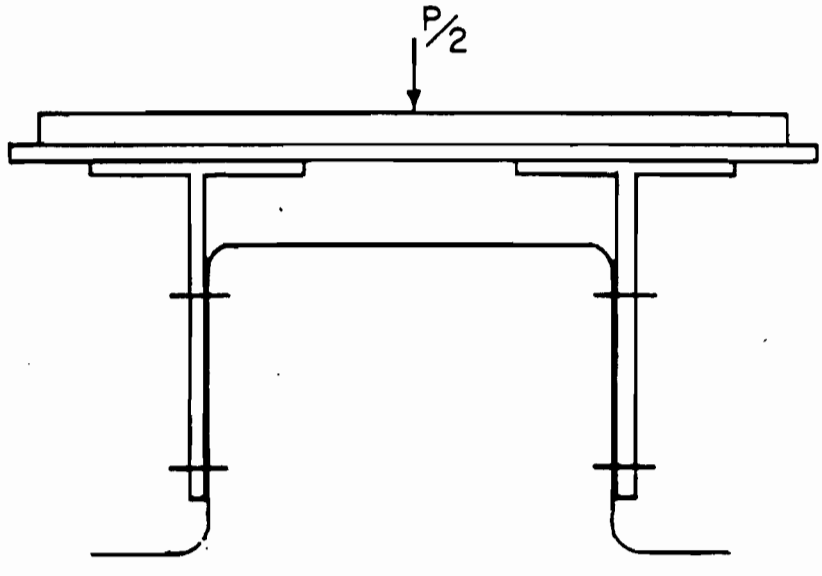

(b) Detail at Loading Points

Figure 3.12 Test Setup for Beams with a Stiffened Flange

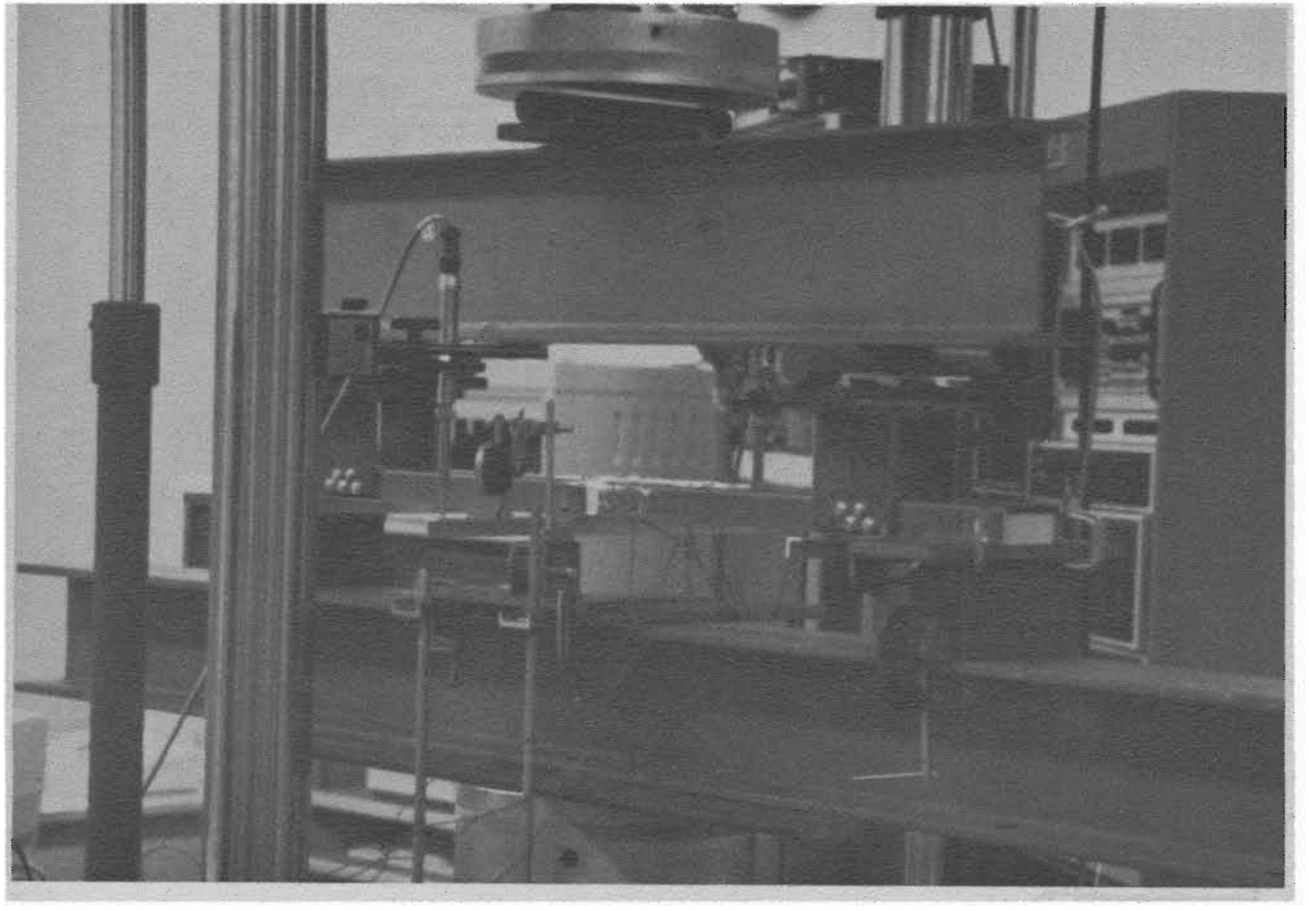

Figure 3.13 Photograph of Test Setup for Beams with a Stiffened Flange

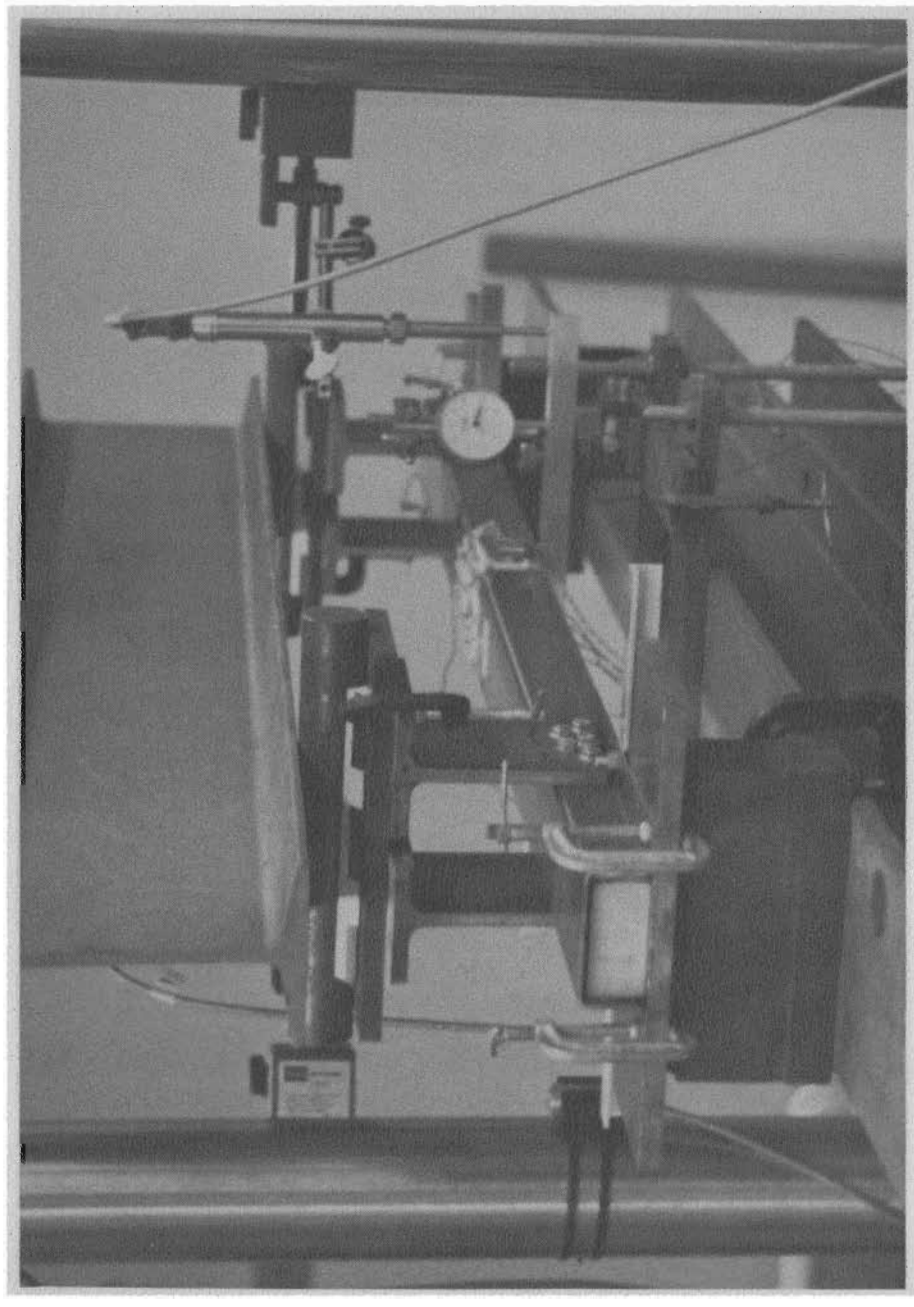

Figure 3.14 End View for the Hat Beam Test Setup

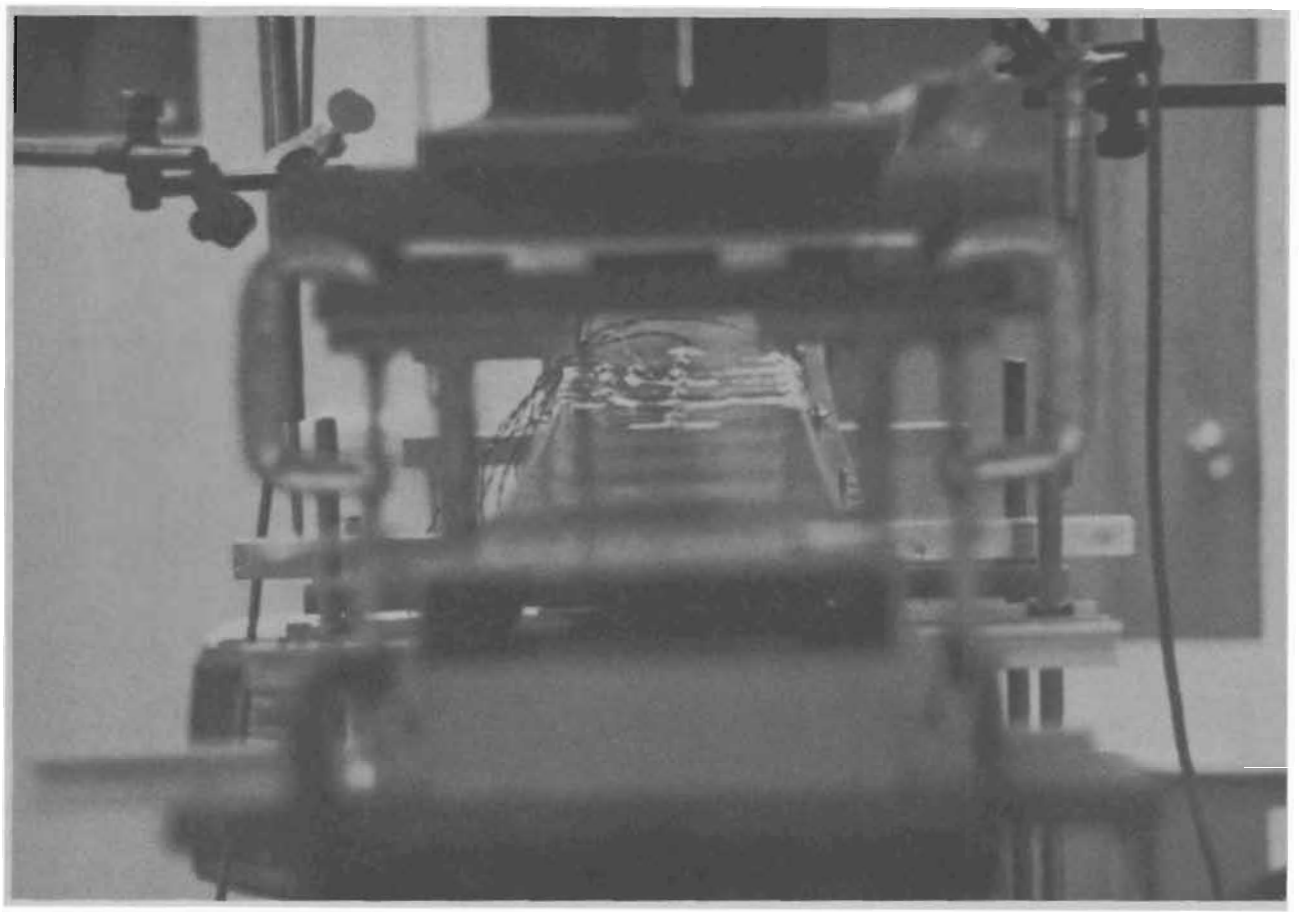

Figure 3.15 Development of Stiffened Flange Buckling Waves During a Slow Test

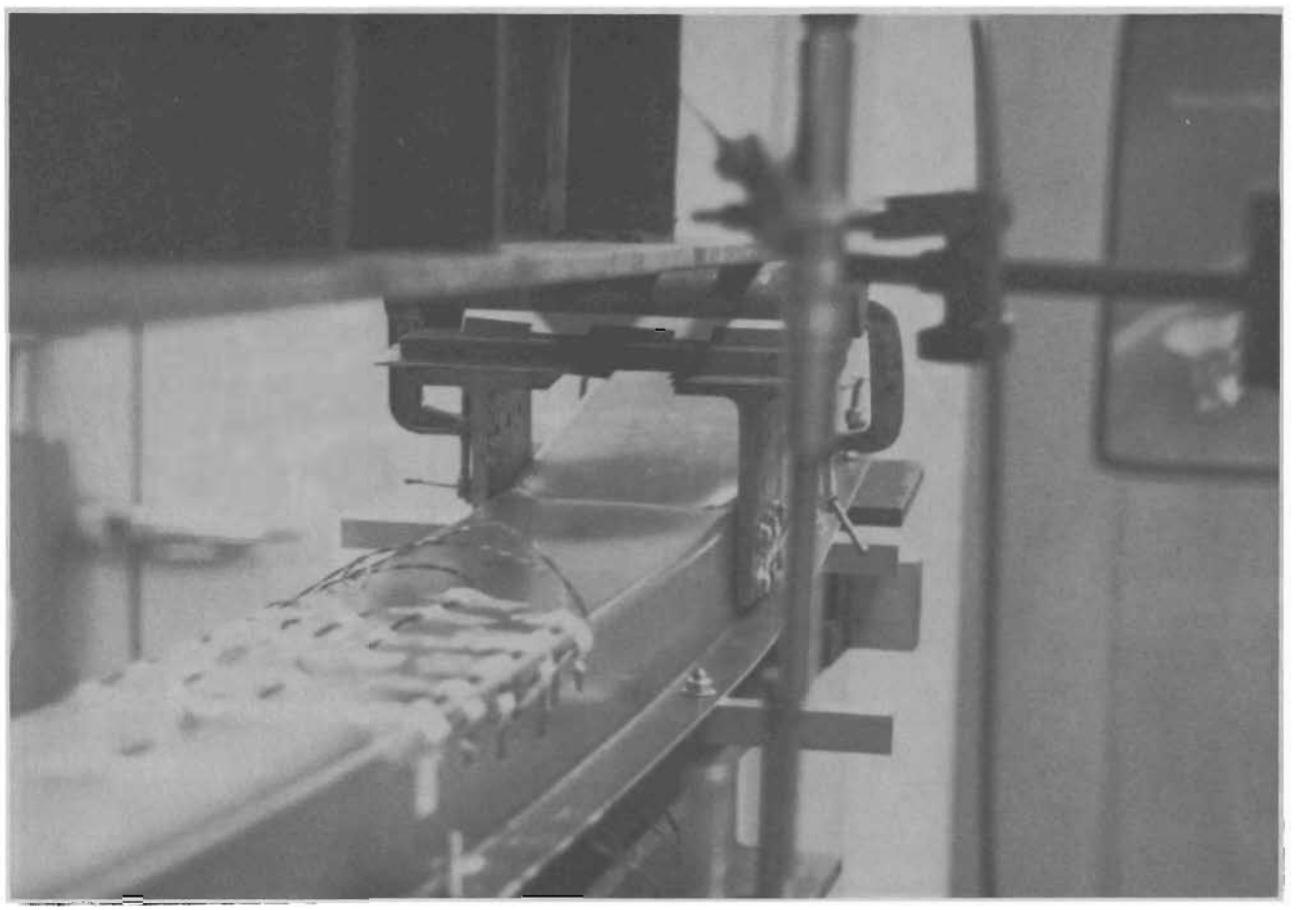

Figure 3.16 Typical Failure of Hat Beams with a Stiffened Flange

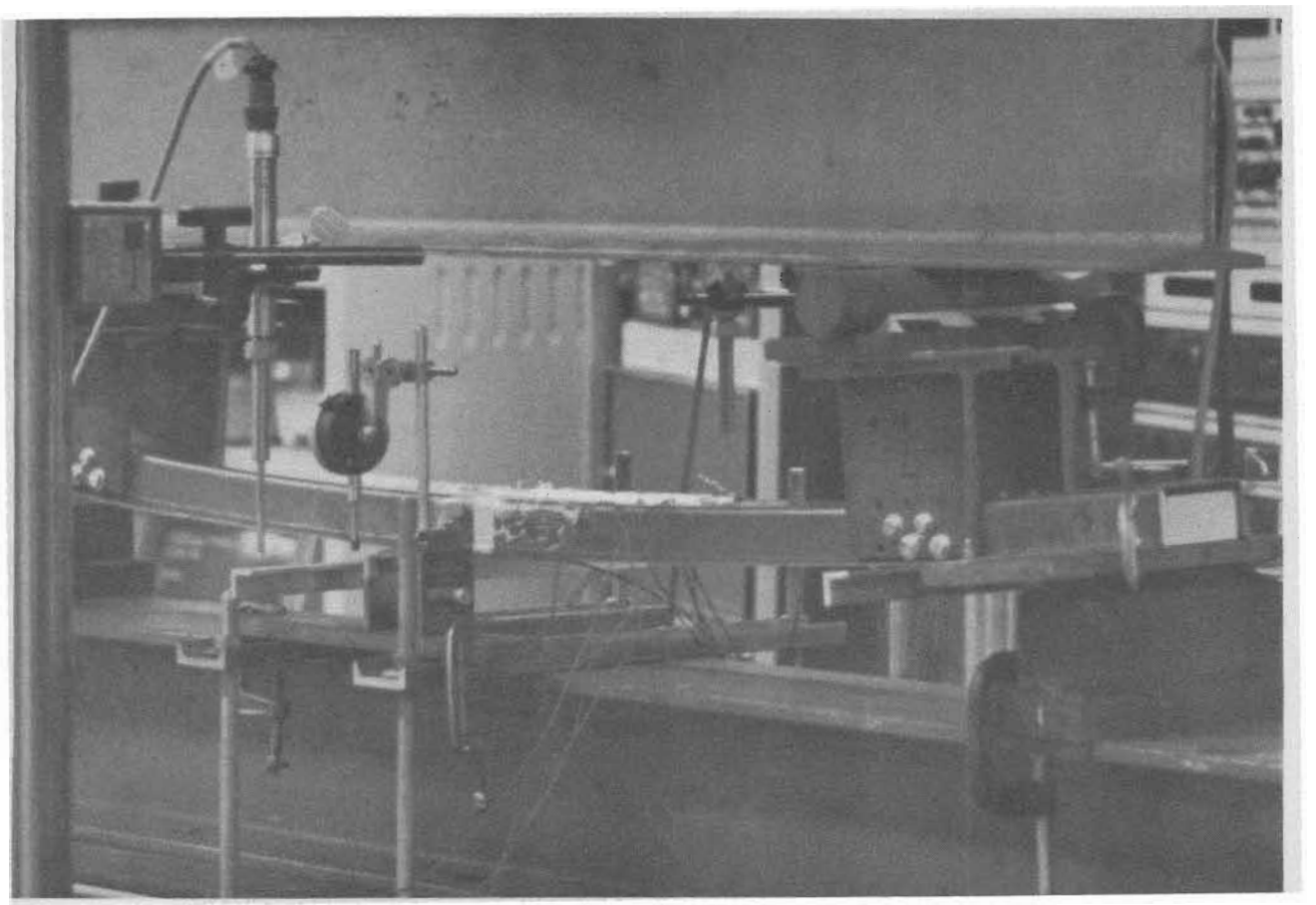

Figure 3.17 Typical Deflected Shape of Beams with a Stiffened Flange

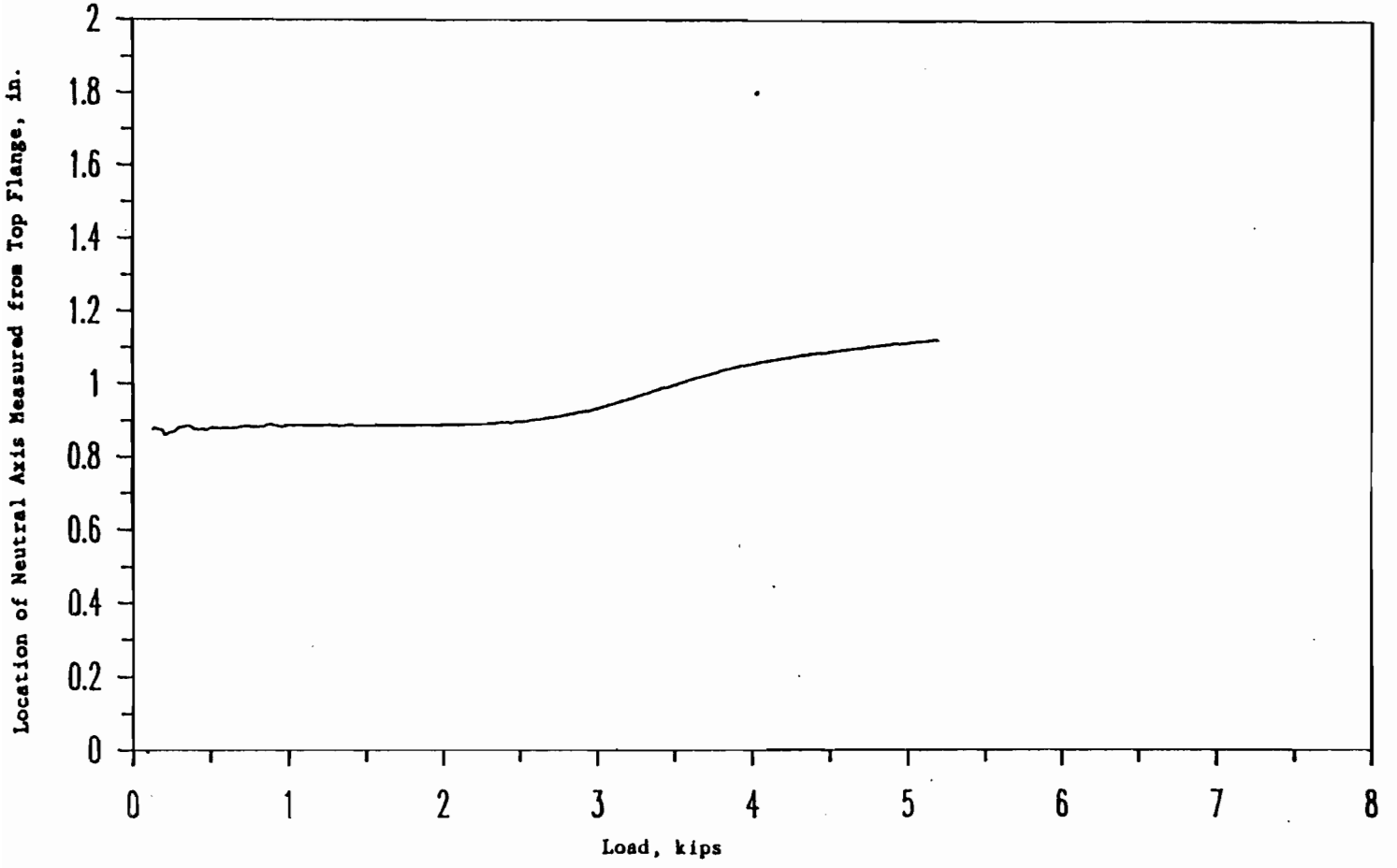

Figure 3.18 Typical Plot of Load vs. Location of Neutral Axis for Beams with a Stiffened Flange (Specimen 3A0A)

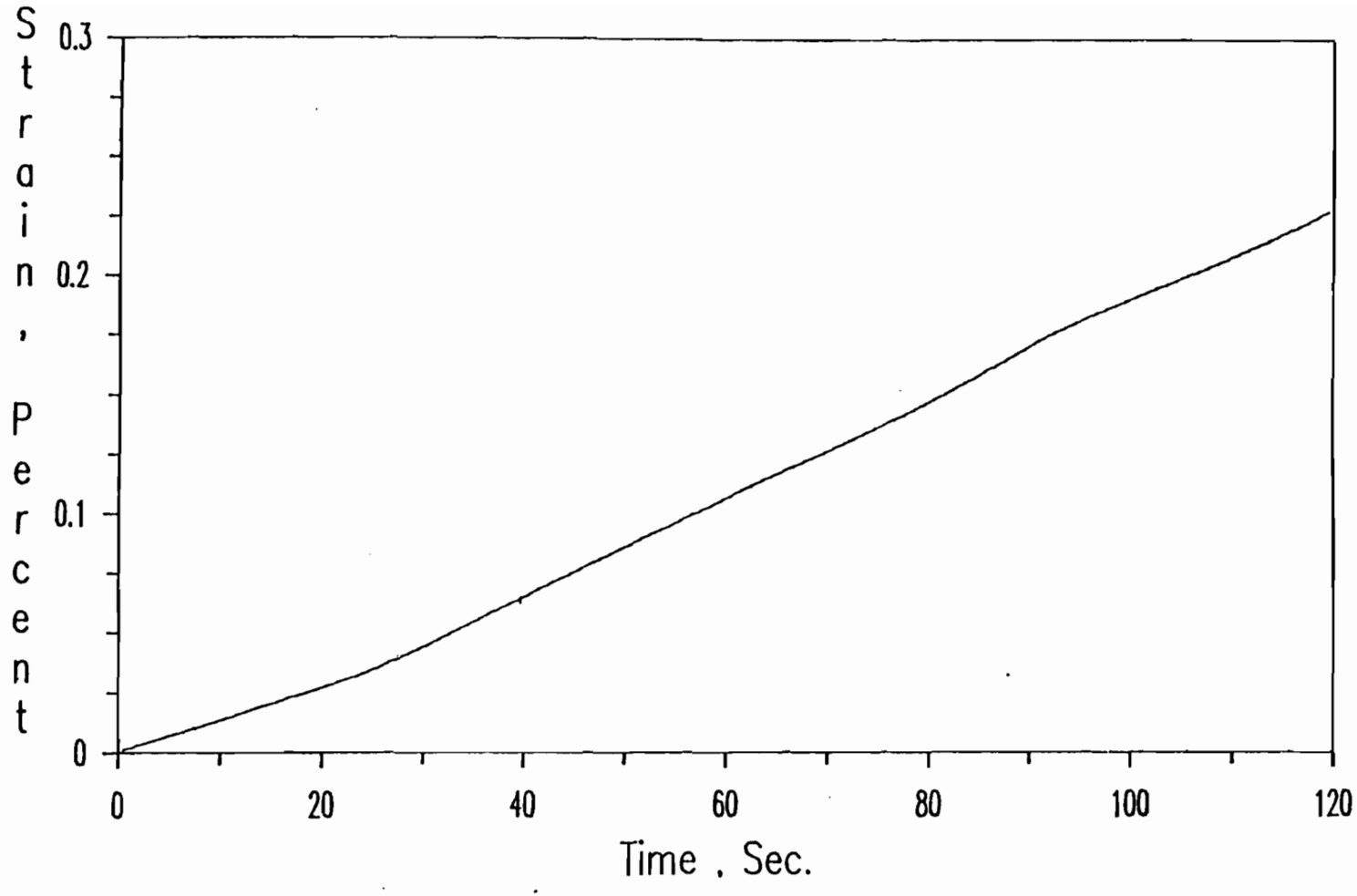

Figure 3.19 Typical Plot of Strain vs. Time for Hat Beams with a Stiffened Flange (Strain Gage # 5 for Specimen 3A1A)

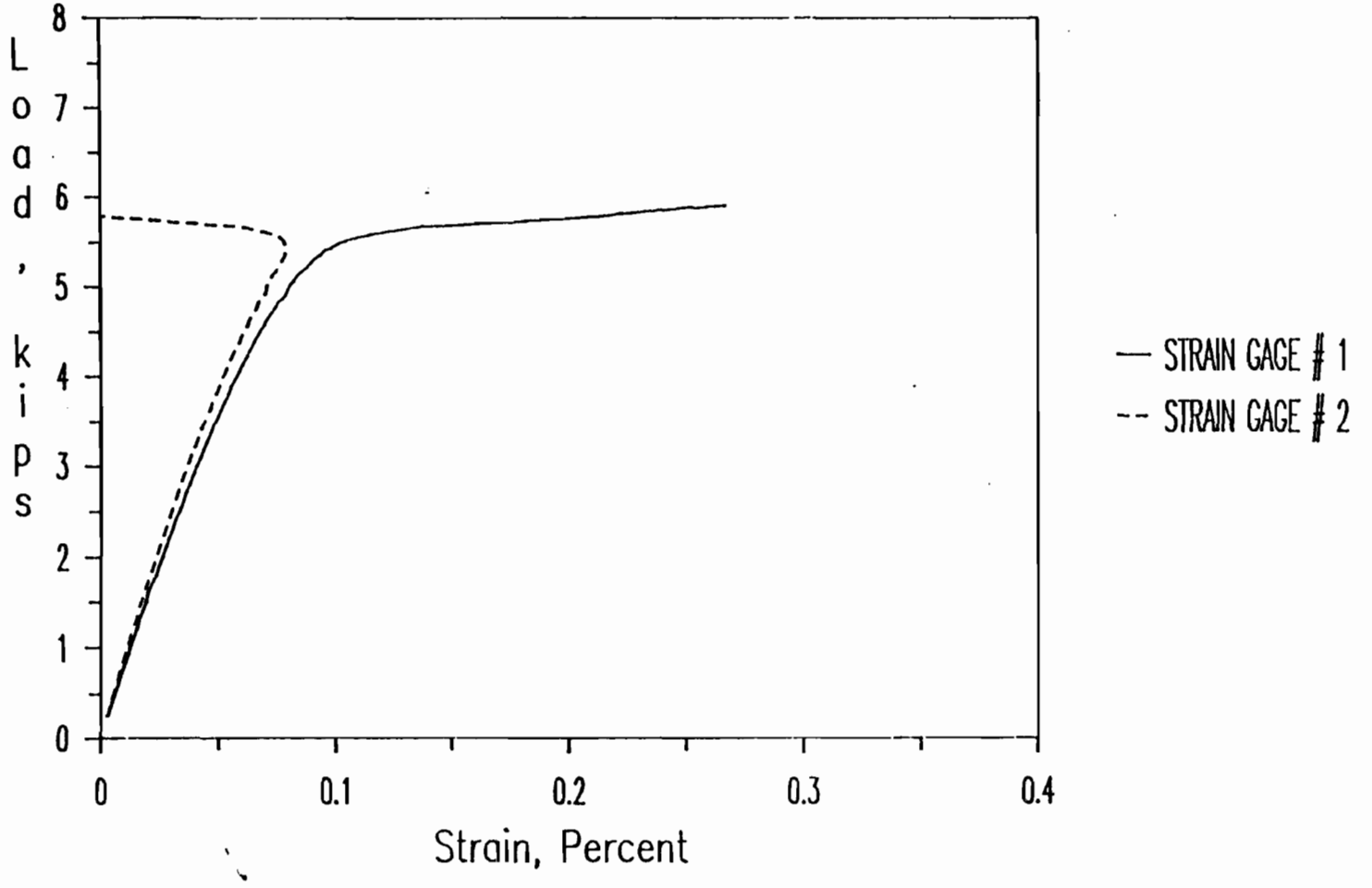

Figure 3.20 Load-Strain Curves of Strain Gages # 1 and 2 Installed at the Center of the Stiffened Flange (Specimen 3C0A)

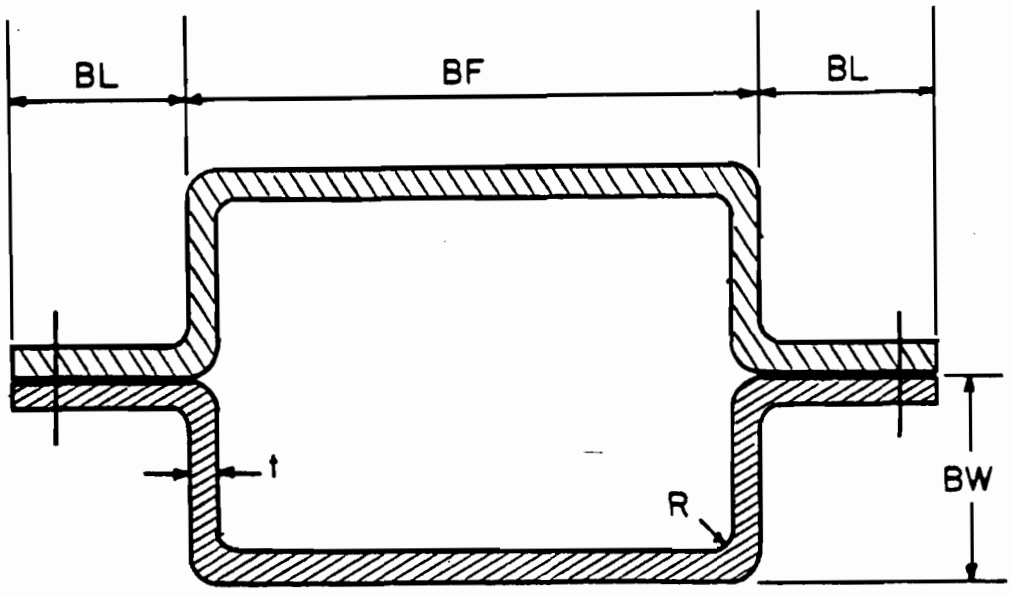

Figure 3.21 Cross Sections of Box-Shaped Stub Columns Used for the Study of Stiffened Elements

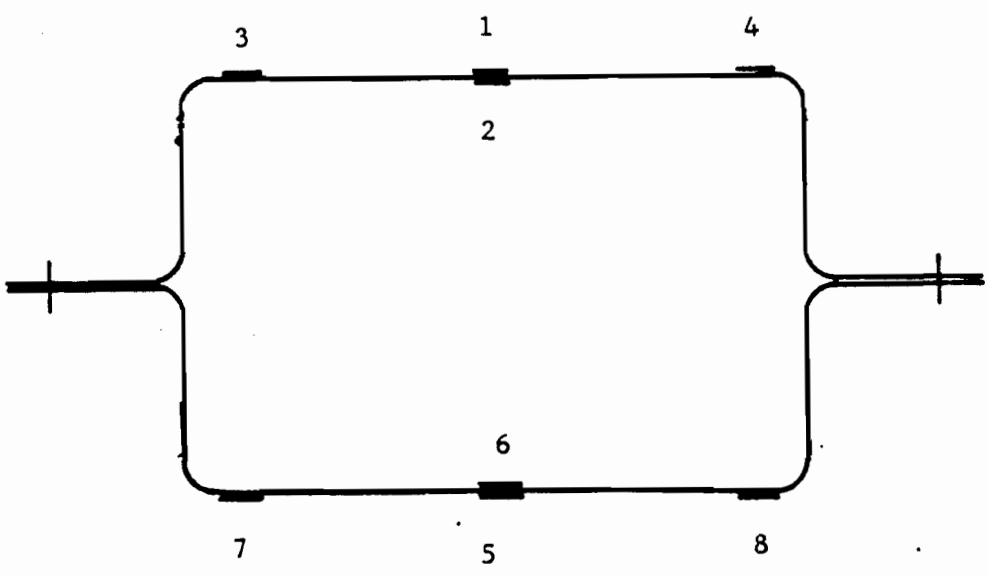

Figure 3.22 Locations of Strain Gages at Midheight of Box-Shaped Stub Columns

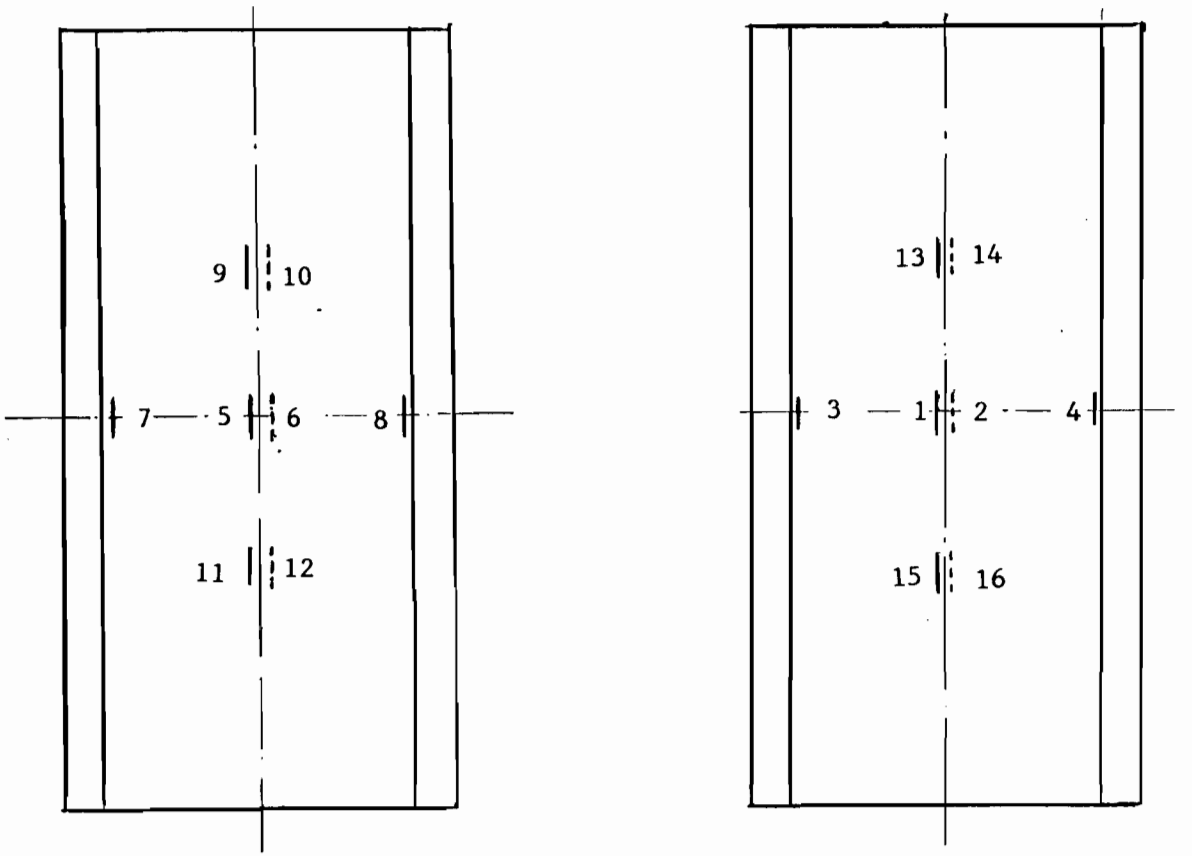

Figure 3.23 Locations of Strain Gages along the Specimen Length for Box-Shaped Stub Column Having Large w/t Ratio

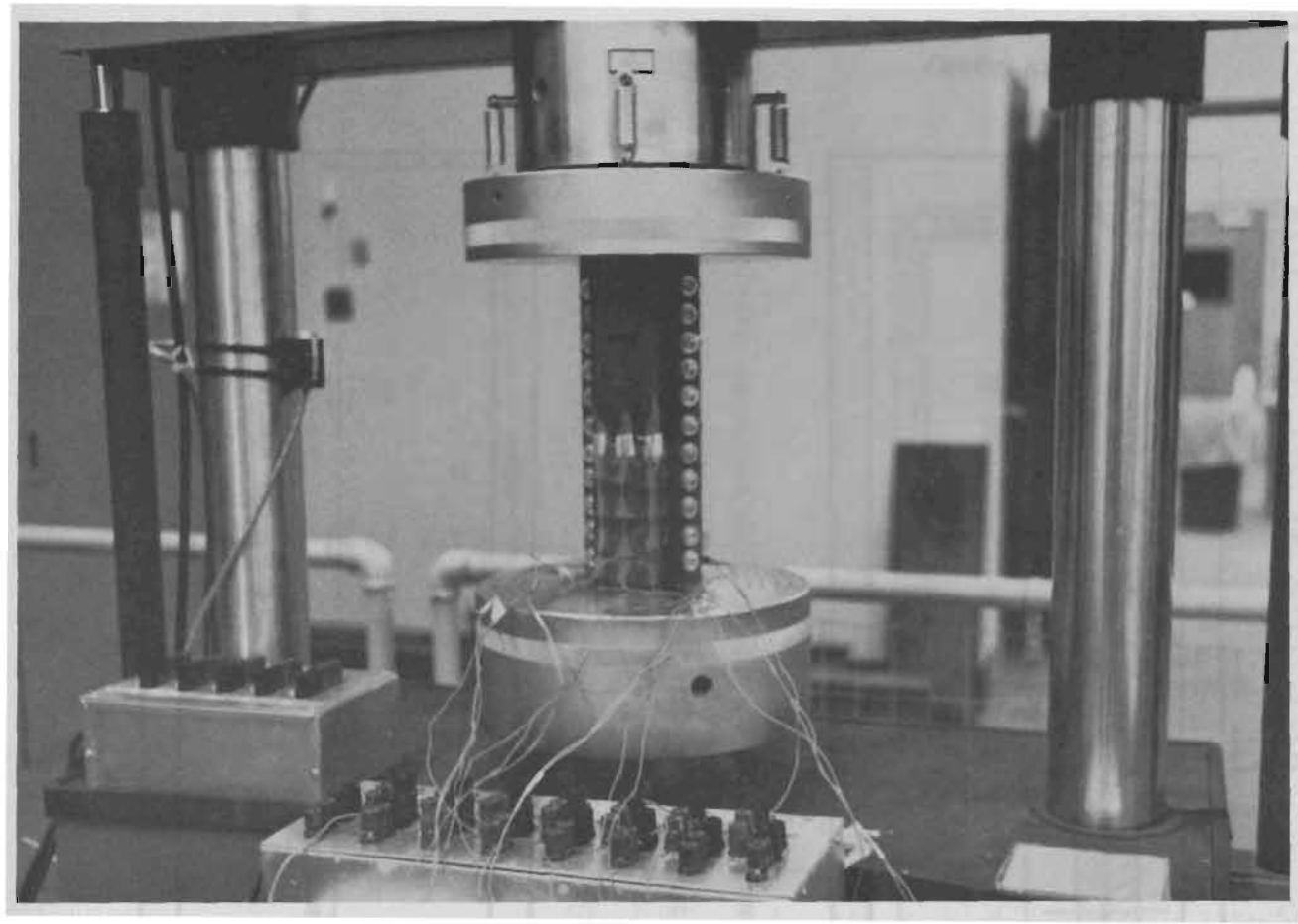

Figure 3.24 Test Setup of Stub Columns with Stiffened Flanges

(Specimen 1B3B)

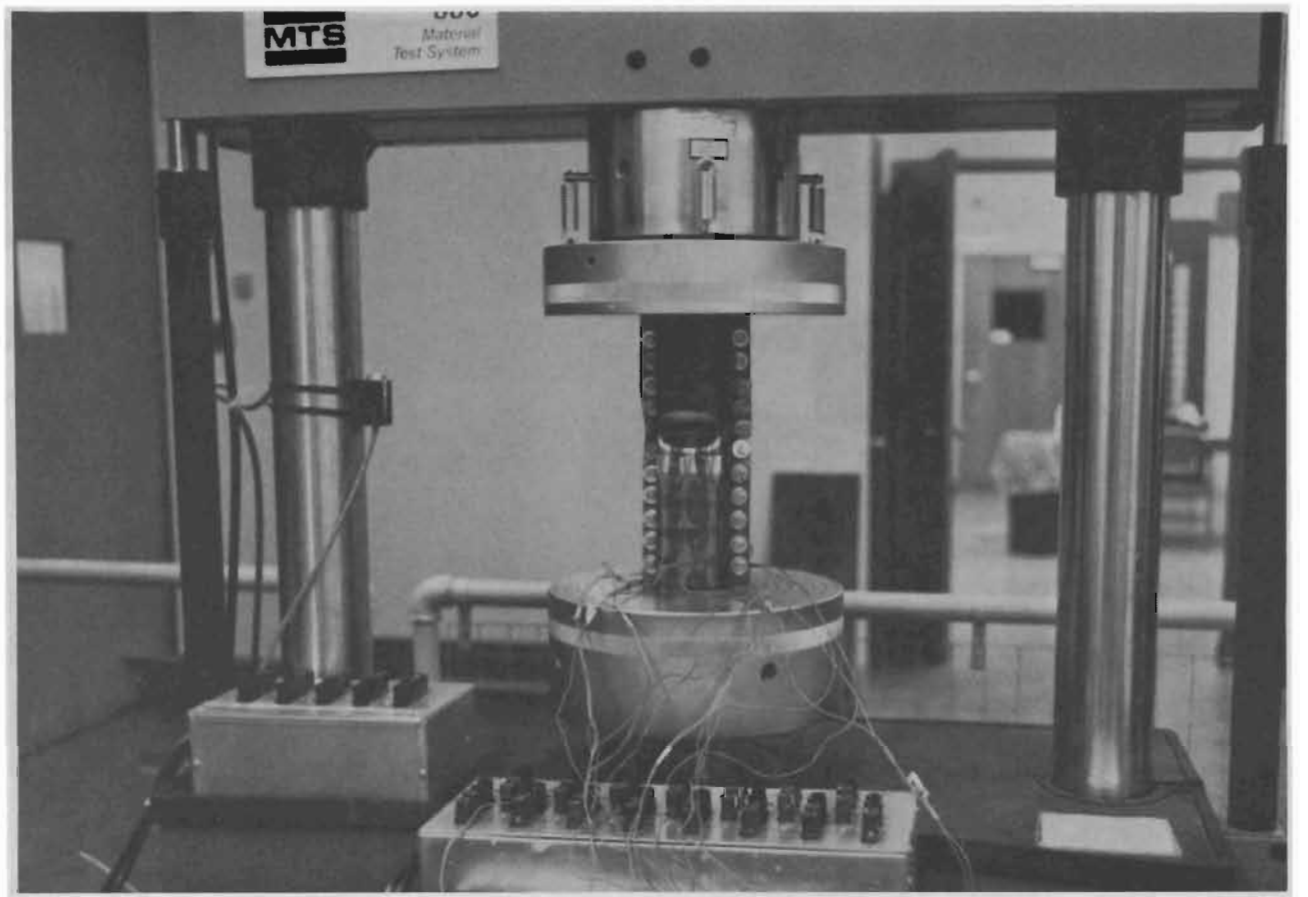

Figure 3.25 Failure of Stub Columns with Stiffened Flanges (Front View)

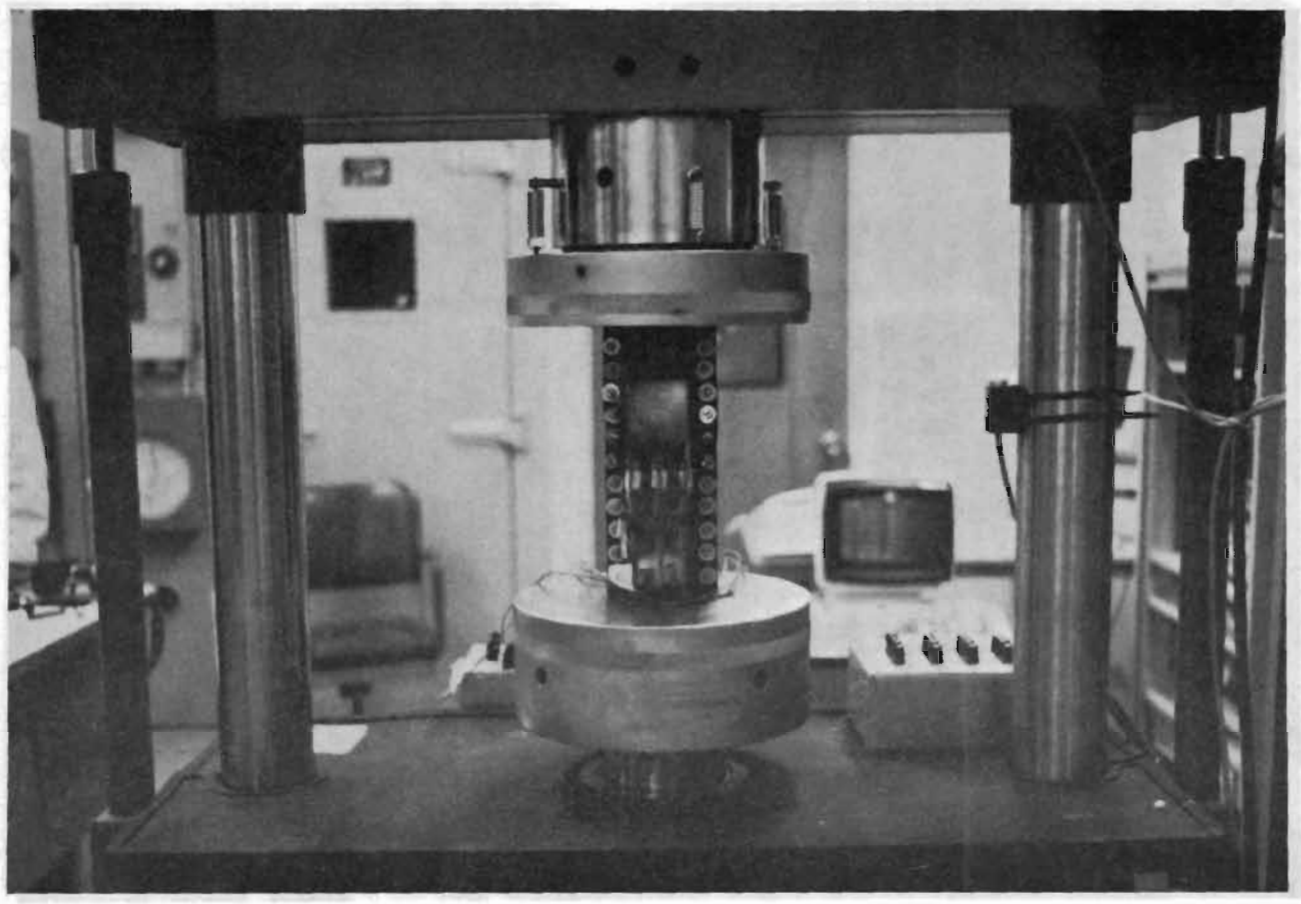

Figure 3.26 Failure of Stub Columns with Stiffened Flanges (Back View)

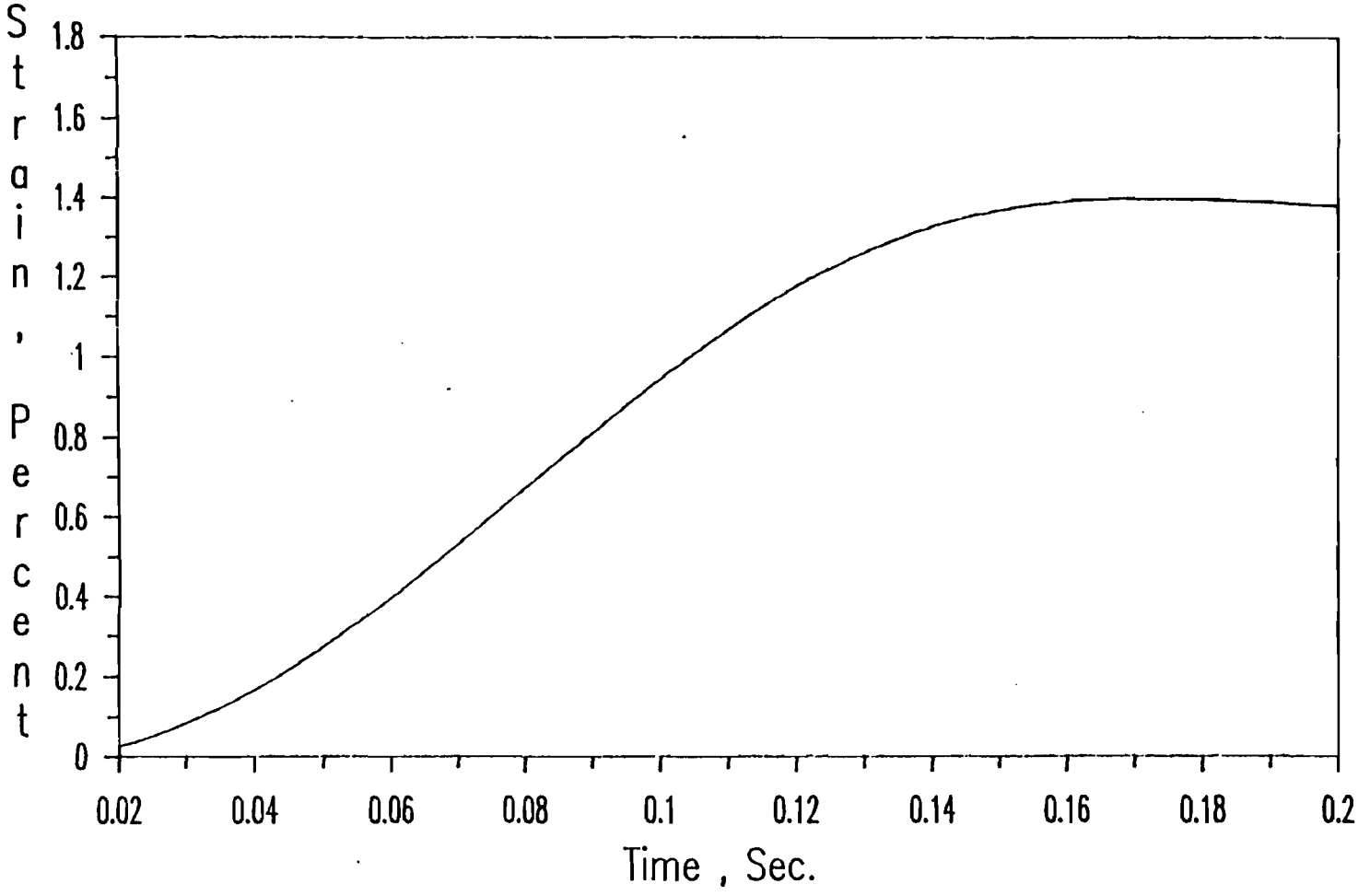

Figure 3.27 Typical Plot of Strain vs. Time for Stub Columns with Stiffened Flanges (Strain Gage # 3 for Specimen 1A3B)

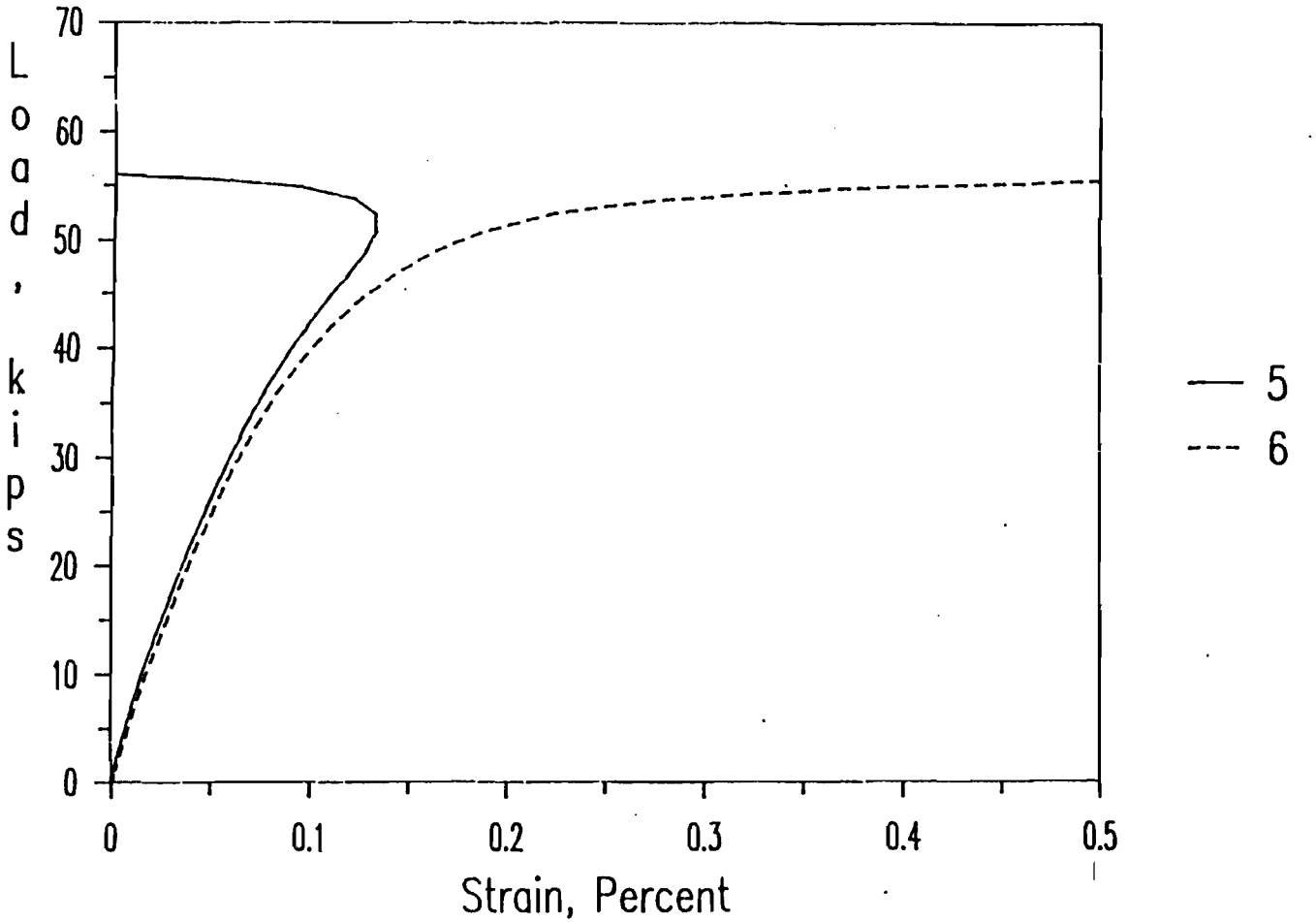

Figure 3.28 Load-Strain Curves of Strain Gages # 5 and 6, Installed at the Center of a Stiffened Flange (Specimen 1C1B)

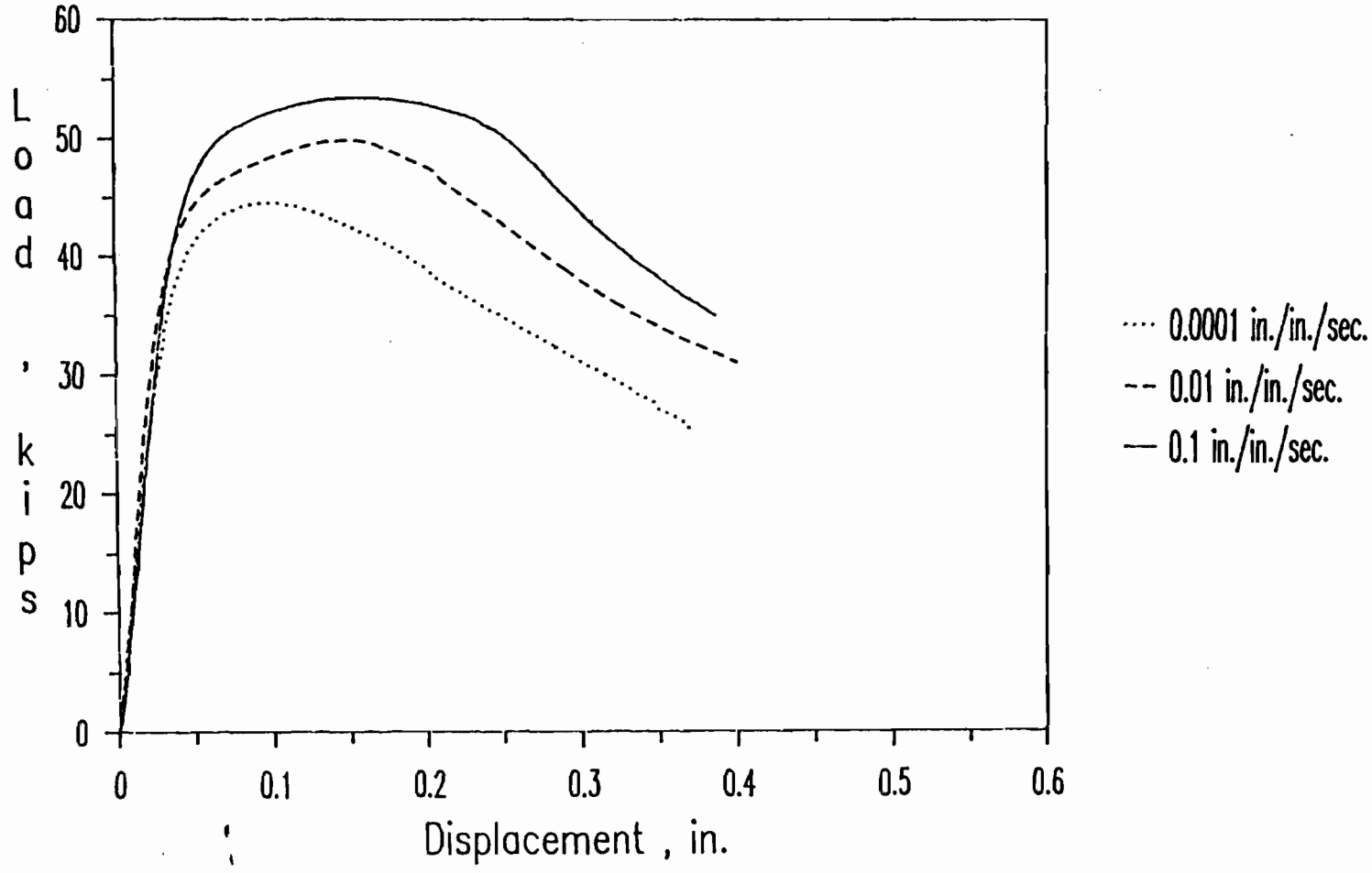

Figure 3.29 Load-Displacement Curves for Stub-Column Specimens 1A1A, 1A2A, and 1A3A

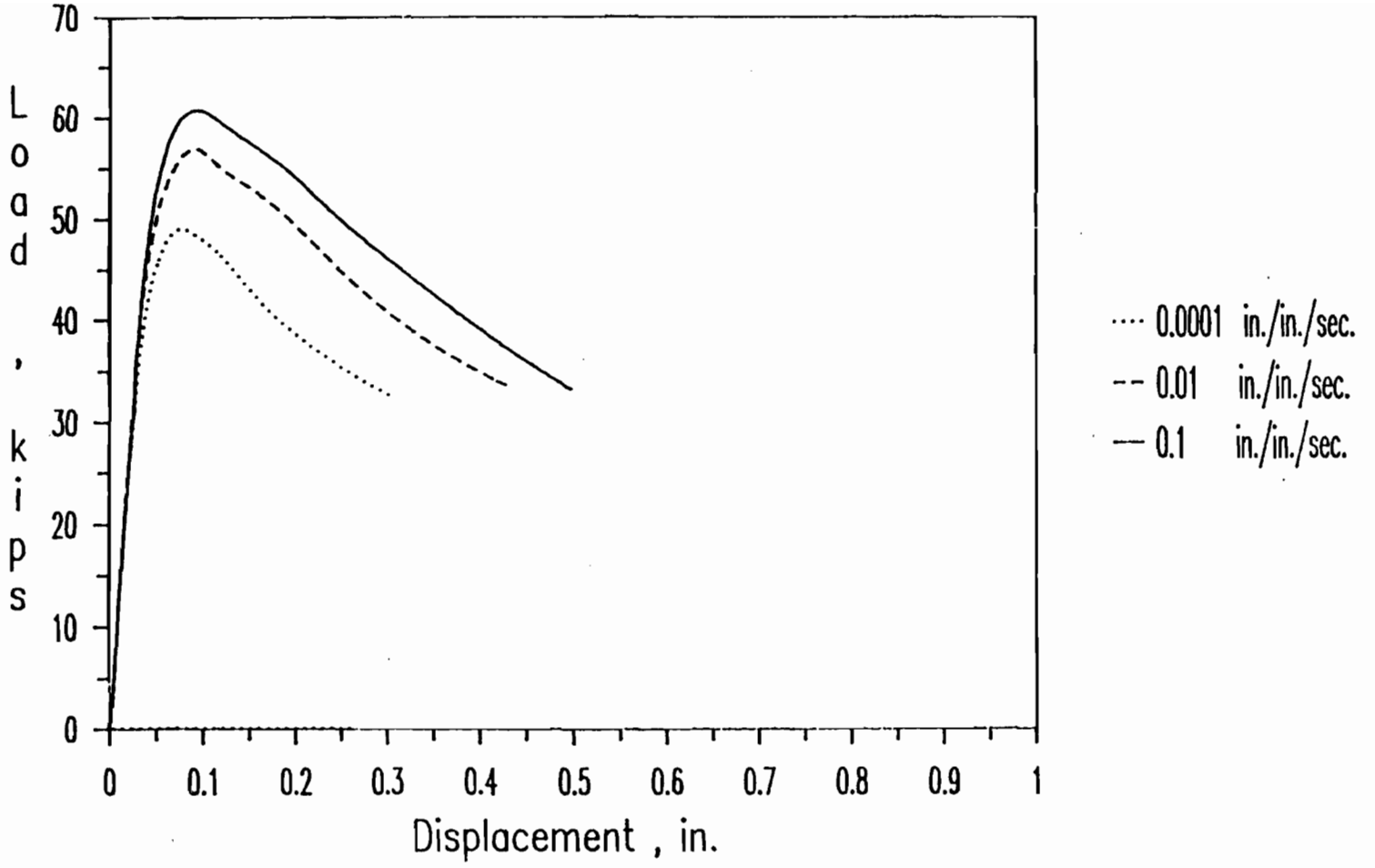

Figure 3.30 Load-Displacement Curves for Stub-Column Specimens 1B1A, 1B2A, and 1B3A

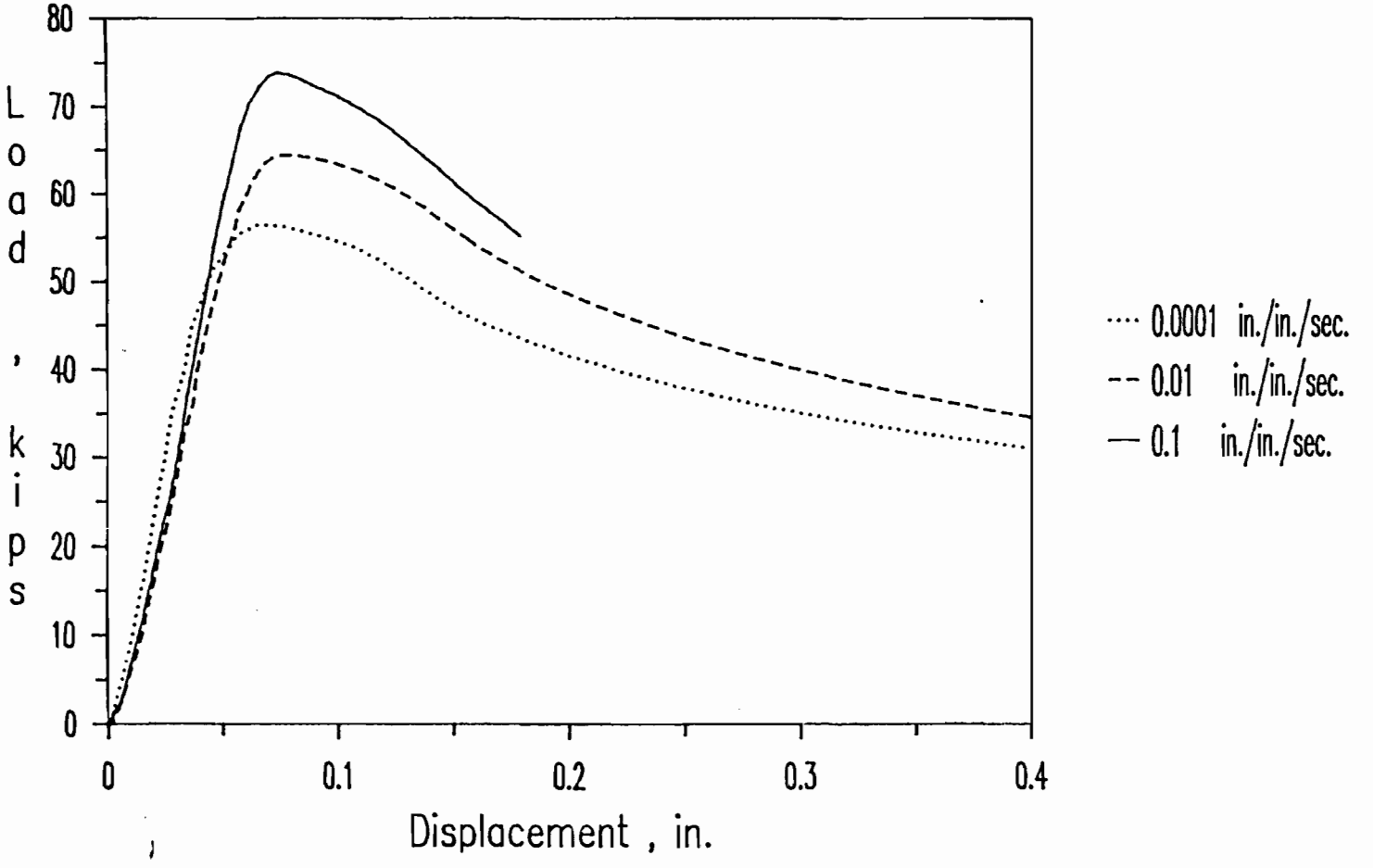

Figure 3.31 Load-Displacement Curves for Stub-Column Specimens 1C1A, 1C2A, and 1C3A

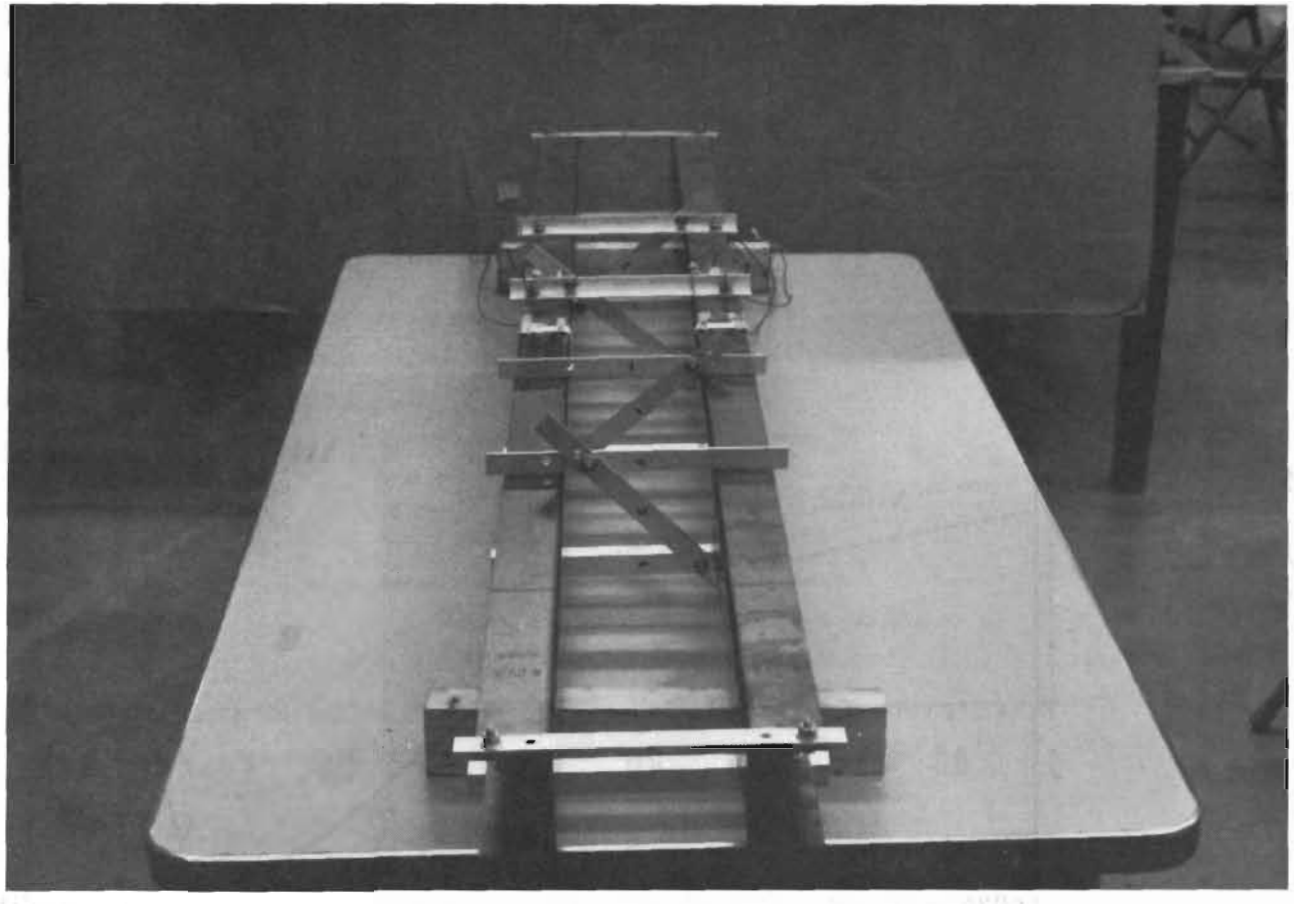

Figure 3.32 Photograph of Channel Beam Specimen Braced by Aluminum Angles

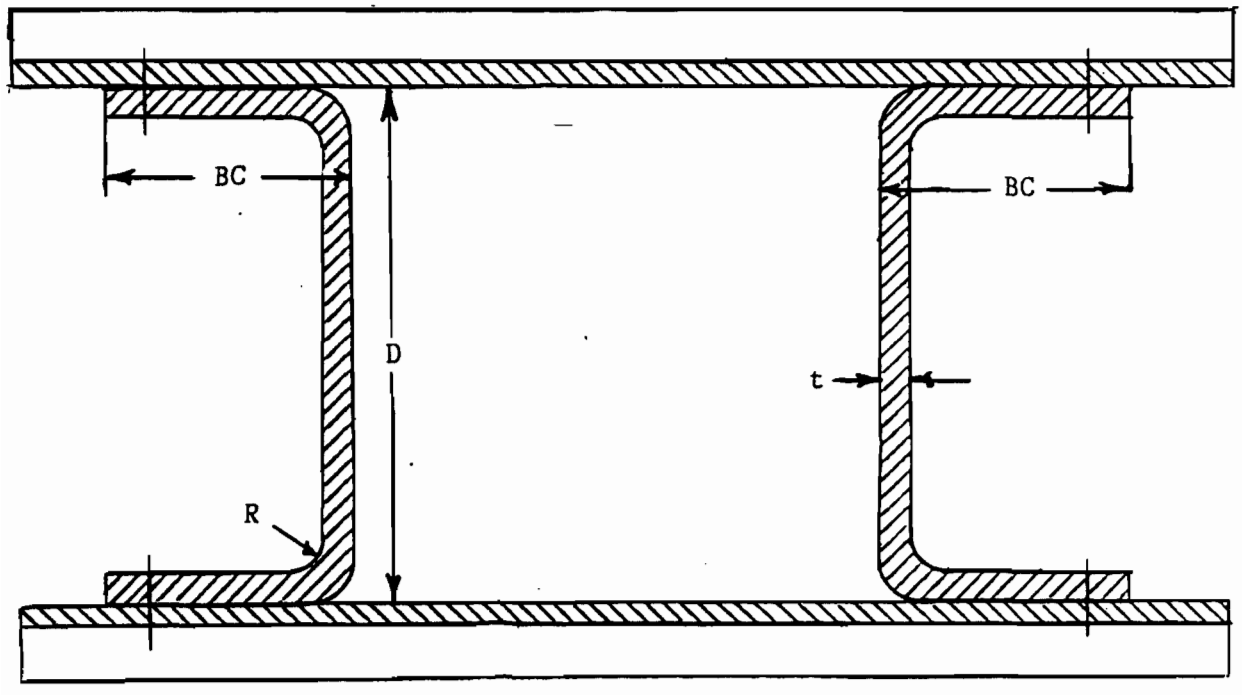

Figure 3.33 Cross Sections of Channel Beams Used for the Study of Unstiffened Elements

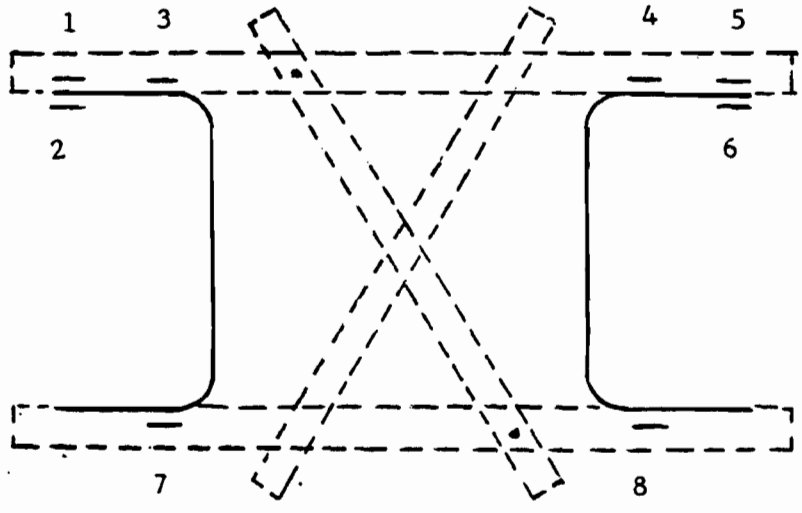

Figure 3.34 Locations of Strain Gages at Midspan Section of Channel Beams

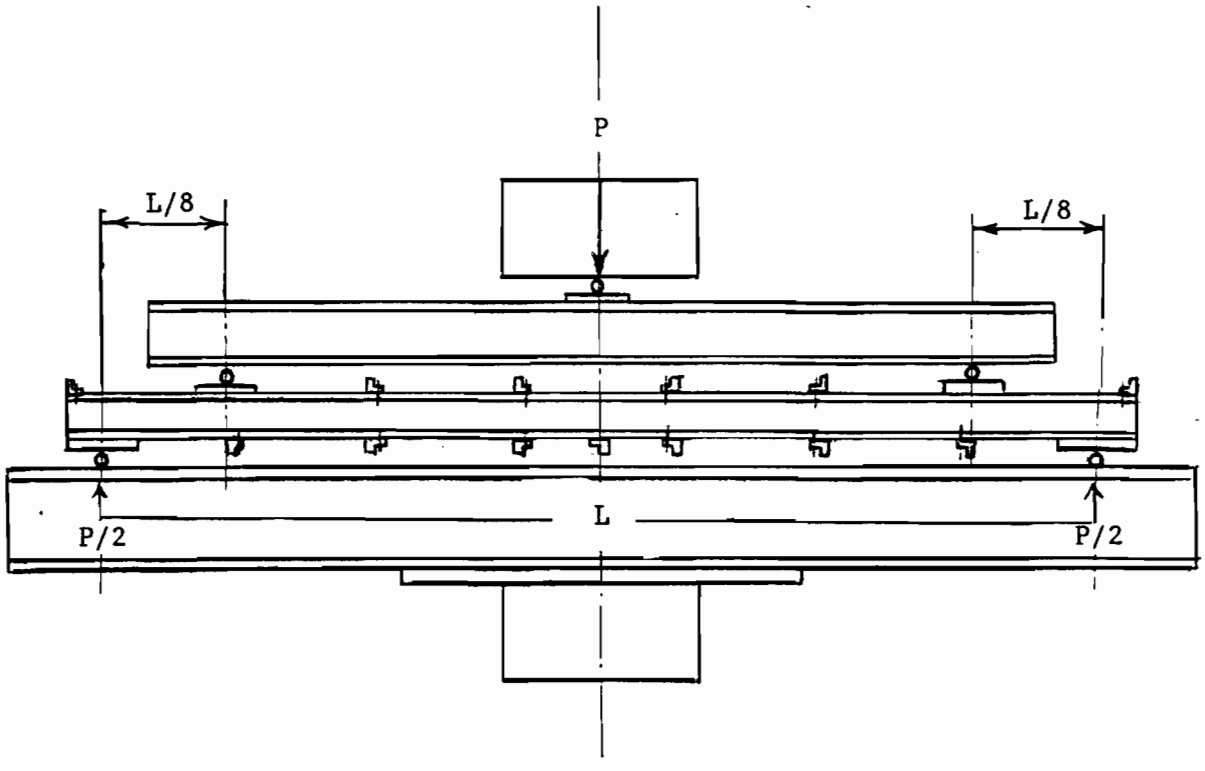

Figure 3.35 Test Setup for Channel Beams with Unstiffened Flanges

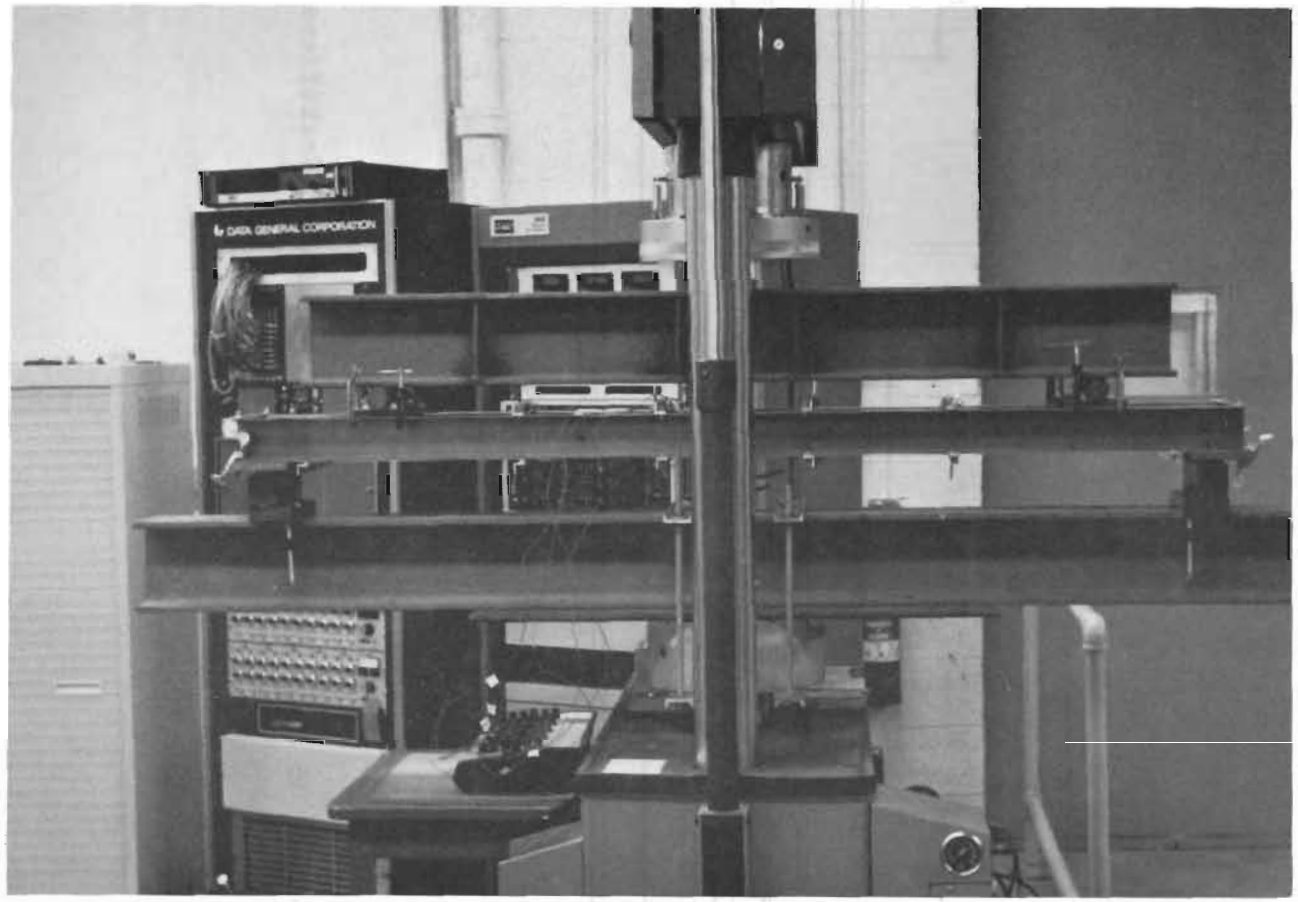

Figure 3.36 Photograph of Test Setup for Channel Beams with Unstiffened Flanges

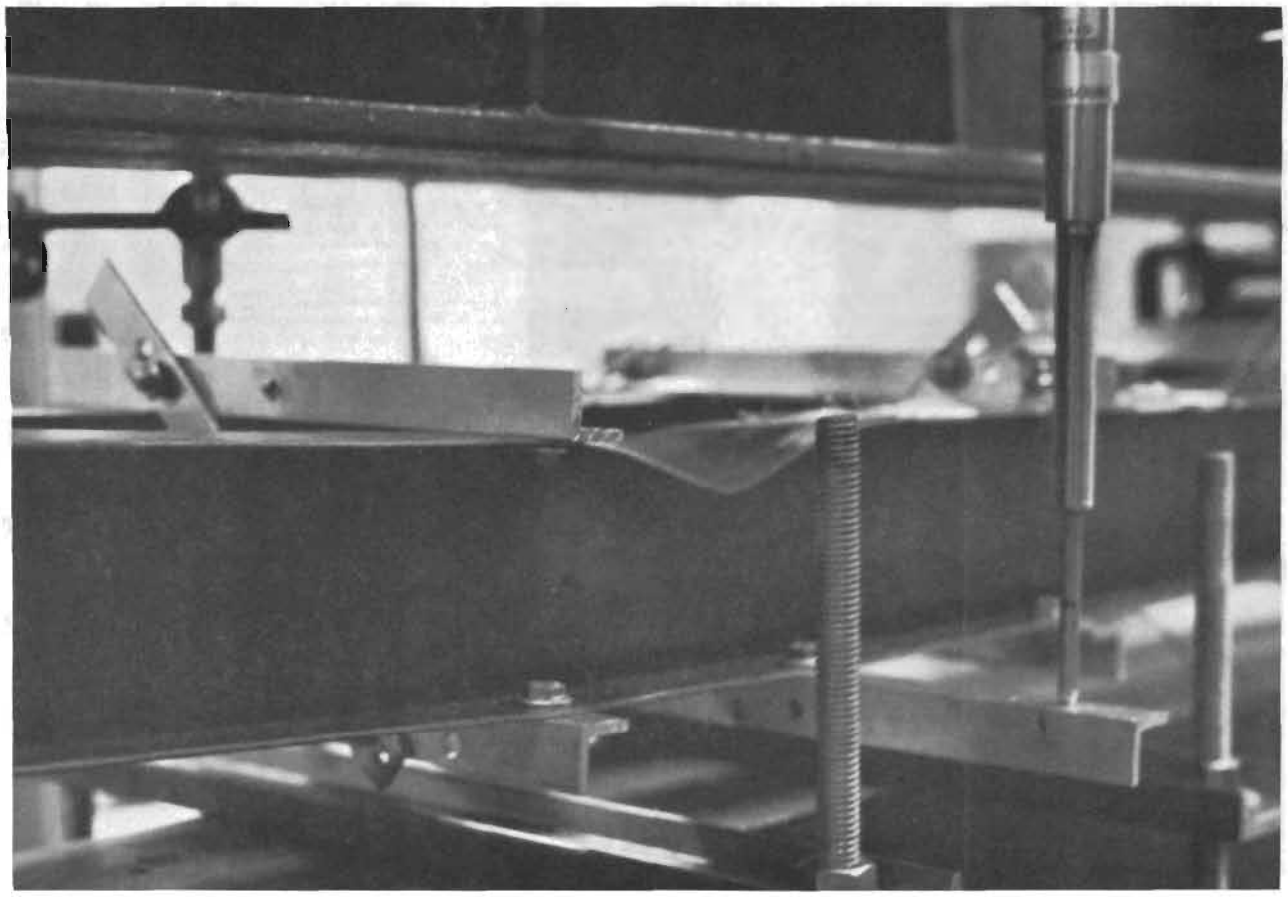

Figure 3.37 Typical Failure of Channel Beams with Unstiffened Flanges

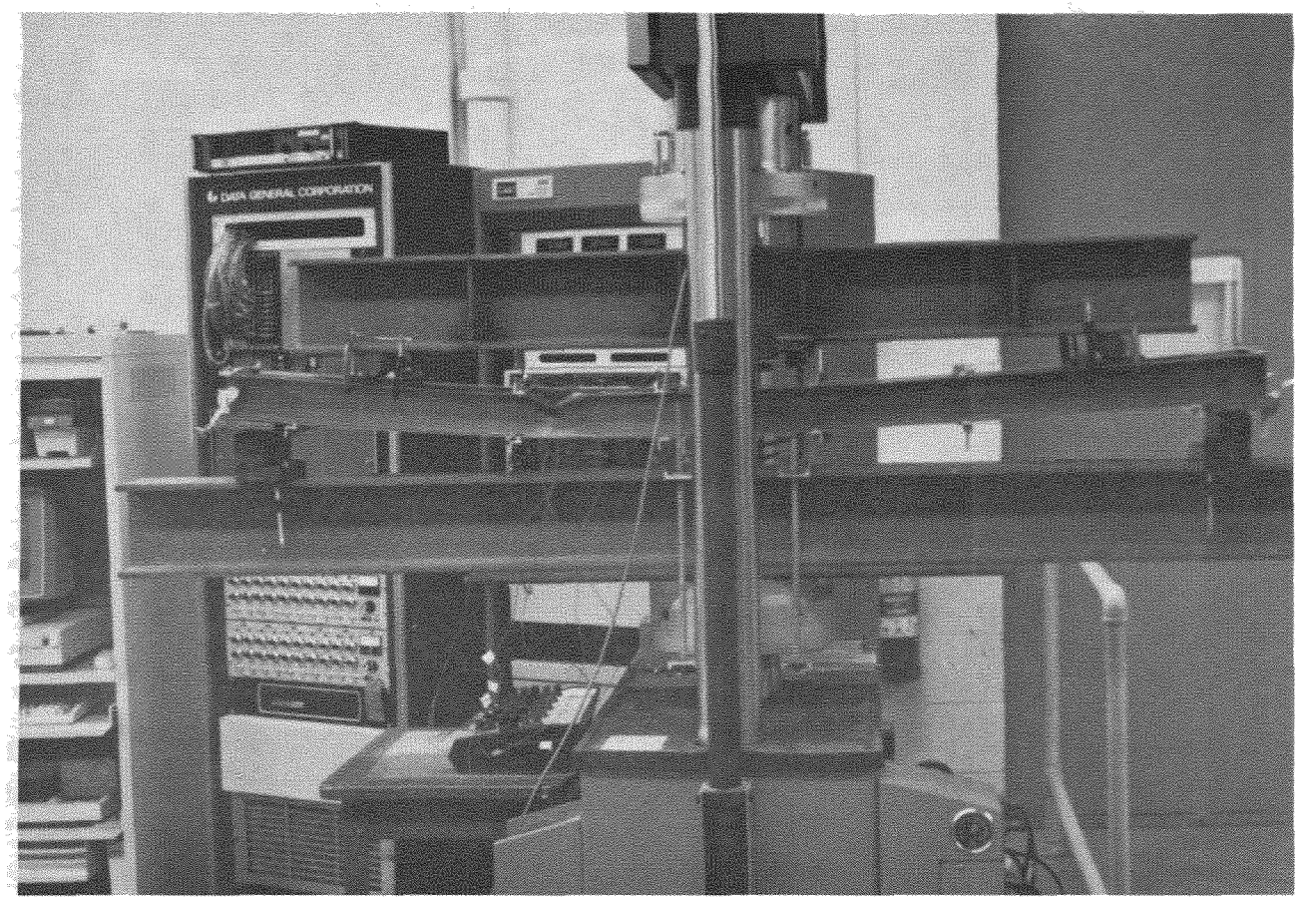

Figure 3.38 Typical Deflected Shape of Channel Beams with Unstiffened Flanges

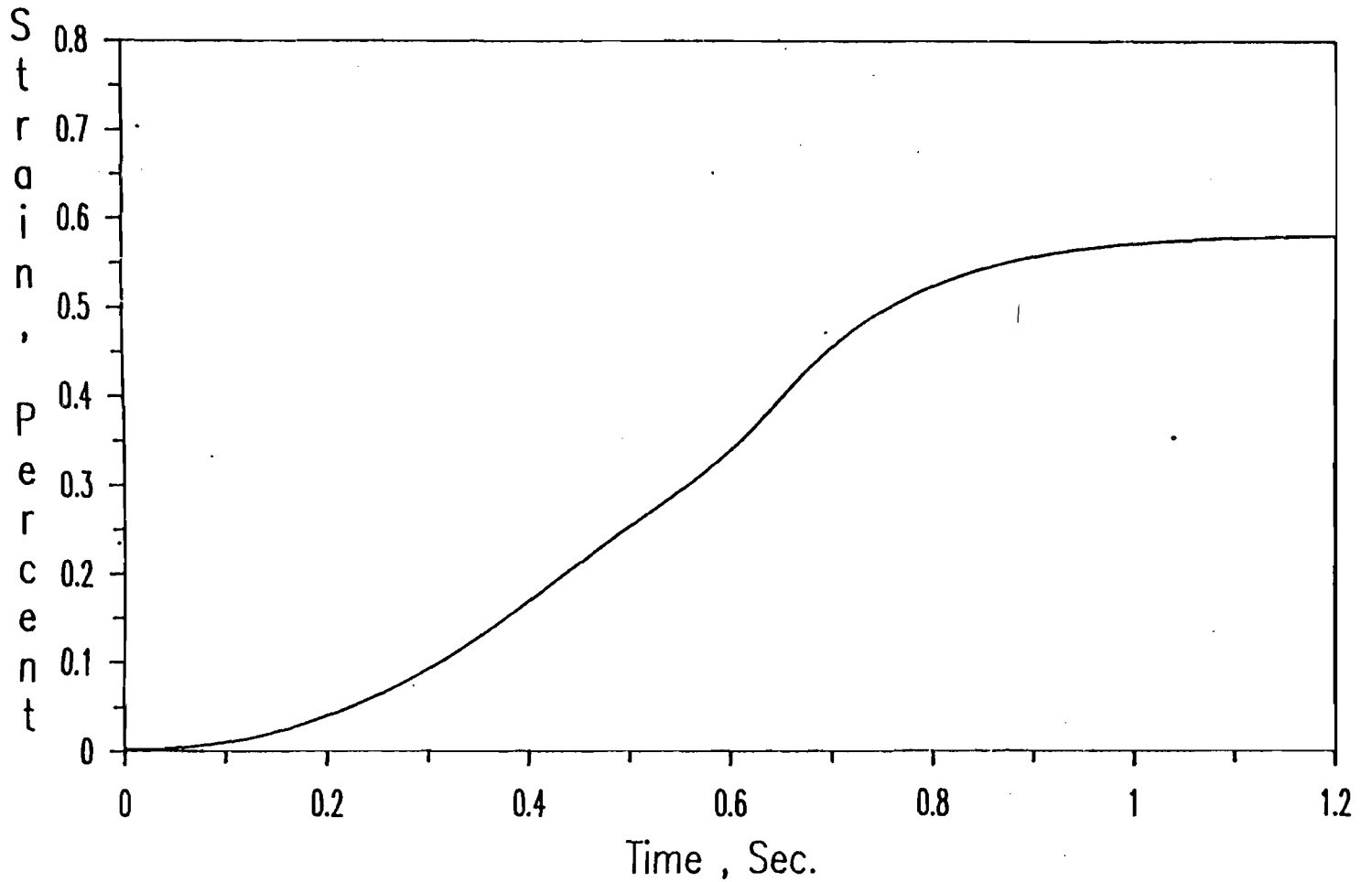

Figure 3.39 Typical Plot of Strain vs. Time for Channel Beams with Unstiffened Flanges (Strain Gage # 3 for Specimen 4C2B)

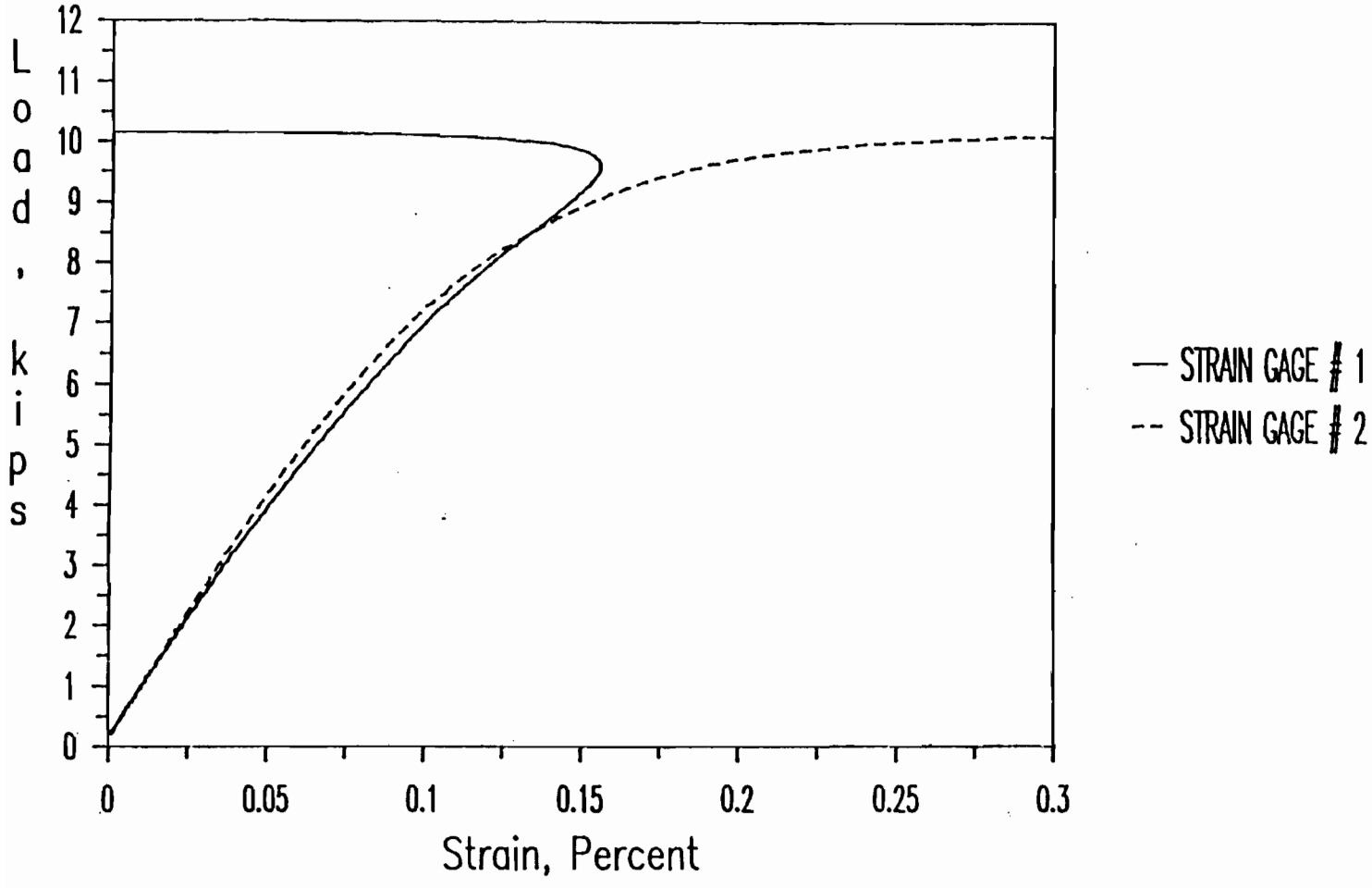

Figure 3.40 Load-Strain Curves of Strain Gages # 1 and 2 Installed at the Tip of an Unstiffened Flange (Spec. 4C2A)

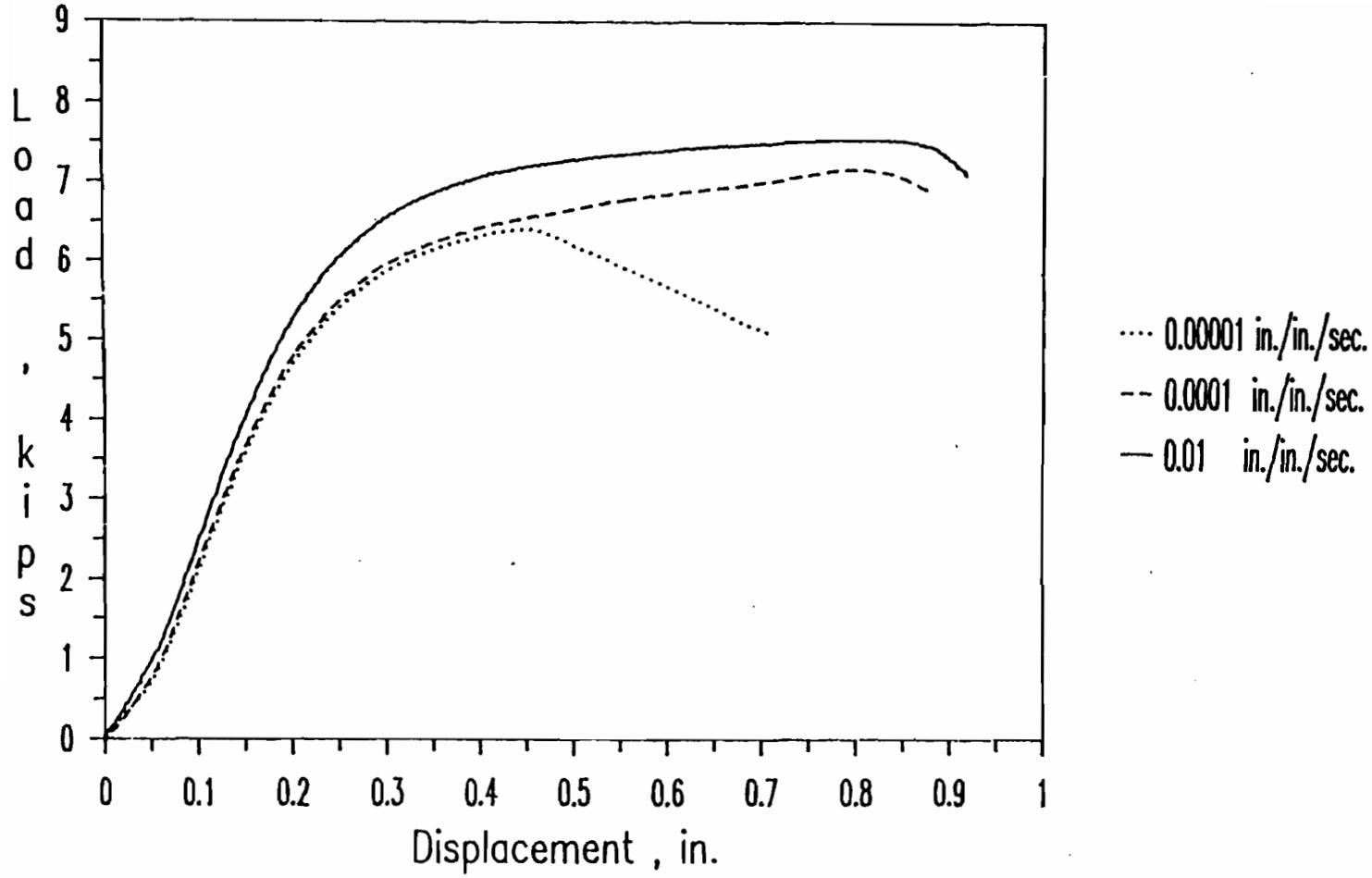

Figure 3.41 Load-Displacement Curves for Channel Beam Specimens 4A0A, 4A1A, and 4A2A

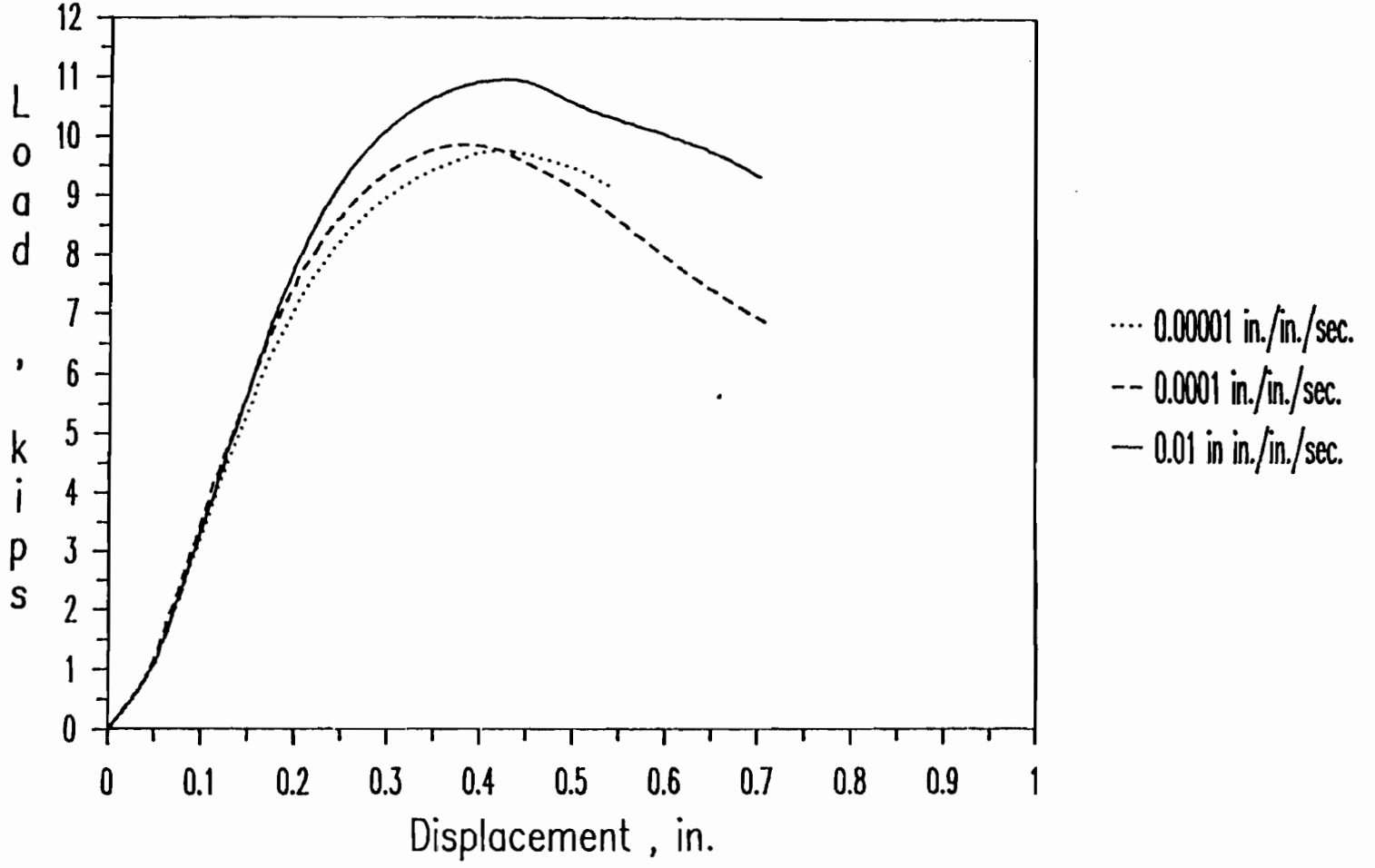

Figure 3.42 Load-Displacement Curves for Channel Beam Specimens 4B0A, 4B1A, and 4B2A

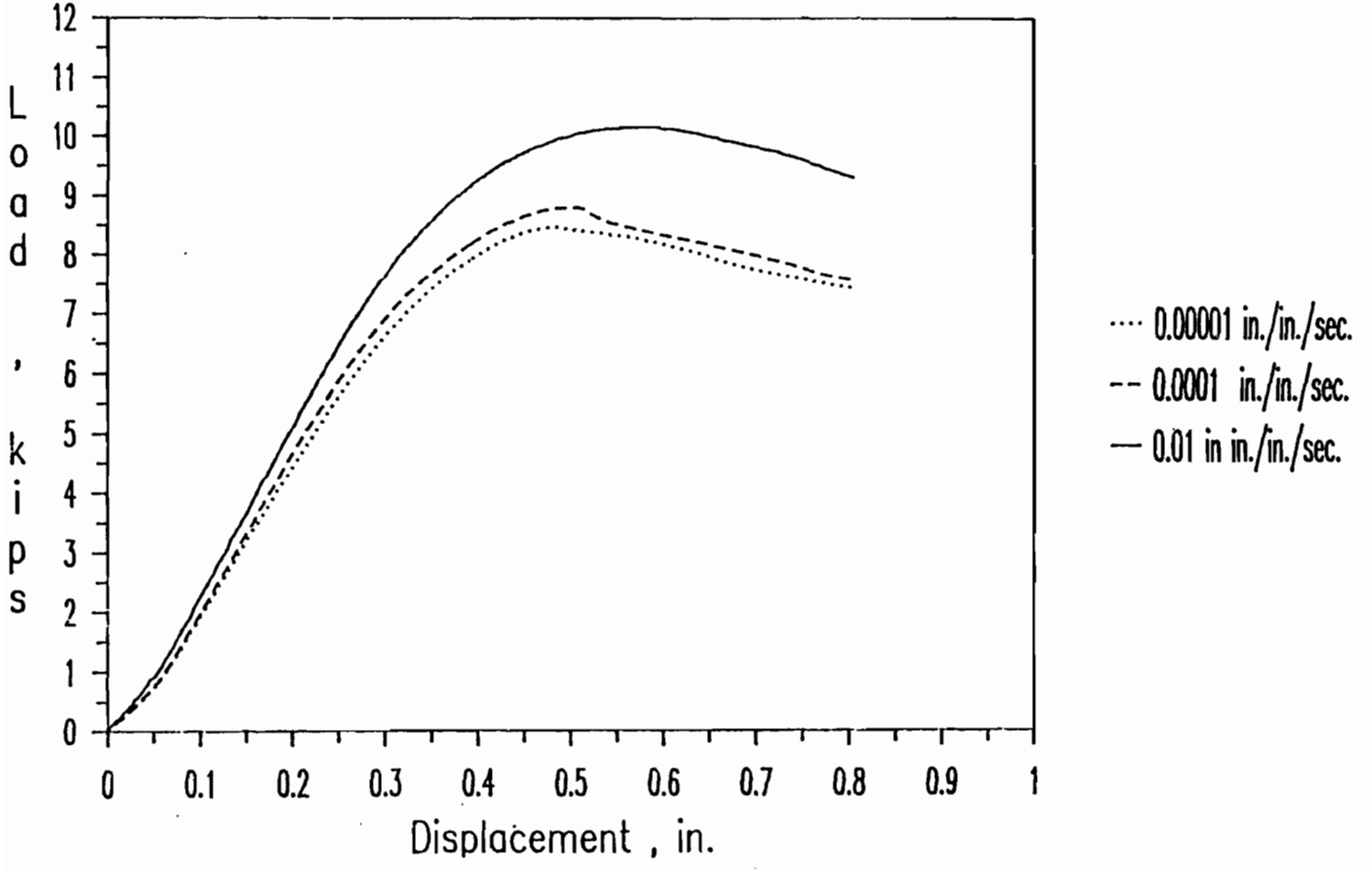

Figure 3.43 Load-Displacement Curves for Channel Beam Specimens 4C0A, 4C1A, and 4C2A

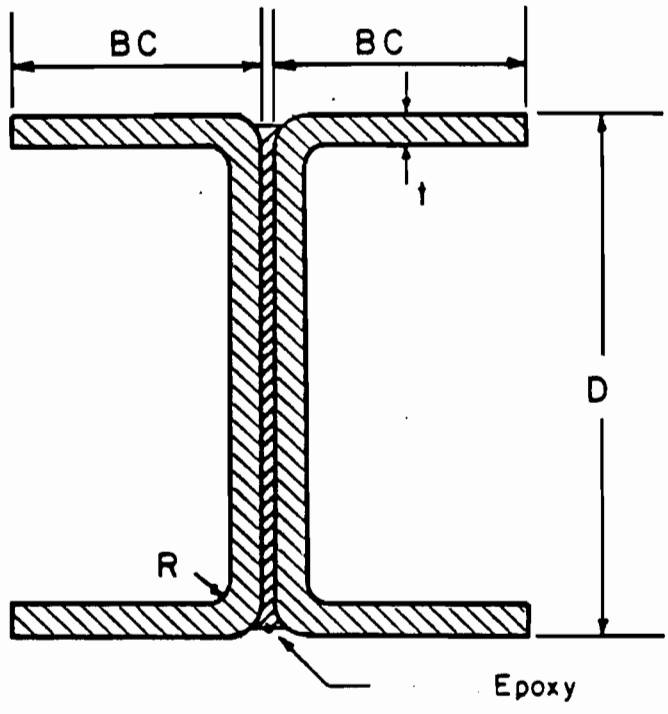

Figure 3.44 Cross Sections of I-Shaped Stub Columns

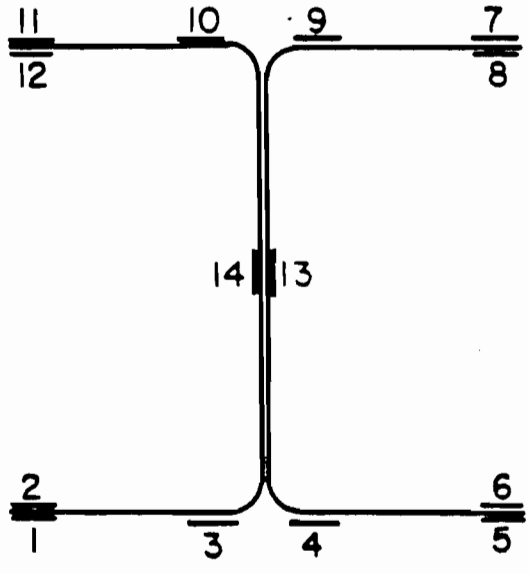

Figure 3.45 Locations of Strain Gages at Midheight of I-Shaped Stub Columns

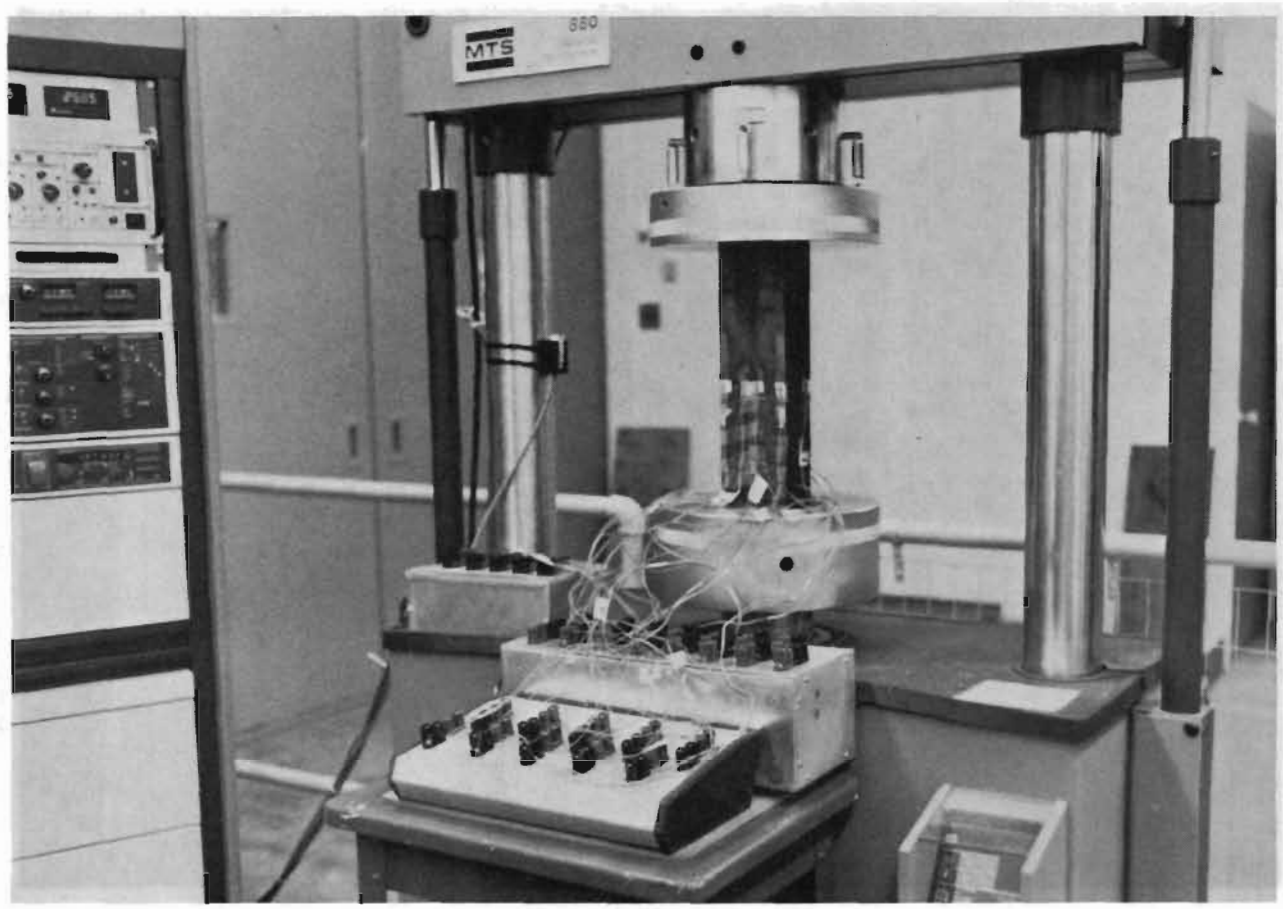

Figure 3.46 Test Setup of Stub Columns with Unstiffened Flanges

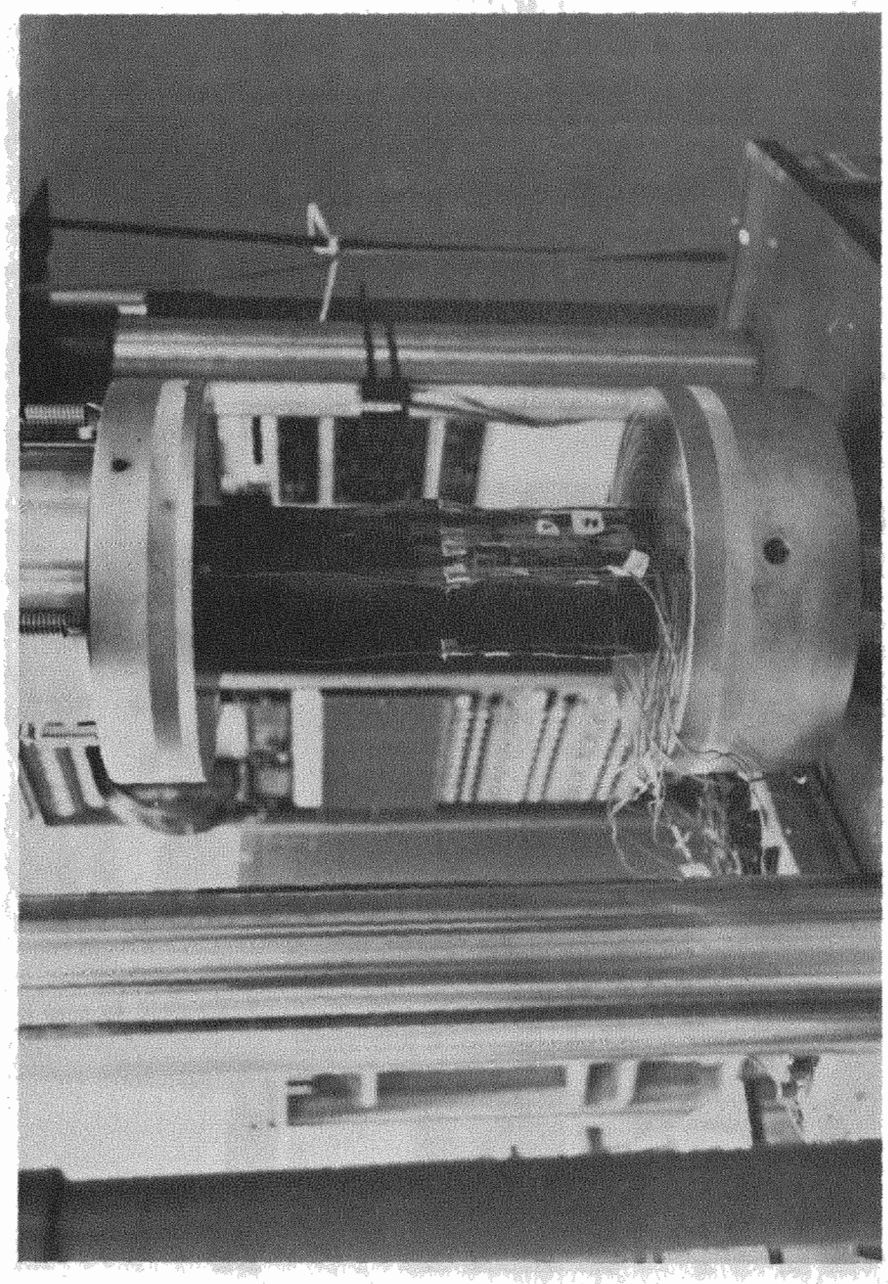

Figure 3.47 Buckling Waves of Unstiffened Flange During a Slow Test

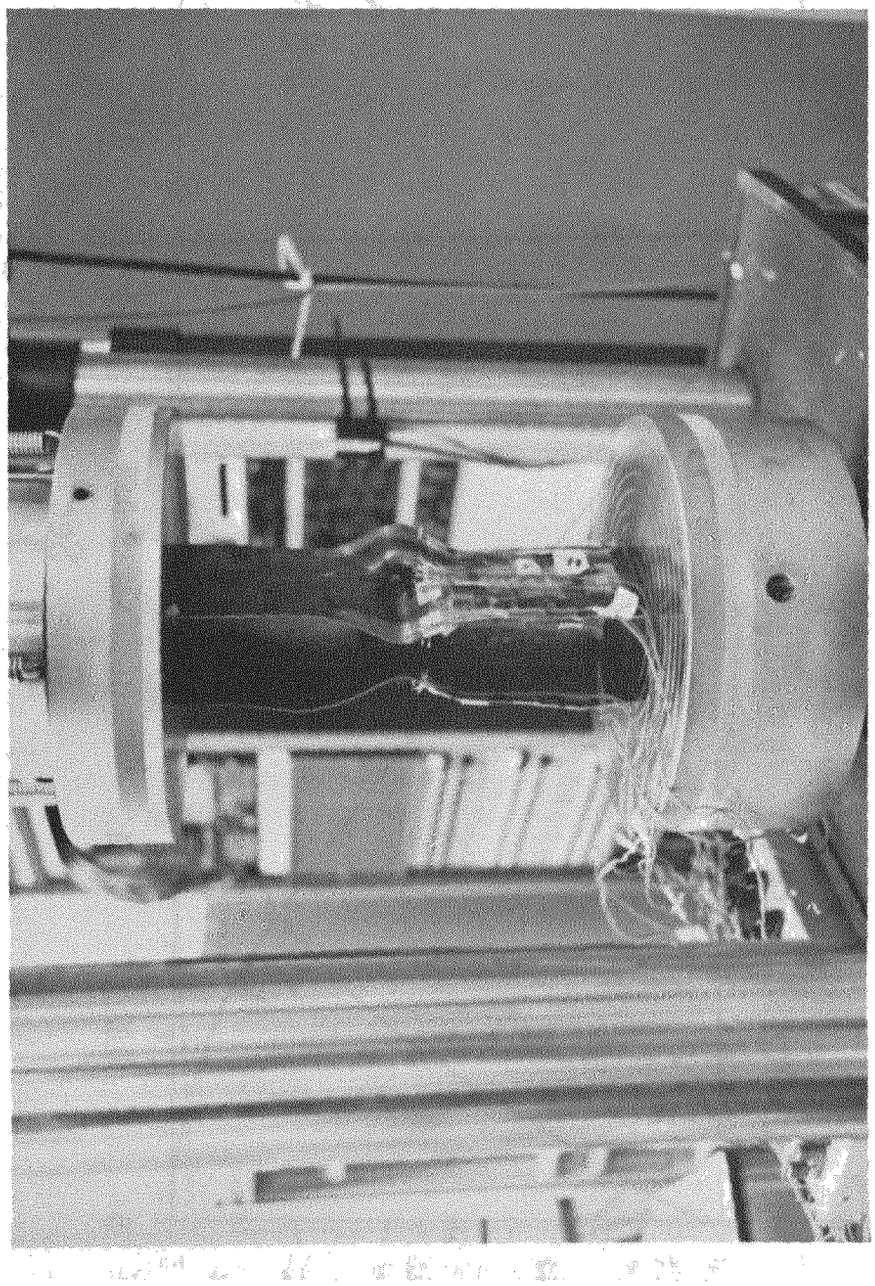

Figure 3.48 Typical Failure of Stub Columns with Unstiffened Flanges

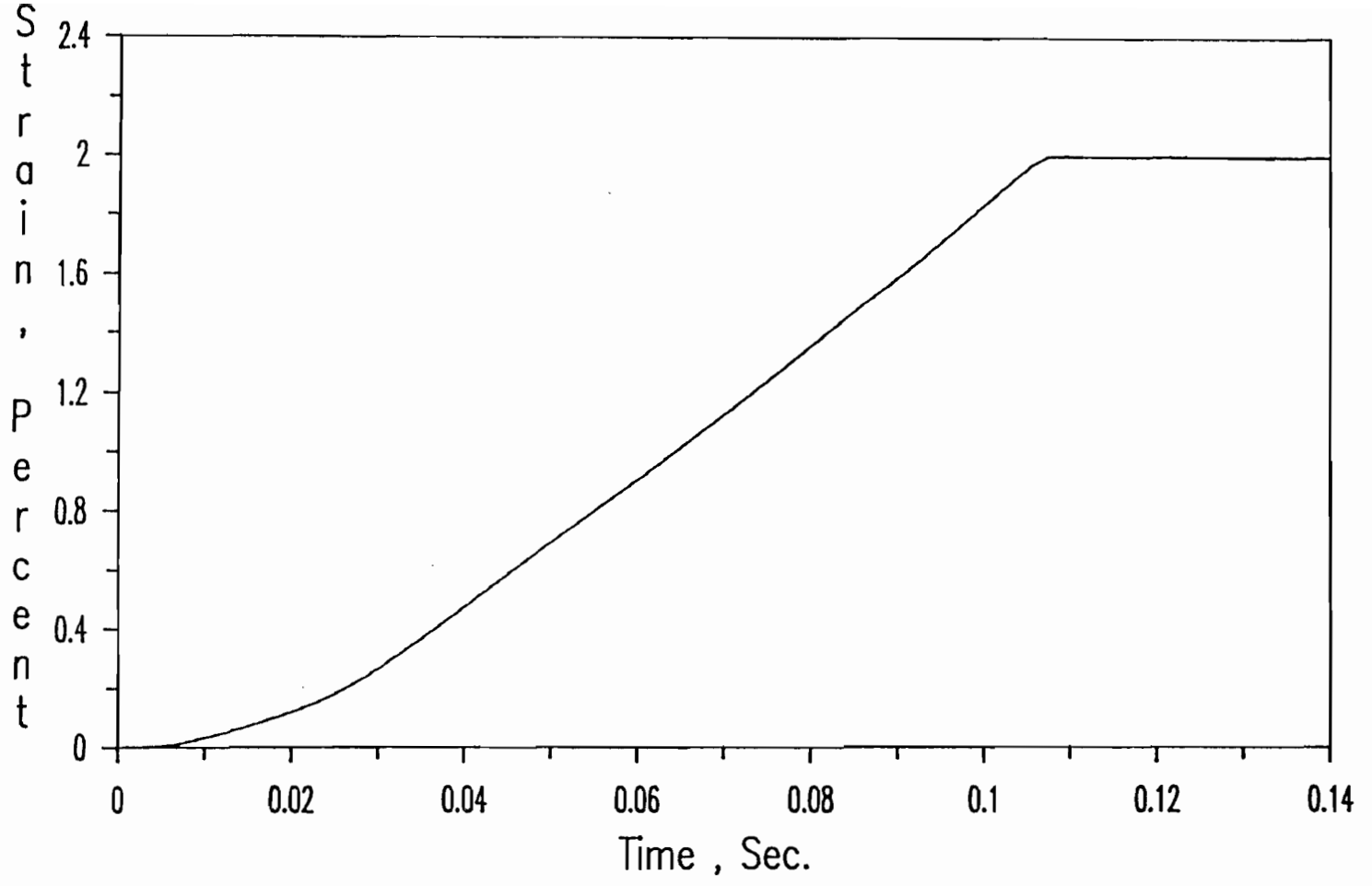

Figure 3.49 Typical Plot of Strain vs. Time for Stub Columns with Unstiffened Flanges (Strain Gage # 3 for Specimen 2B3A)

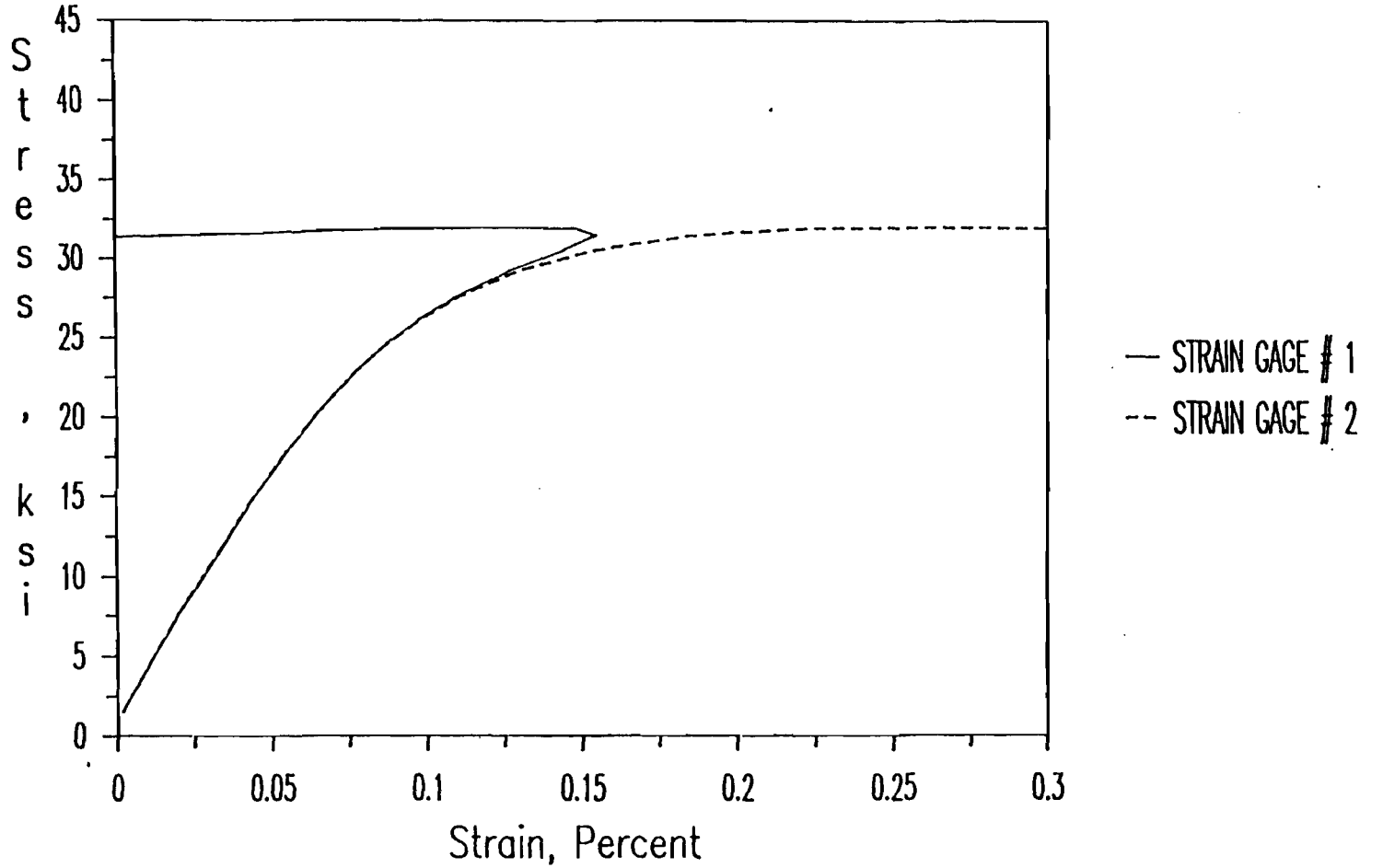

Figure 3.50 Load-Strain Curves of Strain Gages # 1 and 2 Installed at the Tip of an Unstiffened Flange (Spec. 2C0A)

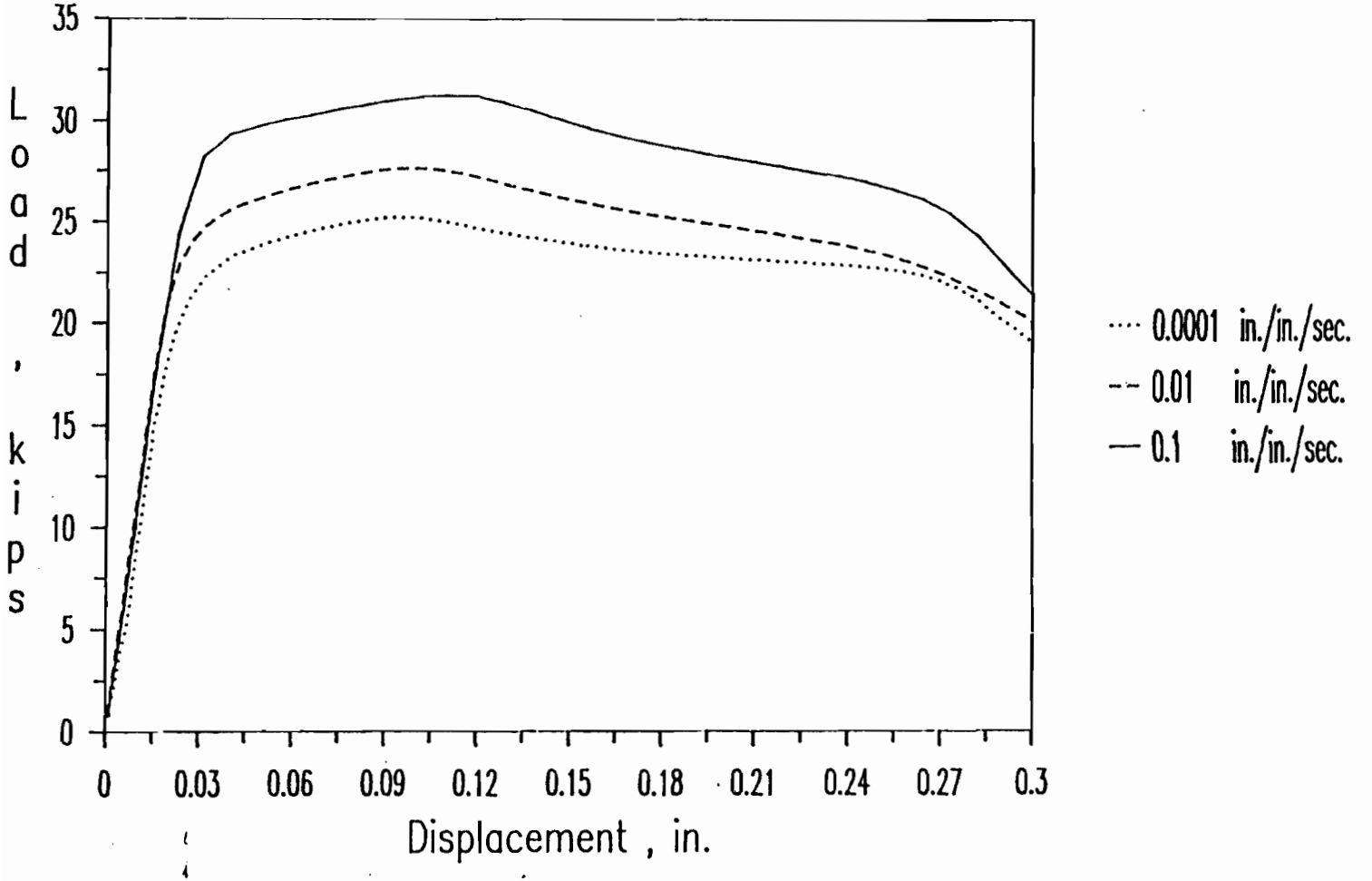

Figure 3.51 Load-Displacement Curves for I-Shaped Stub Columns 2A1A, 2A2A, and 2A3A

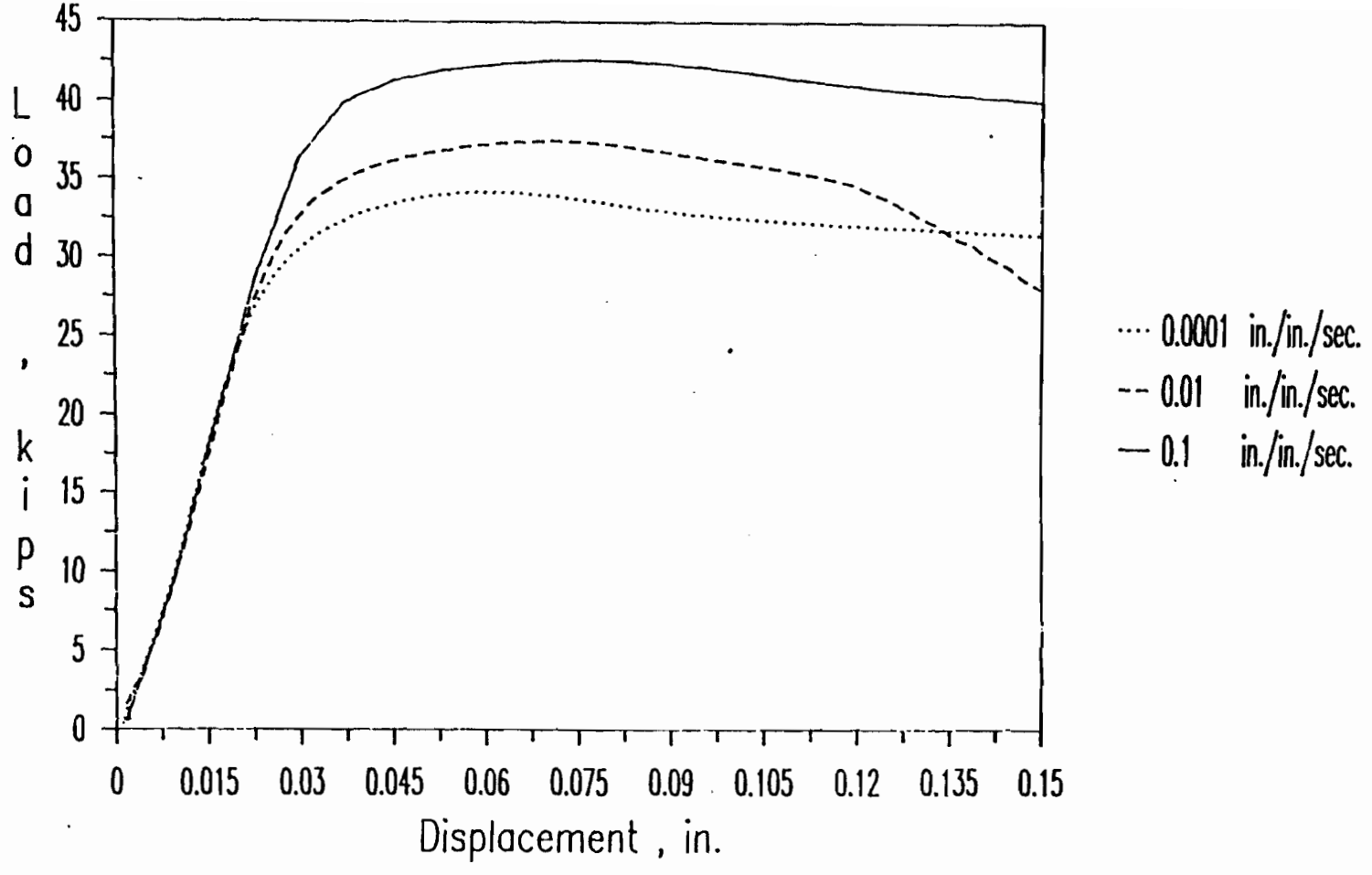

Figure 3.52 Load-Displacement Curves for I-Shaped Stub Columns 2B1A, 2B2A, and 2B3A

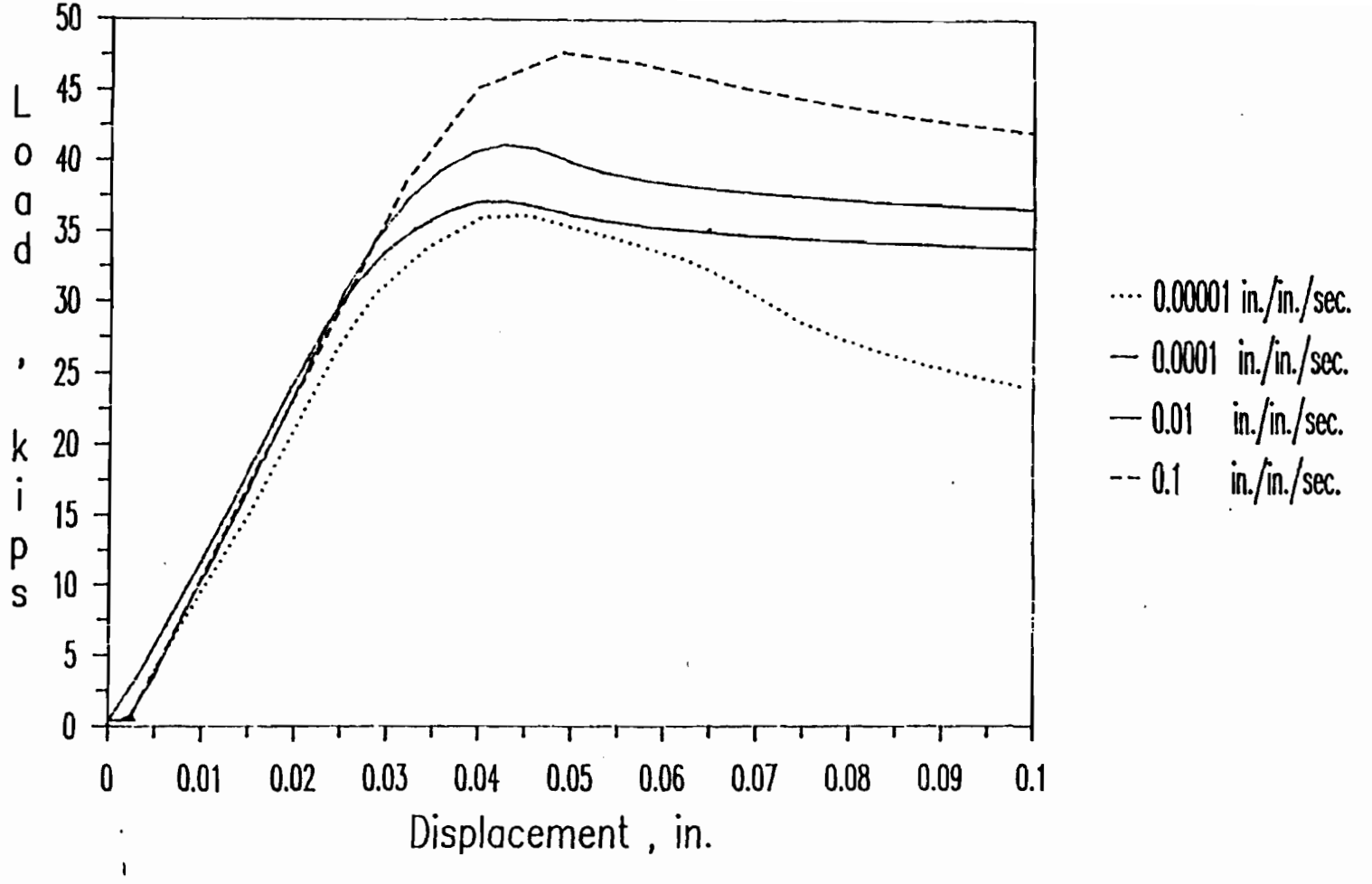

Figure 3.53 Load-Displacement Curves for I-Shaped Stub Columns 2C0A,2C1A, 2C2A, and 2C3A

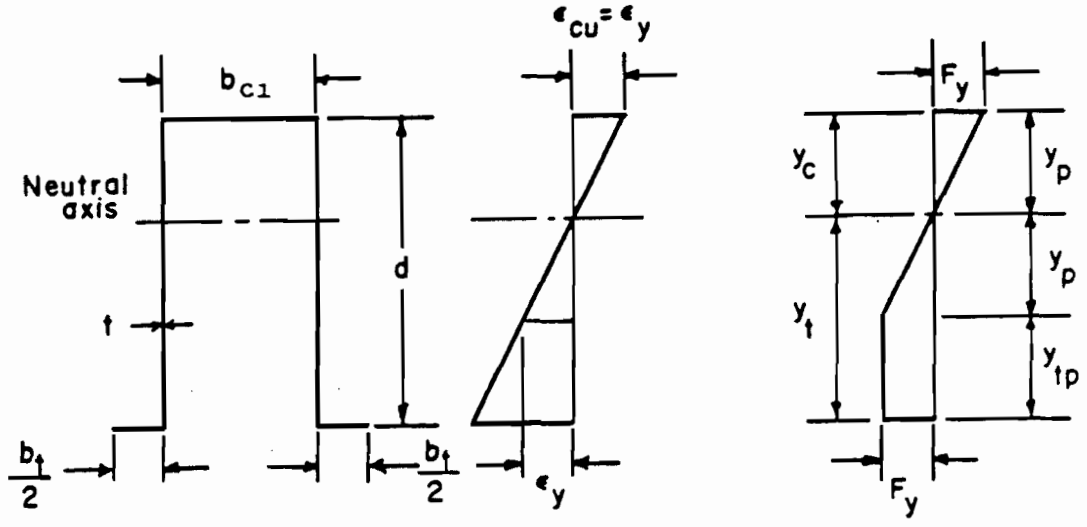

(a)

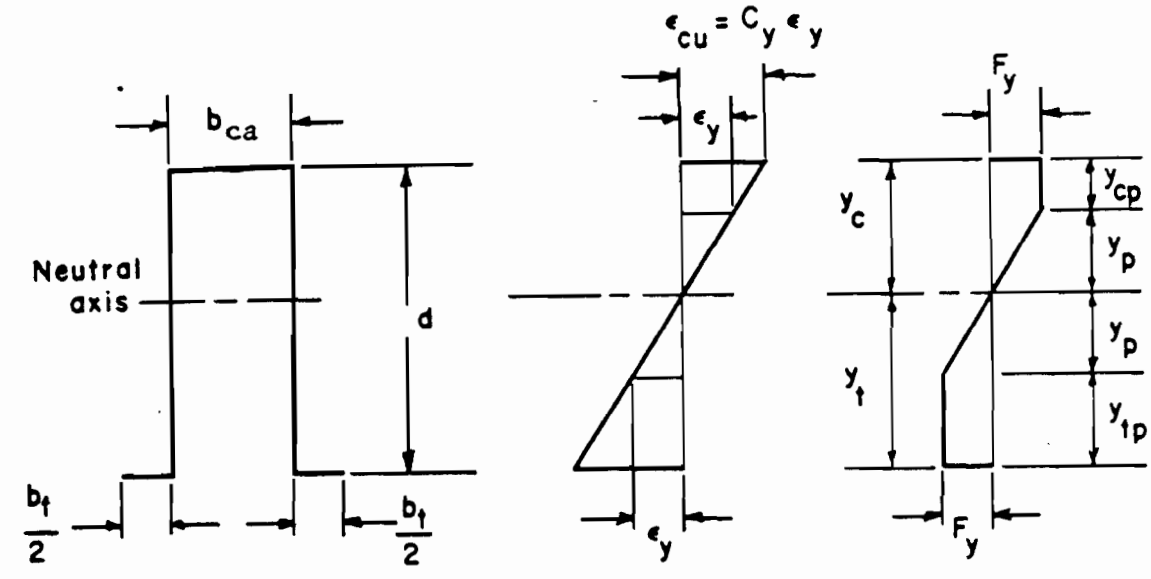

(b)

Fig. 4.1 Stress Distribution in Sections with Yielded Tension Flanges at Ultimate Moments[58]

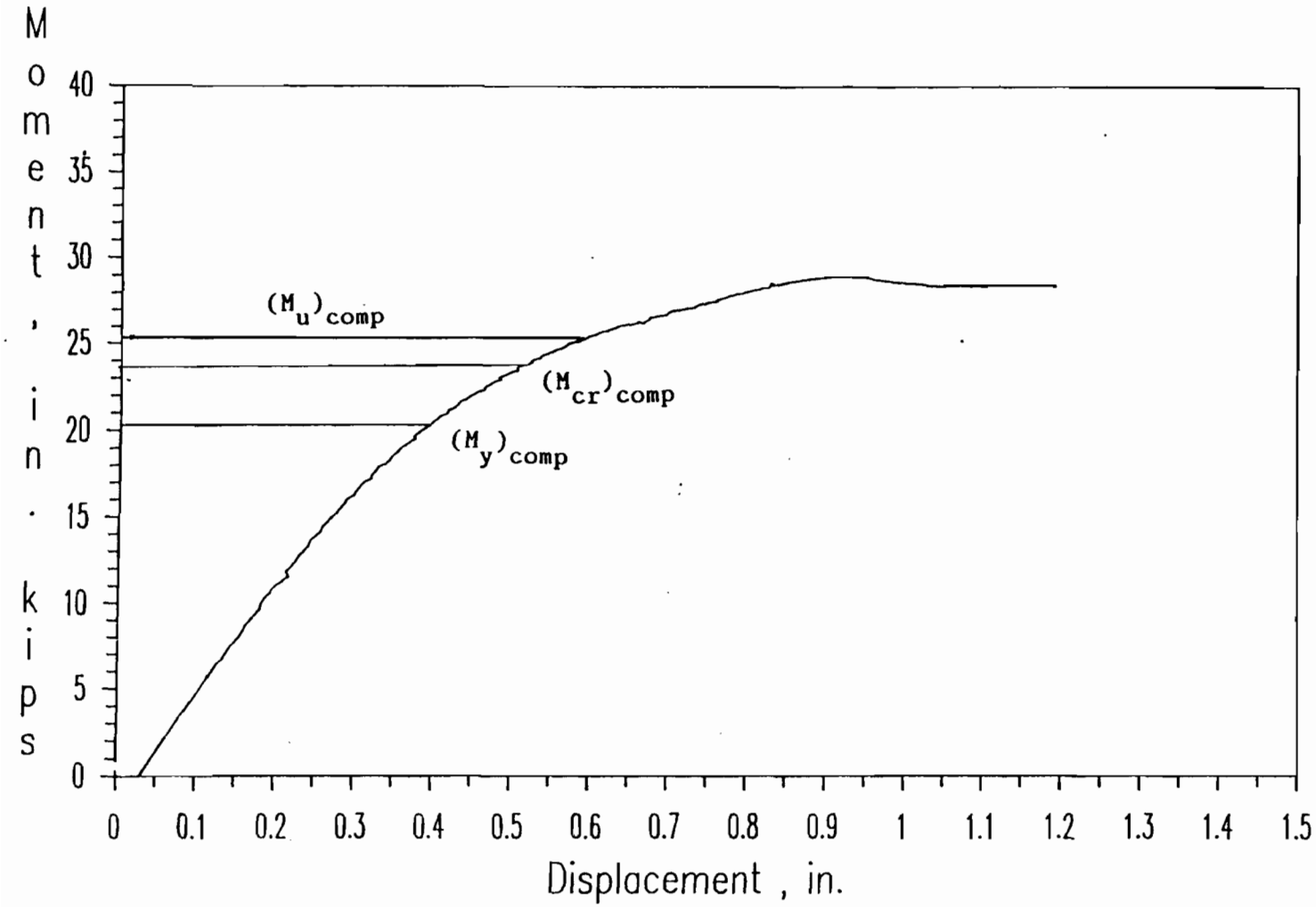

Fig. 4.2 Moment-Displacement Curve for Hat-Beam Specimen 3B0A

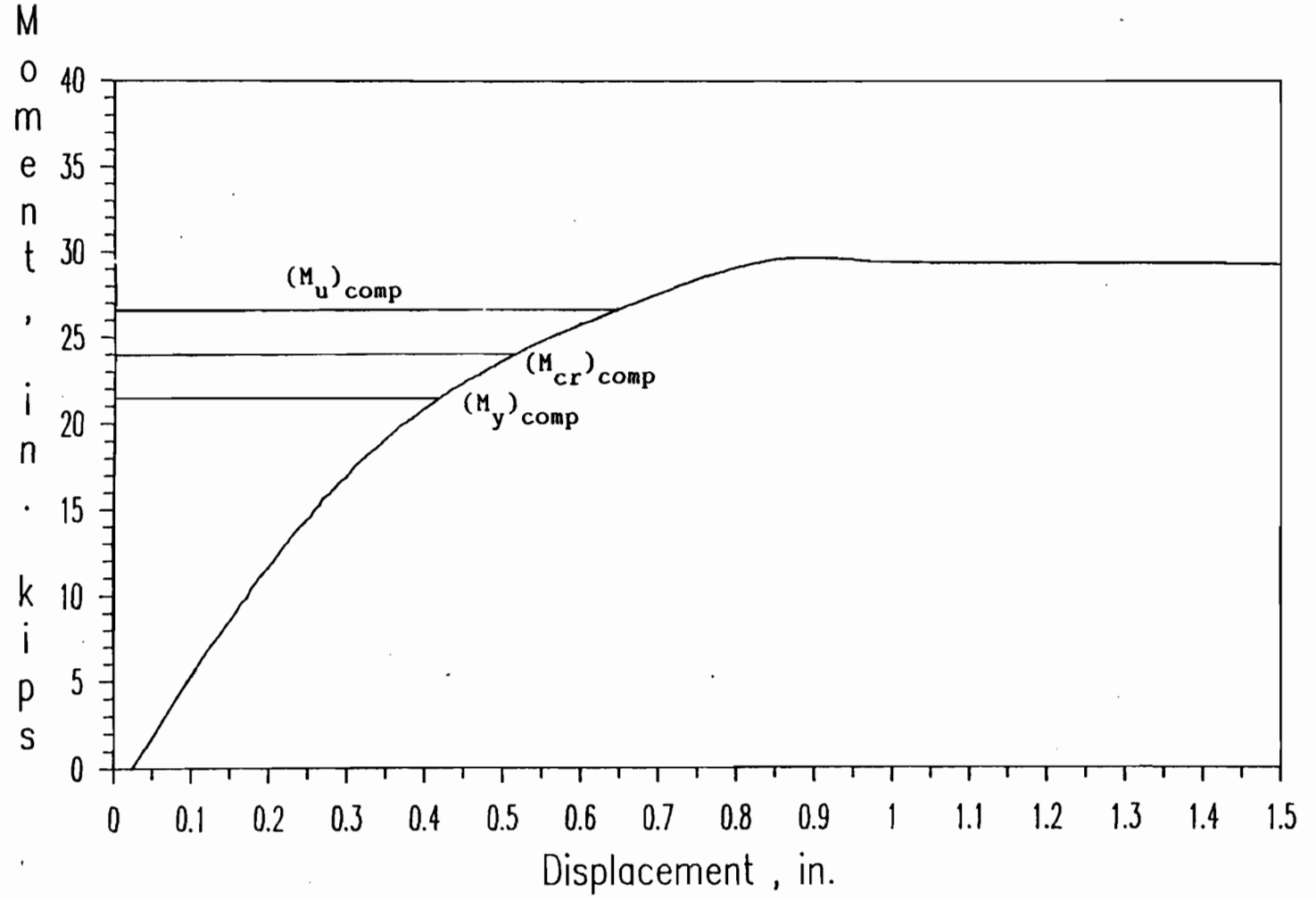

Fig. 4.3 Moment-Displacement Curve for Hat-Beam Specimen 3B1A

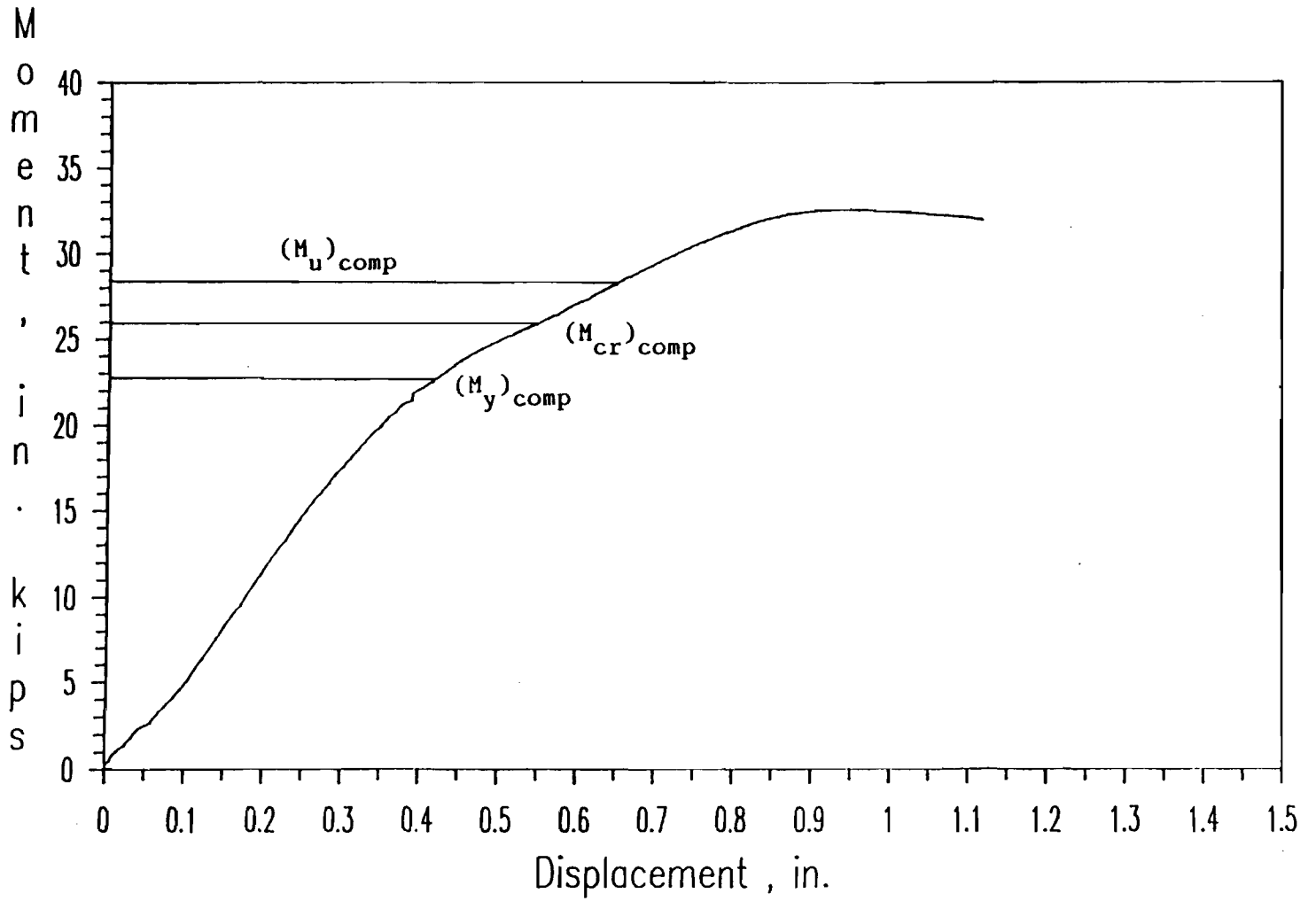

Fig. 4.4 Moment-Displacement Curve for Hat-Beam Specimen 3B2B

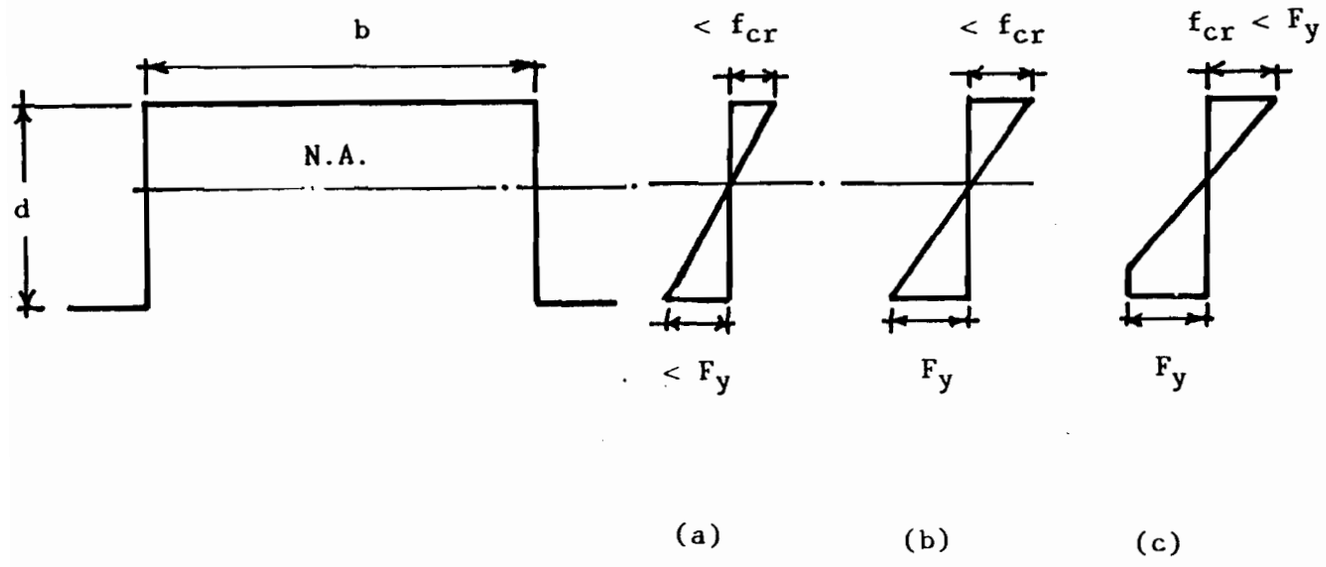

Fig. 4.5 Stress Distribution in Tested Hat Sections

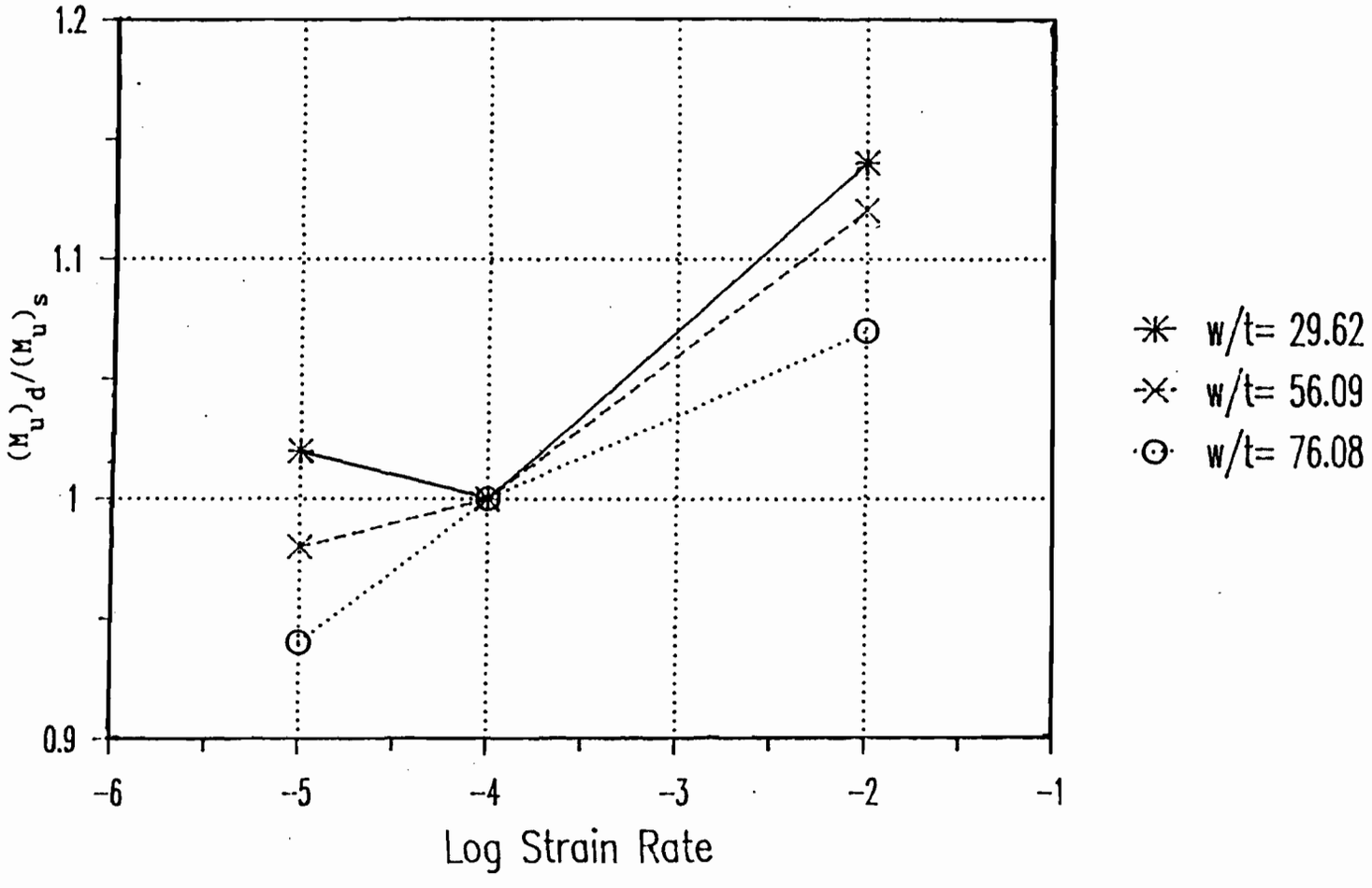

Fig. 4.6 Ratios of Dynamic to Static Average Ultimate Moments vs. Logarithmic Strain Rate for Hat-Beam Specimens

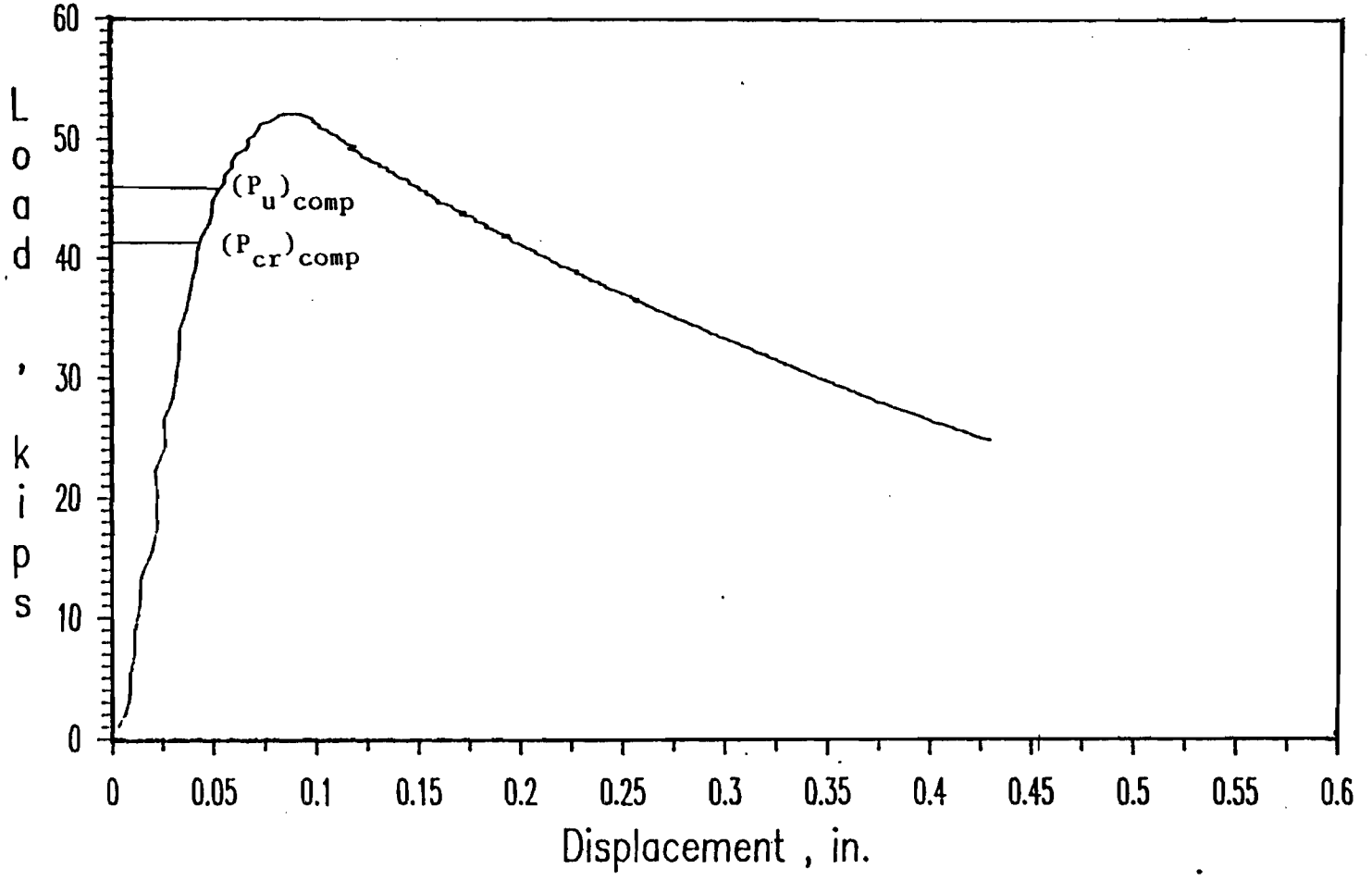

Fig. 4.7 Load-Displacement Curve for Box-Shaped Stub Column Specimen 1B1A

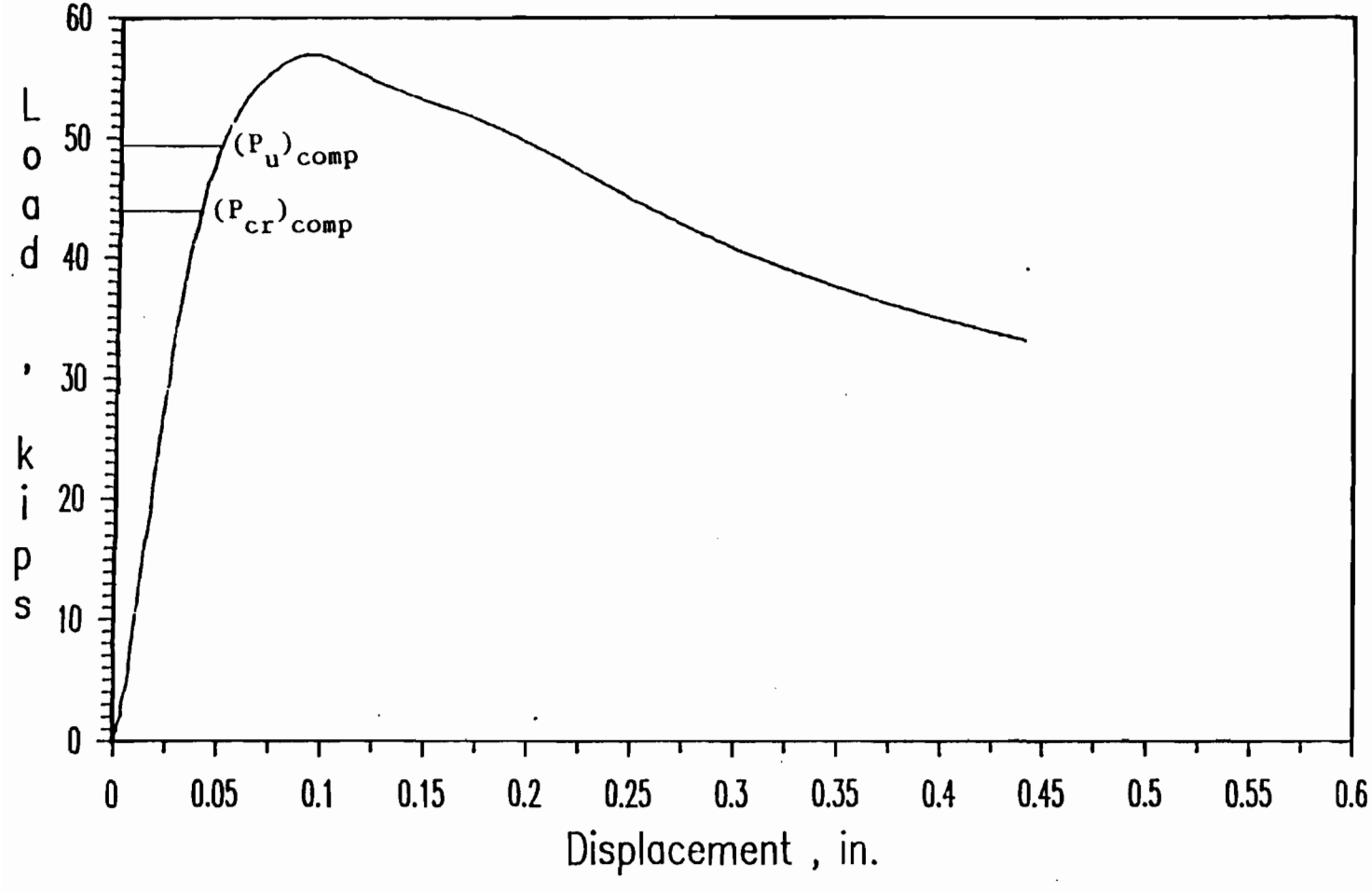

Fig. 4.8 Load-Displacement Curve for Box-Shaped Stub Column Specimen 1B2B

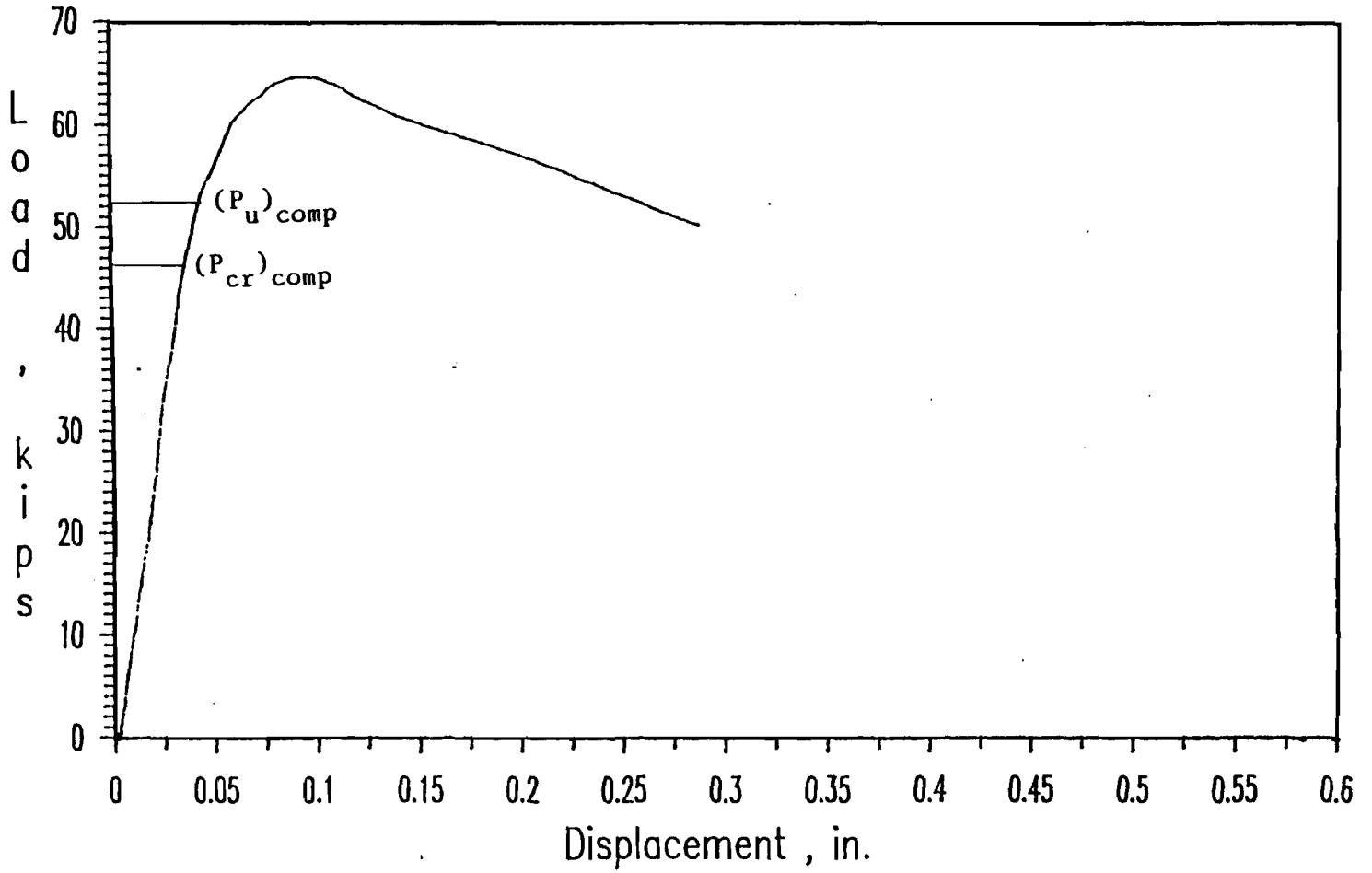

Fig. 4.9 Load-Displacement Curve for Box-Shaped Stub Column Specimen 1B3A

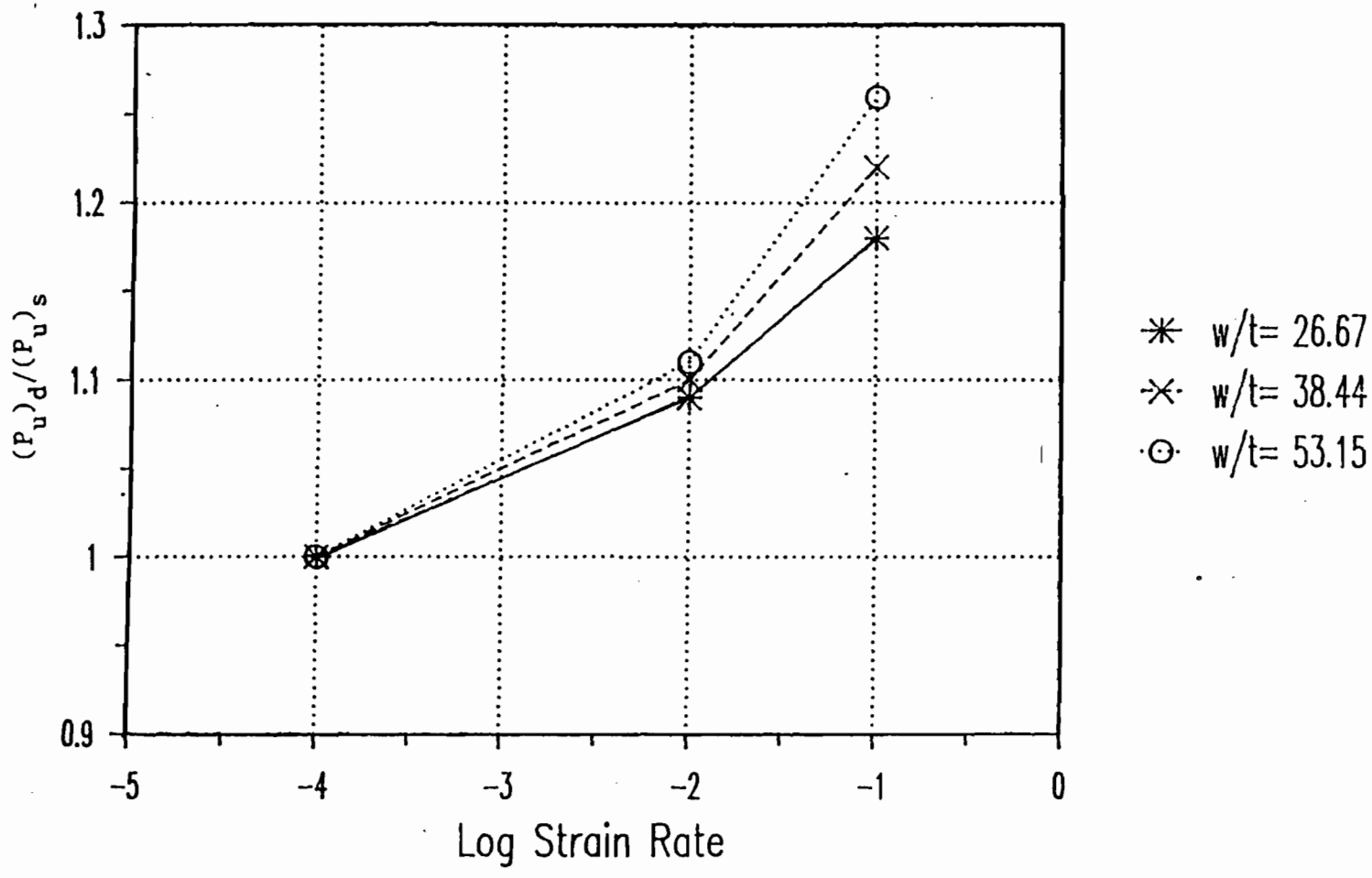

Fig. 4.10 Ratios of Dynamic to Static Average Ultimate Loads vs. Logarithmic Strain Rate for Box-Shaped Stub Columns

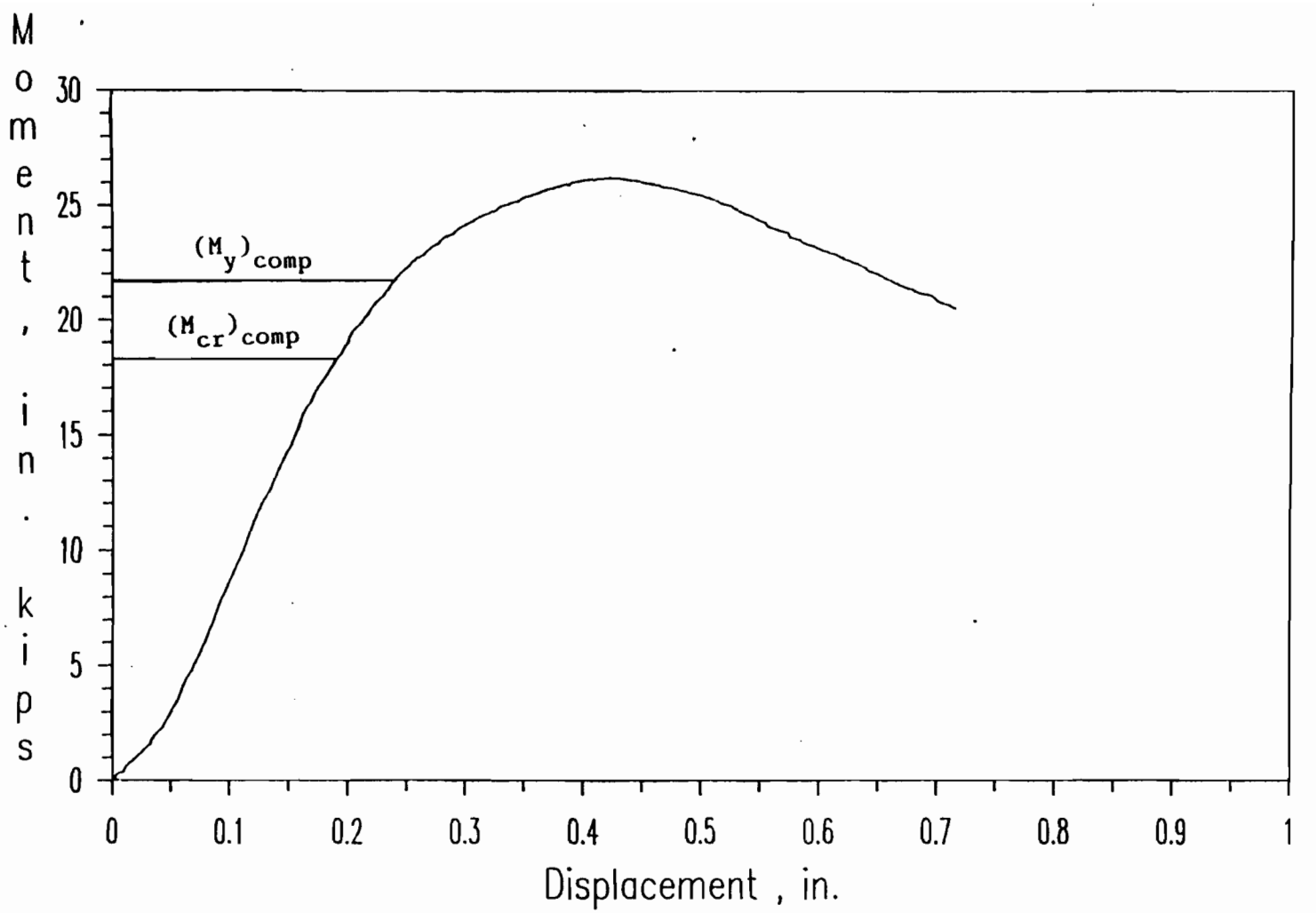

Fig. 4.11 Moment-Displacement Curve for Channel Beam Specimen 4B0A

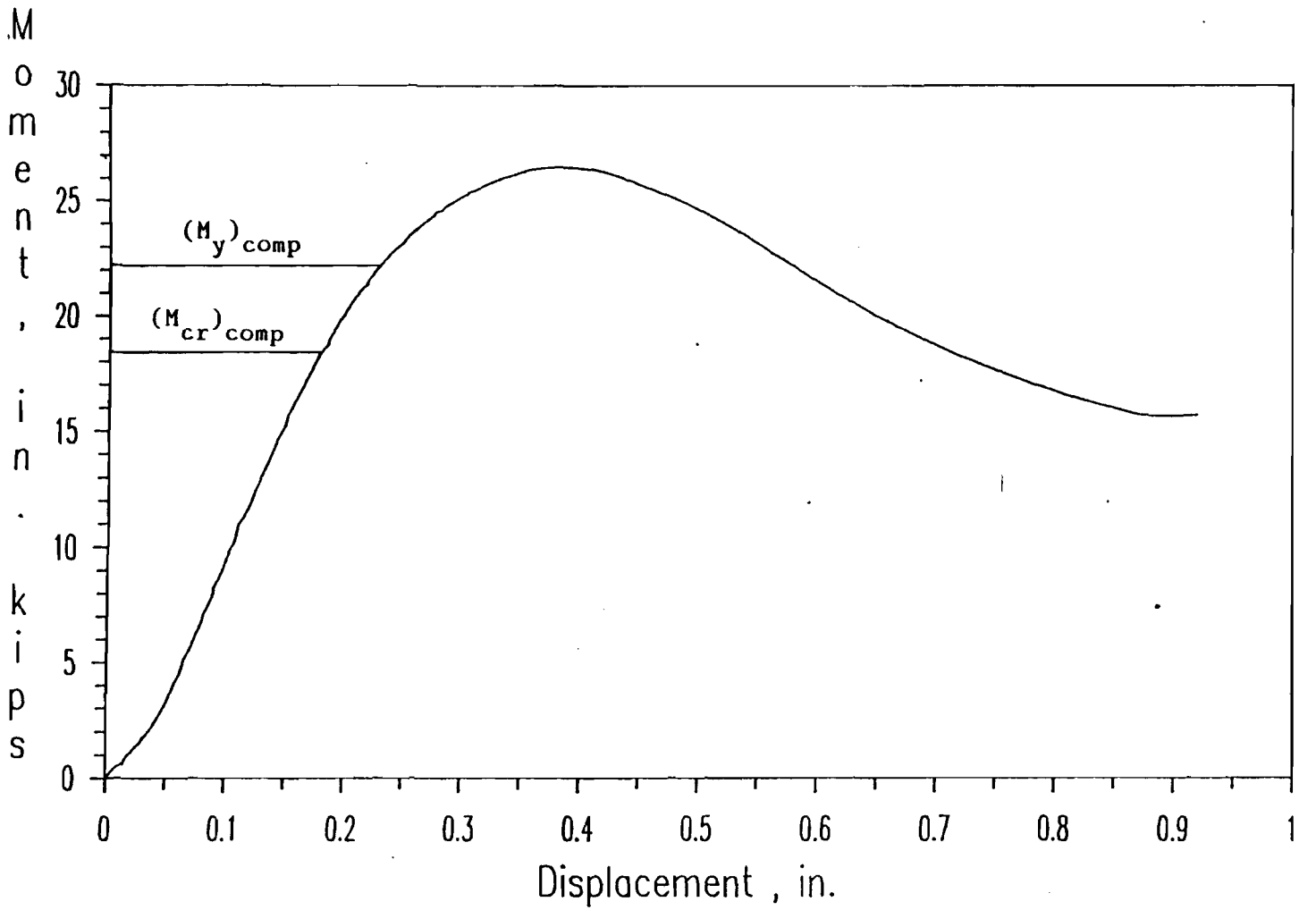

Fig. 4.12 Moment-Displacement Curve for Channel Beam Specimen 4B1B

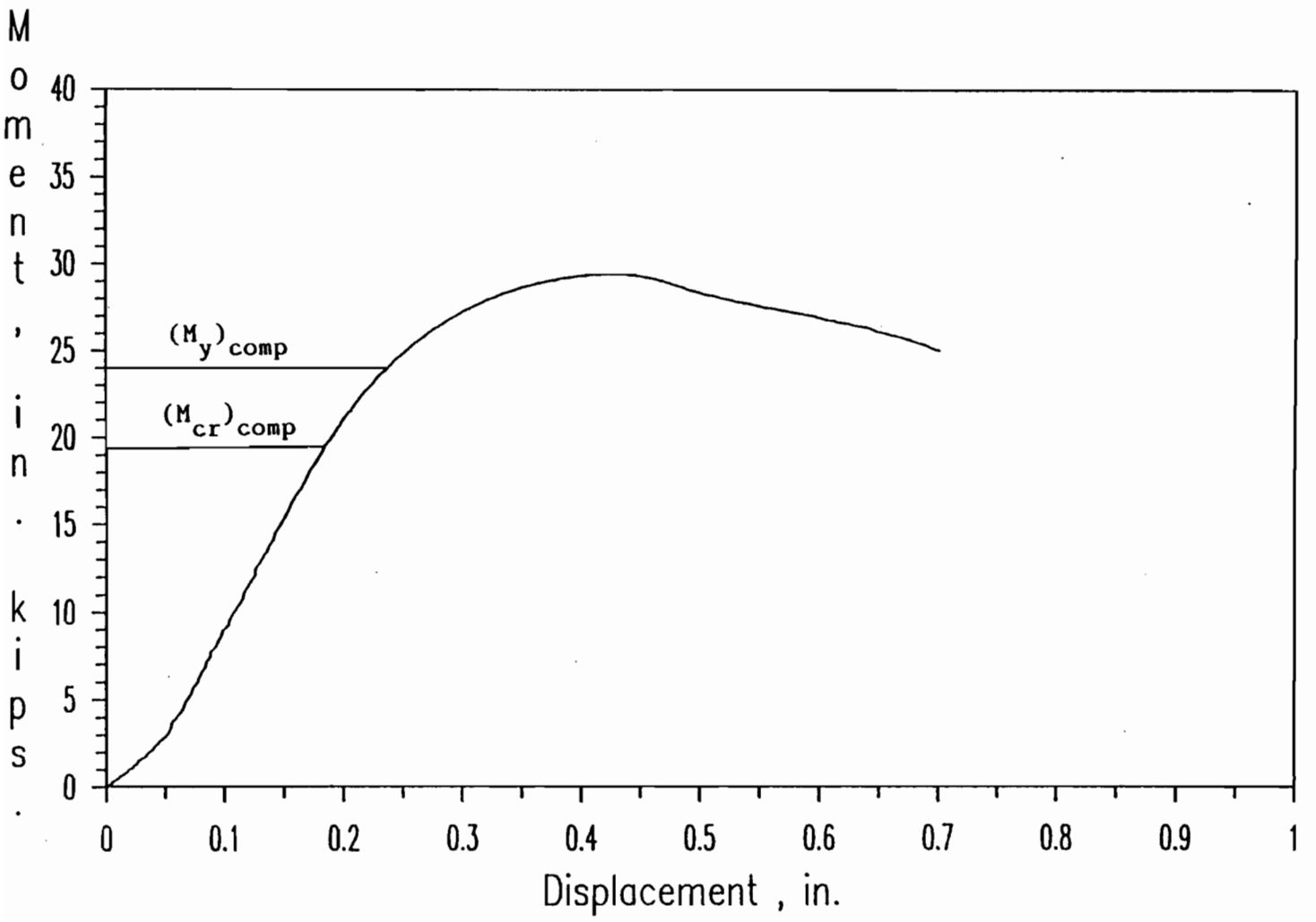

Fig. 4.13 Moment-Displacement Curve for Channel Beam Specimen 4B2B

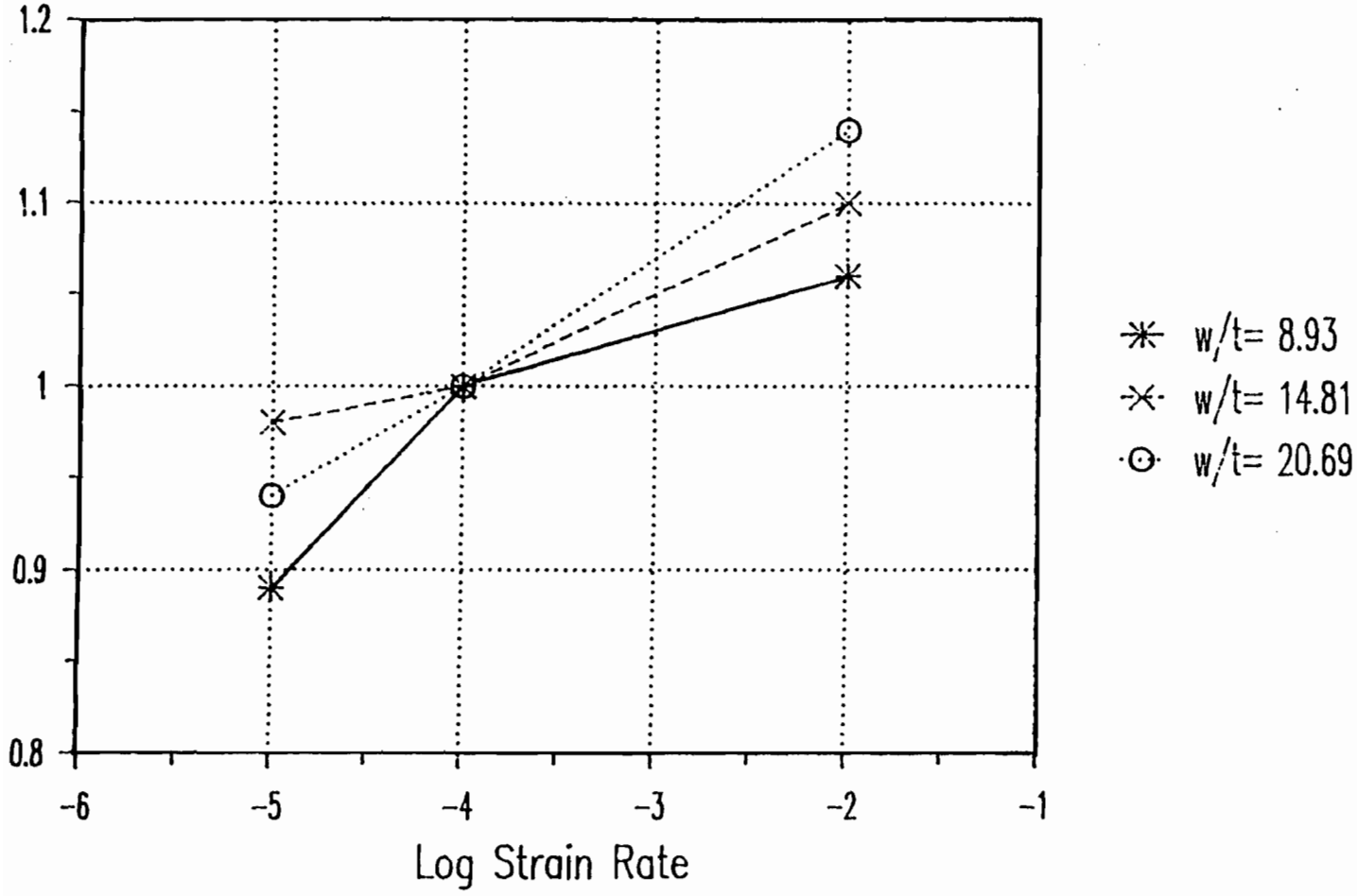

Fig. 4.14 Ratios of Dynamic to Static Average Ultimate Moments vs. Logarithmic Strain Rate for Channel Beam Specimens

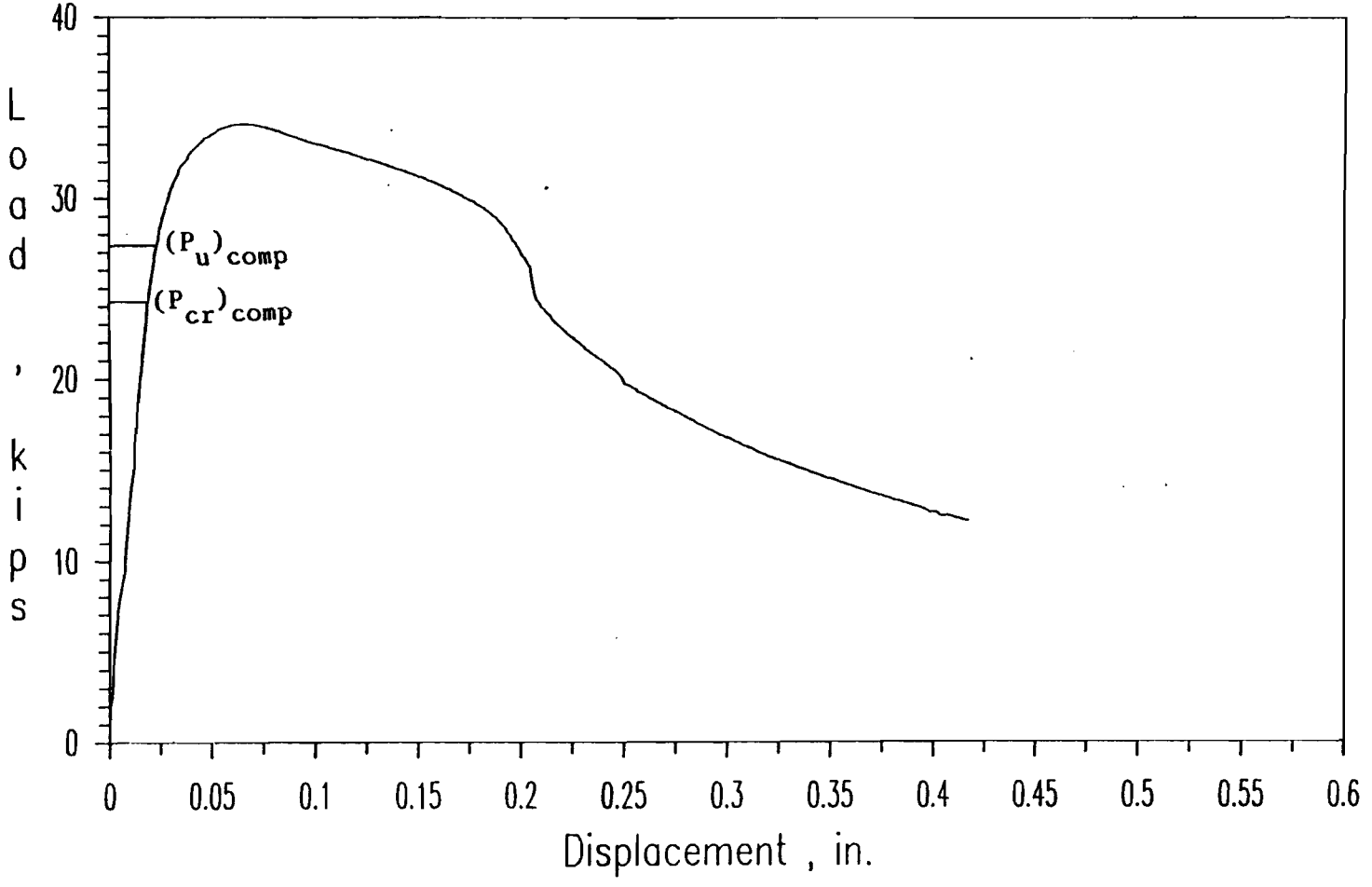

Fig. 4.15 Load-Displacement Curve for I-Shaped Stub Column

Specimen 2B1A

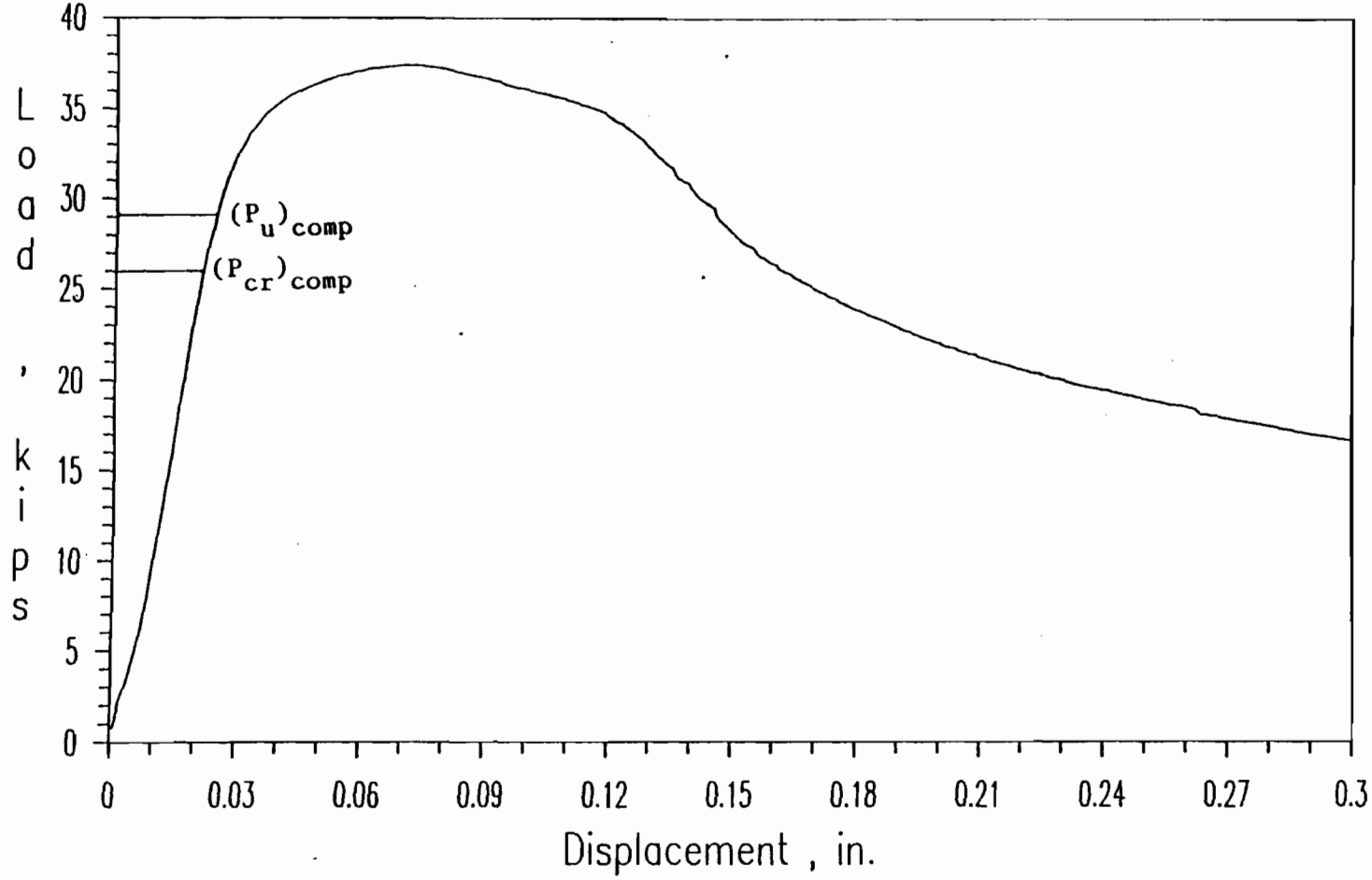

Fig. 4.16 Load-Displacement Curve for I-Shaped Stub Column Specimen 2B2B

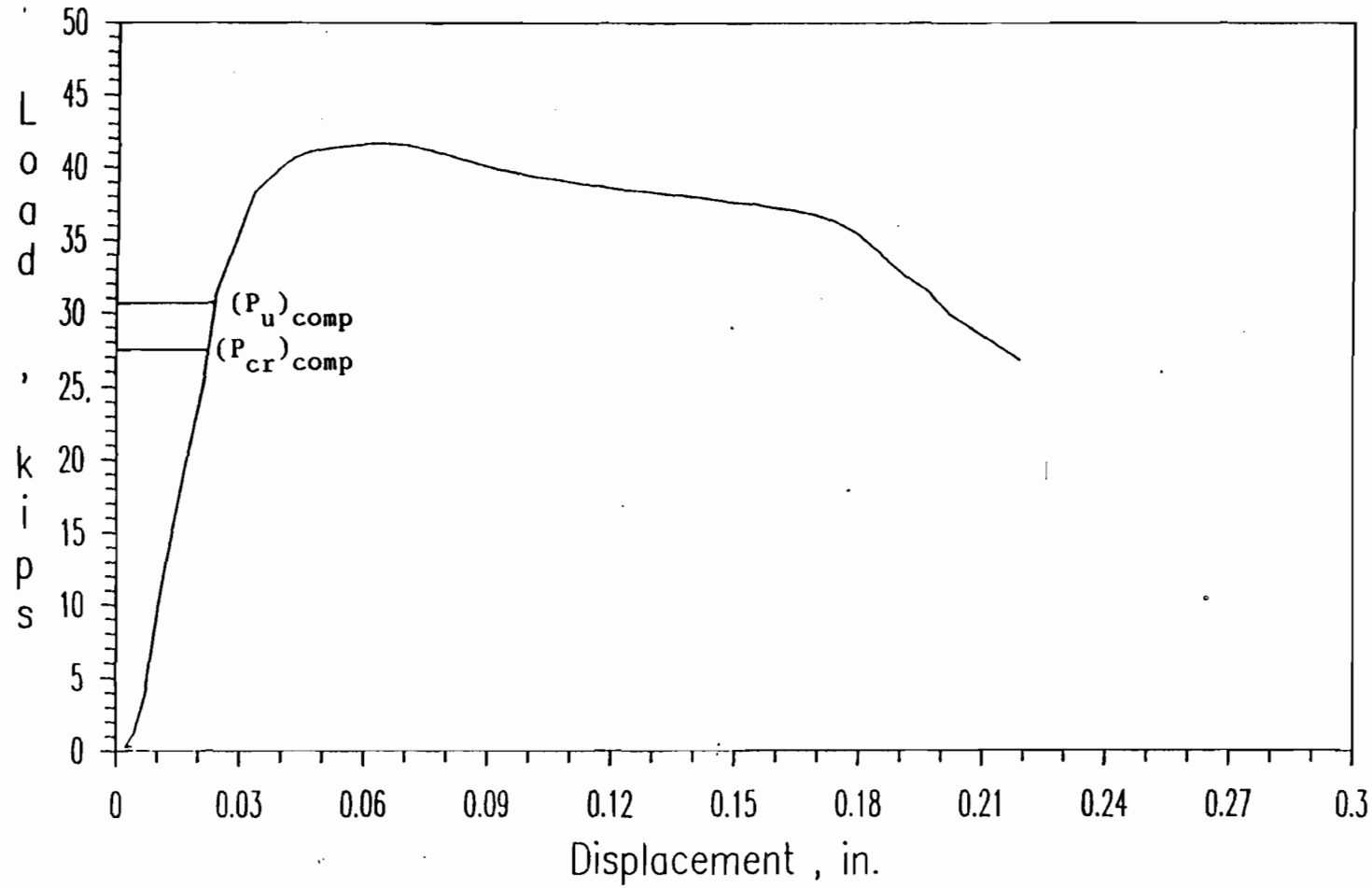

Fig. 4.17 Load-Displacement Curve for I-Shaped Stub Column

Specimen 2B3A

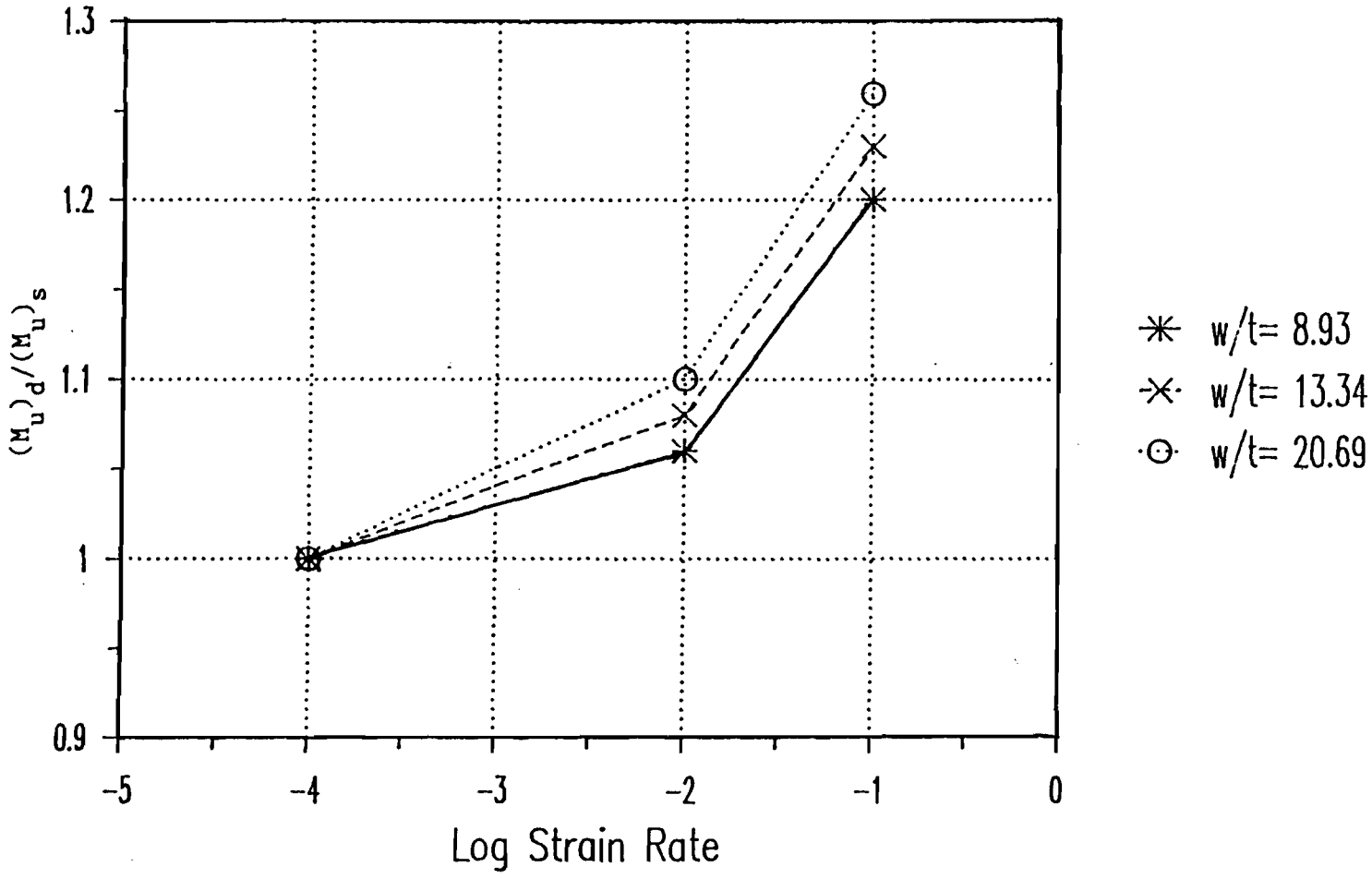

Fig. 4.18 Ratios of Dynamic to Static Average Ultimate Loads vs. Logarithmic Strain Rate for I-Shaped Stub Columns

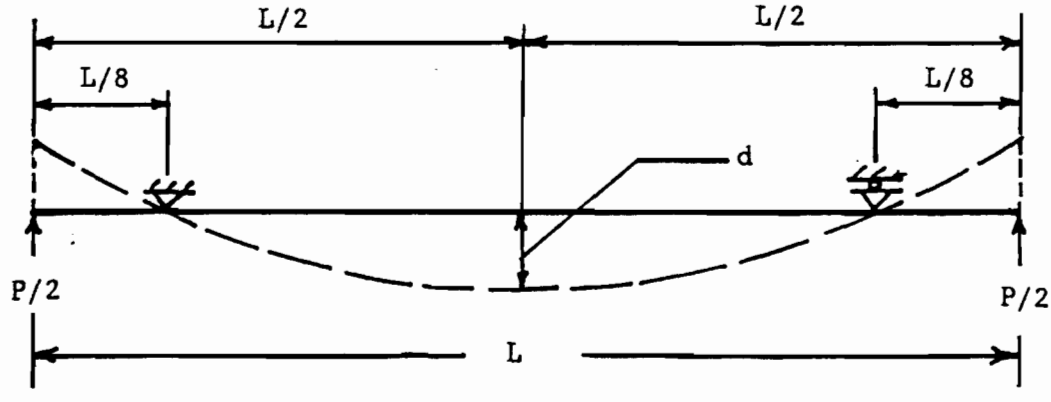

Fig. 4.19 Schematic Diagram for Beam Specimen Showing Midspan Deflection

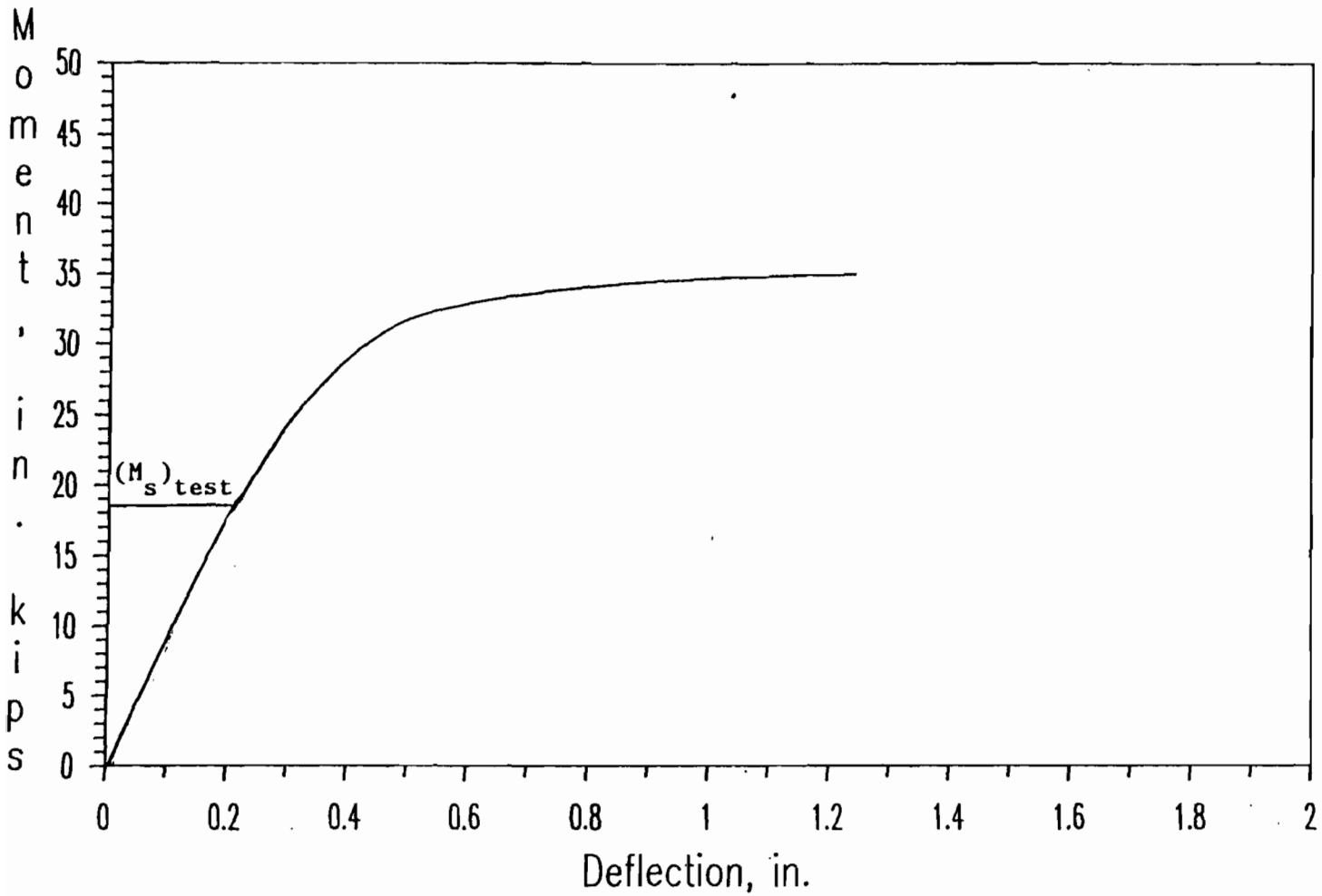

Fig. 4.20 Typical Moment-Deflection Curve for Hat-Beam Specimens

Specimen 3C1B

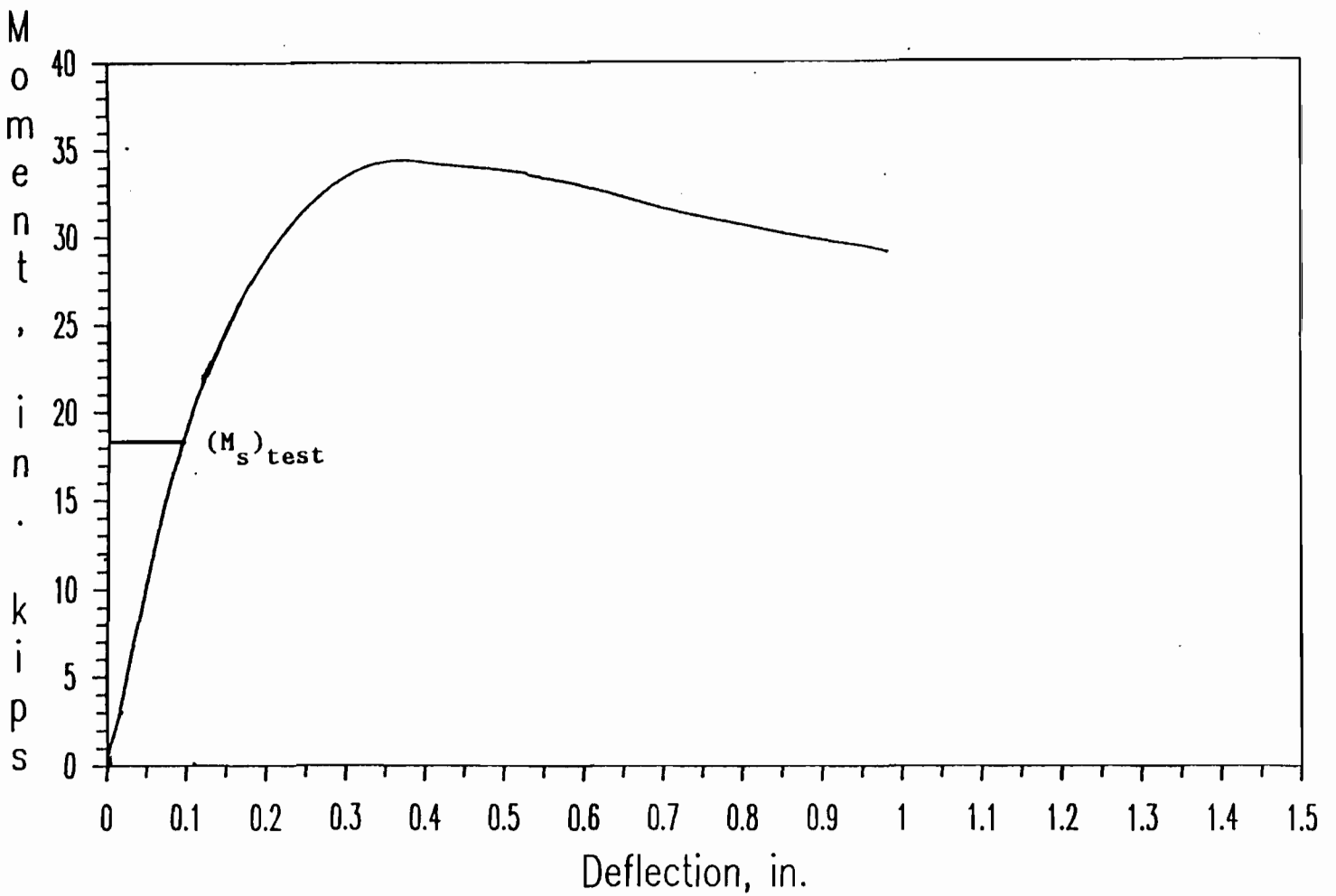

Fig. 4.21 Typical Moment-Deflection Curve for Channel Beam Specimens

Specimen 4C0A

APPENDIX - NOTATION

The following symbols are used in this report:

a	Length of plate
A_e	Effective cross-sectional area of stub columns
A_g	Gross sectional area of stub columns
b	Effective width of a compression element
C_y	Compressive strain factor
d	Depth of the section
	Midspan deflection
D	Flexural rigidity of plate, $Et^3/12(1-\mu^2)$
E	Modulus of elasticity of steel = 29,500 ksi
E_t	Tangent modulus of steel
f	Stress in the compression element
f_d	Compressive stress at the stiffened or unstifffend flange based on the effective section at service moment
f_{cr}	Critical local buckling stress
$(f_{cr})_E$	Elastic critical local buckling stress
$(f_{cr})_I$	Inelastic critical local buckling stress
f_{max}	Maximum edge stress of a compression element
f_x, f_y	Stress components in the x-y plane
F	Stress function
F_{pr}	Proportional limit

F_y	Yield strength
H	Thickness of the beam
I	Moment of inertia
I_e	Effective moment of inertia
k	Buckling coefficient
m	Number of half sine waves in x-direction
	Strain-rate sensitivity exponent
M	Dynamic bending moment
M_0	Static collapse moment
M_{cr}	Critical local buckling moment
M_u	Ultimate moment
M_y	Yield moment
n	Number of half sine waves in y-direction
$\bar{n}$	Constant
p	Constant
P	Coupon axial load
P_{cr}	Critical buckling load
P_y	Yield Load
P_u	Ultimate load
P_m	Mean crush force
q	Lateral uniform load
r	Ratio of the slopes of the elastic and plastic portions of the stress-strain curve

R	Dynamic correction factor
S_e	Elastic section modulus of the effective section
S_{xc}	Elastic section modulus of the full cross section relative to the compression flange
t	Thickness of plate
	Test time
v	Impact velocity
w	Width of plate
α	Constant
β	Constant
ϕ_s, ϕ_u	Stress reduction factors
ε	Engineering or true strain
$\dot{\varepsilon}$	Strain rate
λ, λ_d	Slenderness factors
η	Plasticity reduction factor
$\dot{\kappa}$	Curvature rate
ω	Deflection of plate perpendicular to surface
μ	Poisson's ratio
ν	Constant = $E/(r\ \sigma_0)$
ρ	Reduction factor
σ	True stress
	Dynamic yield stress
σ_0	Static yield stress
τ_{xy}	Shear stress component in the x-z and y-z planes